

IAEA TECDOC SERIES

IAEA-TECDOC-1994

Numerical Benchmarks for Multiphysics Simulation of Pressurized Heavy Water Reactor Transients



IAEA

International Atomic Energy Agency

NUMERICAL BENCHMARKS FOR
MULTIPHYSICS SIMULATION OF
PRESSURIZED HEAVY WATER
REACTOR TRANSIENTS

The following States are Members of the International Atomic Energy Agency:

AFGHANISTAN	GEORGIA	OMAN
ALBANIA	GERMANY	PAKISTAN
ALGERIA	GHANA	PALAU
ANGOLA	GREECE	PANAMA
ANTIGUA AND BARBUDA	GRENADA	PAPUA NEW GUINEA
ARGENTINA	GUATEMALA	PARAGUAY
ARMENIA	GUYANA	PERU
AUSTRALIA	HAITI	PHILIPPINES
AUSTRIA	HOLY SEE	POLAND
AZERBAIJAN	HONDURAS	PORTUGAL
BAHAMAS	HUNGARY	QATAR
BAHRAIN	ICELAND	REPUBLIC OF MOLDOVA
BANGLADESH	INDIA	ROMANIA
BARBADOS	INDONESIA	RUSSIAN FEDERATION
BELARUS	IRAN, ISLAMIC REPUBLIC OF	RWANDA
BELGIUM	IRAQ	SAINT LUCIA
BELIZE	IRELAND	SAINT VINCENT AND THE GRENADINES
BENIN	ISRAEL	SAMOA
BOLIVIA, PLURINATIONAL STATE OF	ITALY	SAN MARINO
BOSNIA AND HERZEGOVINA	JAMAICA	SAUDI ARABIA
BOTSWANA	JAPAN	SENEGAL
BRAZIL	JORDAN	SERBIA
BRUNEI DARUSSALAM	KAZAKHSTAN	SEYCHELLES
BULGARIA	KENYA	SIERRA LEONE
BURKINA FASO	KOREA, REPUBLIC OF	SINGAPORE
BURUNDI	KUWAIT	SLOVAKIA
CAMBODIA	KYRGYZSTAN	SLOVENIA
CAMEROON	LAO PEOPLE'S DEMOCRATIC REPUBLIC	SOUTH AFRICA
CANADA	LATVIA	SPAIN
CENTRAL AFRICAN REPUBLIC	LEBANON	SRI LANKA
CHAD	LESOTHO	SUDAN
CHILE	LIBERIA	SWEDEN
CHINA	LIBYA	SWITZERLAND
COLOMBIA	LIECHTENSTEIN	SYRIAN ARAB REPUBLIC
COMOROS	LITHUANIA	TAJIKISTAN
CONGO	LUXEMBOURG	THAILAND
COSTA RICA	MADAGASCAR	TOGO
CÔTE D'IVOIRE	MALAWI	TRINIDAD AND TOBAGO
CROATIA	MALAYSIA	TUNISIA
CUBA	MALI	TURKEY
CYPRUS	MALTA	TURKMENISTAN
CZECH REPUBLIC	MARSHALL ISLANDS	UGANDA
DEMOCRATIC REPUBLIC OF THE CONGO	MAURITANIA	UKRAINE
DENMARK	MAURITIUS	UNITED ARAB EMIRATES
DJIBOUTI	MEXICO	UNITED KINGDOM OF GREAT BRITAIN AND NORTHERN IRELAND
DOMINICA	MONACO	UNITED REPUBLIC OF TANZANIA
DOMINICAN REPUBLIC	MONGOLIA	UNITED STATES OF AMERICA
ECUADOR	MONTENEGRO	URUGUAY
EGYPT	MOROCCO	UZBEKISTAN
EL SALVADOR	MOZAMBIQUE	VANUATU
ERITREA	MYANMAR	VENEZUELA, BOLIVARIAN REPUBLIC OF
ESTONIA	NAMIBIA	VIET NAM
ESWATINI	NEPAL	YEMEN
ETHIOPIA	NETHERLANDS	ZAMBIA
FIJI	NEW ZEALAND	ZIMBABWE
FINLAND	NICARAGUA	
FRANCE	NIGER	
GABON	NIGERIA	
	NORTH MACEDONIA	
	NORWAY	

The Agency's Statute was approved on 23 October 1956 by the Conference on the Statute of the IAEA held at United Nations Headquarters, New York; it entered into force on 29 July 1957. The Headquarters of the Agency are situated in Vienna. Its principal objective is "to accelerate and enlarge the contribution of atomic energy to peace, health and prosperity throughout the world".

IAEA-TECDOC-1994

NUMERICAL BENCHMARKS FOR MULTIPHYSICS SIMULATION OF PRESSURIZED HEAVY WATER REACTOR TRANSIENTS

INTERNATIONAL ATOMIC ENERGY AGENCY
VIENNA, 2022

COPYRIGHT NOTICE

All IAEA scientific and technical publications are protected by the terms of the Universal Copyright Convention as adopted in 1952 (Berne) and as revised in 1972 (Paris). The copyright has since been extended by the World Intellectual Property Organization (Geneva) to include electronic and virtual intellectual property. Permission to use whole or parts of texts contained in IAEA publications in printed or electronic form must be obtained and is usually subject to royalty agreements. Proposals for non-commercial reproductions and translations are welcomed and considered on a case-by-case basis. Enquiries should be addressed to the IAEA Publishing Section at:

Marketing and Sales Unit, Publishing Section
International Atomic Energy Agency
Vienna International Centre
PO Box 100
1400 Vienna, Austria
fax: +43 1 26007 22529
tel.: +43 1 2600 22417
email: sales.publications@iaea.org
www.iaea.org/publications

For further information on this publication, please contact:

Nuclear Power Technology Development Section
International Atomic Energy Agency
Vienna International Centre
PO Box 100
1400 Vienna, Austria
Email: Official.Mail@iaea.org

© IAEA, 2022
Printed by the IAEA in Austria
March 2022

IAEA Library Cataloguing in Publication Data

Names: International Atomic Energy Agency.
Title: Numerical benchmarks for multiphysics simulation of pressurized heavy water reactor transients / International Atomic Energy Agency.
Description: Vienna : International Atomic Energy Agency, 2022. | Series: IAEA TECDOC series, ISSN 1011-4289 ; no. 1994 | Includes bibliographical references.
Identifiers: IAEAL 22-01487 | ISBN 978-92-0-108522-1 (paperback : alk. paper) | ISBN 978-92-0-108422-4 (pdf)
Subjects: LCSH: Pressurized water reactors. | CANDU reactors. | Simulation methods. | Transients (Dynamics).

FOREWORD

The IAEA organizes International Collaborative Standard Problems (ICSPs) to facilitate cooperation between Member States on activities related to advancing reactor technology, including the development, assessment and validation of computer codes for the design and safety analysis of nuclear power plants.

The objective of the ICSP described in this publication was to develop and facilitate open access to a set of standardized numerical test problems for selected postulated transients in pressurized heavy water reactors. These manufactured test problems are different from typical benchmark problems in that the specification is designed for a stylized model of a generic CANDU-6 pressurized heavy water reactor and a reference solution is not postulated. Nevertheless, the set of four standardized numerical test problems supports the development of simulation codes, methods and coupling frameworks.

This publication contains a description of the four numerical test problems, the multiphysics methodologies applied and the simulations carried out, an independent synthesis of the results, and the lessons learned from the exercise. The supplementary files available on-line provide benchmarks' input and output data.

The IAEA acknowledges the efforts and assistance provided by the contributors listed at the end of this publication. The IAEA officers responsible for this publication were M. Krause and T. Jevremovic of the Division of Nuclear Power.

EDITORIAL NOTE

This publication has been prepared from the original material as submitted by the contributors and has not been edited by the editorial staff of the IAEA. The views expressed remain the responsibility of the contributors and do not necessarily represent the views of the IAEA or its Member States.

Neither the IAEA nor its Member States assume any responsibility for consequences which may arise from the use of this publication. This publication does not address questions of responsibility, legal or otherwise, for acts or omissions on the part of any person.

The use of particular designations of countries or territories does not imply any judgement by the publisher, the IAEA, as to the legal status of such countries or territories, of their authorities and institutions or of the delimitation of their boundaries.

The mention of names of specific companies or products (whether or not indicated as registered) does not imply any intention to infringe proprietary rights, nor should it be construed as an endorsement or recommendation on the part of the IAEA.

The authors are responsible for having obtained the necessary permission for the IAEA to reproduce, translate or use material from sources already protected by copyrights.

The IAEA has no responsibility for the persistence or accuracy of URLs for external or third party Internet web sites referred to in this publication and does not guarantee that any content on such web sites is, or will remain, accurate or appropriate.

CONTENTS

1.	INTRODUCTION	1
1.1.	BACKGROUND	1
1.2.	OBJECTIVE	1
1.3.	SCOPE	1
1.4.	STRUCTURE	2
2.	NUMERICAL TEST PROBLEM DESCRIPTIONS	2
2.1.	OVERVIEW OF GENERIC PLANT MODEL	3
2.2.	STEADY STATE	4
2.3.	ADJUSTER ROD WITHDRAWAL	4
2.4.	COOLANT PUMP RUNDOWN	4
2.5.	INLET HEADER BREAK	4
3.	NUMERICAL TEST PROBLEM SPECIFICATIONS	4
3.1.	STEADY STATE NEUTRONICS MODEL SPECIFICATIONS	5
3.2.	GEOMETRY	5
3.2.1.	Distribution of fuel burnup in the core	9
3.2.2.	Local thermal hydraulics conditions	9
3.2.3.	Structure of the nuclear data library tabulation	11
3.2.4.	Control devices	14
3.3.	SPECIFICATIONS FOR TRANSPORT BASED NEUTRONICS SOLUTIONS	16
3.3.1.	Specification for transport-based neutronic codes	16
3.3.2.	Cross section generation	17
3.3.3.	Core transport model description	19
3.4.	STEADY STATE THERMAL HYDRAULICS MODEL SPECIFICATION	20
3.4.1.	Main simplifications	20
3.4.2.	System components and connections	22
3.4.3.	System models	24
3.5.	TRANSIENTS	26
3.5.1.	Initial conditions prior to transients	26
3.5.2.	Adjuster rod withdrawal	28
3.5.3.	Coolant pump rundown	28
3.5.4.	Reactor inlet header break	29
4.	PARTICIPANT MODEL DESCRIPTIONS	29
4.1.	COMISIÓN NACIONAL DE ENERGÍA ATÓMICA	29
4.1.1.	Codes and methods	29
4.1.2.	Special procedures for processing problem specification data	30
4.1.3.	Coupling framework	30
4.1.4.	Procedure for execution of coupled simulations	32
4.1.5.	Deviations from specifications	32
4.1.6.	Convergence criteria	32
4.2.	CANADIAN NUCLEAR LABORATORIES	33

4.2.1.	Codes and methods.....	33
4.2.2.	Special procedures for processing problem specification data....	34
4.2.3.	Coupling framework.....	34
4.2.4.	Procedure for execution of coupled simulations	36
4.2.5.	Deviations from specifications	37
4.3.	CANADIAN NUCLEAR SAFETY COMMISSION	37
4.3.1.	Codes and methods.....	37
4.3.2.	Special procedures for processing problem specification data....	38
4.3.3.	Deviations from specifications	38
4.4.	CANDU ENERGY INC. AND CANDU OWNER'S GROUP	39
4.4.1.	Codes and methods.....	39
4.4.2.	Special procedures for processing problem specification data....	40
4.4.3.	Coupling framework.....	41
4.4.4.	Procedure for execution of coupled simulations	42
4.4.5.	Deviations from specification.....	43
4.5.	MCMASTER UNIVERSITY	43
4.5.1.	Codes and methods.....	43
4.5.2.	Special procedures for processing problem specification data....	44
4.5.3.	Coupling framework.....	44
4.5.4.	Procedure for execution of coupled simulations	45
4.6.	BHABHA ATOMIC RESEARCH CENTRE.....	47
4.6.1.	Codes and methods.....	47
4.6.2.	Special procedure for processing problem specification data	48
4.6.3.	Coupling framework.....	48
4.6.4.	Procedure for execution of coupled simulation.....	51
4.6.5.	Deviations from specification.....	51
4.7.	KARACHI NUCLEAR POWER PLANT	52
4.7.1.	Codes and methods.....	52
4.7.2.	Special procedures for processing problem specification data....	52
4.7.3.	Coupling framework.....	53
4.7.4.	Procedure for execution of coupled simulations	54
4.7.5.	Deviations from specifications	54
4.8.	PAKISTAN INSTITUTE OF ENGINEERING AND APPLIED SCIENCES	56
4.8.1.	Codes and methods.....	56
4.8.2.	Special procedures for processing problem specification data....	56
4.8.3.	Coupling framework.....	57
4.8.4.	Procedure for execution of coupled simulations	58
4.8.5.	Deviations from specifications	58
4.9.	CERNAVODA NPP	58
4.9.1.	Codes and methods.....	58
4.9.2.	Special Procedures for Processing Problem Specification Data	58
4.9.3.	Coupling framework.....	59
4.9.4.	Procedure for execution of coupled simulations	59
4.9.5.	Deviations from specifications	60
4.10.	GEORGIA INSTITUTE OF TECHNOLOGY	60
4.10.1.	Codes and methods.....	60
4.10.2.	Special procedures for processing problem specification data....	61
4.10.3.	Deviations from specifications	61

5.	SIMULATION RESULTS.....	61
5.1.	ORGANIZATION OF RESULTS.....	61
5.2.	STEADY STATE.....	62
	5.2.1. Coupled converged case.....	62
	5.2.2. Standalone neutronics: diffusion versus transport.....	78
5.3.	ADJUSTER WITHDRAWAL TEST PROBLEM	79
	5.3.1. Standalone neutronics.....	79
	5.3.2. Standalone thermal hydraulics	83
	5.3.3. Coupled converged case.....	86
5.4.	PUMP TRIP TEST PROBLEM.....	96
	5.4.1. Standalone neutronics.....	96
	5.4.2. Standalone thermal hydraulics	98
	5.4.3. Coupled converged case.....	101
	5.4.4. Discussion.....	111
5.5.	INLET HEADER BREAK TEST PROBLEM	111
	5.5.1. Standalone neutronics.....	111
	5.5.2. Standalone thermal hydraulics	114
	5.5.3. Coupled converged case.....	118
6.	LESSONS LEARNED	136
6.1.	PROCESS OVERVIEW	136
6.2.	PREPARATION OF PROBLEM SPECIFICATIONS.....	138
6.3.	PROPAGATION OF CHANGES.....	138
6.4.	ORGANIZATIONAL COMMITMENT	139
6.5.	GENERATION OF RESULTS.....	139
	6.5.1. Issues arising from interpreting specifications	139
	6.5.2. Issues in interpretation of required output.....	139
	6.5.3. Examples of issues arising from different code capabilities	140
	APPENDIX I	141
	THERMALHYDRAULICS MATERIAL PROPERTIES	141
	APPENDIX II	149
	PUMP CHARACTERISTICS	149
	REFERENCES	151
	ANNEX I: SUPPLEMENTARY FILES – DATA	155
	ANNEX II: SUPPLEMENTARY FILES – PARTICIPANT INFORMATION.....	157
	ABBREVIATIONS	163
	CONTRIBUTORS TO DRAFTING AND REVIEW	165

1. INTRODUCTION

1.1.BACKGROUND

The IAEA organizes International Collaborative Standard Problems (ICSP) to facilitate the co-operation on advancing reactor technology related activities, including the development, assessment and validation of computer codes for design and safety analysis of nuclear power plants.

Several countries operating Pressurized Heavy Water Reactors (PHWR) have active research programmes to investigate multiphysics coupled simulations as part of code modernization initiatives. Computer codes used in coupled simulations of PHWR transients traditionally operate independently from one another, even though reactor phenomena are intrinsically coupled. The development of multiphysics reactor simulation code suites presents several technical challenges owing to the need to share data, control execution, and integrate prototype and legacy codes. The choice of a coupling algorithm involves several considerations such as applicability of the proposed multiphysics system to different reactor transients, the state of existing and prototype codes, and the required accuracy in the results of the analyses. These choices can be expected to impact overall simulation accuracy, computing time and resource demands, and the range of applicability of the system.

Currently, no benchmarks or manufactured test problems are available in the open literature for validating, verifying, or even comparing coupled methods for PHWR transients. Numerical test problems require less effort to develop and provide a means to test current and future transient simulation methods. Open access to a database of standardized numerical test problems, representative of PHWR transients, is a first step in filling the currently existing gap in this area.

To address this need, the IAEA initiated in 2016 an ICSP on Numerical Benchmarks for Multiphysics Simulation of Pressurized Heavy Water Reactors to facilitate the development of a set of standardized numerical test problems for selected postulated transients in PHWR. This ICSP is aligned with national programs and aimed at providing peer reviewed results, thus enhancing the confidence in participants' programmes.

1.2.OBJECTIVE

The objective of this ICSP is to develop and facilitate the open access to a set of standardized numerical test problems for selected postulated transients in PHWR. These manufactured test problems are different from the typical benchmark problems in that the specification is designed for a stylized model of a generic CANDU 6 PHWR and a reference solution is not postulated. Nevertheless, the proposed standardized numerical test problems support development of codes, methods, and coupling frameworks.

1.3. SCOPE

The scope of this publication comprises four numerical test problems for steady state and selected postulated transients including anticipated operational occurrences (items 2 and 3) and a design basis accident (item 4), namely:

1. Steady state;
2. Adjuster rod withdrawal;
3. Coolant pump rundown;
4. Inlet header break.

It is expected that differing participants' simulation codes and methods will lead to variation in the submitted solutions to the test problems. The objective of the peer review is to decompose these variances to gain insight on the impact of different simulation approaches to coupled simulation accuracy. It was not mandatory for the participants to execute all the cases in the specification.

Users of this publication include nuclear power plant (NPP) designers, regulators, technical support organizations, utilities, researchers, engineers and students interested in coupled multiphysics computer code development and applications for PHWRs.

1.4. STRUCTURE

This publication contains a description of four numerical test problems, the individual multiphysics simulations carried out, an independent synthesis of the results, and the lessons learned from the exercise. Section 2 describes the numerical test problems, while their detailed specifications are discussed in Section 3. The participants' codes, methods, and coupling framework are presented in Section 4. Section 5 summarizes the results provided by the participants. Section 6 concludes the report by presenting lessons learned in the exercise. Appendix I describes the thermal hydraulics material properties of interests, while Appendix II provides the characteristics of the primary circuit heat transport system cooling pumps.

A set of Excel spreadsheet files supports the numerical test problem specifications, as follows:

- *Core_specs.xlsx*: neutronics core geometry data, burnup distribution and data library;
- *Device_specs.xlsx*: neutronics data/geometry for reactivity control devices;
- *Transport_neutronics.xlsx*: burnup distribution and data library for use with transport neutronics codes;
- *TH_network_specs.xlsx*: network thermal hydraulics geometry and data.

In addition, two data files are provided to support the standalone neutronics and standalone thermal hydraulics simulations of the test problems:

- *SA_neutronics.xlsx*: neutronics response for use with standalone thermal hydraulics simulations, and
- *SA_thermalhydraulics.xlsx*: the corresponding thermal hydraulics response data for use with standalone neutronics simulations.

These files are briefly described in Annex I and contained in the supplementary electronic files to this publication. Annex II provides details on participants.

2. NUMERICAL TEST PROBLEM DESCRIPTIONS

All numerical test problems are based on a common configuration of a stylized PHWR with specified physical parameters. The problems are limited to representing core physics, core thermal hydraulics, and a very simplified ex-core thermal hydraulic network, so that they are not specific to a different PHWR design. Brief descriptions of the proposed numerical test problems are given below. Each problem starts from an initial reactor state and is characterized by key reactor events in time, or as a function of calculated system parameters. Key output parameters will be made available for comparison. Except for the initial reactor state and

boundary conditions, the choices of data, modelling parameters, and methods used to execute the simulation are left to the participants.

The scenarios are inspired by safety analyses commonly carried out for PHWR type reactors. However, these numerical test problems are manufactured and designed to test and compare different simulation approaches. The specifications highlight coupled phenomena, as opposed to providing fidelity to realistic postulated events in a nuclear power station.

Physics and thermal hydraulics models will represent the CANDU6 type heavy water reactor [1][2], fuelled with 37 element natural uranium fuel bundles. The fuel will be distributed to achieve an ‘equilibrium’ critical core, with nominal operating parameters.

2.1. OVERVIEW OF GENERIC PLANT MODEL

The thermal hydraulic network has two loops arranged in two figure of eight configurations, as shown in Fig. 1. As a result, there are four core passes, two passes per loop. There is a total of eight headers, consisting of two inlet and two outlet headers for each loop. The outlet headers in each loop are connected via the interconnect lines. The flow is driven by two primary heat transport system pumps per loop and heat is extracted by two steam generators per loop. The reactor core consists of 380 fuel channels. The participants will have flexibility in grouping channels in the core to reduce the size of the problem. For example, in typical safety scenarios it was shown that seven average channels groups per pass is sufficient to compute key output parameters with acceptable level of accuracy.

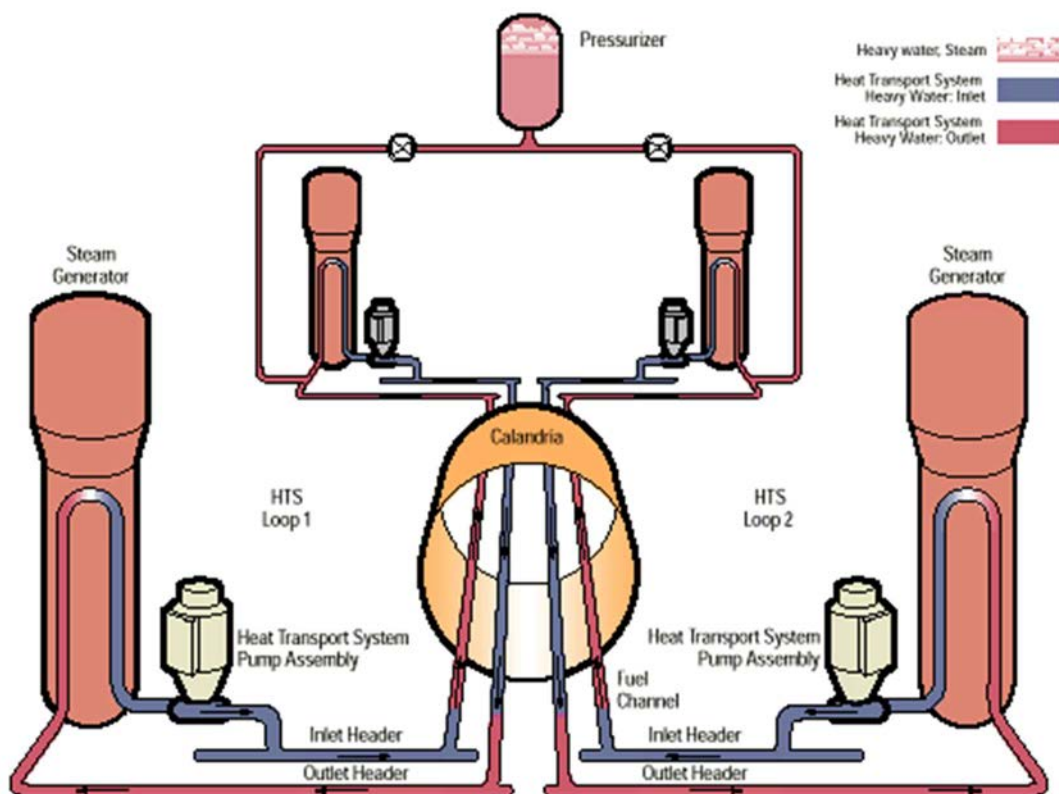


FIG. 1. Schematics of the two of eight thermal hydraulic loops in a pressure tube HWR (reproduced courtesy of Canadian Nuclear Laboratories (CNL)).

In addition to the fuel channels, the heat transport system consists of inlet and outlet feeders also grouped to match the core channel groupings, inlet and outlet headers, risers, boiler

inlet/outlet plenums, primary U-tubes in the steam generators, primary heat transport system pumps and a pressurizer. For the test problems, feed and bleed systems as well as the emergency core cooling (ECC) piping will be excluded, since none of the coupled scenarios proposed will advance to the point of ECC injection. Since feed & bleed functions are achieved by the pressurizer control system these systems will also not be required. To further simplify the input, the secondary side conditions can be entered as a boundary condition, with variable solid-solid heat transfer and boiler coolant temperatures. To achieve a steady state at the desired operating conditions, the participants can adjust the secondary side boundary conditions to match the power input in the core. The participants will also need to implement required control systems to achieve the specified operating conditions, such as the pressurizer controls.

2.2. STEADY STATE

This problem mainly serves to define the converged initial conditions prior to the postulated transient events. The problem has to be solved using the coupled code system.

2.3. ADJUSTER ROD WITHDRAWAL

In this transient it is postulated that two adjuster rods are withdrawn. This represents a reactor physics driven overpower scenario, driving a thermal hydraulics response. A power increase with a spatial tilt is expected within the core leading to an increase in the fuel sheath temperature and potential for intermittent dry-out. The reactor regulating system and shutdown systems are not credited in the simulations. The main quantity of interest is the distribution of channels that exceed the critical channel power.

2.4. COOLANT PUMP RUNDOWN

In this transient, a rundown in heat transport system pump number two is postulated. In this thermal hydraulic driven under cooling scenario, the imbalance between heat removal and heat generation will lead to coolant voiding in the core and positive reactivity insertion. The reactor regulating system and shutdown systems are not credited in the simulations. The main quantity of interest is the distribution of channels that exceed the critical channel power.

2.5. INLET HEADER BREAK

In this transient, a large break in reactor inlet header two is postulated. In this thermal hydraulic driven scenario, depressurization leads to coolant voiding and positive reactivity insertion. The reactor regulating systems is not credited and simulations are performed with and without action of the shutdown systems. The main quantity of interest is the maximum bundle enthalpy.

3. NUMERICAL TEST PROBLEM SPECIFICATIONS

The geometrical description of the reactor physics data, main thermal hydraulic components from the primary heat transport circuit are included in specific Excel files. The *Core_specs.xlsx* file includes the main reactor physics data. Reactor physics device specifications are presented in the *Device_specs.xlsx* while the thermal hydraulic data are included in the *TH_Network_specs.xlsx* file. Each Excel file includes more spreadsheets to cover all types of information required. Additional data are provided in the *transport_neutronics.xlsx* file, for use with transport neutronics codes. In addition, Appendix I provides required solid material

properties and Appendix II the needed pump characteristics, for use by participants in the most consistent manner possible, considering their code and model limitations.

3.1. STEADY STATE NEUTRONICS MODEL SPECIFICATIONS

In this Section the reactor core geometry, the reactor control devices, the distribution of fuel burnup, and the nuclear data library are described. Table 1 presents a summary of key parameters for the core. The nominal thermal power output is 2,000 MW. The ratio of the core fission power to thermal power is fixed to a value of 0.955. This is a representative value for PHWR technology using natural uranium fuel [3][4]. The core is composed of 380 fuel channels, each containing twelve 37 element fuel bundles made of natural uranium dioxide. The core is cooled and moderated using heavy water. The model features highly simplified liquid zone controller, shut-off rods and adjuster rods. Mechanical control absorbers, emergency liquid neutron absorber injection distribution tubes, and other structural components are not included in this model. Ageing effects, such as pressure tube creep and sag, are not included.

TABLE 1. REACTOR CORE SUMMARY DESCRIPTION

Parameter	Value / Type	Unit
Lattice pitch (square)	28.575	cm
Length of bundle	49.53	cm
Core length	594.36	cm
Core radius	379.7	cm
Channel count	380	
Fuel bundles per channel	12	
Core thermal power	2,000	MW _{th}
Thermal to fission power ratio	0.955	
Fuel type	Natural uranium	
Fuel bundle type	37 elements	
Heavy water moderator purity	99.9935	wt% D ₂ O
Heavy water coolant purity	98.39	wt% D ₂ O
# Liquid zone controller	14	
# Shut-off rods	28	
# Adjuster rods	21	
# Mechanical control absorbers	0	

3.2. GEOMETRY

Figure 2 illustrates the basic geometry for the numerical test problems in the *XY* plane. Three regions are represented: fuel, reflector, and out of core. The fuel and reflector regions occupy an approximately cylindrical region bounded by the nominal calandria radius of 379.7 cm. Lattice cells are arranged on a Cartesian grid with a lattice pitch of 28.575 cm and a bundle length of 49.53 cm. The origin of the coordinate system is marked with a circle in the top left corner of Fig. 2. The orientation of the *X*, *Y*, and *Z* axes is also indicated. Mesh planes and device coordinates are based on this coordinate system. The fuel and reflector regions together span a space of 26×26 lattice cells in the *XY* plane and 12 bundle lengths in the *Z* direction. Fuel channels are labelled according to conventional row and column indices, with row ‘I’ skipped. The calandria vessel and end shields are not explicitly represented. Unlike a CANDU 6 PHWR core, this numerical test problem core does not feature a ‘notch’ near the end-shield region.

While there is a heavy water radial reflector in the numerical test problem, there is no axial reflector.

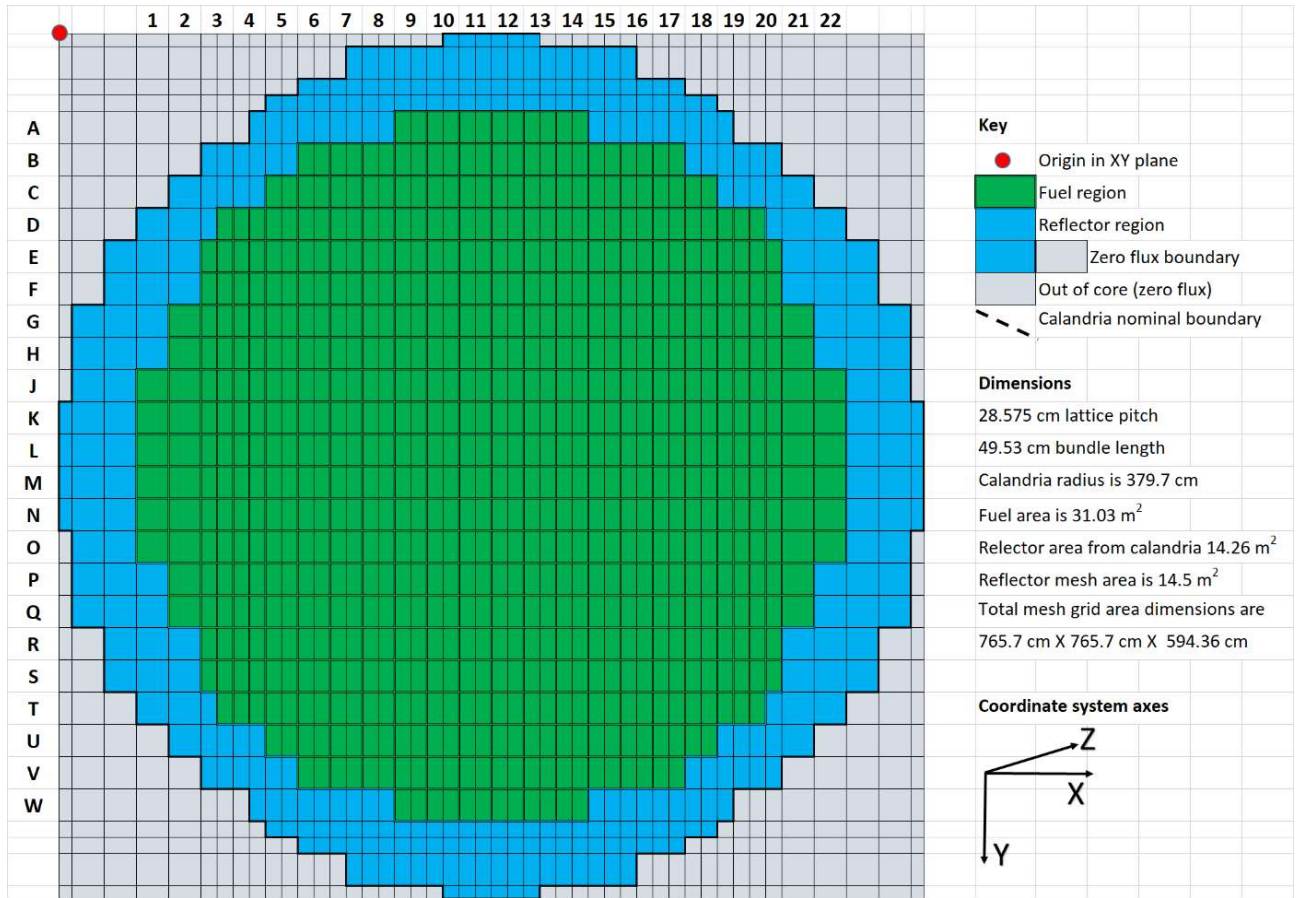


FIG. 2. Layout of fuel, reflector, and out of core regions.

The indicated mesh lines are based on the values of Table 2. The calandria boundary is also presented in Fig. 2. As can be seen, there are regions where the reflector region exceeds the boundary, and other regions where the reverse holds. This inherent inconsistency between a cylindrical boundary and the Cartesian mesh was resolved by adjusting the outer mesh planes to approximately conserve the overall reflector cross sectional area. Given a calandria radius of 379.7 cm and subtracting the area occupied by the 380 fuel channels, the reflector cross sectional area is 14.26 m². The mesh representation and assignment of reflector regions presented in Fig. 2 yields an effective reflector cross sectional area of 14.5 m².

The out of core region (as shown in Fig. 2), are prescribed to have a zero neutron flux. Participants are free to implement this either by imposing a zero flux boundary on the outer Cartesian edges of the reflector cells (indicated by solid black line), or by imposing a zero extrapolation distance on the circular boundary which approximates the calandria. Differences between both approaches are small, as the overall reflector volume is approximately the same and the flux magnitudes are low at the core edges.

Table 2 presents a simplified computational mesh structure for the problem. Core neutron diffusion codes require that a mesh be defined over the problem domain to support a numerical solution. Reactivity control devices and in-core structural components are modeled by perturbing the homogenized macroscopic neutron diffusion cross sections over a specified volume of the core. The affected volumes are defined using parallelepipeds using the coordinates of two opposite corners. Owing to the placement of these devices, mesh structures generally do not

feature regular intervals. Additional X and Z axis mesh planes are chosen to coincide with the bounding planes of the devices. Additional Y axis mesh planes may be added to facilitate the implementation of device movement for transient cases.

TABLE 2. SIMPLIFIED SET OF MESH PLANE COORDINATES

Plane position (cm)				Plane spacing (cm)			
X	X (cont.)	Y	Z	ΔX	ΔX (cont.)	ΔY	ΔZ
0.0000		0.0000	0.0000	N/A		N/A	N/A
11.3750	497.1500	11.3750	24.7650	11.3750	14.2875	11.3750	24.7650
39.9500	511.4375	39.9500	49.5300	28.5750	14.2875	28.5750	24.7650
68.5250	525.7250	54.2375	74.2950	28.5750	14.2875	14.2875	24.7650
97.1000	540.0125	68.5250	99.0600	28.5750	14.2875	14.2875	24.7650
125.6750	554.3000	97.1000	123.8250	28.5750	14.2875	28.5750	24.7650
139.9625	568.5875	125.6750	148.5900	14.2875	14.2875	28.5750	24.7650
154.2500	582.8750	154.2500	173.3550	14.2875	14.2875	28.5750	24.7650
168.5375	597.1625	182.8250	198.1200	14.2875	14.2875	28.5750	24.7650
182.8250	611.4500	211.4000	222.8850	14.2875	14.2875	28.5750	24.7650
197.1125	625.7375	239.9750	235.2675	14.2875	14.2875	28.5750	12.3825
211.4000	640.0250	268.5500	247.6500	14.2875	14.2875	28.5750	12.3825
225.6875	668.6000	297.1250	260.0325	14.2875	28.5750	28.5750	12.3825
239.9750	697.1750	325.7000	272.4150	14.2875	28.5750	28.5750	12.3825
254.2625	725.7500	354.2750	284.7975	14.2875	28.5750	28.5750	12.3825
268.5500	754.3250	382.8500	297.1800	14.2875	28.5750	28.5750	12.3825
282.8375	765.7000	411.4250	309.5625	14.2875	11.3750	28.5750	12.3825
297.1250		440.0000	321.9450	14.2875		28.5750	12.3825
311.4125		468.5750	334.3275	14.2875		28.5750	12.3825
325.7000		497.1500	346.7100	14.2875		28.5750	12.3825
339.9875		525.7250	359.0925	14.2875		28.5750	12.3825
354.2750		554.3000	371.4750	14.2875		28.5750	12.3825
368.5625		582.8750	396.2400	14.2875		28.5750	24.7650
382.8500		611.4500	421.0050	14.2875		28.5750	24.7650
397.1375		640.0250	445.7700	14.2875		28.5750	24.7650
411.4250		668.6000	470.5350	14.2875		28.5750	24.7650
425.7125		697.1750	495.3000	14.2875		28.5750	24.7650
440.0000		711.4625	520.0650	14.2875		14.2875	24.7650
454.2875		725.7500	544.8300	14.2875		14.2875	24.7650
468.5750		754.3250	569.5950	14.2875		28.5750	24.7650
482.8625		765.7000	594.3600	14.2875		11.3750	24.7650

An additional consideration is the need to model control device movements in transients. Numerically, it is preferred if these volumes can be fully defined in terms of the solution mesh. As can be seen in Table 2 and also in Fig. 2 the computational mesh lines are usually aligned

with the positions of the lattice cells. Figures 3 and 4 show the mesh lines in XY and ZY planes, respectively.

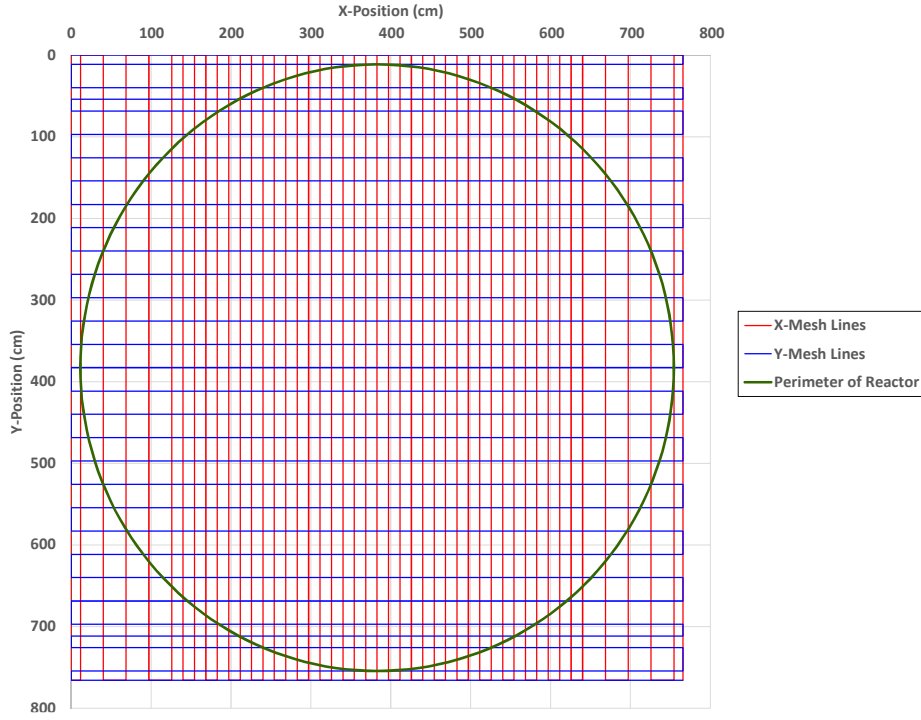


FIG. 3. Illustration of mesh lines in XY plane.

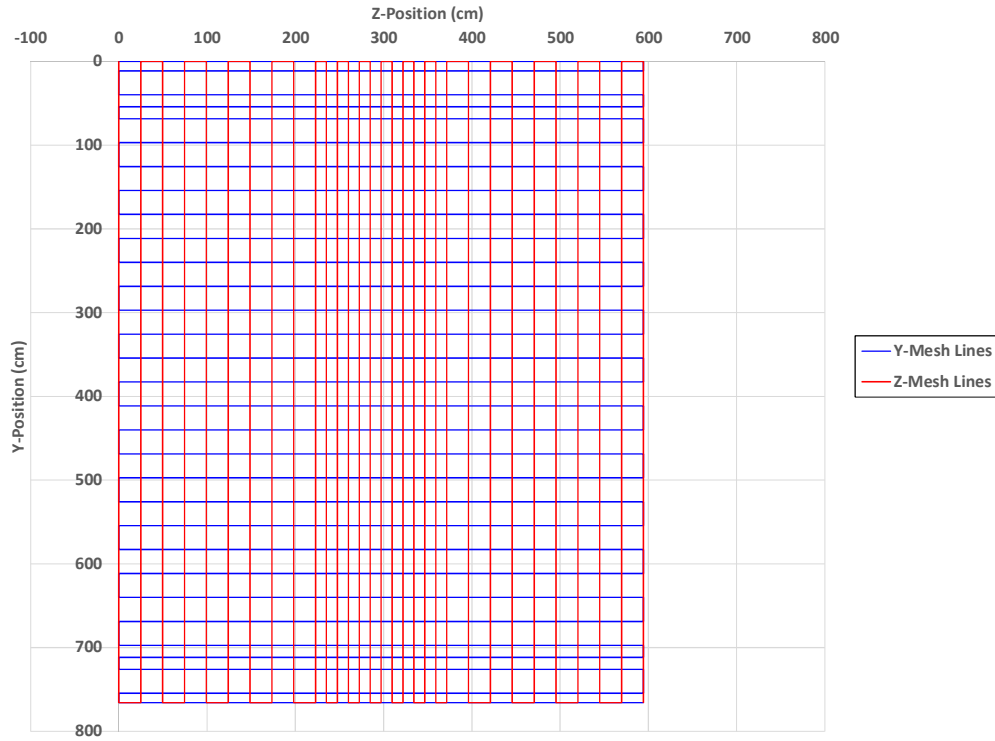


FIG. 4. Illustration of mesh lines in ZY plane.

In some cases, a lattice cell is divided in half, or into quarters by a computational mesh line for finer solution of the neutron flux distribution in either the XY plane or the Z direction. For

example, many of mesh cells in the XY plane are half the size of the lattice pitch, $\Delta y, \Delta x = 28.575 \text{ cm} / 2 = 14.2875 \text{ cm}$, and a number of the mesh cells in the Z direction are one quarter of the bundle length, $\Delta z = 49.53 \text{ cm} / 4 = 12.3825 \text{ cm}$. If reactor core physics codes using finite difference methods to solve the multi-group neutron diffusion equation are being used, then it may be desired by the user to define an even smaller computational mesh size to obtain more accurate estimates of the flux distributions. It is anticipated that participants may need to increase the number of mesh lines in the Y direction with smaller sized computational meshes planes in order to model the vertical movement of the shutoff rods in transient cases and their impact on the core physics behaviour more accurately. Participants are requested to report any significant deviations from the computational mesh presented in Table 2.

3.2.1. Distribution of fuel burnup in the core

In PHWRs, reactivity control is maintained by the combined use of on-line refuelling and reactivity device movement. With the exception of transient fission products, the fuel composition is therefore assumed to be fixed for the duration of each transient. The model features 4,560 ($380 \text{ channels} \times 12 \text{ bundles per channel}$) individual fuel bundle locations in the core. Each is assigned a burnup value, in MW days per tones (MWd/t) of initial heavy elements.

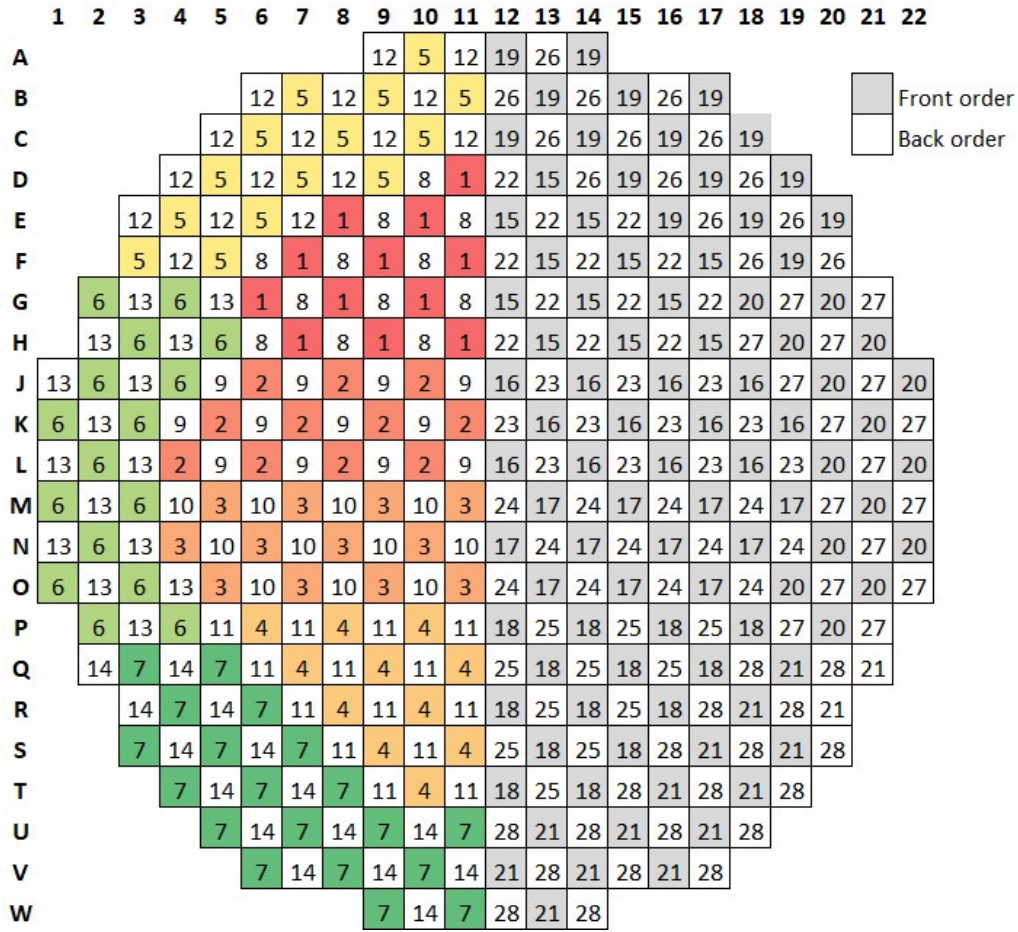
Detailed burnup assignments, by lattice site, are listed in the burnup data worksheet in the Excel file *Core_specs.xlsx*. Each lattice site is assigned a burnup value. Row and column indices follow Fig. 2. The position label refers to the ordering of the fuel bundle within a fuel channel, increasing with the Z axis. A conversion table between bundle irradiation (neutron flux \times time) and burnup is provided for reference.

This prescribed distribution originates from a snapshot of core-follow simulations based on a more detailed model. In such simulations, the core burnup evolution was tracked while satisfying different constraints, such as flux distribution, refuelling scheme, and exit irradiation targets. That model included additional structural elements at the bottom of the core, and its liquid zone controllers were set at different fill levels than what is currently specified (50% fill). Overall, the refuelling and zone levels were adjusted to compensate additional parasitic absorption at the bottom of the core. In the present work, the simplified model does not include these additional components, and the liquid zone controller fill levels are different. The net effect of this variations is that a vertical flux tilt should be expected when evaluating the channel power distribution for the steady state.

3.2.2. Local thermal hydraulics conditions

The thermal hydraulics network is based on a double figure of eight pattern, as illustrated in Fig. 1. The reactor physics simulations require that coolant temperature (T_{cool}) and density (ρ_{cool}) as well as fuel temperatures (T_{fuel}), be provided for each lattice site within the core. However, the thermal hydraulics model provides data in an upstream-to-downstream order, following different flow channels. A mapping is needed to translate the one-dimensional data from thermal hydraulics to the three dimensional data representation required by the reactor physics code. This mapping is based on two considerations. Firstly, each fuel channel is assigned to one of several thermal hydraulics channel groups. This is because the thermal hydraulics model does not represent flow in each fuel channel explicitly. Instead, the flows from multiple channels are treated together. The second consideration is the flow direction. The inlet side of the channel is cooler than the outlet, and hence the coolant density decreases over the length of the channel. In PHWR reactors, the double figure of eight is implemented using alternating flow directions in the core. Figure 5 presents the mapping of thermal hydraulic

channel groups to fuel channels, with flow directions indicated. Twenty eight (28) thermal hydraulic channel groups are used in this problem. Thermal hydraulic channel groups 1–14 are used to represent the left hand side of the *XY* plane, while channel groups 15–28 represent the right hand side in the *XY* plane.



Thermal hydraulic channel groups 1 to 7, in forward order, on left side, are colour-coded.

FIG. 5. Thermal hydraulic channel groups in the PHWR core.

The initial values of coolant density, temperature, and fuel temperature are specified in the ‘TH data’ worksheet in the Excel file *Core_specs.xlsx*. Sample coolant density data are presented in Table 3. Each thermal hydraulics channel group is identified and assigned a data order. The tabulation assumes that data will be provided from the system thermal hydraulics code in an upstream-to-downstream order. For channels using the front-to-back data order, the flow direction is assumed to be parallel along the *Z*-axis, as illustrated in Fig. 5. The first thermal hydraulics data entry (node 1) therefore corresponds to the first core plane.

The correspondence of thermal hydraulics data order to core planes is presented in Table 4. To illustrate, fuel channel D11 (see Fig. 5) is associated with thermal hydraulics channel group 1, which has a front-to-back data order. The coolant density of the first bundle, located in core plane 1, is 0.777 g/cm³. The second bundle is one lattice pitch deeper in the core (core plane #2) and the coolant flows in the same direction. The coolant density is reduced to 0.772 g/cm³. Conversely, fuel channel W28 is associated to thermal hydraulic channel group 28. This channel has a back-to-front data order, indicating that the flow direction is reversed. Bundles located in core planes 1 and 2 are now at the downstream end of the flow, and the corresponding coolant density values are given by the data at nodes 11 and 12.

Fuel and coolant temperatures, as well as coolant densities, are provided as the volume average at each lattice cell point. The liquid temperatures are mass-weighted, as the reactor physics code treat the coolant as a single phase fluid. The fuel temperature provided should represent the average over all 37 element fuel elements within a given fuel bundle assembly.

TABLE 3. AMPLE THERMAL HYDRAULICS INITIAL CONDITIONS AT EACH LATTICE SITE IN THE CORE

Thermal hydraulics channel group	Data order	Coolant density (g/cm ³) in node					
		1	2	...	11	12	
1	Front	0.777	0.772	...	0.673	0.656	
2	Front	0.777	0.772	...	0.673	0.655	
...	
22	Back	0.778	0.773	...	0.619	0.583	
23	Back	0.778	0.773	...	0.652	0.622	
24	Back	0.778	0.773	...	0.667	0.652	

TABLE 4. CORRESPONDENCE TABLE OF THERMAL HYDRAULICS DATA ORDER AND CORE PLANES

Thermal hydraulics data node	Core plane	
	Front	Back
1	1	12
2	2	11
3	3	10
4	4	9
5	5	8
6	6	7
7	7	6
8	8	5
9	9	4
10	10	3
11	11	2
12	12	1

3.2.3. Structure of the nuclear data library tabulation

The Canadian Nuclear Safety Commission has agreed to share a two group nuclear data library to facilitate this ICSP; [2]. The contents of this library are as follows:

- Macroscopic two-group cross sections at reference conditions (T_{fuel} , T_{cool} , ρ_{cool}); specified at 36 burnup nodes;
- Expansion coefficients to evaluate the macroscopic cross sections as coolant density, temperature, and fuel temperature deviate from the reference conditions;
- Neutron kinetic parameters;
- Microscopic cross sections, fission yields, and decay rates for transient fission products.

The library *does not* include decay heat data. If participants require such data for their simulation codes, they should set these data to zero, or as small a numerical value as possible.

For the purpose of this ICSP, the data would only be relevant after the shut-off rods have dropped, at which point the problem effectively ceases to become a coupled exercise.

3.2.3.1. Macroscopic cross section model

The library contains data for the reflector and fuel regions (regions 1 and 2 in Fig. 2). Data are available for the fast (group 1) and thermal (group 2) energy groups. In fuelled regions, data for the following cell-averaged homogenized macroscopic cross sections are available:

- Transport (SIGT), in cm^{-1} ;
- Absorption (SIGA), in cm^{-1} ;
- Production (SIGNF), cm^{-1} , the product of the fission cross section and $\bar{\nu}$;
- Kappa-fission (SIGKF), in $\text{MeV} \cdot \text{cm}^{-1}$, the product of the fission cross section and the average energy release per fission event;
- Group 1 to group 2 scattering (SIG12), in cm^{-1} ;
- Group 2 to group 1 scattering (SIG21), in cm^{-1} ;
- Assembly discontinuity factors on XY plane faces (N, E, S, W), dimensionless;
- Assembly discontinuity factors on bundle end planes (Up, Bottom), dimensionless.

The macroscopic transport and absorption cross sections (SIGT and SIGA) exclude the contribution arising from Xe-135 and Sm-149; see Section 3.2.3.2 for further details.

Assembly discontinuity factors (ADFs) are applied to each surface plane of a lattice cell, without regard to the position of the lattice cell in the core. Of the six surfaces of a lattice cell, two are perpendicular to the core Z axis. The ADFs for these bundle-end planes are set to unity for all values of burnup. The ADFs applied to the remaining lattice cell surface were made identical on symmetry grounds and have burnup dependent values. These factors only used by core diffusion codes that implement nodal methods. Users of finite difference reactor physics core diffusion codes may ignore these data.

All macroscopic cross sections in the fuelled region are represented using a quadratic expansion formula in three variables:

$$\Sigma = \Sigma_0 + a(\sqrt{T_f} - \sqrt{T_{f0}}) + b(\sqrt{T_f} - \sqrt{T_{f0}})^2 + c(T_c - T_{c0}) + d(T_c - T_{c0})^2 + e(\rho_c - \rho_{c0}) + f(\rho_c - \rho_{c0})^2 \quad (1)$$

where:

- | | |
|------------|--|
| Σ_0 | macroscopic cross section of interest at the reference conditions, in cm^{-1} ; |
| T_f | fuel temperature, in $^{\circ}\text{C}$; |
| T_c | coolant temperature, in $^{\circ}\text{C}$; |
| ρ_c | coolant density, in g/cm^3 ; |
| a | linear root fuel temperature effect term; |
| b | quadratic root fuel temperature effect term; |
| c | linear coolant temperature effect term; |
| d | quadratic coolant temperature effect term; |
| e | linear coolant density effect term; |
| f | quadratic coolant density effect term. |

All temperatures are in $^{\circ}\text{C}$, and all densities in g/cm^3 . The macroscopic cross section at the reference conditions and all expansion coefficients are tabulated over 36 burnup values.

Reference conditions for coolant density, coolant temperature and fuel temperature, and presented in Table 5.

TABLE 5. REFERENCE CONDITIONS FOR CROSS SECTION EVALUATIONS

Parameter	Value	Unit
Coolant temperature	288.5	°C
Fuel temperature	687	°C
Coolant density	0.80623	g/cm ³
Coolant purity	98.39	wt% D ₂ O
Moderator purity	99.935	wt% D ₂ O
Moderator temperature	68.0	°C
Moderator Boron	0.1	ppm B

Data for the reflector region are limited to a set of reference cross sections applicable to all values of burnup and are independent of the fuel and coolant variables. Both neutron production and kappa-fission cross section data are set to zero. The data are tabulated in the ‘Cross sections’ worksheet in the Excel spreadsheet file *Core_specs.xlsx*. The first column may take one of the values shown in Table 6.

TABLE 6. DATA TYPES FOR CROSS SECTION FORMULAE

Data type	Unit	Meaning
REF	cm ⁻¹	Reference cross section at nominal conditions
CD1	cm ² /g	Linear term to change in coolant density
CD2	cm ⁵ /g ²	Quadratic term to change in coolant density
CT1	cm ⁻¹ /°C	Linear term to change in coolant density
CT2	cm ⁻¹ /°C ²	Quadratic term to change in coolant temperature
FTSQRT1	cm ⁻¹ /°C ^{1/2}	Linear term to change in coolant temperature
FTSQRT2	cm ⁻¹ /°C	Quadratic term to change in square root of fuel temperature

The first column serves to specify the type of data; the second, the cell type (fuel or reflector); the third, the energy group; and the fourth, the burnup node. The remaining columns hold the data. Data entries labelled as ‘NA’ indicate ‘Not Applicable’. For example, in energy group 1, no relevant data can be applied for scattering from groups 2 to group 1. In addition to the macroscopic cross sections, the prompt fission spectrum is required to calculate the group 1 and group 2 source terms in the neutron diffusion equation. This value is burnup-dependent in principle. In this library, these data are set to unity (1.0) for group 1, and zero (0.0) for group 2, indicating all fission neutrons are assumed to be created in the fast group. These data are listed in the ‘Prompt fission spectrum’ worksheet in the Excel spreadsheet *Core_specs.xlsx* for completeness, and to facilitate later revisions.

3.2.3.2. Macroscopic transient fission product data

The nuclear data library includes data required to model the impact of Xe-135 and Sm-149 on reactor transients. Reactor physics simulation codes typically update the local absorption cross sections to account for the effects of these fission products. The nuclear data library includes:

- Reference microscopic absorption cross sections and related expansion coefficients for Xe-135 and Sm-149;
- Fission product yield data for I-135, Xe-135, and Pm-149;
- Decay rates for I-135, Xe-135, and Pm-149.

Cross section coefficient and yield data are provided over the same 36 burnup nodes as is used for macroscopic cell averaged neutron cross sections. Microscopic cross sections and coefficients are provided for both the fast and thermal group and are provided in units of barns. Yield data is limited to the thermal group.

Microscopic cross sections and coefficients data for Xe-135 and Sm-149 are listed in the SIGA_Xe-135 and SIGA_Sm-149 worksheet tabs of the Excel spreadsheet file *Core_specs.xlsx*, respectively. Yield and decay rate data are listed in worksheets TranFissYields, and TranFissDecayRates respectively. In computing the effective absorption rates for Xe-135 and Sm-149, the cell-average flux is applied. Some codes make use of an F-factor, representing the ratio of the fuel average flux to the cell average flux. Representative values for the thermal and fast F-factors at reference conditions are 0.52 and 1.74 respectively¹. The presence of devices may be assumed not to change the F-factor.

3.2.3.3. Kinetics parameters

Solution of the time-dependent neutron diffusion equation requires that additional kinetics data be available. Kinetics data is provided using six precursor groups to model the impact of delayed neutrons. The library includes the following:

- Decay rates for the delayed neutron precursor groups;
- The delayed neutron fractions, including photo-neutrons;
- The two-group mean neutron speeds;
- The delayed neutron fission spectrum.

Decay rates of the delayed neutron precursors are burnup independent (Table 7). The delayed neutron fission spectrum assumes all neutrons are born in the fast group, for all values of burnup. The remaining data is burnup dependent and provided over the common 36-node grid.

TABLE 7. DECAY RATES OF DELAYED NEUTRON PRECURSOR GROUPS

Precursor group	Decay (1/s)
1	0.0136
2	0.0313
3	0.1233
4	0.3237
5	0.9059
6	3.0480

In file *Core_specs.xlsx*, delayed neutron fractions are stored in worksheet ‘Beta-eff’, while neutron speeds are listed in worksheet as Neutron speeds.

3.2.4. Control devices

In core reactor physics neutron diffusion codes, control devices and several in-core components are typically represented by means of increments to the cross sections applied over a range of mesh cells intersecting the device volume. In the present work, all structural materials such as

¹ R. Farkas (SNC-Lavalin), private communication.

guide tubes, anchors, and flux detector assemblies have been eliminated from the model. Likewise, the mechanical control absorbers used for longer term reactivity control were removed, as are the structures related to the liquid poison safety shutdown system. Only the following incremental devices are defined:

- 28 shut-off rods;
- 14 liquid zone controllers;
- 21 adjuster rods.

All device locations are consistent with CANDU 6 type PHWRs, with minor modifications made to align X and Y planes with typical mesh boundaries. Shut-off rods are initially located out of the core and will be inserted using a time dependent position profile during the simulated transients to shut down the reactor. Liquid zone controllers are assumed to be 50% filled, and adjuster rods are in their nominal position, where the centre of the devices intersects the Y -plane at the core centre. In a CANDU 6 core, there are three types of adjuster rods, three types of liquid zone controllers, and one type of shut-off rod. The liquid zone controllers feature both air- and water-filled fractions. As a result, ten different incremental cross sections tables are defined:

- Three for the different types of adjuster rods: ADJ01, ADJ02, and ADJ03;
- One for the shutoff rods: shut-off rods;
- Three for the water-filled portion of the liquid zone controllers: LZCR01, LZCR02, LZCR03;
- Three for the air-filled portion of the liquid zone controllers: ZCAIR01, ZCAIR02, ZCAIR03.

Incremental devices are defined as follows:

- A unique identifier to name the device;
- The name of the incremental cross section table used to represent the device;
- The three dimensional coordinates of the opposing corners of a regular parallelepiped, which are labelled $(X1, Y1, Z1)$ and $(X2, Y2, Z2)$ respectively. However, in the listing describing the devices, the data is listed by the three pairs of coordinates, $X1, X2$; $Y1, Y2$; and $Z1, Z2$.

In the present model, 77 individual devices are defined using 10 incremental cross section tables:

- 21 adjuster rods;
- 14 water-filled liquid zone controller segments;
- 14 air-filled liquid zone controller segments;
- 28 shutoff rods.

Data for device positions and incremental cross sections are listed in the Excel spreadsheet file *Device_specs.xlsx*. For each device, two three-dimensional coordinates are listed to define a regular parallelepiped representing the volume of space occupied by the device. Device coordinates are listed in the Positions tab, while the cross sections are listed in the Incremental_XS worksheet. As discussed above, the pairs of X , Y , and Z values that define the position and extent of the parallelepiped that represents the control device are shown in the

Excel file, as $X1$, $X2$; $Y1$, $Y2$; and $Z1$, $Z2$. The following incremental cross section data are available:

- Fast and thermal transport;
- Fast and thermal absorption;
- Group 1 to group 2 scatter;
- Group 2 to group 1 scatter;
- Fast and thermal nu-fission;
- All other parameters, such as fast/thermal k_{app} -fission, fast ADF left, fast ADF right, thermal ADF left, and thermal ADF right, are set to zero. Thus, use of the reactivity devices are assumed to have no impact on these other parameters.

In the present Specification, the liquid zone controller fill levels are uniformly fixed at the 50% fill level. Each of the 14 liquid zone controller devices specified in the Positions worksheet of the *Device_specs.xlsx* Excel data file is represented by two devices sharing identical coordinates. One device, of incremental cross section type ZCAIR, represents the incremental cross sections for a liquid zone controller emptied of water (fill level of 0). The other device, of incremental cross section type LZCR, represents the incremental cross sections when the fill level is 100%. For each liquid zone controller, participants are instructed to apply the ZCAIR incremental cross sections over the entire volume defined by the device coordinates. Participants should then add the LZCR (water-filled) incremental cross sections based on the water fill level.

3.3. SPECIFICATIONS FOR TRANSPORT BASED NEUTRONICS SOLUTIONS

In this section, specifications are provided to implement a stylized model of a full core CANDU reactor suitable for use with transport neutronics codes. This specification differs from the main specification in the following points:

- Burnup distribution was simplified to eight individual values;
- Cross section data are provided for the nominal and voided conditions only;
- Adjuster rods are the only reactivity control devices which are implemented.

The specification published in reference [1] was expanded to a full core with the burnup distribution given in the Burnup table worksheet of the *transport_neutronics.xlsx* file. The 2-group region-wise macroscopic cross section library developed in reference [1] are provided in the cross sections worksheet of this same file. They are applicable for deterministic, stochastic, and hybrid transport calculations.

3.3.1. Specification for transport-based neutronic codes

Each CANDU 6 fuel bundle consists of 37 natural uranium fuel pins clad in Zircaloy: a centre pin surrounded by three rings of fuel pins as depicted in Fig. 6. The fuel pins are surrounded by heavy water coolant inside of a pressure tube. The pressure tube is encased within a calandria tube, beyond which is heavy water moderator. There is a small gap between the pressure and calandria tubes which, for present purposes, is defined to be a vacuum. The fuel bundle dimensions are given in Table 8.

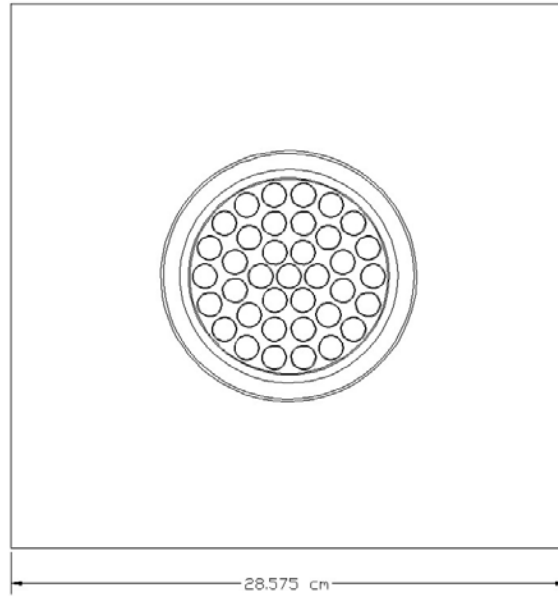


FIG. 6. Cross sectional view of CANDU 6 lattice cell, reproduced from [1].

TABLE 8. FUEL BUNDLE DIMENSIONS

Parameter	Dimension (cm)
Fuel pin outer radius	0.6103
Clad outer radius	0.6522
Rod length	49.5260
Ring 1 radius	1.4480
Ring 2 radius	2.8755
Ring 3 radius	4.3305
Pressure tube inner radius	5.1689
Pressure tube outer radius	5.6032
Calandria tube inner radius	6.4478
Calandria tube outer radius	6.5875
Radial (x - y) lattice pitch	28.5750
Axial (z) lattice pitch	49.5300

The structure of the CANDU fuel bundle has several components. In this numerical test problem, only the fuel pins and the end plates (or end regions) are modelled. The end plate is represented by a homogenized disk consisting of 29% zircaloy and 71% heavy water by volume. This disc, which is centered within the pressure tube at each end of the bundle, is 0.001 cm thick with a radius of 5.1 cm.

3.3.2. Cross section generation

The collision probability code HELIOS [5] (Version 1.8) was used to generate macroscopic material cross sections at each of the eight burnup points described in the previous sections. The isotopic atom densities of the fuel were obtained by depleting a fresh (natural uranium) fuel bundle to 13,000 MWd/t uranium using zero current boundary conditions. At each of the eight burnup points of interest, branch off calculations were performed to calculate two group macroscopic cross sections for four fuel regions (corresponding to the four fuel rings), clad, pressure tube, calandria tube, coolant and moderator. This two group library, which is taken

directly from [1], is provided in the cross sections' worksheet of the Excel workbook *transport_neutronics.xlsx*. The tables provide the transport, capture, and fission cross sections (all in cm^{-1}); the fission neutron yield; the fission neutron spectrum; and the multigroup scattering matrix. The transport correction [6] was applied to the macroscopic P_0 scattering cross sections ($\Sigma_{0,g \rightarrow g'}$) to produce the group-to-group scattering matrices:

$$\Sigma_{s,g \rightarrow g'} = \Sigma_{0,g \rightarrow g'} - \delta_{gg'} \bar{\mu}_0 \sum_{g'=1}^2 \Sigma_{0,g \rightarrow g'} \quad (2)$$

where $\bar{\mu}_0$ is the average cosine of the scattering angle and $\delta_{gg'}$ is the Kronecker delta. The 47-group HELIOS reactor cross section library was used for the calculations of the two group library. The voided state cross sections were calculated by repeating the branch off calculations with the coolant density reduced to 0.001 g/cm^3 . Table 9 shows the fresh bundle atom densities.

TABLE 9. FRESH BUNDLE ATOM DENSITIES

$1000 \times Z + A^a$	Fuel	Coolant	Moderator	Clad	Calandria tube	Pressure tube
1001		8.6803E-04	4.7189E-05			
1002		4.7715E-02	6.4260E-02			
5010			1.1003E-09	2.3269E-07	2.3300E-07	9.5142E-08
5011			4.9386E-09			
8016	4.6375E-02	2.4292E-02	3.2154E-02			
24050				3.2693E-06	3.2737E-06	2.6516E-07
24052				6.2974E-05	6.3058E-05	5.1075E-06
24053				7.1399E-06	7.1494E-06	5.7908E-07
24054				1.7737E-06	1.7761E-06	1.4386E-07
26054				8.5967E-06	5.5338E-06	1.9203E-06
26056				1.3483E-04	8.6791E-05	3.0118E-05
26057				3.1154E-06	2.0054E-06	6.9592E-07
26058				4.1147E-07	2.6487E-07	9.1914E-08
28058				3.1730E-06	2.4964E-05	1.5909E-06
28060				1.2220E-06	9.6145E-06	6.1272E-07
28061				5.3132E-08	4.1802E-07	2.6640E-08
28062				1.6918E-07	1.3311E-06	8.4827E-08
28064				4.3344E-08	3.4102E-07	2.1733E-08
40000 ^b				4.2059E-02	4.2127E-02	4.1803E-02
92234	1.2751E-06					
92235	1.6687E-04					
92238	2.3014E-02					

^a Z is the atomic number and A is the isotope mass number.

^b Material 4000 is a pseudo-isotope corresponding to natural zirconium.

Reflector cross sections were calculated by extending half of a lattice cell (depleted to 4,000 MWd/t uranium) with 68 cm of heavy water in one direction and assuming vacuum conditions beyond. The portion of moderator extending exactly one lattice pitch (28.575 cm) beyond the fuel cell boundary was homogenized and collapsed to two energy groups to produce reflector cross sections (geometry as shown in Fig. 7). The cross sections were collapsed using the flux spectrum directly from the transport calculation (i.e. with no critical spectrum correction).

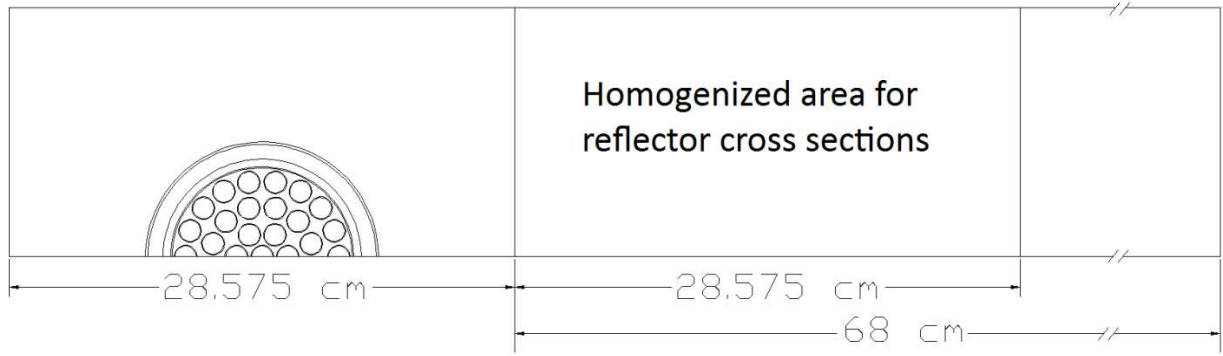


FIG. 7. Configuration used for reflector cross section generation (reproduced from [1]).

3.3.3. Core transport model description

The stylized core model consists of 380 horizontal fuel channels, each comprised of 12 fuel bundles. The channels are refuelled online from both ends of the reactor in an alternating checkerboard configuration, thus causing the axial burnup distribution of any given channel to be roughly the inverse of the adjacent channels. This spatial distribution of burnup is preserved in the current stylized model, but the number of unique burnup points in the reactor was reduced to simplify the description of the numerical test problem while maintaining the same qualitative core attributes. Specifically, the burnup values of the fuel bundles have been rounded to one of the eight following points: 32.69, 78.38, 342.37, 818.87, 1638.73, 3608.15, 6381.44 and 8721.49 MWd/t uranium. The burnup distribution is provided in the ‘Burnup distribution’ worksheet of the *transport_neutronics* Excel workbook distributed with the specifications package.

Core specifications from Table 1 remain in effect, with the following exceptions:

- Liquid zone controllers and shutoff rods are not enabled.
- The heavy water reflector modelled in the transport code is presented in Fig. 8.
- Only half of the core is presented for brevity.
- The boundary condition at the outer boundary of the reflector is taken as that surrounded by a pure infinite absorber, i.e., no re-entrant neutrons.

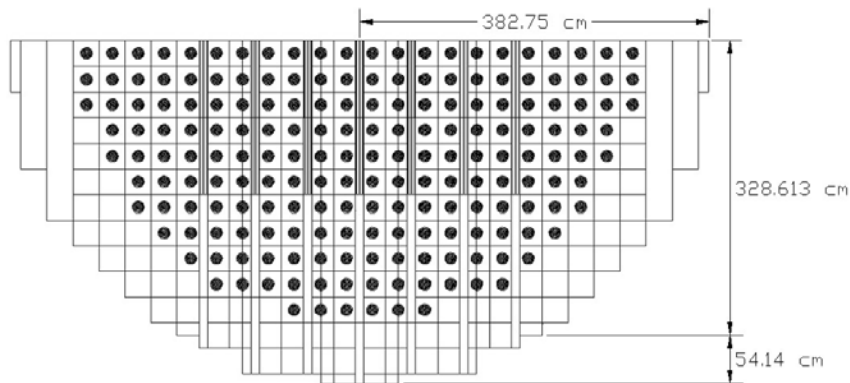


FIG. 8. Cross sectional view of the stylized core model; only one half of the core is shown (reproduced from [1]).

This specification contains only one type of adjuster rod. Each rod consists of a solid stainless-steel cylinder (shim) that is centred in a stainless steel tube. The shim and tube are composed of two vertical segments with slightly different diameters. The inner segment extends 85.725

cm from the midplane, while the outer segment extends from the end of the inner segment to a point 171.45 cm from the midplane. The dimensions of the inner and outer adjuster rod segments are given in Table 10. The adjuster rod assembly (shim and tube) is cantered within a zirconium guide tube. Heavy water fills the gaps between the steel shim and the inner steel tube and between the inner steel tube and outer guide tube. The adjuster rods are located interstitially perpendicular to the fuel channels, arranged vertically in three rows of seven at $z = 222.89, 297.18$ and 371.48 cm where $z = 0$ is the exterior boundary of the first axial plane. The x positions are $0, \pm 57.15, \pm 114.3, \pm 171.45$ cm. The guide tube extends from the end ($y = \pm 171.45$ cm) of the adjuster rod to the boundary ($y = \pm 342.9, \pm 371.475, \pm 371.475, \pm 382.753, \pm 371.475, \pm 371.475, \pm 342.9$). The centre of the core is taken as the origin for the (x, y) coordinate. The adjuster rods are modelled in two segments. The vertical extents of the inner and outer segments in the y -direction are listed in Table 10.

TABLE 10. ADJUSTER ROD DIMENSIONS

Component dimension	Inner element	Outer element
	0.000 cm–85.725 cm	85.725 cm–171.450 cm
Shim outer radius (cm)	0.650	0.710
Steel tube inner radius (cm)	3.607	3.607
Steel tube outer radius (cm)	3.725	3.690
Guide tube inner radius (cm)	4.519	4.519
Guide tube outer radius (cm)	4.572	4.572

3.4. STEADY STATE THERMAL HYDRAULICS MODEL SPECIFICATION

This section describes the thermal hydraulics network based on a stylized PHWR idealization developed at CNL for the system thermal hydraulics computer code ARIANT². The model consists of two figure of eight loops with a core of 380 fuel channels, per Fig. 5. Although the model is highly simplified, it provides sufficient detail to capture the main characteristics of flow distribution among the channels and the overall pressure drops across the core with typical flow rates through the main coolant pumps in the primary circuits.

3.4.1. Main simplifications

Simplifications in the plant network and control systems minimize the modelling effort. Operating characteristics of the main coolant pumps, distribution of various losses in the reactor circuit, piping geometry, and core power are representative of a typical PHWR plant. Despite these simplifications, the model can be used to simulate a steady state thermal hydraulic scenario, where the operating parameters such as the total flow rate, header pressures, etc. are comparable to those in the reactor. However, simplifications listed below are expected to result in deviations for postulated upset scenarios, therefore, rendering the results not applicable for actual reactor safety analyses.

The following simplifying assumptions have been made:

1. Boiler (steam generator) primary sides are represented in sufficient detail to represent the overall hydraulic resistance offered by the boiler tubes in the steam generators. However, the secondary side is represented by a constant heat transfer coefficient and a

² Formerly known as CATHENA4.

constant secondary side temperature for the steady state run. The heat transfer area for each boiler is given in Table 11. It should be noted that these values can also be calculated from the thermal hydraulics specifications spreadsheet for each primary pipe component that are arranged in the configuration of an inverted U tube. For the transient thermal hydraulics analysis, the secondary side heat transfer coefficient is modified to closely resemble typical heat transfer rates observed during the initial phase of a large break loss of coolant accident (LBLOCA). For different scenarios, the participants will agree on the value of the secondary side heat transfer coefficients. For the steady state operation, CNL recommends using values of 30,000 W/m²/K and 535 K for, respectively, the heat transfer coefficient and the secondary side average fluid temperature.

TABLE 11. BOILER HEAT TRANSFER AREA

Component	Area (m ²)
wbXXin	3.27
wbXXtsu	59.36
wbXXupl	450.88
wbXXupm	464.13
wbXXupu	343.87
wbXXtpa	119.49
wbXXtpb	119.49
wbXXdnu	343.87
wbXXdnm	464.13
wbXXpre	450.88
wbXXtsd	59.36
wbXXout	3.42

2. The pressure and inventory control system are also simplified. The pressurizer is represented by a large vertical pipe connected to a pressure boundary condition. The pressure boundary condition is set at 10 MPa at thermodynamic equilibrium (saturated) conditions. The pressurizer is connected to loop 1 through OHD3³ and loop 2 through OHD7 (see Fig. 9).
3. The pressure tubes are assumed insulated, allowing the users to neglect the modelling of convective/conductive/radiative heat transfer from the pressure tube to calandria tube. This simplifying assumption will therefore preclude any scenario that involve the moderator or scenarios involving pressure tube calandria tube contact.
4. The emergency core cooling system piping was removed as none of the planned scenarios necessitate the inclusion of this subsystem of the plant.
5. There are no non-condensable gases present in the simplified network. The net coolant mass in the simplified plant with the pressurizer should be close to 136,000 kg, including the pressurizer component which has a coolant mass of 31,000 kg. This value can also be calculated and verified from the component volumes and initial densities in the thermal hydraulics specifications spreadsheet. Minor deviations may be acceptable but should be noted in the final report. The coolant fluid is treated as pure D₂O. Thermo-physical properties of the coolant are independent of the actual coolant purity specified

³ OHD: outlet header

in Table 1. There are no provisions to correct the average coolant density communicated to the neutronics code for changes in coolant purity.

The focus of the ICSP numerical test problem is thermal hydraulics/neutronics coupling and reactor response to rapidly changing core conditions early in the transient. The ECC systems are triggered usually after several minutes of operation, even for a LBLOCA, well after the reactor was shut down.

3.4.2. System components and connections

The idealization is shown in Fig. 9 with corresponding piping geometry data in spreadsheet *TH_Network_specs.xlsx*. The thermal hydraulics network consists of two loops connected to the pressurizer via two separate lines via OHD3 (in loop 1) and OHD7 (in loop 2); the loops are also connected through the purification line, via the suction side of primary pump 1 (loop 1) and pump 3 (loop 2). Two lines of interconnects allow flow bypass between OHD1 and OHD3 (loop 1) and OHD5 and OHD7 (loop 2). There is a total of 380 channels, 190 channels per loop, and 95 channels per pass. Fuel channels with similar mass flow rates and power levels are grouped to minimize the computational effort. The suggested grouping for this numerical test problem is seven groups for each core pass as given in Table 12 where the first number (a) in the a/b/c triplet denote the number of channels in the thermal hydraulics group, the second number (b) denote the thermal hydraulics channel identification number and the third number (c) denote the corresponding channel group, as shown in Fig. 5.

TABLE 12. CORE THERMAL HYDRAULIC CHANNEL GROUPINGS

Group #	Pass-1	Pass-2	Pass-3	Pass-4
1	12/11/1	12/21/8	12/31/15	12/41/22
2	11/12/2	12/22/9	12/32/16	11/42/23
3	12/13/3	11/23/10	11/33/17	12/43/24
4	11/14/4	14/24/11	14/34/18	11/44/25
5	14/15/5	16/25/12	16/35/19	14/45/26
6	16/16/6	15/26/13	15/36/20	16/46/27
7	19/17/7	15/27/14	15/37/21	19/47/28
Total	95	95	95	95

Example 1: ‘12/11/1’ refers to 12 channels, in Pass 1, Group 1, with thermal hydraulic group number 1.

Example 2: ‘19/47/28’ refers to 19 channels in Pass 4, Group 7, with thermal hydraulic group number 28

Detailed piping geometry (pipe length, end-to-end elevation change, pipe flow area, hydraulic diameter, and pipe roughness) minor losses (K -factor) and recommended nodalization for each group is given in the Excel spreadsheet file *TH_Network_specs.xlsx* under the ‘components’ worksheet. It should be noted that although a pipe volume can be computed from the product of pipe length and pipe flow area, in some instances total volume has also been specified. For thermal hydraulics codes that cannot accept more than two geometry variables for a pipe component, the participants should consider the following guidelines:

- For fuel channels, preserve total pipe length and flow area should be preserved. That is, the thermal hydraulics code should calculate the pipe volume internally, and
- For header components, preserve total volume and cross sectional area. If necessary, the participants are expected to add an extra node to ensure correct length.

For those participants who may need detailed dimension specifications for the inlet header break problem, the following values may be used:

- Inlet header internal diameter: 0.370 m
- Inlet header volume: 0.6875 m³ (also provided in thermal hydraulic specifications)
- Inlet header total length: 6.407 m
- Inlet header pipe (exclusive of end caps): 6.0 m

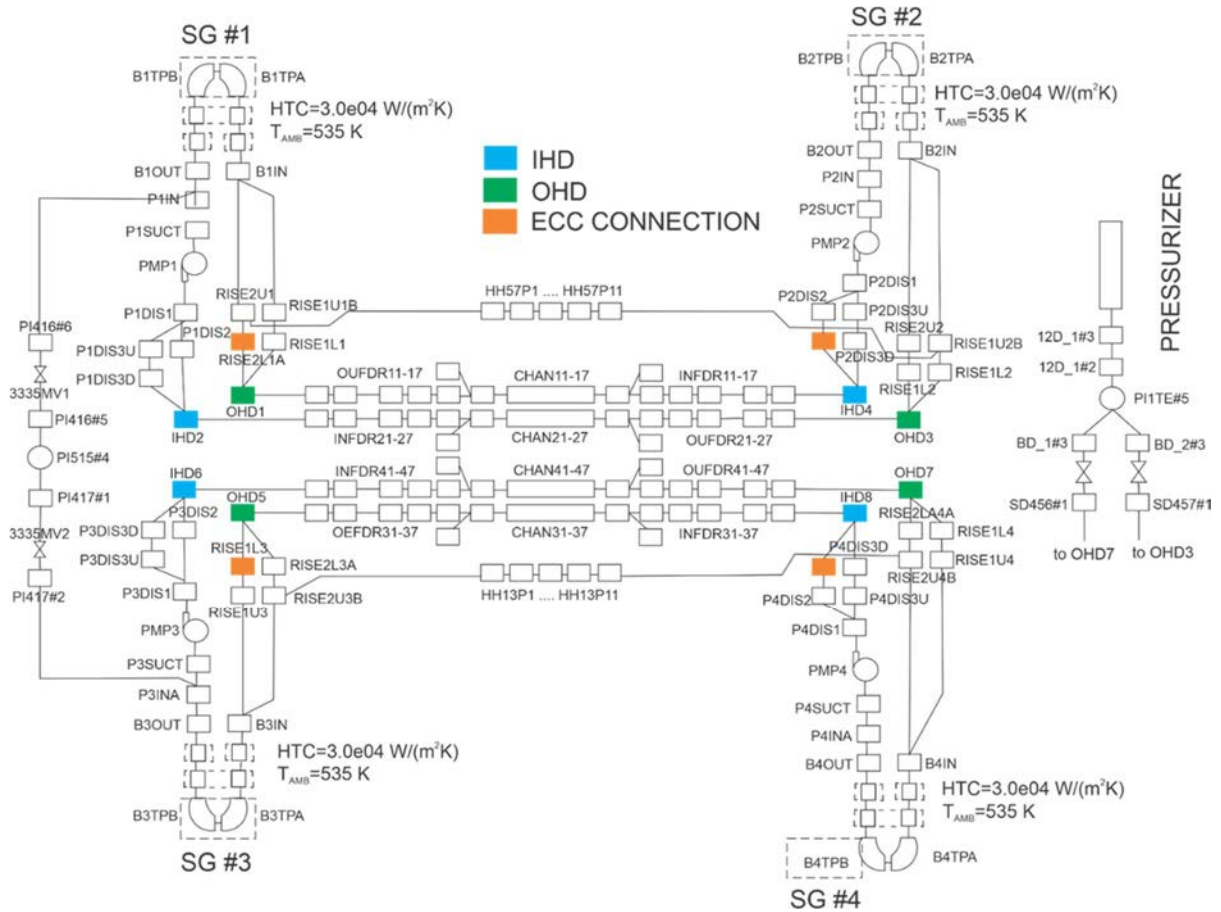


FIG. 9. Simplified thermal hydraulics network for numerical test problem.

The data are arranged to follow the figure of eight configurations. For example, piping details for loop 1, pass 1 start from IHD4⁴, and continue on inlet feeders of pass 1, channel groups 11 to 17, outlet feeders for pass 1, OHD1 followed by piping for boiler 1 primary side and pump 1 suction and discharge piping. This network of thermal hydraulic components is followed by pass 2 of loop 1. Similarly, this pattern is repeated for loop 2 for pass 3 and pass 4. This section of the input specifications covers all core passes, all eight (8) headers, four (4) main pumps and four (4) boilers/steam generators with associated intermediate piping, corresponding minor loss coefficients and recommended nodalization for each component.

The second part of the components worksheet in the *TH_Network_specs.xlsx* file provides detailed geometry specifications for header-to-header interconnect lines for both loops, followed by piping for loop 1 to loop 2 piping (all intermediate piping for purification system was removed as discussed earlier) and the pressurizer component with associated piping.

⁴ IHD: inlet header

The component connections specifications are given under the ‘connections’ worksheet in the *TH_Network_specs.xlsx* Excel spreadsheet file.

3.4.3. System models

Model specifications are given in ‘System_Models’ worksheet in *TH_Network_specs.xlsx*:

- All junction resistance values at links connecting components described under the components worksheet tab;
- Specification of the discharge model to be used;
- All valves and orifices in the thermal hydraulics network including initial orifice area (for valves) and associated discharge coefficients;
- All pumps in the circuit with their associated rated operating characteristics (homologous pump data is provided in 0).

3.4.3.1. Initial and boundary conditions

The ‘Boundary_Conditions’ worksheet in the *TH_Network_specs.xlsx* Excel spreadsheet file specify the pressurizer boundary condition. This condition is imposed on the circuit to achieve the steady state in the plant model when all four main pumps are running. To ensure that all participants perform steady state analysis with the same initial conditions, it is essential that all steady state inlet header temperatures converge at 260 °C.

The participants are permitted to adjust secondary side conditions slightly to achieve the required inlet header temperatures. Prior to initiating the iterations required to achieve convergence in the steady state, all participants should initiate the pressurizer with a fill level of 100%, as detailed in the specification worksheets. It is expected that the equilibrium water level will drop by differing amounts depending on the participant’s simulation system.

For all piping and connections specified under the ‘Components and Connections’ worksheet in the *TH_Network_specs.xlsx*, spreadsheet a set of initial conditions are provided. These are selected such that the state of the plant at the start of a steady state thermal hydraulics run is as close to the steady state values of operation as possible. For piping components, node pressure, steam and liquid water enthalpies, steam volume fraction and initial mass flow rate in each node are provided. For connections between the piping components, initial two phase mass flow rate is specified.

3.4.3.2. Wall heat transfer models

The ‘Wall_Heat_Transfer_Models’ worksheet in the *TH_Network_specs.xlsx* Excel spreadsheet specify the information for the two groups of the solid body heat transfer models, namely fuel element models and boiler/steam generator tube models.

3.4.3.3. Fuel bundles / fuel elements

The first group contains specification of the 336 models (4 coolant passes \times 7 fuel channel groups per pass \times 12 bundles per channel) representing the average fuel element in one of the 37 element bundles. The simplifying approximation for modelling is that all fuel elements in a particular fuel bundle have the same characteristics including element power, and fuel temperature. Thus, the heat transfer calculation is performed for a bundle averaged fuel element, for an average bundle within fuel channel group. A fuel element has two material layers in

radial direction with a gap region in between. The fuel arrangement is the UO_2 fuel pellet, gap and the clad. Dimensions and required material properties (such as thermal conductivity, heat capacity, mass density, and others) are provided in Appendix I.

The bundle power for each of these models are specified in cells from column AN32 to AN62 through column AY32 to AY62 of the separate worksheet *Bundle_Power* worksheet in *TH_Network_specs.xlsx*. The specifications provide converged initial temperatures for all solid heat structures modelled, including the fuel element radial region values. In total, there are 336 different average bundle power levels specified.

3.4.3.4. Boiler / steam generator tubes

The second group contains specification of the models that form the four simplified boiler/steam generator models. Each boiler is specified by the twelve wall models. The first model defines inlet while the last outlet of the boiler. The remaining 10 models portray the 3,542 small diameter parallel Inconel pipes. The inner surface of these pipes is exposed to primary side coolant flow while the outer surface to the secondary side coolant flow. Dimensions and required material properties are provided. The secondary side boundary conditions are assumed to remain unchanged for all problems. The heat transfer areas corresponding to primary side boiler tubes are given in Table 11.

3.4.3.5. Material properties

The fuel model is comprised of a three-region CANDU fuel element at standard dimensions (see specifications spreadsheet *TH_Network_specs.xlsx* for detailed fuel geometry information), namely an inner UO_2 , and an outer Zircalloy region with a gap in between. Material properties for UO_2 and Zircalloy can be found in Appendix I. The gap properties are also provided in *TH_Network_specs.xlsx* in terms of a gap conductance and surface emissivities. For those participants where a gap model does not require surface emissivities but other parameters such as a total gap conductivity, a workaround is provided in the Appendix I. Similarly, material properties used in steam generator, namely, Inconel, carbon steel and stainless steel are also given in Appendix I.

3.4.3.6. System control models

The control system was highly simplified since most of the control logic for ECC, pressure and inventory control system, and others have been removed. The control system provided in this specification, however, is sufficient to achieve a steady state operating condition. These system controls the valves around the pressurizer (PRZBC1 and PRZBC2). Control of these valves are achieved through the input table OPNPBC but the participants can choose their own method for control. These valves are closed once a steady state is achieved and the system pressure is stabilized. The valves are closed prior to initiation of any plant transient to ensure that the pressurizer is isolated from the externally imposed pressure boundary condition. Prior to initiating the iterations required to achieve convergence in the steady state, all participants should initiate the pressurizer with a fill level of 100%, as detailed in the specification worksheets. It is expected that the equilibrium water level will drop by differing amounts depending on the participant's simulation system.

Only one numerical test problem involves movement of the shutdown rods. Movement will be initiated on the basis of a specified core power threshold.

3.5. TRANSIENTS

3.5.1. Initial conditions prior to transients

The reactor operates at 100% nominal power without interruption. This case has to be executed in three variants:

- **Coupled neutronics/thermal hydraulics.** Starting from the specified initial conditions. Results based on a time-converged solution should be reported using the template file *PI_RES_template.xlsx*. Please note that some results require that dedicated standalone neutronics simulation be performed using the converged thermal hydraulics local conditions.
- **Standalone steady state neutronics.** Starting from the specified thermal hydraulics initial conditions, a standalone neutronics steady state simulation is performed. Results should be reported using template file *PI_SAPH_RES_template.xlsx*.
- **Standalone thermal hydraulics.** Starting from the specified bundle power distributions, a standalone thermal hydraulics simulation is performed. Results based on a time converged solution should be reported using the template file *PI_SATH_RES_template.xlsx*.
- **Standalone neutronics with shutdown.** A standalone neutronics transient simulation is performed using the thermal hydraulics initial conditions of the steady state specification. These initial conditions are assumed to be time invariant. The reactor trip occurs at $t = 0$ s. The time evolution of the lower edge of the shutoff rods follows Table 13. At trip time, the lower edges of the rods are at zero insertion, corresponding to the topmost y axis mesh plane. The rods start their insertion immediately, however there is a 0.28 s delay before their lower edge breaches the fuelled region of the core. The rods reach their full insertion 1.75 s after the trip was initiated. When fully inserted, the bottom edge of all rods is at 715.75 cm, and their top edge lies a 0 cm. Results should be reported using template file *PI_SAPH_RES_template.xlsx*.

TABLE 13. SHUT-OFF ROD POSITION PROFILE

Time (s)	Shut-off rods position (cm)
0.00	0.00
0.25	54.24
0.50	164.49
0.75	274.74
1.00	384.99
1.25	495.25
1.50	605.50
1.75	715.75
5.00	715.75

To facilitate issue diagnosis and inform comparisons of participant solutions, supplemental standalone neutronics simulations are required to compute time independent neutronics outputs. These should be performed using in-core local thermal hydraulics data derived from the coupled solutions. These are detailed in the following Subsections.

3.5.1.1. Full-core void worth

Bundle wise thermal hydraulic local conditions are perturbed by setting all coolant densities values to 0.001 g/cm³. The static effective neutron multiplication is computed from a standalone neutronics simulation. The coolant voiding reactivity worth (CVW1), in the unit of mk, is computed as follows:

$$CVW1 = \frac{1}{k_{ref}} - \frac{1}{k_{voided}} \times 1000 \quad (3)$$

where k_{ref} is the standalone steady state neutron multiplication factor of the unperturbed system, and k_{voided} is the neutron multiplication factor obtained when the coolant density is reduced to 0.001 g/cm³.

3.5.1.2. Half-core checkboard void worth

Bundle wise thermal hydraulic local conditions are perturbed in core pass 2, thermal hydraulics groups 8–14, by setting the coolant density values to 0.001 g/cm³. The static effective neutron multiplication is computed from a standalone neutronics simulation. The coolant voiding reactivity worth (CVW2), in mk, is computed as:

$$CVW2 = \frac{1}{k_{ref}} - \frac{1}{k_{hc voided}} \times 1000 \quad (4)$$

3.5.1.3. Liquid zone controller worth

The fill level of the liquid zone controllers is set to 1.0 (full fill). The static effective neutron multiplication is computed from a standalone neutronics simulation. The procedure is repeated using a fill level of 0.0 (zero fill). The full liquid zone controller worth is computed in mk as:

$$LZCW = \frac{1}{k_{full}} - \frac{1}{k_{empty}} \times 1000 \quad (5)$$

3.5.1.4. Adjuster rod worth

Adjuster rods are withdrawn from the core and the effective neutron multiplication factor is computed from a standalone neutronics simulation. The adjuster rod worth (ADJW) reactivity worth of the rods is computed in mk as:

$$ADJW = \frac{1}{k_{full}} - \frac{1}{k_{empty}} \times 1000 \quad (6)$$

3.5.1.5. Fuel temperature worth

Bundle-wise thermal hydraulic local conditions are perturbed by setting all fuel temperatures to a value of 2,000 °C. The static effective neutron multiplication is computed from a standalone neutronics simulation. The reactivity worth of increasing the fuel temperature, in mk, is computed as:

$$FTW = \frac{1}{k_{ref}} - \frac{1}{k_{2000 \text{ deg C}}} \times 1000 \quad (7)$$

3.5.2. Adjuster rod withdrawal

Following a period of stable steady state operation, adjuster rods 7 and 14 begin moving out of the core at time $t = 0$ s. The rods travel upwards at a uniform rate of 10 cm/s. No reactor trips are credited, and the simulation is halted at time $t = 25$ s. Results should be reported using Excel file *P2_RES_template.xlsx*. Two standalone variants are included:

- Standalone neutronics: thermal hydraulics feedback is modelled using the data listed in the Adjuster withdrawal worksheet of file *SA_thermalhydraulics.xlsx*. Results should be reported using Excel file *SAPH2_RES_template.xlsx*.
- Standalone thermal hydraulics: neutronics feedback is modelled using the data in the Adjuster withdrawal worksheet of file *SA_thermalhydraulics.xlsx*. Results should be reported using Excel file *SATH2_RES_template.xlsx*.

Note that the problem specification data provided for the standalone variants are based on coupled solutions derived from earlier specifications. As a result, it will not be possible to perform a consistency test between participant standalone solutions and their corresponding coupled solutions.

3.5.3. Coolant pump rundown

Following a period of stable steady state operation, heat transport pump #2 begins a rundown at $t = 0$ s. The pump speed profile is listed in Table 14. No reactor trips are credited, and the simulation is halted at time $t = 25$ s. Results should be reported using Excel file *P3_RES_template.xlsx*. Two standalone variants are included:

- Standalone neutronics. Thermal hydraulics feedback is modelled using the data listed in the ‘Pump rundown’ worksheet of file *SA_thermalhydraulics.xlsx*. Results should be reported using Excel file *SAPH3_RES_template.xlsx*.
- Standalone thermal hydraulics. The neutronics feedback is modelled using the data listed in the ‘Pump rundown’ worksheet of file *SA_neutronics.xlsx*. Results should be reported using Excel file *SATH3_RES_template.xlsx*.

TABLE 14. PUMP 2 RUNDOWN DATA

Time (s)	Pump speed (rpm)	Time (s)	Pump speed (rpm)
0.0	1791.0	13.0	792.8
1.0	1570.0	14.0	757.0
2.0	1400.0	15.0	723.0
3.0	1300.0	16.0	690.7
4.0	1200.0	17.0	660.2
5.0	1149.8	18.0	631.3
6.0	1097.8	19.0	604.0
7.0	1048.0	20.0	578.2
8.0	1000.4	21.0	553.9
9.0	954.9	22.0	531.1
10.0	911.4	23.0	509.6
11.0	869.9	24.0	489.5
12.0	830.4	25.0	470.7

Note that the problem specification data provided for the standalone variants are based on coupled solutions derived from earlier specifications. As a result, it will not be possible to perform a consistency test between participant standalone solutions and their corresponding coupled solutions.

3.5.4. Reactor inlet header break

Following a period of stable steady state operation, a break is postulated to occur in IHD2 at time $t = 0$ s. The break area is 0.0645 m^2 and the break opening time is 100 ms. The break opens with a linear profile of break area vs time. The header break external pressure is set to atmospheric pressure. When the core power reaches or exceeds 120% of nominal, the shutoff rods start to move according to Table 13. Coupled simulations are halted at time $t = 5$ s. Results should be reported using Excel file *P4_RES_template.xlsx*.

3.5.4.1. Coupled variant without shutoff rod movement

In this variant, the simulations are performed without crediting movement of the shutoff rods. Results should be reported using Excel file *P4_NOSOR_RES_template.xlsx*.

3.5.4.2. Standalone reactor physics variant

In the standalone physics variant, the thermal hydraulics feedback is provided in the ‘Header break’ worksheet of file *SA_thermalhydraulics.xlsx*. The trip time is specified as 0.8448 s. Results should be reported using Excel file *P4_SAPH_RES_template.xlsx*.

3.5.4.3. Standalone thermal hydraulics variant

In the standalone thermal hydraulics variant, the physics response is provided in the ‘Header break’ worksheet of file *SA_neutronics.xlsx*. Results should be reported using Excel file *P4_SATH_RES_template.xlsx*.

Note that the problem specification data provided for the standalone variants are based on coupled solutions derived from earlier specifications. As a result, it will not be possible to perform a consistency test between participant standalone solutions and their corresponding coupled solutions.

4. PARTICIPANT MODEL DESCRIPTIONS

4.1.COMISIÓN NACIONAL DE ENERGÍA ATÓMICA

4.1.1. Codes and methods

PUMA v6.0.5 [7] was used for neutronic calculations and RELAP5/3.3 [8] for thermal hydraulic calculations. The coupling scheme was implemented using a specially developed python interface. Specification data was also read directly from specification files using a dedicated python interface to generate models.

PUMA solves the diffusion approximation of the neutronic transport equation in a finite difference scheme. It has capabilities to solve eigenvalue, adjoint, and spatial cinematic problems. It is organized in a modular way and allows the user a high degree of customization

regarding how the calculations are carried out. It allows general multigroup cross sections with multiple interpolation tables. Transient calculations are done with a quasi-static approximation, with a backwards finite difference scheme and cross section data is revised at each time step in response to changes in local conditions.

RELAP5 computer code is a light water reactor transient analysis code developed for the U.S. Nuclear Regulatory Commission (NRC) for use in rulemaking, licensing audit calculations, evaluation of operator guidelines, and as a basis for a nuclear plant analyser. Specific applications of this capability have included simulations of transients in LWR systems, such as loss of coolant, anticipated transients without scram, and operational transients such as loss of feedwater, loss of offsite power, station blackout, and turbine trip.

RELAP5 is a highly generic code that, in addition to calculating the behaviour of a reactor coolant system during a transient, can be used for simulation of a wide variety of hydraulic and thermal transients in both nuclear and nonnuclear systems involving mixtures of steam, water, non-condensable and solute.

The RELAP5 hydrodynamic model is a one-dimensional, transient, two fluid model for flow of a two phase steam water mixture that can contain non-condensable components in the steam phase and/or a soluble component in the water phase. The model contains several options for invoking simpler hydrodynamic models. These include homogeneous flow, thermal equilibrium, and frictionless flow models. These options can be used independently or in combination. The homogeneous and equilibrium models were included primarily to be able to compare code results with calculations from the older codes based on the homogeneous equilibrium model.

The two fluid equations of motion that are used as the basis for the RELAP5 hydrodynamic model are formulated in terms of volume and time averaged parameters of the flow. Phenomena that depend upon transverse gradients, such as friction and heat transfer, are formulated in terms of the bulk properties using empirical transfer coefficient formulations. In situations where transverse gradients cannot be represented within the framework of empirical transfer coefficients, such as subcooled boiling, additional models specially developed for the particular situation are employed. The system model is solved numerically using a semi implicit finite difference technique. The user can select an option for solving the system model using a nearly implicit finite difference technique, which allows violation of the material Courant limit. This option is suitable for steady state calculations and for slowly varying, quasi steady transient calculations.

For the header break problem, the default RELAP choked flow correlation was used. No difference was observed with Henry-Fauske with default parameters and it allowed much greater time steps. A difference of approximately 900 kg/s in the maximum flow through the break was observed compared to using Henry-Fauske in frozen condition.

4.1.2. Special procedures for processing problem specification data

No special procedures were required.

4.1.3. Coupling framework

For steady state calculations a steady state simulation was used in the neutronic model and a transient simulation for the thermal hydraulics. Information was exchanged each 100 s of thermal hydraulic simulated time and this was repeated until the convergence criteria were met.

For transient calculations both codes run independently, sharing information after a fixed time interval, throughout the interval the information received in the exchange is assumed to be constant. For all transients a time exchange interval of 10 ms was used. Both, steady state and transient simulation schemes, are presented in Fig. 10. A sensitivity analysis was done with time steps of 20 ms and 5 ms and the results obtained didn't show significant differences between 10 ms and 5 ms timesteps for the proposed transients.

A procedure for running a transient coupled simulation took the following steps:

1. PUMA simulated a steady state condition with initial thermal hydraulic conditions.
2. RELAP simulated a steady state condition with initial power distribution.
3. Coupled steady state was reached using the described scheme for steady state coupling.
4. Pressurizer was isolated from the thermal hydraulic model.
5. PUMA model was modified to a transient one.
6. A 10 s full transient simulation in steady state condition was carried out, with the transient scheme described above, to check that every variable was in equilibrium and no perturbation is added to the transients.
7. Perturbations for the corresponding transient problem were introduced and the system was evolved until the final specified time.

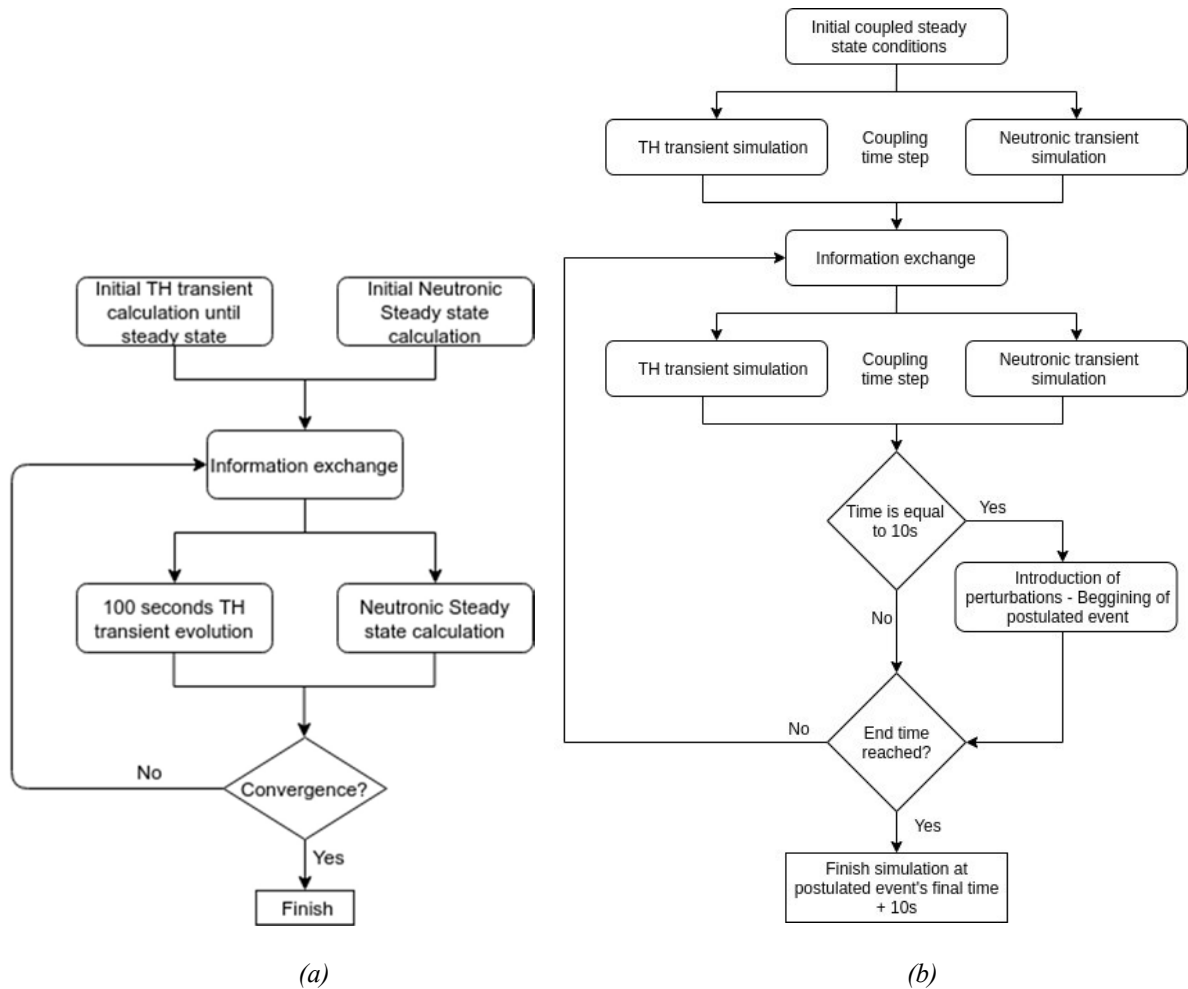


FIG. 10. (a) Steady state and (b) transient coupling schemes.

The coupling interface adds the power to the corresponding channels in the neutronic model to generate power distribution per channel and bundle for the thermal hydraulic model. The internal time step for power evolution in PUMA was reduced until the maximum power difference was negligible. A 2.5 ms time step was used.

RELAP5 generates coolant and fuel temperature and coolant density distributions, which are copied to the corresponding neutronic channels. No modification is applied to these values and all neutronic channels corresponding to a thermal hydraulic channel are assumed to have the same thermal hydraulic characteristics. Automatically RELAP5 tries to increase the time in a user specified range, provided a courant limit is not exceeded in any volume. A parametric analysis was carried out to select a maximum time step that would assure both the absence of numerical instabilities and convergence of the result. A time step range of 0.0001–0.1 ms was used internally in RELAP for all transients.

PUMA requires that both the square root and the value of fuel temperature are provided. The latter is not used to modify cross sections, but it is deemed useful for graphical representation.

4.1.4. Procedure for execution of coupled simulations

See Section 4.1.3.

4.1.5. Deviations from specifications

A +1°C difference was added to secondary side temperatures, so as to get an average 260°C in inlet headers. A mean Samarium value was considered for the reactor and the actual distribution was not considered. A mean neutron velocity as a function of burn-up was used for every burn-up step.

For components for which specified data results in the inner junction areas being bigger than the component area, preference was given to the former. This was done because an error arose during simulation as it considers this situation as a modelling discrepancy.

Concentrated loss specified for volumes was distributed uniformly in the junctions of the given volume. In some node volumes, a junction was added in the middle if a concentrated loss was specified for that volume. It was not possible not to include energy dissipation in balance equations. It is reflected in a difference in power generated in core and power extracted in the steam generator for the steady state.

Fuel temperatures are reported as volumetric average of only the pellet and not the full heat-structure that would include the cladding. This could lead to higher values being reported if the bulk of participants report the average including cladding.

4.1.6. Convergence criteria

The parameters and limits listed in Table 15 were considered to reach convergence. When the difference for all variables between two steps are below the limit, the simulation is considered converged. It was observed that the variable that took the longer to converge was the pressurizer level. In average it took 1,000 s of simulated time to reach convergence.

TABLE 15. STEADY STATE CONVERGENCE CRITERIA

Convergence test	Limit	Unit
Δk_{eff}	0.001	mk
Max(Δ bundle power)	0.005	%
Pressurizer level	1	mm
Max(Δ (header pressure))	0.001	MPa
Max(Δ (header void))	0.0005	n/a
Max(Δ (header T))	0.01	°C
Max(Δ (Pump flow))	0.2	kg/s
Max(Δ (Heat structure T))	0.01	°C

4.2.CANADIAN NUCLEAR LABORATORIES

4.2.1. Codes and methods

The CNL prepared solutions to the numerical test problems using NESTLE-C (version 3.1.2) and ARIANT (version 1.0.0.24). These updated code versions include a coupling interface which eliminates the need for third party software, such as SALOME [9]. However, the coupling algorithm is generally unchanged from [10], which was based on SALOME to enable coupling.

ARIANT is a one dimensional, non-equilibrium, two fluid, two phase thermal hydraulics code. Written in Fortran 95/2000, its highly modular structure facilitates maintenance as it is easier to identify code issues or to implement code modifications during the development cycle. ARIANT's use of dynamic memory allocation means the problem sizes are only limited by available computer memory.

The intended range of ARIANT application includes, but is not limited to, PT-HWR power reactors, nuclear test facilities such as the NRU, MAPLE, and SLOWPOKE, as well as experimental facilities (RD-14M, CWIT, LASH). ARIANT incorporates various modules enabling the user to perform complete simulations of power plants or experimental facilities. For example, a highly detailed heat transfer module enables the user to model a partially voided PHWR fuel bundle in three dimensions to any desired resolution. The code includes a neutron point kinetics model for basic neutronics calculations; however, this model was supplemented by linking to NESTLE-C in order to incorporate a more detailed representation of the reactor core physics. ARIANT incorporates a complete control system module that provides all the necessary tools required to simulate the control systems in a power plant such as various trip functions, controls required for power manoeuvring, etc. In short, all controls required to operate a nuclear power plant can be simulated using ARIANT control modules.

ARIANT employs a fully implicit numerical integration scheme using Newton's iterative method [11] and is hyperbolic within its range of application [12]. The field equations are discretized using a finite volume scheme and are solved in their non-linear form without any need for linearization. One of the benefits of this approach is that pressure and density fields computed at each time step are consistent and no additional mass and energy corrections are necessary after the solution of the system of equations. Implicit methods are inherently stable even for very high Courant numbers. In theory, implicit integration schemes are unconditionally stable. However, in practice, caution is still required to ensure initial conditions are selected to ensure the initial state is reasonably close to the radius of convergence of the scheme.

NESTLE-C [13] is a few group neutron diffusion code based on the nodal expansion method. The code is a derivative of NESTLE [14], with specific modifications to enable PT-HWR simulations. NESTLE-C is capable of solving eigenvalue, adjoint, and fixed source, and transient problems. CNL is currently maintaining NESTLE-C on behalf of the Canadian Nuclear Safety Commission. Originally limited to solving two or four energy group problems, NESTLE-C was updated to accommodate a general multigroup structure using cross sections generated by the SERPENT code [15][16]. In addition, a covariance data library is available to support nuclear data sensitivity and uncertainty propagation studies [17]. NESTLE-C can solve the time independent eigenvalue problem using either a finite difference or nodal expansion method. The nodal expansion is based on a quartic expansion of the flux. Moment closures and continuity relations are used to construct a system of equations representing node-to-node interface currents. The solution of this system is used to correct the coupling coefficients used in the finite difference solver. The finite difference solver outer iterations are accelerated using either the Chebyshev polynomial or Weiland Shift methods. The fixed source problem is solved using the same framework, with the addition of the external source terms. Transient problems are cast as a series of fixed source problems. The time dependent neutron precursor terms are incorporated in the source term. Cross section data is revised at each time step in response to changes in local conditions. Flux solutions obtained using the corrected fixed source formulation are linked between time steps using a backward Euler scheme.

As of version 3.1.2, NESTLE-C is implemented using double precision arithmetic and uses dynamically allocated arrays. The code can be compiled in two modes: standalone executable and dynamically linked library. The standalone executable is used for all standalone versions of the Problems. The dynamic library is called by ARIANT in order to implement all coupled Problems.

4.2.2. Special procedures for processing problem specification data

No special procedures were required.

4.2.3. Coupling framework

NESTLE-C provides bundle-wise power at each lattice site in the reactor core. ARIANT provides volumetric averaged values of the coolant and fuel temperatures, as well as the coolant density. An operator splitting approach is used to implement solutions to the coupled neutronics/thermal hydraulics problems. Both codes march in time in parallel steps, using common time synchronization points. Fig. 11 illustrates the process. Data which are exchanged are assumed to be constant between exchange times, hence convergence studies are required to ensure the data exchange intervals are not too long. In the present work, coupled solutions to Problems 2 and 3 using a 50ms data exchange interval show little variation from solutions based on a 5ms data exchange interval. However, for problem 4 (header break), additional sensitivity was observed. All results presented by CNL are based on simulations using a 5ms data exchange interval.

ARIANT controls the overall simulation time for all coupled problems. Internally, ARIANT uses an automatic time step control logic which maximizes the time step size within user specified limits. This is made possible through the use of an internal time step redo capability. The limits were set as 0.01–1 ms. NESTLE-C simulations are performed with internal time steps of 1 ms. A simulation proceeds through the following steps:

1. ARIANT model initialization at time $t = 0$.

2. NESTLE-C model initialization at time $t = 0$. Initialize data synchronization data arrays and local thermal hydraulics data arrays used by NESTLE-C. The time-independent neutron diffusion equation is solved to initialize equilibrium transient fission products and the excess reactivity normalization constant.
3. ARIANT reads list of synchronization times from memory linked to NESTLE-C arrays.
4. ARIANT identifies the next synchronization time t' . Both codes execute from t to t' .
5. ARIANT transmits three vectors representing updated thermal hydraulics data. The transfer is implemented using a library call which overwrites data in NESTLE-C thermal hydraulics data arrays. NESTLE-C transmits a vector representing the 4,560 bundle powers.

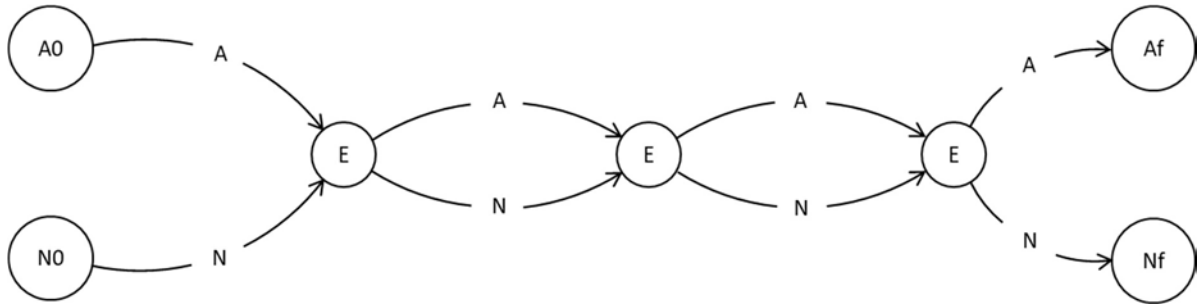


FIG. 11. Coupled execution scheme. From initial conditions (A0, N0), NESTLE-C and ARIANT execute in parallel, exchanging data at pre-defined time intervals (E).

Steps 4 and 5 are repeated until ARIANT determines the simulation has terminated. The data transfers between the codes requires that different data unfolding operations be performed to translate the data into forms which are consistent for each code. ARIANT stores the thermal power for each of the thermal hydraulics channel groups. NESTLE-C provides power at each of the 4,560 bundles in the core. When NESTLE-C provides power, the full array of 4,560 bundle powers is transferred to ARIANT. The data are ordered as 12 axial planes of 380 values. Each value is mapped to the corresponding thermal hydraulics channel group and summed to obtain the total power in each thermal hydraulics channel group.

NESTLE-C maintains an internal array representative of the in-core local thermal hydraulic conditions. Specifically, the coolant density, temperature, and fuel temperature. The data are stored using a time dependent grid which is initialized at run time from an input file. In standalone transient simulations, this file is interpolated in time to provide NESTLE-C with up-to-date estimates of local thermal hydraulics conditions. No interpolation is performed in coupled simulations. Instead, new thermal hydraulics data overwrite the initial thermal hydraulics data and the code always applies these new data between data exchange times.

Separate data sets are provided for each thermal hydraulics channel group. However, NESTLE-C needs to account for the flow direction when mapping these data to the core geometry. In NESTLE-C, this is implemented by grouping the first 14 thermal hydraulics groups as being in front-to-back order, while the latter groups are in back-to-front order. As a result, the numbering of thermal hydraulics groups used by NESTLE-C differs from that used by ARIANT. Prior to transmitting the updated thermal hydraulics data, ARIANT re-orders the data from its representation to that used by NESTLE-C. Figure 12 illustrates the thermal hydraulics numbering scheme used by NESTLE-C, which needs to be translated from the specification presented in Fig. 5.

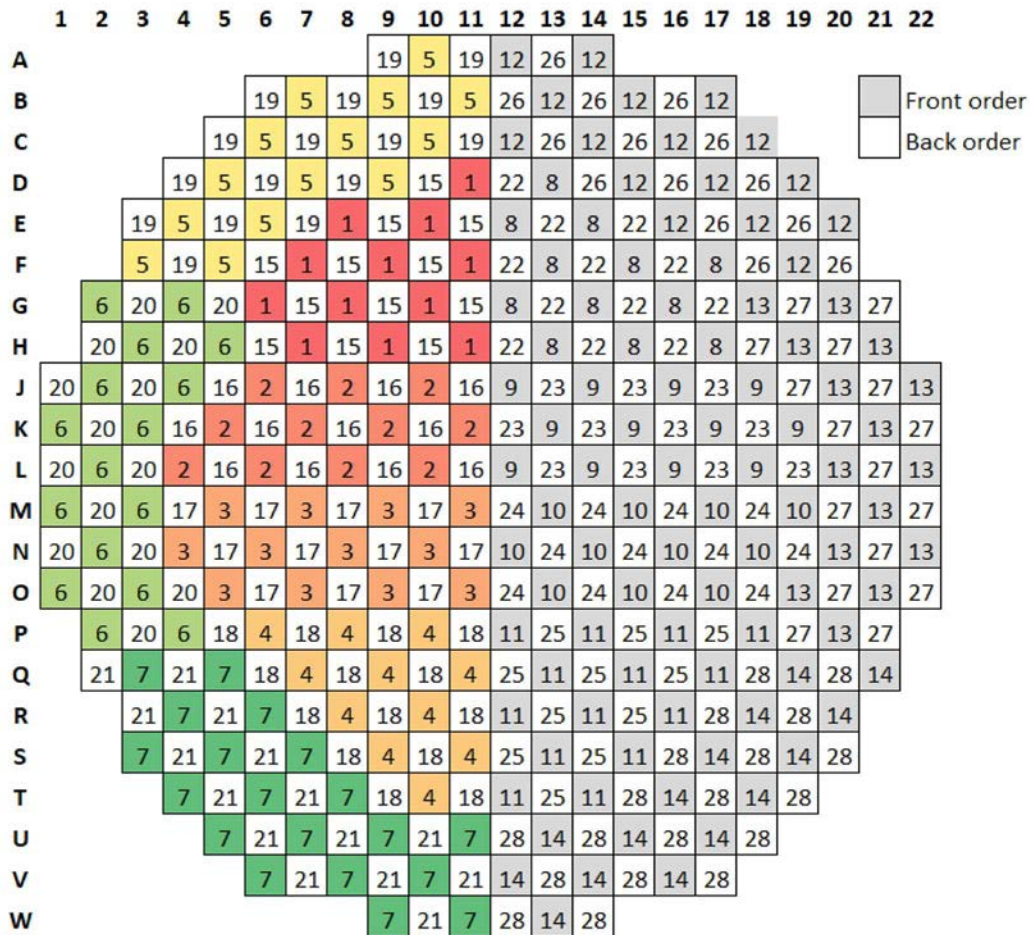


FIG. 12. Thermal hydraulics group numbering, NESTLE-C convention.

4.2.4. Procedure for execution of coupled simulations

Prior to executing coupled simulations, a series of standalone NESTLE-C and ARIANT simulations are performed in an iterative manner, see Fig. 13. Starting from the Problem 1 specifications, NESTLE-C is first executed. The resulting power distribution is translated to ARIANT input and a standalone ARIANT simulation is then performed. The pressurizer loop isolation valve is left open for the first 100 s of this simulation. The isolation valve is then closed, and the simulation continues for another 100 s. The resulting in-core local thermal hydraulics conditions are then communicated to NESTLE-C, and a new iteration cycle is initiated. Once five such cycles are completed, convergence testing is initiated. The process terminates once convergence is achieved, or once the maximum number of iterations is reached. Initial conditions are then copied over to the respective coupled cases and the coupled simulations are launched.

Table 16 lists the convergence criteria. Both neutronics and thermal hydraulics outputs are factored. Convergence is tested by comparing values obtained between successive iterations. Several outputs are treated as vectors, such as channel powers, header pressures etc. For these outputs, two types of criteria are specified: the root mean square difference between the distributions (RMS), and the maximum absolute difference (MAXDIF). In the present work, the system converged within a total of 5 iterations. However, this is largely due to the fact that the Problem 1 specifications were based on older NESTLE-C/ARIANT simulations. The initial conditions were therefore already close to the converged state.

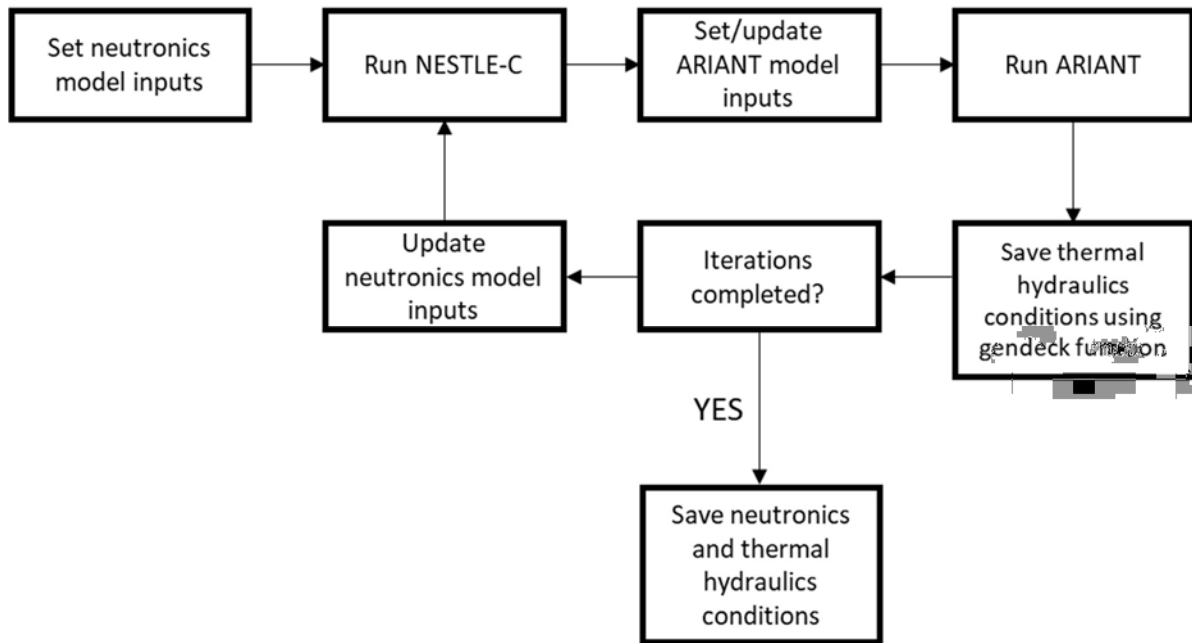


FIG. 13. Workflow for NESTLE-C/ARIANT steady state iterations).

TABLE 16. STEADY STATE CONVERGENCE CRITERIA

Test	Limit	Unit	Test	Limit	Unit
Δk_{eff}	0.10	mk	Header V MAXDIF	1E-5	N/A
$\Delta \text{max channel power}$	0.10	MW	Pump flow RMS	0.5	kg/s
Channel power RMS	0.05	MW	Coolant density RMS	0.005	g/cm ³
Channel power MAXDIF	0.05	MW	Coolant density MAXDIF	0.001	g/cm ³
Header P RMS	0.0005	MPa(a)	Coolant temperature RMS	0.1	°C
Header P MAXDIF	0.001	MPa(a)	Coolant temperature MAXDIF	0.1	°C
Header T RMS	0.005	°C	Fuel temperature RMS	0.1	°C
Header T MAXDIF	0.01	°C	Fuel temperature MAXDIF	0.1	°C
Header V RMS	1.00E-03	n/a			

4.2.5. Deviations from specifications

No deviations from specifications.

4.3. CANADIAN NUCLEAR SAFETY COMMISSION

4.3.1. Codes and methods

The version of the NESTLE computer code for CANDU applications, herein referred to as the NESTLE-C core simulator, was developed under sponsorship by the CNSC as a ‘standalone’ computer code [18]. NESTLE-C was developed from the original version of NESTLE [19], applicable to light water reactors and used in several research projects supporting CNSC staff regulatory reviews. The code was converted in 2012 to the Fortran 90 standard by the University of Tennessee under a research contract sponsored by the CNSC [20]. Other code updates were carried out to modularize and modernize NESTLE-C in a manner consistent with the latest updates performed with the parent NESTLE code for light water reactor applications [21]. The code was transferred in 2014 to CNL for further development and maintenance.

NESTLE-C is a few-group neutron diffusion code based on the nodal expansion method. NESTLE-C can solve eigenvalue, adjoint, fixed source, and transient problems. Originally limited to solving two or four energy group problems, NESTLE-C was updated to accommodate a general multigroup structure using cross sections generated by the SERPENT code. NESTLE-C can solve the time independent eigenvalue problem using either a finite difference or nodal expansion method. The nodal expansion is based on a quartic expansion of the flux. Moment closures and continuity relations are used to construct a system of equations representing node-to-node interface currents. The solution of this system is used to correct the coupling coefficients used in the finite difference solver. The finite difference solver outer iterations are accelerated using either the Chebyshev polynomial or Weiland Shift methods.

For this work, NESTLE-C Version 3.0 was used to model the standalone physics variant of Problem 1. A particular focus of this work was to enable a comparison of the NESTLE-C results to those from the transport code COMET [22]. Four distinct cases were run including the reference, full core voided, full core checkerboard voided and half a core checkerboard voided case, with each problem being performed both with and without the presence of adjuster rods. Detailed comparisons of these trials can be found in *COMET_NESTLE-C_CP_Comparison.xlsx* and *COMET_NESTLE-C_Key_Parameter_Comparison.xlsx* in the CNSC submission.

4.3.2. Special procedures for processing problem specification data

The NESTLE-C input file structure is well suited to the information contained in the specification data files. No special procedures beyond the general reorganization of the data were required to translate the inputs into a format amenable to NESTLE-C.

The NESTLE-C output provides a relative power distribution in lieu of the absolute bundle or channel powers. A post-processing utility was developed in 'R' to obtain the bundle power and channel power maps from the NESTLE-C output files. A copy of this script can be found in the *File_Converters* folder of the submission.

There was no code coupling required in service of this problem.

4.3.3. Deviations from specifications

The NESTLE-C input structure is broken into a series of files relating to; Geometry, Fuel Burnup, Devices, Modelling Methodology, Thermal hydraulics, Cross Sections and Kinetics. As stated in Section 4.1.1, this work was structured to facilitate comparisons between the COMET and NESTLE-C codes. To that end, there are some noted differences between the specifications and the inputs used in NESTLE-C. For each input file category, the sources of the inputs used in the problems are detailed below:

Geometry: The x - y - and z -core geometry, meshing, lattice dimensions and bundle dimensions were taken from the *core_specs.xlsx* file. Boundary conditions were matched to those specified in Section 3.3.

Fuel Burnup: The burnup distribution and values were matched to those specified in Section 3.3. It is noted that this distribution is slightly augmented from the one in the *transport_neutronics.xlsx* file.

Devices: Adjusters of a singular type (with inner and outer regions) were included with incremental cross sections aligned with the GATECH model for COMET. Adjuster guide tubes

were included only in the regions where adjusters are present and were extended neither above nor below them. Adjuster x -positions were aligned with the *device_specs.xlsx* file whereas y - and z -positions were aligned. No zones or other reactivity devices were simulated in this work.

Modelling methodology: Two solution methods were used in this work; the finite difference method (FDM) and the nodal expansion method (NEM). Results for both solution methods are provided.

Thermal hydraulics: The coolant density, coolant temperature and fuel temperature are aligned with the GATECH model for COMET. For voided cases, a value of 0.001g/cm^3 is used.

Cross sections: Cross section coefficients, reference conditions and isotopic composition were taken from the *core_specs.xlsx* file.

Kinetics: Kinetics data is not applicable to the standalone steady state (transport) neutronics case.

Other: For consistency with the GATECH model for COMET, the NESTLE-C power density was tuned to get a core power of 1,900 MW, rather than 2,000 MW.

4.4.CANDU ENERGY INC. AND CANDU OWNER'S GROUP

4.4.1. Codes and methods

To perform the multi-physics simulations two primary codes were used: one for the neutronic calculations and one for thermal hydraulic calculations. The neutronic code used was RFSP version 3.5.2.2 [23], while the thermal hydraulic code used was CATHENA version 3.5.5.1 [24]. Both are summarized below.

RFSP is a code used to perform neutronic analysis of a CANDU type reactor core. The code is modular including the ability to calculate instantaneous or time average flux distributions using finite difference two group diffusion theory. RFSP is used throughout the Canadian nuclear industry for design, safety and compliance monitoring simulations. Its primary function for the purposes of this work is to solve both the time independent and time dependent neutron diffusion equations in three dimensions and two energy groups using a mesh based numerical scheme. The time dependent solutions are obtained using the Improved Quasi Static (IQS) method. In the present case, the neutron kinetics module CERBERUS is used for this calculation. Owing to the nature of the problem, several RFSP functions that would typically be used to perform transient problems like the ones here needed to be bypassed to comply with the problem specifications. These are discussed in greater detail below.

CATHENA is a one dimensional, two fluid thermal hydraulics computer code designed for the analysis of two phase flow and heat transfer in piping networks. The hydrodynamic model used in CATHENA is a one dimensional, two fluid nonequilibrium representation of two phase fluid flow. The model consists of individual mass, momentum, and energy equations for the gas and liquid phases together with flow regime dependent constitutive relations that describe mass and momentum, and energy transfers across the interface and between each phase and the piping walls. The thermal hydraulic model in CATHENA includes pipe, volume, reservoir, T -junction, and tank components and uses a staggered mesh, one step, semi-implicit, finite difference solution method, which is not transit time limited. In the numerical solution method used, a linear system of finite difference equations is constructed as a result of the time and spatial integration of the partial differential mass, momentum, and energy conservation

equations over finite time steps and finite space (nodes or links) intervals. In the CATHENA numerical method, the time step is selected based on the rates of change of a set of parameters including pressure, void fraction, phase enthalpies, phase velocities, and wall temperatures.

4.4.2. Special procedures for processing problem specification data

The RFSP code was used for the physics modelling of the transients. However, the neutronic modelling and test problem specification format are based on input frameworks for other codes, for which some of the methods and formatting are not consistent with RFSP modelling. Consequently, many functions that reside within RFSP that are normally used in analysis were performed by scripts outside of the code. They include:

- Calculation of fission product concentrations (Xe-135, I-135, Sm-149, Pm-149);
- Calculation of the impact on cross sections by the above fission product concentrations;
- Calculation of the impact of local (fuel temperature, coolant temperature, and coolant density) parameters on the homogenized cross sections.

Moreover, while the specification supplies a burnup distribution and the homogenized two-group cross sections as a function of burnup, the typical method of introducing these cross sections (i.e. input fuel tables where cross sections are a function of fuel thermal irradiation) cannot be used. Instead, the fuel thermal irradiation in the RFSP model was co-opted to be used as an index in order to deliver the script calculated cross sections to their appropriate location in the model. The reason for this approach is that RFSP code has no mechanism allowing the user to supply arbitrary cross sections for the diffusion solver.

These scripts were prototyped using Python notebooks. The notebooks facilitated description, organization and review while the scripts were being developed. This scripting mainly supplemented RFSP, although it also executed RCCTS code, which drove the coupling with CATHENA code. The delineation of what each analysis code and script is responsible for is presented in Fig. 14 for the steady state and transient case simulations.

In summary the scripts were responsible for the following:

- Computing bundle-wise reference two group macroscopic cross sections based on the ones supplied by the numerical test problem specification as a function of burnup;
- Applying corrections to these cross sections to account for thermal hydraulic properties using the quadratic expansion formula as supplied by the numerical test problem specification;
- Computing the cell-wise concentration of fission products (either by iteratively computing the steady state concentrations or by iteratively computing the concentrations by advancing through a time-step);
- Applying the correction to the macroscopic cross sections based on the computed fission product concentrations and microscopic two-group cross sections supplied by the test problem specifications;
- Producing input tables to RFSP, using the format of WIMS-AECL uniform parameter tables and WIMS grid tables, with the computed (and corrected) macroscopic cross sections from the test problem specifications;
- Running RFSP, CATHENA and RCCTS codes.

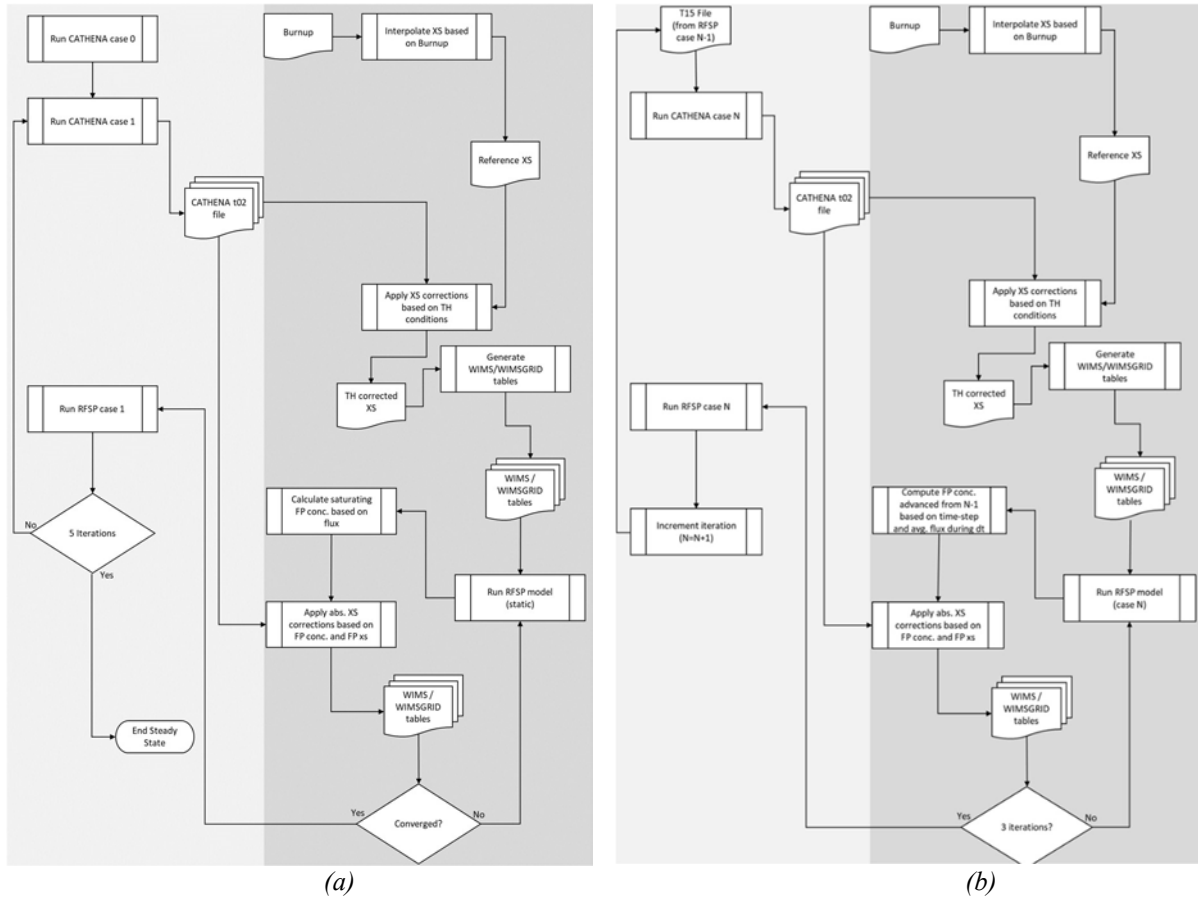


FIG. 14. CEI code coupling framework for coupled (a) steady state and (b) transient calculations.

4.4.3. Coupling framework

A third code, RCCTS, was used to supplement the scripts used to couple the codes. The delineation between the two is illustrated in Fig. 14. The RCCTS module is a Perl suite of routines that execute a sequence of alternating RFSP and CATHENA runs to model hypothetical power transients in a CANDU reactor core for safety analysis.

The key interface information to ensure consistent mapping of data between RFSP and CATHENA codes is the geometry and order of the thermal hydraulic channel grouping. CATHENA does not model each channel individually, but groups them into a smaller number of subsets with consistent flow direction, called channel groups. The in-core portion of each channel group is further broken into a number of nodes equal to the number of bundles in a channel. A certain order is chosen within CATHENA for data to be output for each bundle node of each channel group. An input file is prepared for RFSP that identifies each channel with an ordinal number, from 1 to the total number of channel groups. This defines the order in which the data is expected from CATHENA, and in which data is prepared for input to CATHENA.

The RCCTS code's routines prepare files from the CATHENA output containing average coolant density, coolant temperature and fuel temperature at each bundle node for each channel group at two different times bracketing the time step. These files are input to RFSP. RFSP, in turn, interpolates the thermal hydraulic input data to the correct times for its internal calculations and calculates the total power at each bundle-node location within each thermal hydraulic channel group at the end of the user-specified time step. RCCTS then transfers this information to CATHENA for the next iteration or calculation step. This data transfer between

the two analysis codes is done at user-specified time intervals during the transient calculation. At every time step, each scientific code is executed sequentially: first CATHENA then RFSP.

The RCCTS portion of the overall analysis process is highlighted for steady state and transient calculations in Fig. 14. The initial ‘case 0’ is a standalone CATHENA steady state calculation that sets up the thermal hydraulic reference conditions. The fully coupled steady state calculation is typically referred to as ‘case 1’. This is where minor changes may be made to the reactor conditions relative to the reference conditions. The ‘case 2’ run executes RFSP only, to calculate the adjoint flux required by the Improved Quasi-static methodology for solving the time-dependent neutron diffusion equation. Beyond this, each subsequent ‘Case N’, for $N = 3, 4, \dots$, corresponds to a transient time step.

The script also includes methods that facilitate the set-up of the necessary simulation files, directory structure and certain environment variables required to ensure proper execution of the simulation. It has the capabilities to simulate both slow and fast transients using RFSP dynamic calculation modules along with the tripping of shutdown system number 1.

The RCCTS routines also analyse the RFSP output by preparing data such as tables of power and reactivity, including directional power tilts versus time, and calculation of the maximum total enthalpy associated with the hottest (highest relative radial power) element of the bundle determined by RFSP to have the highest time integrated power to the end of the simulated transient. In addition, the script also consolidates CATHENA output for plotting purposes.

A sensitivity case using a different transient time step may also be carried out as a separate ‘once only’ simulation to confirm adequacy of the chosen time steps. The parameters of interest are the time dependent reactivity and reactor power. They do not vary significantly with a reduction in time step. Steady state convergence is discussed in the subsequent section, including the parameters used to test for convergence.

RCCTS code was used in these simulations to manage the interaction between the two analysis codes. However, due to the non-standard RFSP modelling required to comply with the test problem data specifications, significant supplemental scripting was necessary to facilitate the RCCTS coupling of RFSP and CATHENA (e.g., to cover transient fission products—see Section above).

4.4.4. Procedure for execution of coupled simulations

The first ‘case 0’, is a long 1,000 s thermal hydraulics only simulation performed with the power distribution supplied by the test problem specifications. Only the steady state ‘case 1’, a 100 s thermal hydraulic simulation using the power distribution from the previous neutronics calculation, is iterated by repetition of the CATHENA–RFSP sequence. The methodology to couple RFSP and CATHENA is described in above. Convergence is confirmed by checking that the bundle-node powers change by less than a specified criterion between the last two iterations—this was achieved within five iterations.

The steady state k_{eff} is, as expected, not exactly unity. Also, the flux solution to the eigenvalue equation does not in itself determine the reactor power. RFSP uses the user input power value as well as ‘ H -factors’ derived from the fuel and material properties to scale the power distribution for the steady state. Relative changes calculated for the transient conditions are then applied to this reference power to give the power distribution at each time step.

4.4.5. Deviations from specification

There were no deviations from the specification. However, there are two noteworthy subtleties:

- RFSP did not use the ADF supplied by the specifications. The used version of RFSP code does not have this capacity.
- The neutronic boundary conditions were an extrapolated zero flux at the calandria radius supplied by the specifications as opposed to a zero flux at the mesh face.

4.5. MCMASTER UNIVERSITY

4.5.1. Codes and methods

PARCS v32m21 [25][26] was used for diffusion calculations and TRACE v5p5 [27]–[29] was used for system thermal hydraulics calculations. Steady state and transient coupling were facilitated by custom built Python scripts. Python scripts were also used to extract data from the specifications and generate aspects of the reactor physics and thermal hydraulics models. Additional lattice physics work was performed with the SCALE [30] code system, specifically the NEWT [31] and TRITON [32] modules, to generate an independent set of two group fuel cross sections, and with the SERPENT [33] code, to generate an independent set of control device incremental cross sections. All problems were run with both sets and SCALE results can be obtained upon request.

PARCS code is the U.S. NRC code that solves the steady state and time dependent multi-group neutron diffusion equation in Cartesian or hexagonal reactor geometries. The code allows for several solution methods, including higher order nonlinear nodal kernels, such as the nodal expansion method, and the more standard fine mesh finite difference solver. Cross sections are read into PARCS through PMAX file, which can be generated from the output of a large number of lattice physics transport codes (compatible with SCALE, HELIOS, and SERPENT for example) using the GenPMAX utility [34]. The PMAX file format is very flexible and can allow for any number of different fuel cross sections sets to be defined, each of which can contain multiple thermal hydraulic branch partial derivative cross section coefficients, as a function of burnup. Any number of incremental cross sections can also be defined as a function of burnup. Currently, PARCS allows 12 different thermal hydraulic feedback branches. PARCS also includes adjoint calculation capability, equilibrium and transient Xenon calculations, decay heat calculations, control rod de-cusping, flexible boundary conditions and completely customizable control rod positioning.

TRACE code is also the U.S. NRC code, originally developed for light water reactor analysis, that is being integrated into the Canadian Industry Standard Toolset for CANDU safety analysis. It includes models for multidimensional two-phase flow, nonequilibrium thermodynamics, and generalized heat transfer, among others. The equations described two phase flow and heat transfer are solved using finite volume numerical methods. A TRACE model is built using component models. Each physical piece of equipment in a reactor can be represented as some type of built in TRACE component, which is further nodalized into some number of cells over which the equations are solved. In this work, the PIPE, PUMP, HTSTR, POWER, and BREAK (boundary conditions) components were used. A fundamental philosophy of the TRACE code system is limiting the user effect. As such, the user is limited in their ability to choose or modify key constitutive relations and closure models such as single and two phase pressure drop correlations, two phase heat transfer correlations, etc. In this way, the TRACE code is less flexible than traditional tools used for CANDU safety analysis, such as CATHENA,

but at the same time, is more straightforward to use. With respect to compliance with the numerical test problem specifications activities, there were two major restrictions on this point: (1) the inability to turn off pressure drop due to area change, and (2) the inability to specify or modify break flow correlations.

4.5.2. Special procedures for processing problem specification data

ARIANT and CATHENA are node and link codes, which means that a single flow area, hydraulic diameter, and K -factor are defined for each node, and a single velocity is calculated for each node. TRACE and RELAP on the other hand are node and two cell edge codes, which means that two flow areas, hydraulic diameters and K -factors are defined for each cell edge, and two cell edge velocities are calculated. These differences are summarized in Fig. 15, where bolded quantities are calculated by the code, and un-bolded quantities are input parameters. Note that initial values for the bolded parameters are still required as input.

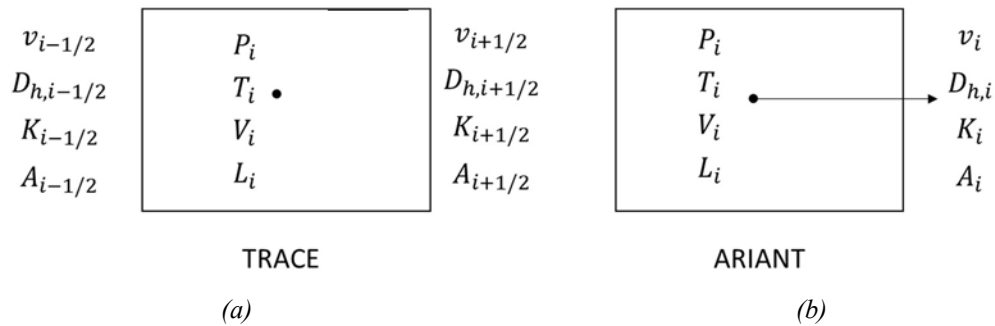


FIG. 15. (a) TRACE/RELAP nodalization and input requirements vs. (b) ARIANT/CATHENA nodalization and input requirements. Notation: v : fluid velocity, D_h : cell or cell edge hydraulic diameter, K : cell or cell edge minor loss co-efficient or K -factor, P : fluid pressure, T : fluid temperature, V : cell volume, L : cell length, A : cell or cell edge flow area.

Problem specifications were originally based on simplified ARIANT models. Because of differences in input requirements, a set of rules was developed to translate the ARIANT input deck into a TRACE input deck. However, it was found that a direct implementation of these rules with no additional modifications or tuning resulted in very poor pressure drop agreement throughout the system, but reasonable temperature agreement. As such, additional modifications to the system model had to be performed.

4.5.3. Coupling framework

The transient coupling methodology used in this work is a straightforward marching algorithm where information (power distribution and thermal hydraulics variables) is exchanged between PARCS and TRACE code on a constant, user defined information exchange time step, as shown in Fig. 16. Since no convergence criteria is used between iterations, information exchange time step sensitivity studies were performed for all transients. It was found that an information exchange time step of 0.05 s was sufficient for the header break transient (0.1 s was too coarse), while 0.1 s was sufficient for both the adjuster pull and pump rundown transients. The PARCS internal time step was set to 0.01 s, such that the end of the PARCS calculation would always line up with the end of the coupled time step, taking either 5 or 10 steps before information is exchanged. TRACE on the other hand, requires the user to provide a range of internal time steps, so it has flexibility if the conditions in the system are varying rapidly. In this work, a range of $0.01-1 \times 10^{-6}$ s was used, such that the maximum time step would always be 5 or 10 times smaller than the coupled time step. TRACE uses a sophisticated internal algorithm to determine which internal time step value to use during the calculation, and will always add

additional time steps, if necessary, so that the calculation ends very close to the user defined end time. As such, while TRACE could take much more than 5 or 10 internal time steps before information is exchanged, it will always be exchanging information at the correct problem time.

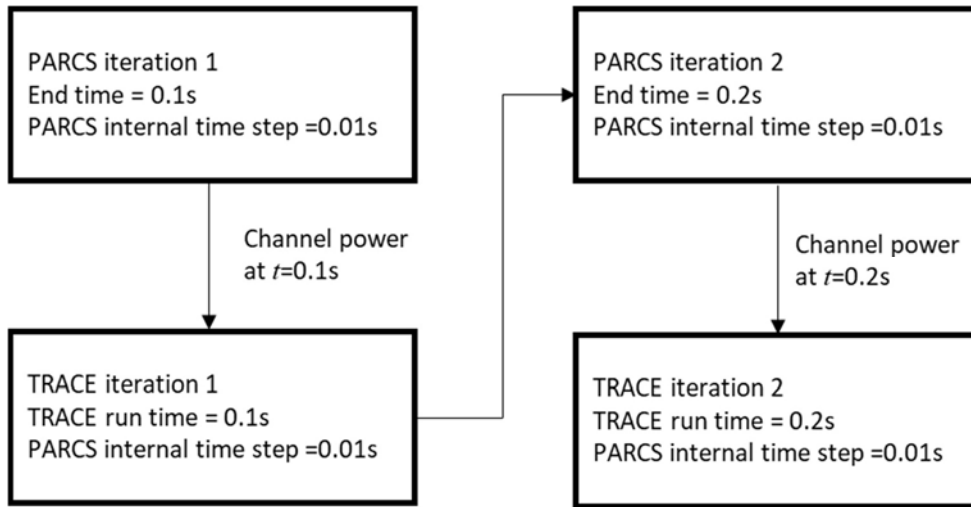


FIG. 16. Illustration of the marching algorithm used in the transient coupling methodology.

4.5.4. Procedure for execution of coupled simulations

Steady state initial conditions that are used to initiate the transient calculations were obtained through a series of steady state Picard iterations between TRACE and PARCS, see Fig. 17. In this method, the two codes are run in the steady state calculation mode with reasonable convergence criteria (or runtimes if convergence cannot be obtained) and information is exchanged between codes at the end of every calculation. The initial channel power and thermal hydraulic variable distributions defined in the Specifications were used to initiate the iterations. This process is repeated until a set of converged initial conditions have been generated. In the context of this exercise, the initial conditions refer to the PARCS channel power distribution, and TRACE thermal hydraulics variable distributions (fuel temperature, coolant temperature and coolant density). While convergence criteria are typically used to define the end of the steady state iterations, the initial conditions can only be said to be converged if they yield a constant core power during a subsequent coupled null transient (a do nothing transient). As such, in the McMaster methodology, no specific steady state convergence criteria were used. Instead, after each steady state iteration a null transient test was performed to see if a constant core power was obtained. It was found that as little as 3 Picard iterations were required to generate converged initial conditions that yielded a constant core power during coupled null transients. This was tested with both the specified cross sections and the independently generated SCALE cross sections. These results can be seen in Fig. 18 and Fig. 19. The transient calculations were initiated from these same conditions. For PARCS, a tight convergence criterion of 1×10^{-10} was used on all steady state parameters (k_{eff} , global and local fission sources). For TRACE, however, it was found that with the burnup distribution defined in the Specifications, the code would never converge to reasonable steady state convergence criteria (1×10^{-3}) due to the presence of vapour in the system. However, when run as a standalone code using the ideal power distribution defined in the 2018 Specifications, TRACE converges on all parameters in 27 s to a value of 1×10^{-3} . In either case, it was found through inspection of key system results (header pressures, pump mass flow rates), that a sufficient steady state is achieved after 50 s of TRACE runtime.

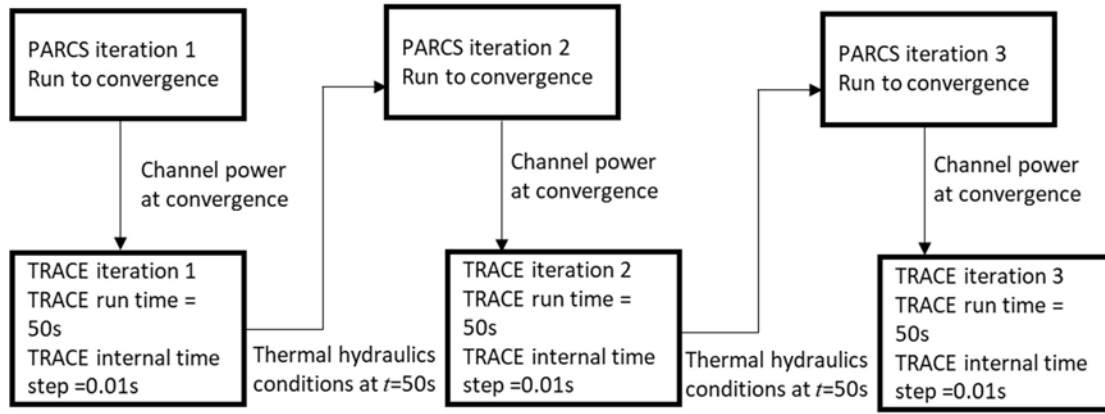


FIG. 17. Illustration of steady state Picard iteration methodology.

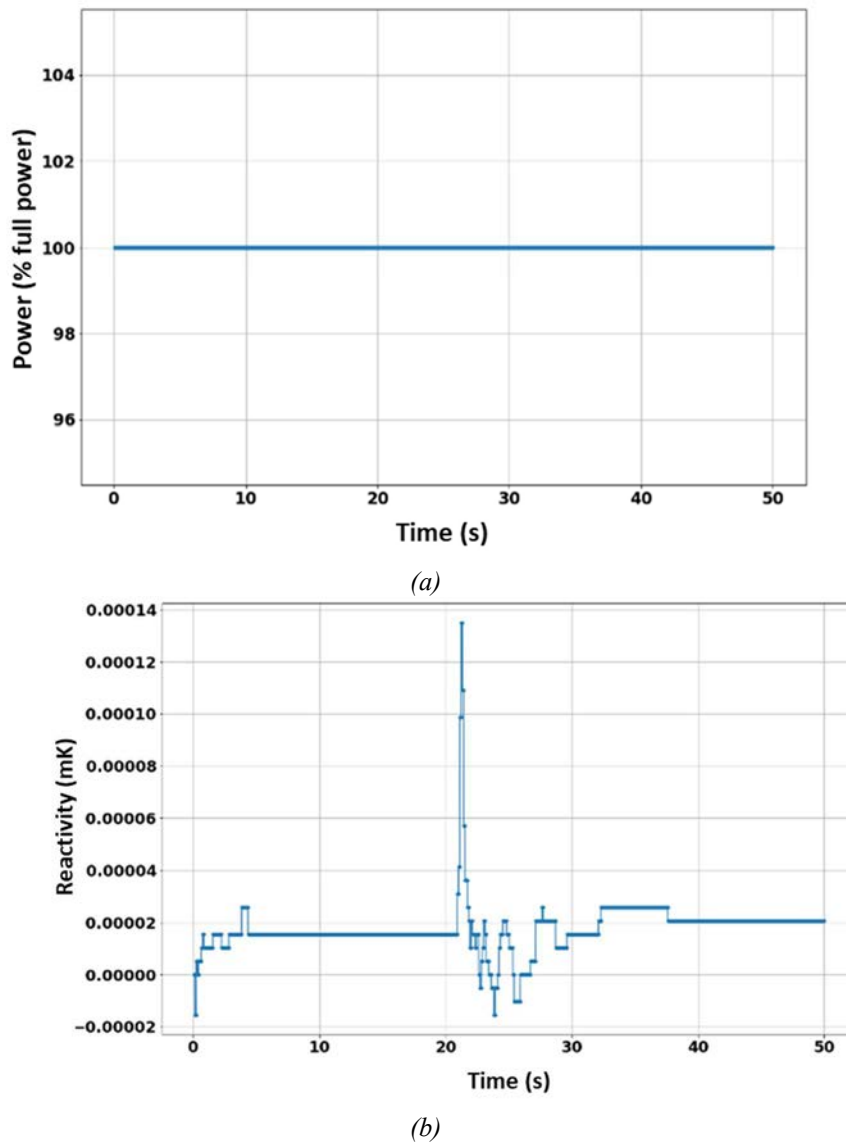
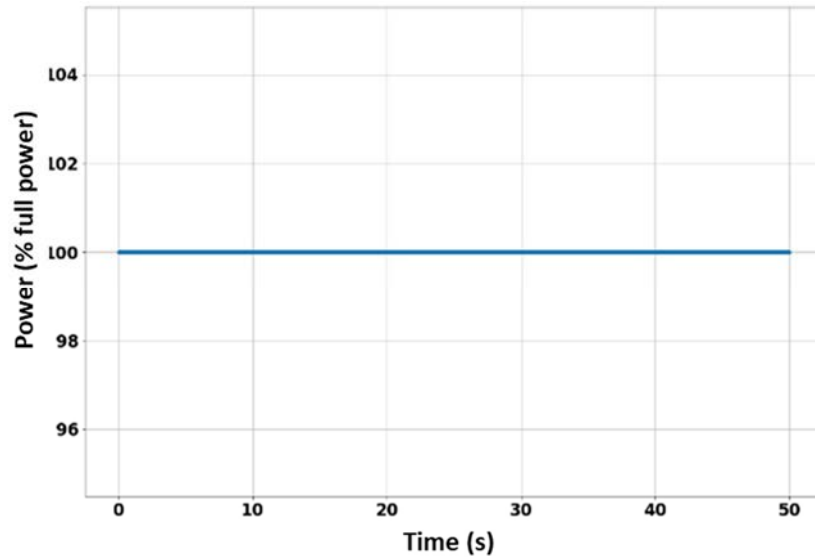
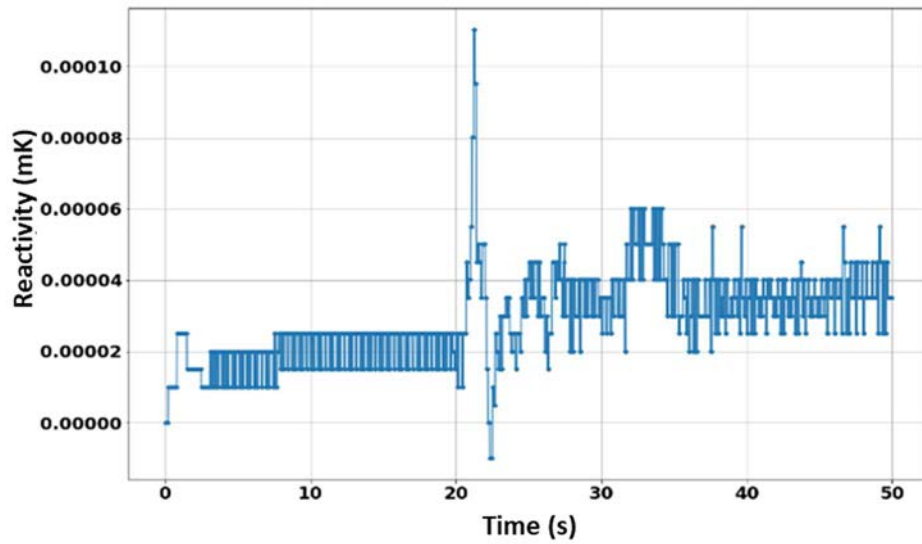


FIG. 18. Coupled null transient results with specification cross section data: (a) normalized core power, (b) core reactivity.



(a)



(b)

FIG. 19. Coupled null transient results with SCALE cross section data: (a) normalized core power, (b) core reactivity.

4.6. BHABHA ATOMIC RESEARCH CENTRE

4.6.1. Codes and methods

The thermal hydraulic safety analysis code RELAP5/3.2 [35] was used for modelling of reactor. It is capable of modelling a wide range of system configurations from single pipes to different experimental facilities to full scale reactor systems. The configurations can be modelled using an arbitrary number of fluid control volumes and connecting junctions, heat structures, core components, and system components. Flow areas, volumes, and flow resistances can vary with time through either user control or models that describe the changes in geometry associated with damage in the core.

The RELAP5 heat structures are one dimensional models with slab, cylindrical, or spherical geometries. Other system components available to the user include pumps, valves, electric

heaters, jet pumps, turbines, separators, and accumulators. The code is based on a nonhomogeneous and non-equilibrium model for the two-phase system that is solved by a fast, partially implicit numerical scheme to permit economical calculation of system transients. In addition to calculating the behaviour of a reactor coolant system during a transient, can be used for simulation of a wide variety of hydraulic and thermal transients in both nuclear and nonnuclear systems involving mixtures of steam, water, non-condensable, and solute. The code includes many generic component models from which general systems can be simulated. The component models include fuel rods, control rods, pumps, valves, pipes, heat structures, reactor point kinetics, electric heaters, jet pumps, turbines, separators, accumulators, and control system components. In addition, special process models are included for effects such as form loss, flow at an abrupt area change, branching, choked flow, boron tracking, and non-condensable gas transport. The heat transfer model is an important model as the chemical reactions are governed by the accurate temperature determination of fuel pins. Heat generated in the fuel pins is conducted through the fuel pins and transferred to the surrounding environment by means convection and radiation. The code is validated against several PWR standard problems as well as for RD-14 M Standard Problems PHWRs [36].

4.6.2. Special procedure for processing problem specification data

A special procedure was used to apply the specified standalone thermal hydraulics power tables. The table provided consists of power map of entire core at 0.1 s time interval. This is equivalent to specification of 28 channels by 12 bundles in every channel. This tantamount to 336 data points at every 0.1 s time interval. Hence total data handled is 84,000. To convert this data, which was provided in excel sheets, Linux bash scripts were developed which can read the data from the data files and convert it into the format of input deck suitable to RELAP5. Since RELAP5 has a limitation of 99 data points to be used in general table, several such tables were generated using the above mentioned bash scripts, each consisting of 99 points. The replacement option of RELAP5 was used in combination with restart option to replace the 99 points table with next 99 points and so on. This way, it was possible to simulate the transient by providing the entire power table data in the form of several restart files. Thus, to cover 25 s transients one initial run of 5 s and four restart runs each of 5 s are used.

4.6.3. Coupling framework

Thermal hydraulic model: RELAP5/3.2 code specific model was developed as per the given guideline of the ICSP. The nodalization of primary heat transport system is furnished in Fig. 20. The nodalization includes loop 1 and loop 2 flow paths, feeders, headers, primary coolant pumps and steam generator. Twelve number of control volumes are used to model for one group of coolant channel.

There are 28 groups to model 380 coolant channels of the reactor. Nodalization of Pass 1 of loop 1 is shown in Fig. 21.

Seven groups of the channels have been considered for the reactor core modelling. Similar modelling for other passes and loop 2 is carried out following the guidelines. Fuel bundles and steam generator tubes are modelled with solid cylinder and hollow cylinder heat structures respectively. Each node of the channel heat structure represents several fuel elements, i.e. 37 multiply the number of fuel channels represents one thermal hydraulics channel group.

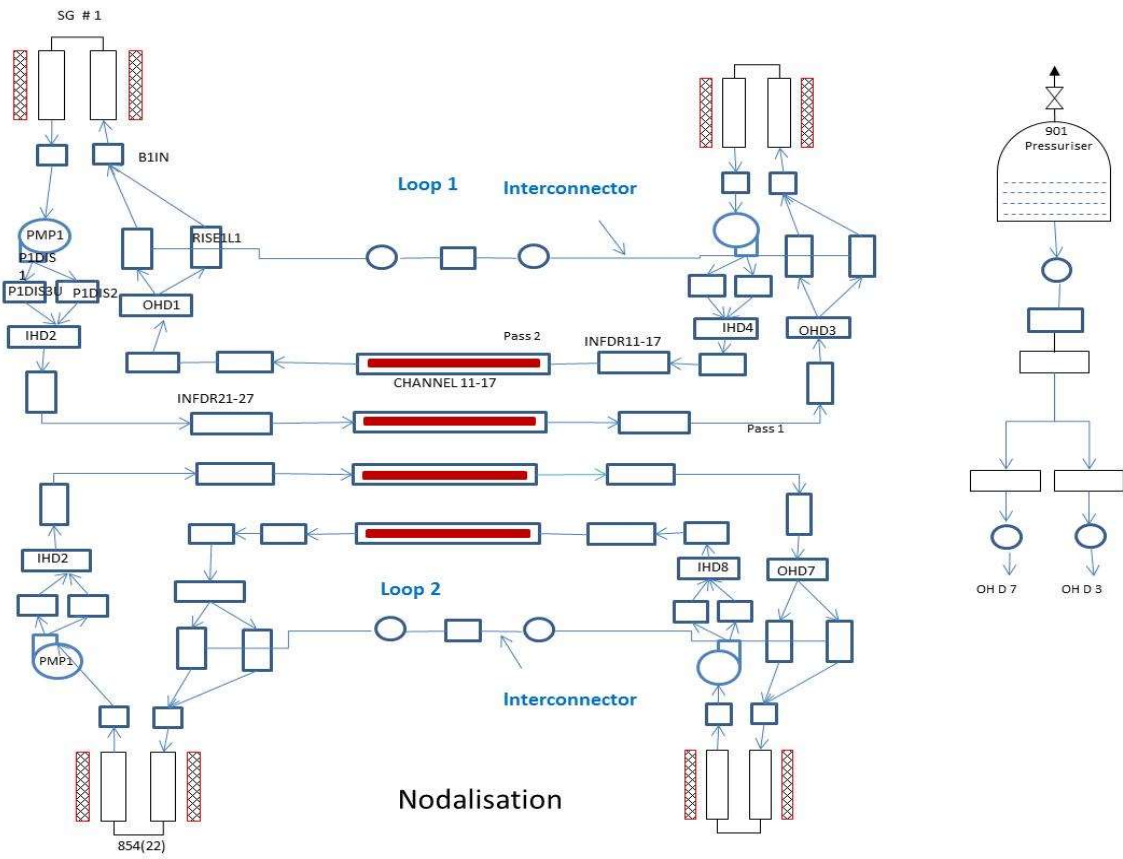


FIG. 20. Nodalization of primary heat transport system.

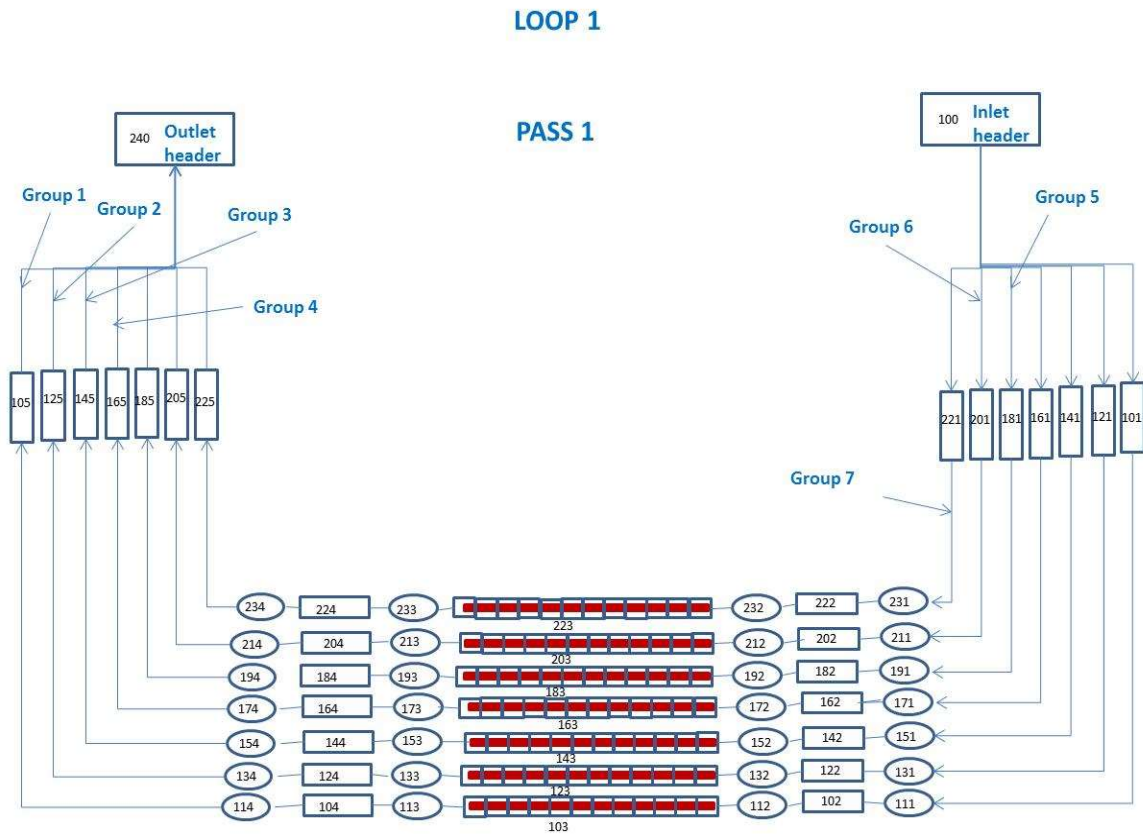


FIG. 21. Nodalization of pass1 (loop 1) PHWR reactor.

Reactor physics model: Multipoint kinetics with internal coupling technique was used for modelling of reactor physics for two loops of PHWR. The reactor is treated with two nodes representing loop 1 and loop 2. However, for LBLOCA transients four nodes are considered for the core. The set of equations together with the geometry shown in Fig. 22 are used for modelling of reactor physics:

$$\frac{dP_h}{dt} = \alpha_{hh} \frac{P_h}{l_h} + \alpha_{kh} \frac{P_h}{l_h} + (\rho_h - \beta_h) \frac{P_h}{l_h} + \sum_{i=1}^{m_d} \lambda_i C_{ih} \quad (8)$$

$$\frac{dC_{ih}}{dt} = \beta_{ih} \frac{P_h}{I_h} - \lambda_i C_{ih}; i = 1, 2, \dots, m_d \quad (9)$$

$$\frac{dP_k}{dt} = \alpha_{kk} \frac{P_k}{l_k} + \alpha_{hk} \frac{P_h}{l_k} + (\rho_k - \beta_k) \frac{P_k}{l_k} + \sum_{i=1}^{m_d} \lambda_i C_{ik} \quad (10)$$

$$\frac{dC_{ik}}{dt} = \beta_{ik} \frac{P_k}{l_k} - \lambda_i C_{ik}; i = 1, 2, \dots, m_d \quad (11)$$

$$\alpha_{hh} = \omega_{hh} v_h I_h \quad (12)$$

$$\alpha_{kh} = \frac{\omega_{hk} \sum_{jh} V_h v_h I_h}{\sum_{jh} V_k} \quad (13)$$

$$\omega_{ihk} = \frac{D_i A_{hk}}{V_h \Delta_{hk}} \quad (14)$$

$$\omega_{ihh} = \sum_{k=1, k \neq h}^z \omega_{ihk}, i = 1, 2 \quad (15)$$

where:

\sum_f	macroscopic fission cross section
λ_i	decay constant of i^{th} delayed neutron group
β_i	delayed neutron fraction of i^{th} group
D	diffusion coefficient
α	coupling coefficient
v	neutron velocity
A	interface area between nodes
V	volume of a node
P	power of a node
C_i	delayed neutron concentration of i^{th} group expressed in terms of power
m_d	number of delayed neutron groups
l	prompt neutron lifetime

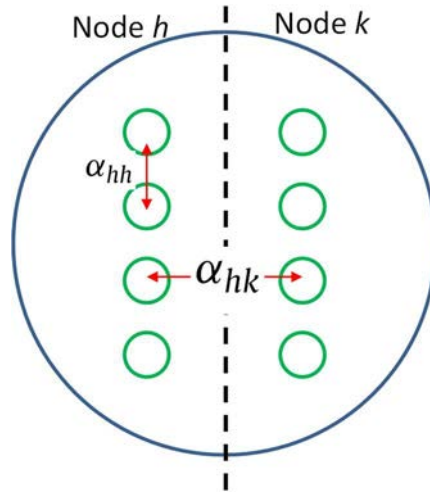


FIG. 22. Multipoint representation of a reactor core

Details of the multipoint model formulation and comparison of the formulation with standalone reactor physics code is furnished in [37].

Control variable feature of RELAP5 code is used for formulation of above equations. The local thermal hydraulics parameters (coolant density and voids) are used to calculate the total reactivity feedback. A predefined (i) coolant density vs. reactivity table, (ii) void vs. reactivity table (iii) fuel temperature vs. reactivity table and (iii) time vs. shutdown reactivity table are used to calculate the total reactivity feedback. The reactivity tables are generated *a priori* using lattice physics calculations performed using CLUB [38] and the IAEA supplied ENDF/BVI 69 group nuclear data library.

Data transfer: The reactivity feedback is further used in the above-mentioned formulation to calculate powers of each node of core heat structures, representing fuel bundles. The code convergence is based on mass error and no neutronic parameters are involved in code convergence. A time step sensitivity in the range of interval of 1 ms to 1 μ s is tested with respect to break flow rate (in case of LBLOCA) and exchange of information (thermal hydraulics and neutronics). Based on the study, 1ms time step is chosen for execution of the code as not much difference is observed on maximum break flow rate, void generation and power rise for the LBLOCA transient. Hence all the cases are run with 1ms time step.

4.6.4. Procedure for execution of coupled simulation

The thermal hydraulic steady state is achieved without reactivity feedback for 1000 s and with a constant power input of 2,000 MWth. After achieving the thermal hydraulic steady state, the multipoint kinetics model is evoked in the restart. The excess reactivity is balanced with a bias value to keep the reactivity very close to zero and power at 2,000 MWth. After attending a steady state with reactivity feedback, a steady state is declared to be achieved with respect to thermal hydraulics as well as for reactor physics.

4.6.5. Deviations from specification

Thermal hydraulic specifications have been followed; however, the number of thermal hydraulics groups has been reduced from 28 to 7. Flow loss coefficients are adjusted to get an acceptable pressure drop profile. However, the total flow rate settled at a slightly lower value (–0.1%) of the specified value. The steady state reactor pressurizer level was found to reach equilibrium at a height of 14.19 m as opposed to 11.4 m. The neutronics model differs

significantly from the specifications, owing to the use of the multi-point kinetics model. An additional parameter coupling coefficient is used to couple the core regions represented by different elements of the multi-point kinetics model.

4.7. KARACHI NUCLEAR POWER PLANT

4.7.1. Codes and methods

RELAP5/3.4 [35] is used for thermal hydraulic simulation using the nodalization as provided in the numerical test problem specifications as required RELAP input syntax. The RELAP nodalization feature are summarized in the following:

- Two loops, four passes;
- Each pass has seven flow channels;
- Each flow channel has twelve fuel nodes;
- Thus $12 \times 7 \times 4 = 336$ fuel axial nodes;
- 12 axial and 13 radial nodes for each fuel heat structure;
- Four pumps with homologous curve, six valves and three breaks;
- Total number of volumes = 1,335;
- Total number of flow paths = 1,375;
- Total number of heat structures = 1,166;
- Total mesh points of heat structures = 7,880;
- Steam generator tube heat transfer coefficient and sink temperatures slightly reduced;
- Primary coolant mass ≈ 125.7 tons D₂O and volume = 158.8 m³;
- Heat transport pumps data as provided in Appendix II;
- Heat structure properties as per specifications;
- Point kinetics for core power transient.

CITATION-2 code [39] was used for three dimensional flux/power distribution. The code is a steady state code that uses finite difference method for solving multi-group diffusion equation. Since CITATION is a steady state code, the coupling assumes that the transient term $\frac{1}{v} \frac{\partial \phi}{\partial t}$ is small compared to the other terms of diffusion equation. Point kinetics is used to predict core bulk power transient. The spatial power distribution follows the steady state distribution at each time step as calculated by CITATION code. Important features of CITATION nodalization is summarized in the following:

- The meshing and spacing is based exactly on the data provided in the specifications:
 - X direction: 46;
 - Y direction: 30;
 - Z direction: 30;
 - Total mesh points: 41,400.
- The boundary condition is set to zero flux at all boundaries;
- Burnup dependent cross sections used as provided in the specification.

A FORTRAN program provides the interface between RELAP and CITATION for data exchange and input preparation for CITATION at each time step.

4.7.2. Special procedures for processing problem specification data

The RELAP nodalization is similar to that provided in the specifications as shown in Fig. 9. The input file is prepared by keying in all data manually from TH_Network_Specs.xlsx. The

initial axial and radial power are taken from the ‘Bundle_Power’ worksheet for the 12×28 nodes. The fuel and clad thermal properties are taken from Appendix I.

4.7.3. Coupling framework

The hydrodynamic part of RELAP code provides the coolant density and coolant temperature whereas the heat structures of RELAP provides fuel temperature. These three variables for each of the 12×28 volumes in the core are used as feedback parameter to update cross sections for the CITATION code. The CITATION code provides the core power distribution for the 46×30×30 mesh points which are separately lumped into 12×28 thermal hydraulic node. It should be mentioned that power is produced in the active nodes only and not in all 46×30×30 mesh points. The lumped 12×28 power values are supplied to RELAP code along with reactivity (in dollars) which is derived from effective multiplication factor provided by CITATION. This is explained in Fig. 23. The data transfer between the two codes is done through a FORTRAN program. The same program calls both RELAP and CITATION during each time step.

For the core bulk power calculation by RELAP, the reactivity (in dollars) is provided to RELAP from k_{eff} calculated by CITATION. The normalized power calculated by RELAP is multiplied by 2,000 MW and fed back to CITATION code input. The Coolant density, Coolant Temperature and Fuel Volume Averaged temperature of the 12×28 RELAP nodes are processed by FORTRAN program for mapping them into CITATION mesh points of core region using mapping array. Data is transferred at each computation step. A time step of 0.05 s is used for steady state convergence till 100 s. The transient is simulated at a time step of 0.01 s. CITATION convergence criteria required maximum relative changes in the flux and eigenvalue of 10^{-4} and 10^{-5} respectively.

For RELAP, the simulation is done on time marching. The time stepping is 0.05 s for steady state up to 100 s. During transient a time step of 0.01 s is used. The convergence of any iterative calculations is dealt internally by the code.

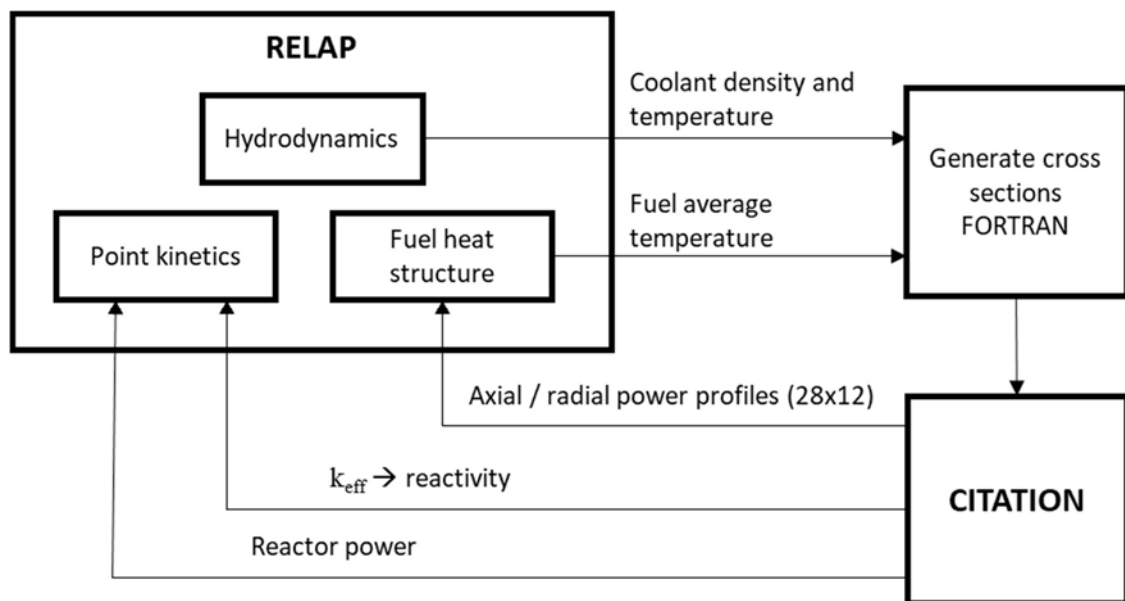


FIG.23. Coupling framework for CITATION and RELAP5 Mod 3.4

4.7.4. Procedure for execution of coupled simulations

The steady state of coupled calculations is obtained in 100 s as follows. In the first calculation step, the CITATION code is allowed to run to provide an initial estimate of power distribution to RELAP. The cross sections for this run of CITATION are based on thermohydraulic data of RELAP input file prepared from ‘Initial_Conditions’ Tab TH_Network_Specs.xlsx. For subsequent runs till 50 s, the CITATION code is not allowed to run and the RELAP parameter are allowed to converge at constant power (2000 MW). After 50 s, the CITATION code is allowed to run using RELAP TH condition. The power profile computed by CITATION is passed to RELAP without reactivity feedback to RELAP till 55 s (i.e., next 5 s). The k_{eff} converges during this period (5s). At 55s, this is assigned the initial value ($k_{eff,0}$) for reactivity calculations. The codes are run for the next 5s (i.e., 60 s) again without reactivity feedback to RELAP. The reactivity feedback is started after 60 s till 100 s to obtain a coupled converged steady state. Any transient is started after 100 s. The pressurizer is isolated from the boundary condition at 90 s (Fig. 24 illustrates).

The reactivity transient is calculated by employing the converged value of k_{eff} provided by CITATION code as:

$$\rho(t) = \frac{k_{eff}(t) - k_{eff}(0)}{k_{eff}(t)} \quad (16)$$

where:

$k_{eff}(t)$ effective multiplication factor provided by CITATION code at time (t);
 $k_{eff}(0)$ effective multiplication factor when steady state is achieved in RELAP/CITATION coupling.

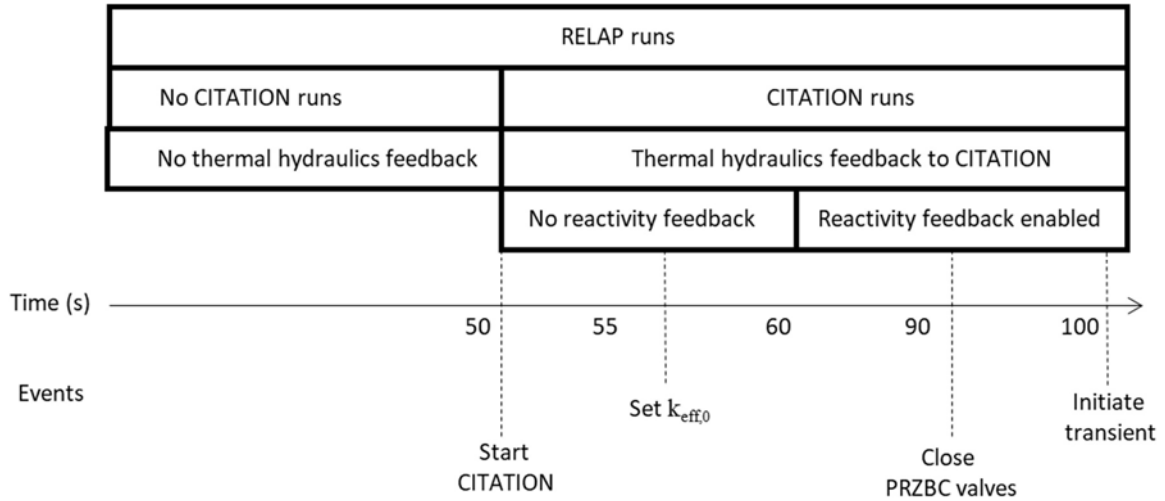


FIG 24. CITATION and RELAP5 Mod 3.4 steady state iterative process.

4.7.5. Deviations from specifications

The hydrodynamic data is based on the specifications except for the VOLUME components, which are special components for which no momentum balance is supposed to be applied. Since, RELAP does not have any special model, these components are bypassed. However, to conserve the loop inventory, their physical volumes is added in the neighbouring volumes.

The volumes specified in the specifications are not used for all components except for Inlet / Outlet Endfittings Dead Volumes and Pump Discharge Volume PnDIS1. These volumes shown significant difference with the RELAP calculated volumes as product of flow area and length given in the specifications. For these components, the flow area is conserved, and the length is internally calculated by RELAP as $\text{Length} = \text{Volume}/\text{Flow Area}$.

The sink temperature of the steam generator secondary side is slightly lowered (530 K instead of 535 K) to come up with an IHD temperature equal to 260°C. Otherwise, the IHD temperature came out around 263°C.

The single ended break is simulated with Henry–Fauske Break Discharge. The given discharge coefficient ($C_v = 0.61$) gave a significantly small initial break discharge flow ($\sim 3,800$ kg/s). The value of C_v was changed to 0.85 to get an initial break flow of about 5,000 kg/s as predicted by ARIANT code.

The heated equivalent diameter (D_h) for fuel channel is calculated using $4 \times \text{Flow Area}/\text{Heated Perimeter}$. The value comes out to be 9.1 mm.

When a junction connects two volumes having different flow areas, RELAP optionally uses smooth area change or Abrupt area change to compute the junction pressure drop. Smooth area change option is used everywhere except the connection between:

- Headers and feeders;
- Boiler inlet/outlet and the neighbouring volumes;
- Volumes specified in the specifications ‘System_Model’ tab column H for reversible loss due to area change.

The CITATION code is a steady state code and RELAP point kinetics is used to predict bulk reactor power transient. The point kinetics require the lumped core–wide effective fractions of delayed neutrons instead of spatial burnup dependent data. Thus, β values, given in the ‘beta–eff’ worksheet of the ‘core_specs.xlsx’ workbook, are not used. Instead, point kinetics data supplied in older specifications (deleted in the final specifications) was used as shown in the Table 17.

TABLE 17. STEADY STATE CONVERGENCE CRITERIA

Point Kinetics Constants		
Precursor Group	Delayed Neutron Fractions	Decay Constants (s⁻¹)
1	0.000295	6.120E–04
2	0.001165	3.155E–02
3	0.001033	1.218E–01
4	0.002350	3.175E–01
5	0.000780	1.389E+00
6	0.000197	3.784E+00
Neutron mean prompt lifetime (s):		9.02E–04

For Xe–135/Sm–149, the average core flux was used for generation of macroscopic cross section. That is, Xe–Sm effects on whole core basis, not on cell basis.

4.8. PAKISTAN INSTITUTE OF ENGINEERING AND APPLIED SCIENCES

4.8.1. Codes and methods

The reactor physics codes used in the simulation are OpenMC⁵ and WIMSD/4 whereas the thermal hydraulics simulations were carried out using RELAP/SCDAPSIM.

OpenMC is an open source Monte Carlo neutron/photon transport simulation code initially developed at the Massachusetts Institute of Technology in 2011 [40]. Since then, it was improved through contribution from the international user's community. It solves k -eigenvalue transport problem under static conditions for a critical or a sub-critical system using continuous energy or multi-groups. The problem geometry can be developed using built-in models or can be imported from the supported solid geometry software. The accuracy and execution time of OpenMC depend on the number of histories and generations. For present problem, a dedicated study was carried out to see the effect of these parameters on variation of k_{eff} . The values of these parameters, where k_{eff} converges, were used in the simulation.

The WIMS is a reactor lattice physics code developed by AEE Winfrith [41] to calculate neutron flux distribution and an infinite medium multiplication factor for a unit cell. Over the years, it was altered as needed to adjust special types of problems thereby giving rise to the family of WIMS codes. WIMSD/4 is one of its variants. It solves neutron transport equation over the lattice cell to get neutron flux and infinite multiplication factor in a discrete energy and spatial mesh. For this purpose, it requires multigroup isotopic microscopic cross section library and the lattice cell geometry as input.

RELAP/SCDAPSIM Mod 4.0 is the latest version of its kind developed by the SCDAP Development Training Program, administrated and distributed by Innovative System Software [42]. It is a best estimate system code used to simulate a wide range of plant conditions from normal operation to severe accident of light water reactors. It has built-in hydrodynamic and heat structures components along with process models, trips and control systems to simulate reactor transients.

The RELAP5 and the OpenMC are run on different platforms and need a special program to communicate with each other. A program in python is written to execute the reactor physics and thermal hydraulic software and process data obtained in the output files. This program executes OpenMC and process the output file to calculate the channel power and the peaking factor for each thermal hydraulic channel. Then it updates the RELAP5 input file, execute RELAP5 and process the output file to get thermal hydraulic parameters. Then the program updates the fuel temperature, coolant temperature and coolant density in the material.xml file and executes OpenMC for the next iteration.

4.8.2. Special procedures for processing problem specification data

The bin power and burnup have been calculated from the weighted average of the individual bundles given in the problem specifications. The isotopic density calculations for the specified burnup have been achieved using WIMSD/4.

⁵ <https://docs.openmc.org/en/stable/>

4.8.3. Coupling framework

The coupling scheme used in this work is presented by the flow chart as depicted in Fig. 25. A Program in Python is developed which not only executes the codes but also processes and transfers the data between different codes. A step by step description of the coupling scheme is given below:

1. The first step is determination of the isotopic concentrations once at the beginning of the simulation. This is done by WIMSD/4. The Information about the geometric data, fresh fuel material composition and burn-up time inputted from specification sheets to calculate the isotopic concentrations at the given burnup steps.
2. This is followed by preparation of necessary input files (materials.xml, geometry.xml, settings.xml, tallies.xml and plot.xml) required to run OpenMC. These files remain unchanged except the materials.xml file which is updated at each iteration.
3. The OpenMC is then executed. The output file is processed to get bundle and channel powers and their distribution along channel. The Euclidian norm of the core bundle powers is also evaluated.
4. The Python program writes Channel powers into RELAP5 code input file and execute the RELAP5. The thermal hydraulics parameters are extracted from output of RELAP5 and used as an input to OpenMC for next iteration as mentioned in step 2.
5. Steps 2–4 are repeated iteratively using the Python program till result are converged. Convergence criteria is minimum difference of the Euclidian norm between two consecutive iterations.

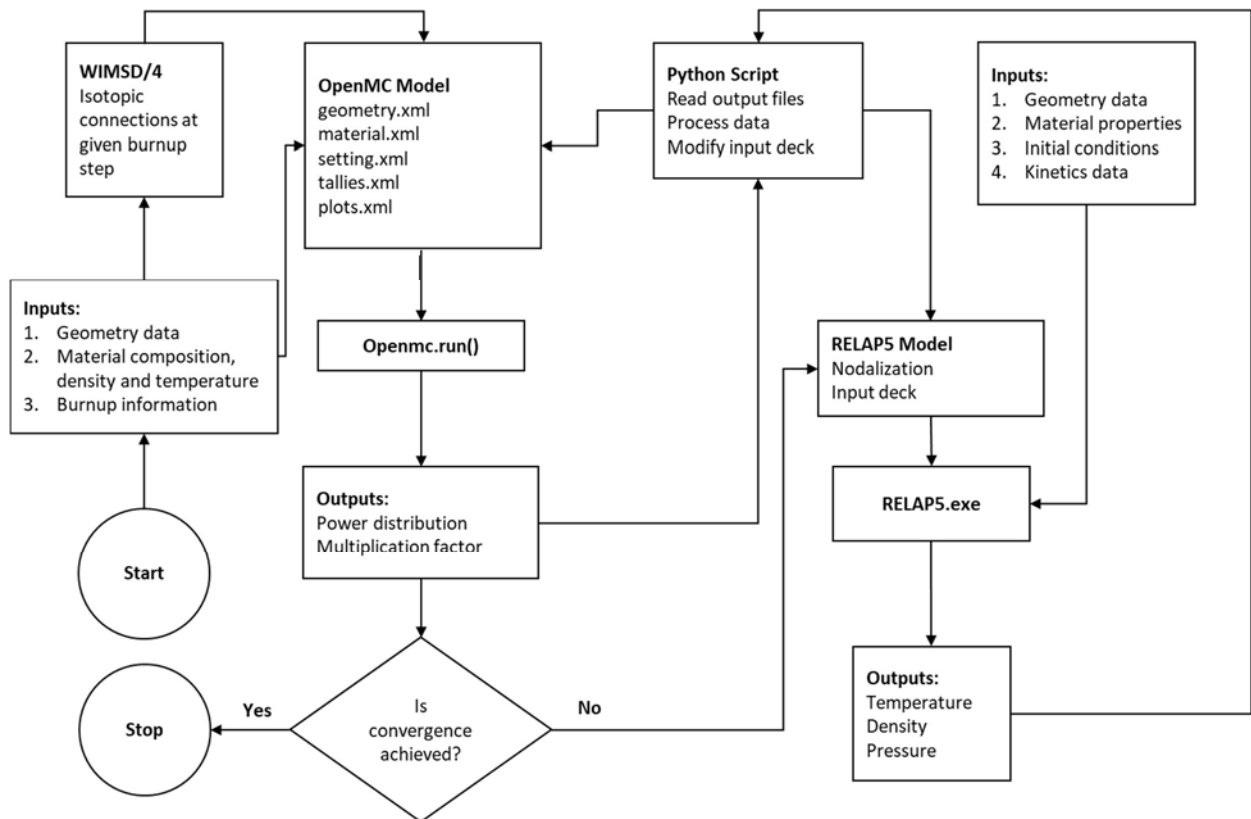


FIG. 25. Flow chart for the coupling of the reactor physics and thermal hydraulic codes.

4.8.4. Procedure for execution of coupled simulations

A program written in Python to manage the steady state coupling of two codes. The OpenMC is used for neutronics calculation and RELAP5 for thermal hydraulic simulation. The transient coupled simulation is not carried out for Problem 2–4.

4.8.5. Deviations from specifications

k_{eff} values calculated as 0.99105 taking B–10 concentration equivalent to (8.1×10^{-7}) atomic weight fraction in moderator. Small adjustments in geometric data were made to achieve the thermal hydraulics steady state values i.e. minor adjustments in loss coefficients to achieve desired flows rates and pressure drops. Transient problems 2–4 are not included in this study.

4.9. CERNAVODA NPP

4.9.1. Codes and methods

RFSP IST is an acronym for Reactor Fuelling Simulation Program Industry Standard Toolset. It is a computer program to do neutronic (static, quasi static and dynamic) calculations for CANDU reactors. The code is modular and has many capabilities including the ability to calculate instantaneous or time–average flux distributions. RFSP is capable of simulating reactor–operating histories, including refuelling and burnup steps. RFSP also incorporates the capability for spatial kinetic calculations, including coupling to thermal hydraulics computer programs. In the present work, our team used RFSP, version 3.5.4.1 [43].

RFSPCB version 2.1.0.2 [44], a suite of routines driven by a Perl script which run RFSP coupled with a thermal hydraulics code CATHENA Mod 3.5d Rev. 2 [45]. CATHENA is an acronym for CANAdian THERmalhydraulic Network Analyses. It is one–dimensional two–fluids thermal hydraulic code. The code is generally applicable to transient, two–phase flow for light water or heavy water in piping networks.

4.9.2. Special Procedures for Processing Problem Specification Data

The irradiations for every fuel bundle were calculated by interpolation using irradiation–burnup conversion table.

The fuel and reflector channel layout, dimension of mesh, lattice arrays and mesh spacing in X , Y and Z directions, location and incremental cross section for movable devices, cross section for REFLECTOR, the β and λ parameters for delayed neutron, 28 thermal hydraulics channel groups arrangement were taken and handled in RFSP format from the following files, listed in the numerical test problem specifications: *Core_specs.xlsx*: neutronic core geometry data, burnup distribution and data library, *Device_specs.xlsx*: neutronic data/geometry for reactivity control devices and *TH_network_specs.xlsx*: network thermal hydraulics geometry and data.

Two types of cross sections for fuel are required by RFSP. The first is the uniform–parameter WIMS tables that were calculated by interpolation. Irradiation interval was of 0.1 n/kb, resulting in 42 irradiation steps. The second is the WIMS grid based tables for reference and perturbed cases. For reference, the cross sections for the 34 irradiation steps, (0.0–4.0) n/kb were taken files and handled in RFSP format. The benchmark specification of cross sections is incompatible with typical RFSP usage which relies on rigorously formatted WIMS tables. RFSP has no way to readily introduce arbitrarily calculated cross sections. For instance, saturating fission product effects in RFSP are either modelled explicitly or captured using

thermal ^{135}Xe cross sections. In the specifications they are captured using two group calculations for ^{135}I – ^{135}Xe and ^{149}Pm – ^{149}Sm . A similar dichotomy exists for local thermal hydraulics condition effects on cross sections. The macroscopic transport and absorption cross sections (SIGT and SIGA) exclude the contribution arising from Xe–135 and Sm–149 and were not recalculated. Following the test problem specifications, all macroscopic cross sections in the fuelled region for perturbed case are recalculated using a quadratic expansion formula in three variables:

$$\Sigma = \Sigma_0 + a(\sqrt{T_f} - \sqrt{T_{f0}}) + b(\sqrt{T_f} - \sqrt{T_{f0}})^2 + c(T_c - T_{c0}) + d(T_c - T_{c0})^2 + e(\rho_c - \rho_{c0}) + f(\rho_c - \rho_{c0})^2 \quad (17)$$

4.9.3. Coupling framework

The coupling processes were run on a standard PC, under Windows platform. The WINDOWS executable files have been used and the duration of the process was dependent by the transient time simulated and by the minimum time step used.

4.9.4. Procedure for execution of coupled simulations

The coupling process is presented in Fig. 26. Separate input models have been prepared for the reactor physics and thermal hydraulic computer codes. The steady state reactor power distribution was obtained by running separately the reactor physics code. The total power and the axial power distribution were transferred to CATHENA model. The CATHENA code was run long enough until the steady state conditions have been achieved. The average coolant density, coolant temperature and fuel temperature obtained at the end of the respective steady state simulation were transferred to reactor physics code. The reactor physics code was run, and a new set of channel power and a new axial power distribution was obtained. The differences between two subsequent channel power distributions were calculated. If the differences between two subsequent steps were below 1%, the steady state was assumed that was reached. Otherwise, the iterative process continued until the acceptance criteria were obtained. During the transient, the very small internal time steps were imposed in order to ensure converge at each time step.

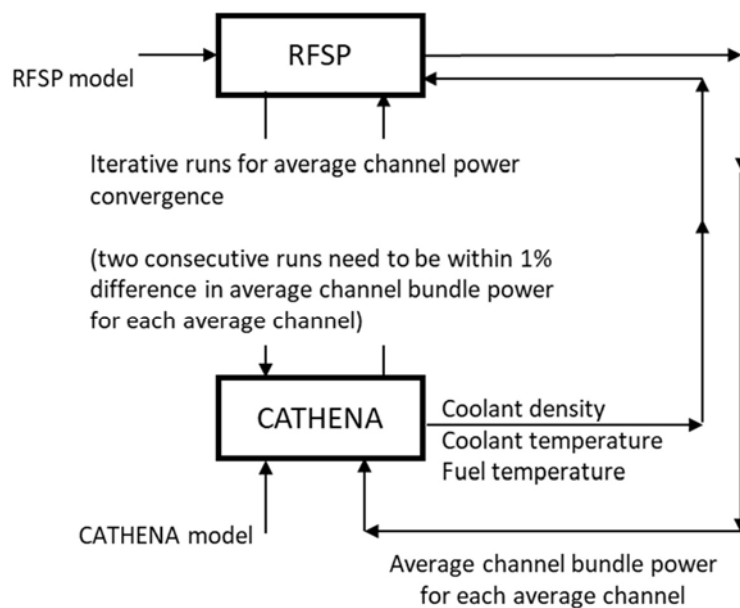


FIG.26. Coupling scheme for RFSP3.5.4.1 and CATHENA Mod 3.5d Rev. 2.

4.9.5. Deviations from specifications

The input for the thermal hydraulic computer code was based on the technical specifications.

The 12 components from each average channel (i.e. CHAN_{xy}_01 to CHAN_{xy}_12) from technical specifications were coupled into one single component representing the respective average fuel channel. The length and the elevation change were calculated as the sum of the individual pipe lengths / elevations change. The flow area / hydraulic diameter / roughness is the same for all 12 components and value presented for one component was included in the model for the average channel. The pipe flow resistances due to minor losses were combined (as a sum) in one equivalent value. The number of axial nodes imposed was 12 (corresponding to the number of bundles in the channel). The volume for the average channel component was calculated as the sum of the volumes of all 12 components for that average channel.

The total power for one average channel was determined by adding the power for all bundles and all components for the respective average channel. The axial relative power distribution was determined by adding the individual data (for the same bundle, corresponding to all average channel components), divided by the total amount (sum of all bundle powers for all components from one average channel).

To get the inlet header temperatures close to 261°C, as specified, the prescribed heat transfer coefficient at the outer surface was slightly changed. The value presented in the specification was kept for steam generator #1 while for steam generator #2 it was increased to 3.24×10^4 . In the same time, for boiler #3, the value was decreased to 2.90×10^4 while for boiler#4 it was increased to 3.15×10^4 , compared to 3.0×10^4 (specifications data for each steam generator).

4.10. GEORGIA INSTITUTE OF TECHNOLOGY

4.10.1. Codes and methods

The coarse mesh transport COMET method, described in detail in [22], is a hybrid stochastic/deterministic tool for the determination of eigenvalue and fission density distribution of a variety of nuclear reactors. COMET solves multigroup and continuous energy eigenvalue, adjoint, fixed source problems, relying solely on transport theory. At the lattice level, COMET performs its modelling and simulation transport calculations as a series of pre-computations, creating a database of response functions necessary to solve any reactor core configuration composed of unique fuel assemblies/bundles and reflector blocks. Since the response function library is generated by Monte Carlo, this allows it to solve problems in full fidelity, with neither homogenization approaches nor low order approximations that can compromise the accuracy of the solution. Even fuel particle level detail can be captured using this method. At the core level, a deterministic iterative process then uses the response function library to construct the core solution. COMET was implemented into Cartesian, hexagonal and cylindrical geometries to perform whole core transport calculations for various reactor cores. Extensive benchmark calculations in water reactors [46], prismatic gas cooled (thermal) reactors [47] and advanced burner fast reactor [48] have shown that its accuracy is close to that of Monte Carlo, while the computational efficiency exceeds that of whole core Monte Carlo or fine mesh transport methods by several orders of magnitude.

For this work, COMET was used to obtain the multigroup reference solutions for the following cases of Problem 1: full core voided, full core checkerboard voided and half core checkerboard voided cases, with each problem being performed both with and without the presence of adjuster rods.

4.10.2. Special procedures for processing problem specification data

No special procedures were required since the COMET input file structure is well suited to the information contained in the specification data files. This is a single physics problem and therefore no coupling of physics was required.

The COMET output provides a normalized bundle and pin power distributions in the core and their uncertainties. A post-processing script in python was developed to obtain the channel power maps from the COMET output files.

4.10.3. Deviations from specifications

Since the Monte Carlo method was used to generate the response function library for COMET, the geometry details and material heterogeneities were fully modelled in the fuel bundle, adjuster rods and reflectors. For consistency with the deterministic transport and diffusion models, the external circular core boundary was approximated as corrugated rectangular meshes and no-re-entry boundary condition was assumed in COMET core calculations. It noted that COMET can model the exact (circular) boundary easily.

5. SIMULATION RESULTS

These numerical test problems are different from the typical benchmark problems in that the specification is designed for a stylized model of a generic CANDU 6 PHWR and a reference solution is not postulated. Detailed specifications have been developed for each test problem. However, the participants were not required to strictly follow the specifications, i.e., except for the initial reactor state and boundary conditions, the choices of data, modelling parameters, and methods used to execute the coupled transient simulation were left to the participants. It is expected, therefore, that differing participant's simulation codes and methods will lead to variation in the submitted solutions to the test problems. The objective is to decompose these variances, in order to gain insight on the impact of different simulation approaches to coupled simulation accuracy.

5.1. ORGANIZATION OF RESULTS

Each test problem is limited to representing reactor physics and system thermal hydraulics phenomena. The steady state was first executed for (a) testing of coupling methods and sensitivities, plus 'tuning of models' in order to (b) achieve similar starting conditions for better comparison of challenging problems results. Two additional sub-problems are defined under each test problem:

1. Neutronics simulations with postulated thermal hydraulics conditions;
2. Thermal hydraulics simulations with postulated power transient.

The purpose of these additional sub-problems is (a) separate testing of neutronics and thermal hydraulics methods and codes, in order to (b) gather complete information for better comparison of the challenging test problem results.

The sub-problems play a significant role in the discussion of the results and identification of main contributors to the differences. The following are illustrative examples of potential main contributors to the differences in the results:

1. Neutronics simulations with postulated thermal hydraulics conditions
 - Method: diffusion, transport;
 - Boundary conditions;
 - Formulation of the diffusion equations;
 - Deviations from the proposed specification;
 - Conversion of data in the specification to the standard input specific to each code (burnup to irradiation, etc);
 - Treatment of saturated fission products (Xe, Sm);
 - Other.

Agreement between results would be a first screening filter for the contributors to the variances in the results of the coupled simulations of the test problems.

2. Thermal hydraulics simulations with postulated power transient.
 - Models;
 - Deviations from the proposed specification;
 - Conversion of the specification to the specific models in individual thermal hydraulics codes, i.e., approximations, omissions, etc.—these are somehow different from the deviations from the proposed specification;
 - Other.

Agreement between results would be a first screening filter for the contributors to the variances in the results of the coupled simulations of the test problems.

3. Coupled neutronics– thermal hydraulics:
 - Differences in the coupling procedure/algorithm;
 - Temporal convergence of the inter-code information transfer: neutronics and thermal hydraulics use different methods to determine the time steps in their internal calculations. Information is transferred at intervals at least equal to the longer of the time steps used by the codes. Since the time steps aren't changed in the coupled calculation from what they would be for independent code runs, it may be argued that the coupling does not lead to any additional requirements for assessment of internal time steps;
 - Spatial convergence of the inter-code information transfer: neutronics codes have a more refined radial/azimuthal mesh (one or two nodes per bundle) when compared to thermal hydraulics (24 channel groups). The information passed from neutronics is collapsed into representative values for the thermal hydraulics channel groups and similarly, when information is passed from thermal hydraulics, it is expanded for neutronics using typically a set of time-independent axial flux values. There is potential impact of using time-independent flux shapes instead of transient axial flux shapes;
 - Other.

Analysis of results from the standalone problems should somehow simplify the discussion of the results for the coupled problem and help focus on issues related to coupling techniques.

5.2. STEADY STATE

5.2.1. Coupled converged case

This problem presents contributions from all participants. Table 18 presents a comparison of neutronic parameters that were selected as the Figure of Merit (FOM) for this problem. The

multiplication factor and all the parameters presented in Section 3.5.1 were included. Multiplication factors have an acceptable dispersion, with a standard deviation of 3 mk. There is also an acceptable agreement in neutronic parameters, except for the FTW, for which the standard deviation is higher than the mean of the reported values. Due to its small absolute value, it was observed that lesser modifications in how this value is obtained can cause important differences. For the rest of the parameters the standard deviation is lower than 10%. It is noteworthy that results from the Cernavoda and CEI teams differ slightly, despite the use of common simulation tools (RFSP and CATHENA). This can be attributed to differences in the approach used to translate test problem specifications into input compatible with RFSP.

Table 19 shows a comparison of thermal hydraulic parameters. The analysis includes pressurizer level (PRESL), power generated by the fuels (P_FUEL), transferred to the coolant (P_COOL) and transferred to the steam generators (P_SGEN), the maximum outlet header void (MAXVOID) and the total mass of coolant on the system (TOTMASS).

For the pressurizer steady state level, a good agreement is found among participants, with the exception of BARC. Most of the participants reach a stationary condition with the pressurizer totally full of liquid water. Some participants found this to be dependent on initial pressurizer level used.

Concerning the loop heat balance, RELAP users show a higher power being evacuated to the secondary side than what is being generated in the core. This is associated with dissipation effects that cannot be turned off in the simulations. CATHENA/ARIANT users show no difference between these values. CEI and McMaster show instead a negative difference between power evacuated to the secondary side and power generated in the core.

TABLE 18. NEUTRONIC PARAMETERS FOR STEADY STATE COUPLED SIMULATIONS

FOM	KEFF	CVW1	CVW2	ADJW	LZCW	FTW
Unit	–	mk	mk	mk	mk	mk
Mean	0.9980	16.2	4.7	15.9	7.1	–0.5
Std. Dev.	0.003	0.5	0.4	0.8	0.3	1.1
CNL	0.9997	16.6	4.9	15.8	7.8	–0.7
CNEA	0.9999	16.2	4.8	14.5	7.0	–0.4
Cernavoda	1.0008	15.6	4.8	15.7	7.0	–
KANUPP	0.9942	16.6	5.0	16.6	6.9	–0.3
McMaster	0.9982	16.7	5.0	17.0	7.1	–2.3
CEI	0.9997	16.3	4.9	–	7.0	1.1
PIEAS	0.9911	16.6	4.7	–	–	–
BARC	1.0006	15.1	3.8	–	–	–

For the reported void fraction, there are two different behaviours: CATHENA/ARIANT users present values close to 0.1, while RELAP/TRACE users have values close to 0.01. BARC presents a higher maximum void compared to the rest of RELAP/TRACE users and this could be due to the use of a different number of thermal hydraulics channel groups. Total masses show a big dispersion and a clear correlation between total mass and void fraction cannot be established for all users.

TABLE 19. THERMALHYDRAULICS PARAMETERS FOR STEADY STATE COUPLED SIMULATIONS

FOM	PRESL	P_FUEL	P_COOL	P_SGEN	MAXVOID	TOTMASS
Unit	m	MW	MW	MW		kg
Mean	11.66	2000.18	2000.21	2000.32	0.10	130868
std. dev.	0.97	0.59	0.69	14	0.11	6572
CNL	11.03	1999.75	1999.87	1999.97	0.08	133843
CNEA	11.40	2000.02	2000.02	2010.57	0.01	138316
Cernavoda	11.40	2000.00	2000.00	2000.03	0.08	134831
KANUPP	11.39	2001.73	2002.00	2008.70	0.03	127838
McMaster	11.40	2000.00	2000.00	1998.80	0.01	137616
CEI	11.10	2000.00	2000.10	1967.30	0.13	132743
PIEAS	11.40	1999.95	2000.00	2000.00	0.12	118909
BARC	14.20	2000.00	1999.71	2017.17	0.18	122851

Table 20 shows a comparison of the maximum channel and bundle power and their location. The standard deviation of those values and the maximum of the mean channel power distribution are also reported. There is good agreement regarding maximum channel and bundle power values, with relative standard deviations lower than 10%. Regarding the location of such maximum there is a bulk of participants that report the same position while two of them found a different one. It should be noted that BARC is one of these participants and is not modelling differences in power within a thermal hydraulics group, so results are expected to differ.

TABLE 20. MAXIMUM CHANNEL AND BUNDLE POWERS FOR STEADY STATE COUPLED SIMULATIONS

FOM	Maximum channel power at 25 s	Maximum channel power location	Maximum bundle power at 25 s	Maximum bundle power location
Unit	MW	–	kW	–
Mean	6.94	S9	855.0	S9_07
Std. Dev.	0.53	–	41.7	
CNL	7.58	S9	929.5	T12_07
CNEA	6.92	S9	851.9	S9_07
Cernavoda	6.93	S9	851.6	S9_07
KANUPP	7.08	S9	883.0	S9_07
McMaster	6.93	S9	866.7	S9_07
CEI	7.02	S9	861.8	S9_07
PIEAS	8.22	P11	869.3	Q10_06
BARC	6.27	M12	768.8	M13–M15–M17–M19–N12–N14–N16–N18–O13–O15–O17_07

Figures 27 and 28 show the distribution of coolant temperature and pressure respectively along the system. differences between extreme values lower than 4 °C and 0.7 MPa, with the exception of the exit of the core (before the outlet header), where the differences on coolant temperature reach 12 °C. The highest differences in pressure are found between pump discharge and core inlet.

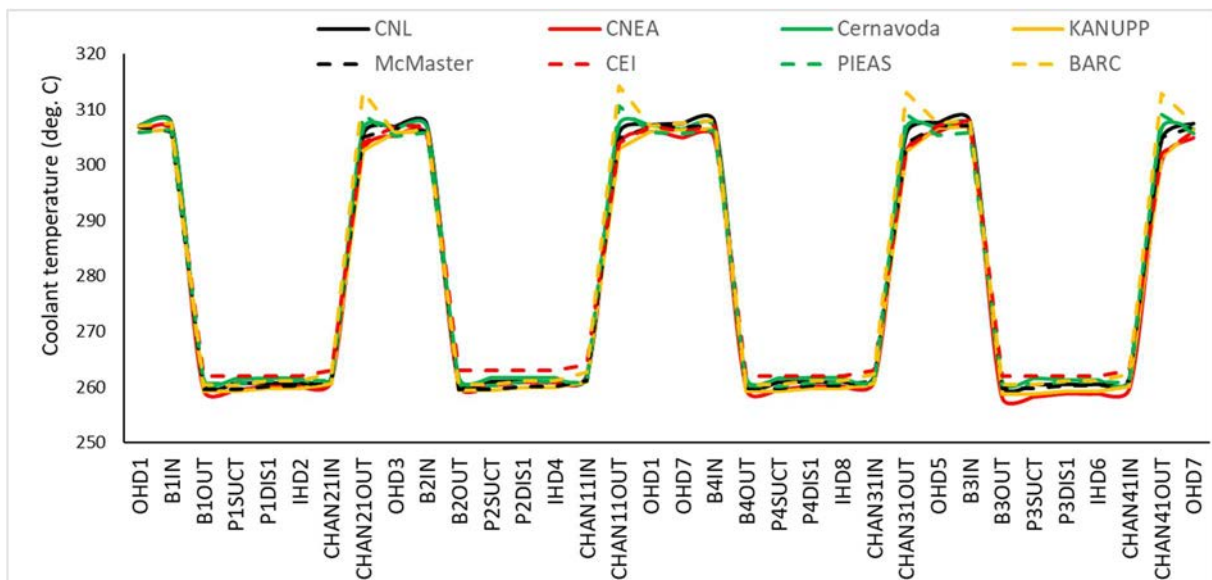


FIG. 27. Coolant temperature profile along the network.

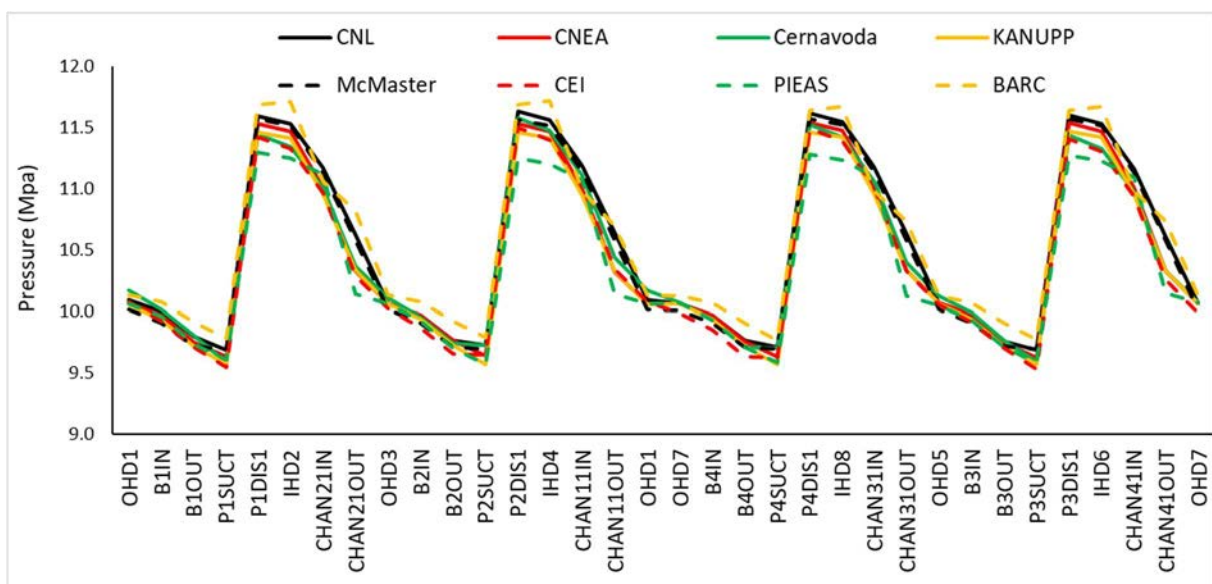


FIG. 28. Pressure profile for steady state coupled simulations.

Figure 29 shows the void fraction profile along some relevant components of the circuit. The results are consistent with the analysis of the maximum void in the outlet header presented in table TP1_1. CATHENA/ARIANT users present higher void fractions along the circuit than RELAP/TRACE users, with the exception of BARC, who presents the highest void fractions in components of loop 1.

A noteworthy feature of BARC results is the strong asymmetry in the void fraction between the two loops. While in one of the loops its void fraction is the maximum from all the contributions (being the only participant that presents a non-null void fraction at the exit of the thermal hydraulics channel 1 pass 1), in the other loop the void fraction is more similar (although a bit higher) to the rest of RELAP/TRACE users. This result could be related to the modifications made in their model.

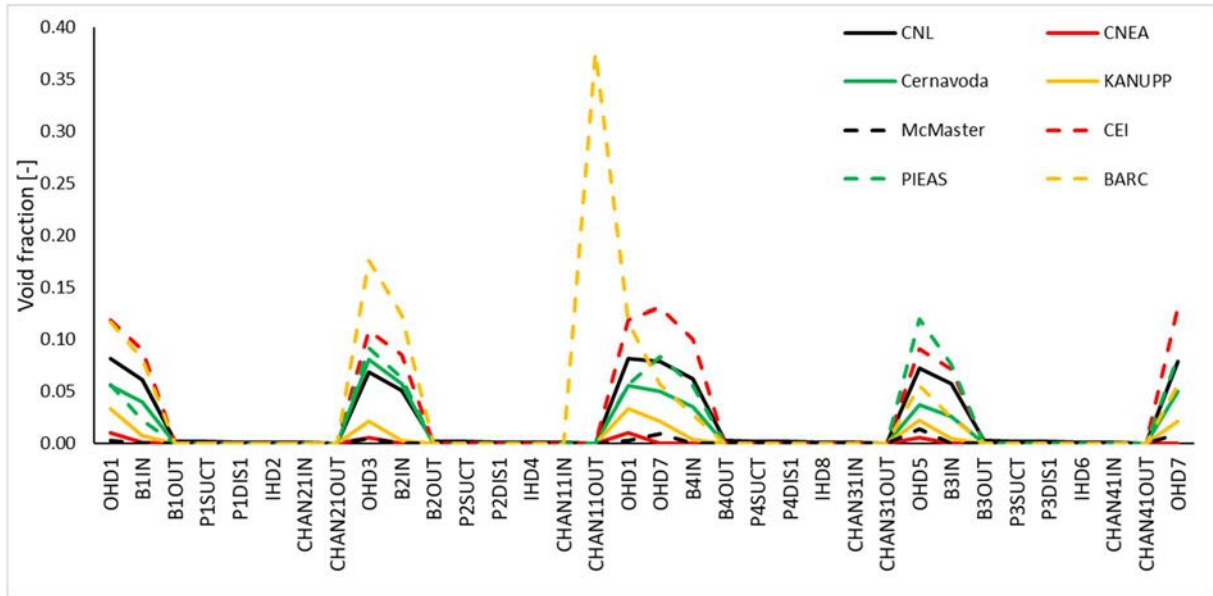


FIG. 29. Void profile for steady state coupled simulations.

Figure 30 shows mean channel power and the relative standard deviation. Higher dispersion of results is found near the border of the core, especially towards the bottom part. Figures 31 to 34 present the participant's differences to the mean channel power. CNEA, McMaster, KANUPP and CEI present a particularly similar power distribution, with up to 10% lower powers than the mean in the periphery of the core and up to 7% larger ones in a ring halfway between the centre and border of the core.

CNL presents a significant shift of power to the lower region of the core, where the channel power is up to 19% higher than the mean; this shift is offset by significantly lower power in the peripheral channels of the upper region; there is also a noticeable difference in the channels affected by liquid zones. Cernavoda presents a flatter power distribution than the mean, with an up to 10% lower power in the centre compensated by an increase of up to 20% of the power channel in the periphery. The opposite behaviour presents PIEAS, with up to 40% more of power at the centre of the core and up to 36% lower in the periphery. Finally, BARC presents higher values in the centre of the core up to 20%, lower values in the middle (up to 35%) and higher values towards the periphery, up to 45%. Additionally, it shows a tilt upwards.

Figure 35 shows mean values and relative standard deviation for fuel temperature. Higher dispersion is found in the middle of radially outermost channel groups. Figure 36 shows mean values and relative standard deviation for coolant temperature distribution. A good agreement is found. Figure 37 shows mean values and relative standard deviation for coolant density distribution. Higher dispersion is found towards the exit of the last channel of each pass and some other channels of pass 1 and 2.

Figure 38 shows participant differences to mean values for fuel temperature distribution. CNEA and CERNAVODA present higher temperatures overall than the mean and BARC lower ones. PIEAS presents a flatter distribution. Figure 39 shows participant differences to mean coolant temperature distribution. A good agreement is found. Two participants show higher differences than the rest. Figure 40 shows participant differences for coolant density distribution. Results are consistent with maximum void fractions in header reported. However, a dispersion of results between participants with similar maximum void fractions in headers is observed. BARC and PIEAS present the biggest differences to the mean.

There is a generally good agreement in steady state parameters and distributions. However, there are some differences that should impact transient simulations and ought to be considered to analyse those results. Some participants tend to have closer results than others, and two groups associated with the thermal hydraulic codes that are used can be identified in some cases. This should be considered when analysing transient results.

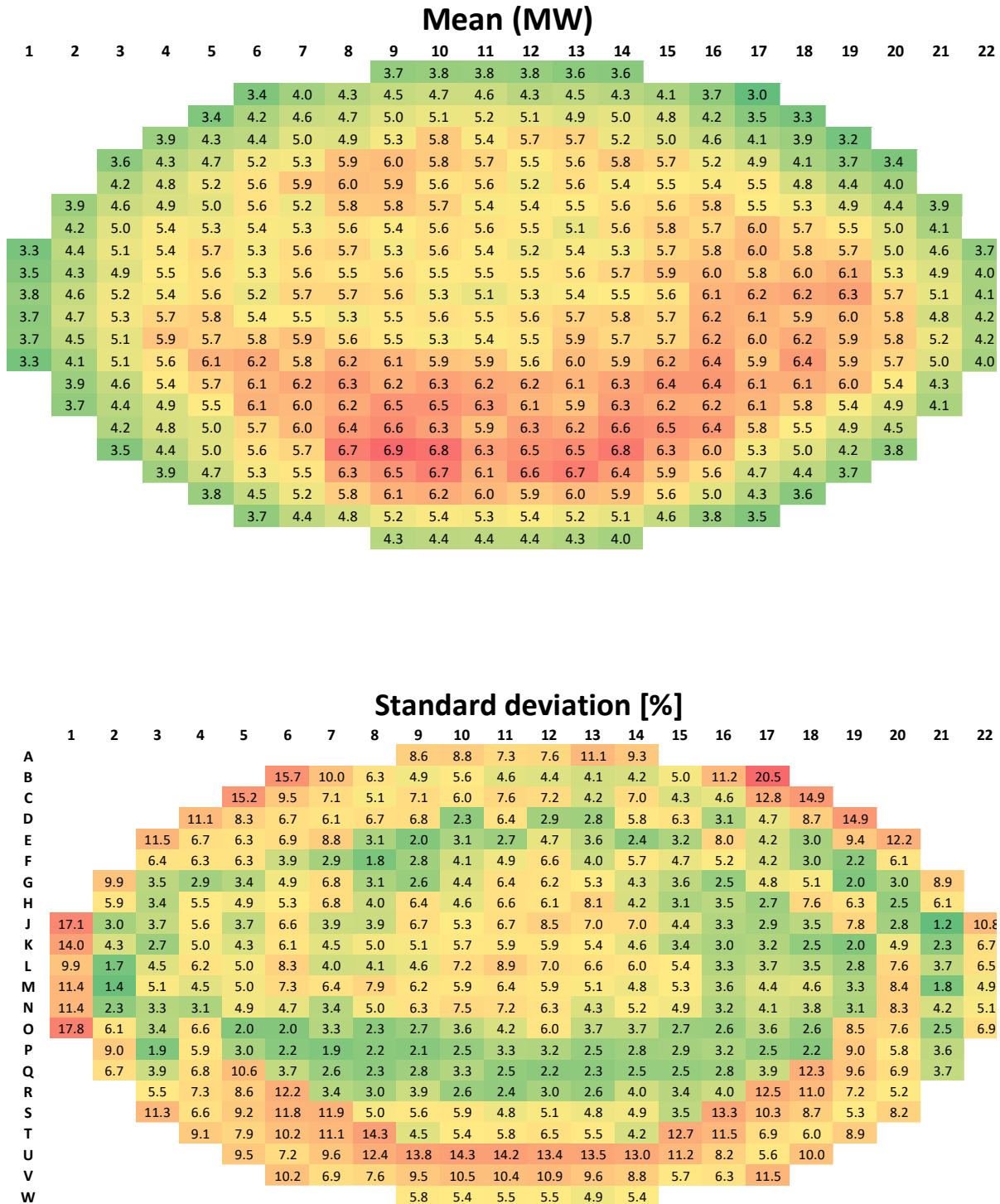


FIG. 30. Mean power channel and relative standard deviation for steady state coupled simulations (MW).

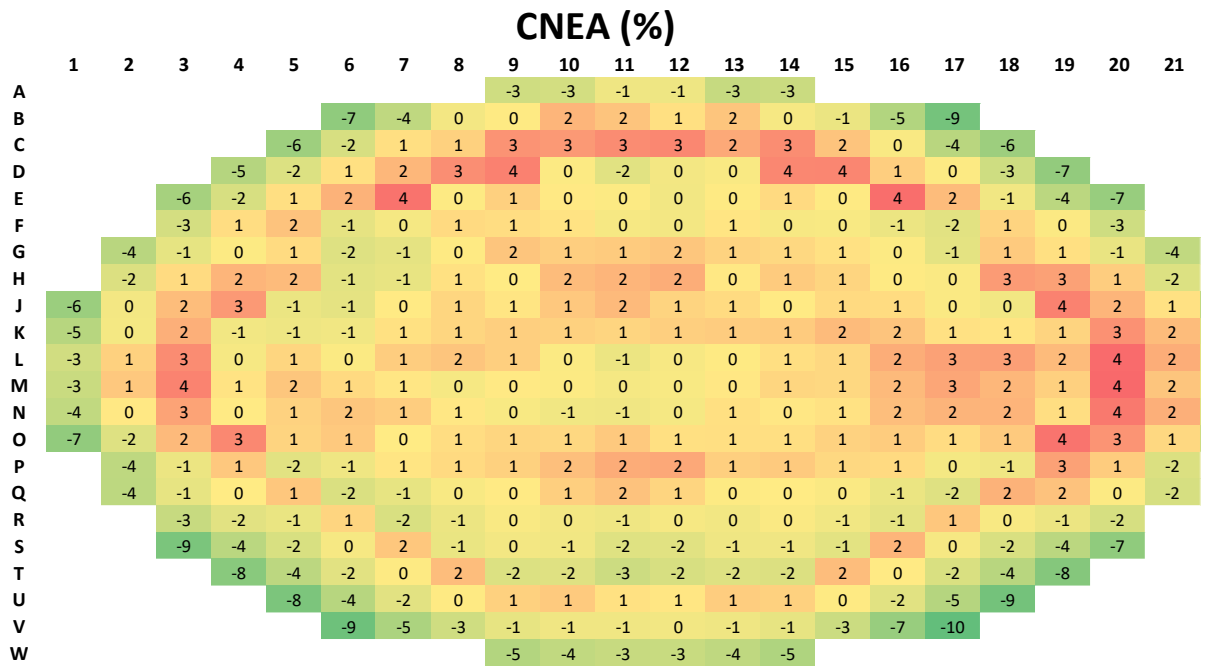
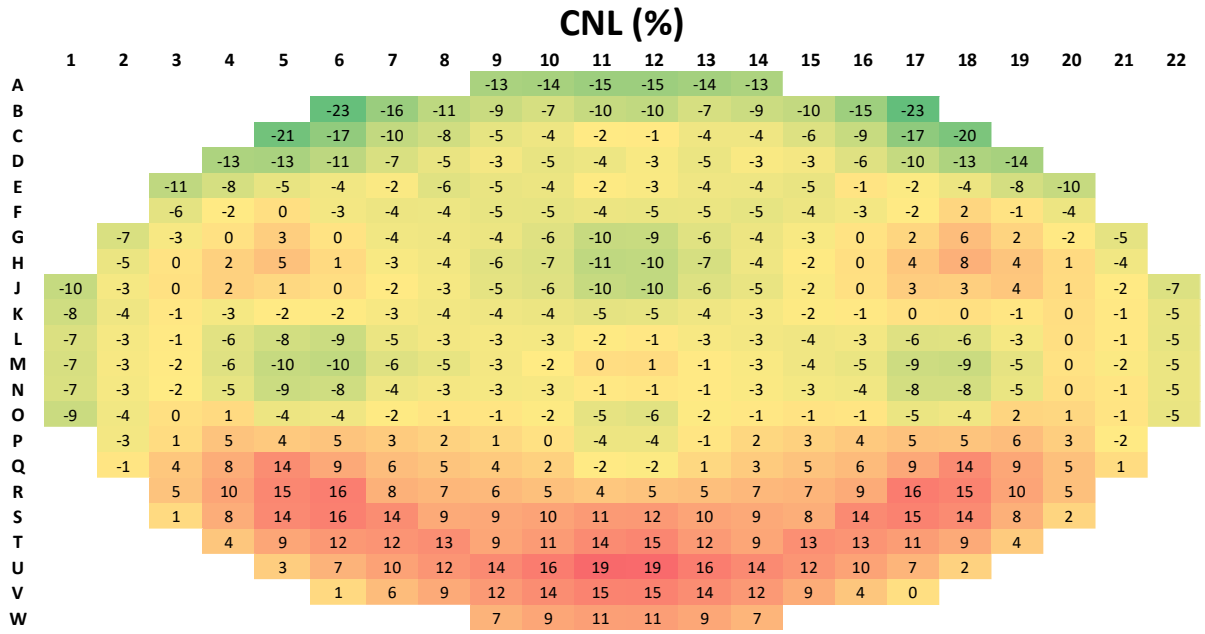


FIG. 31. Power channel differences to the mean for steady state coupled simulations (MW) for CNL and CNEA. A negative value means the participant has lower channel power than the average.

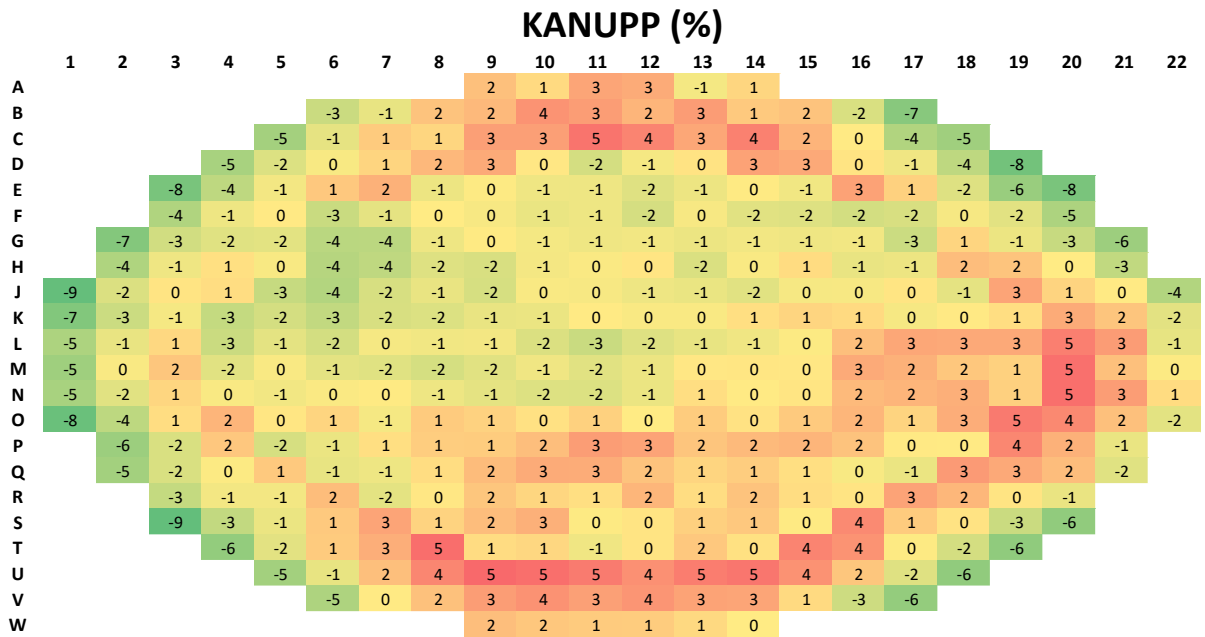
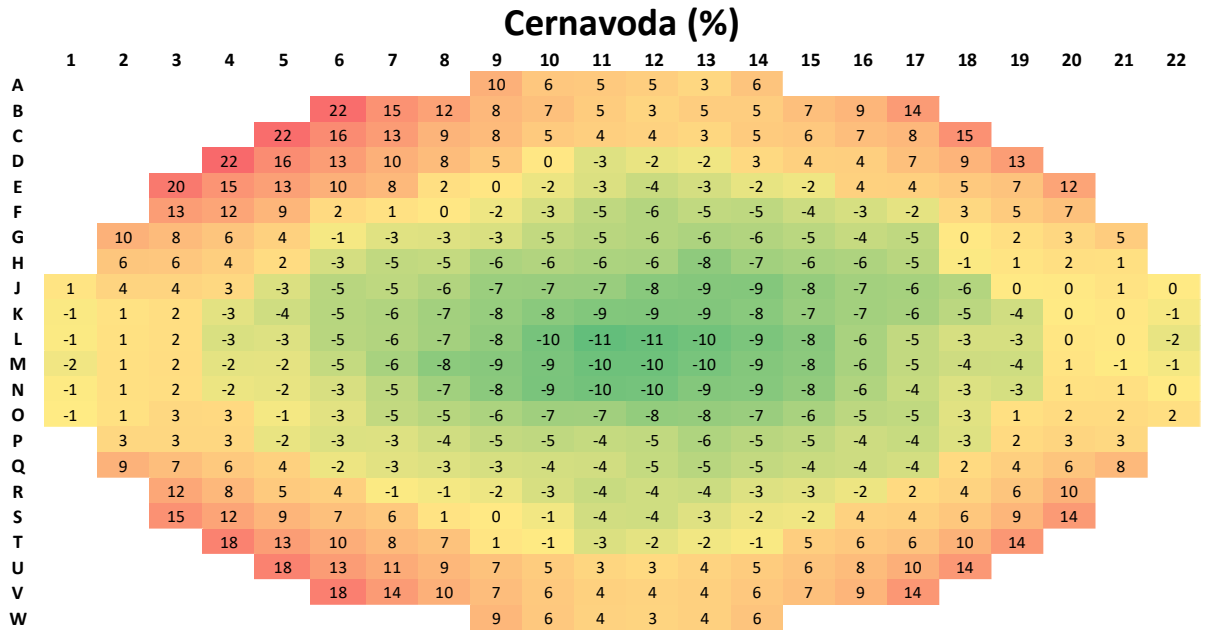


FIG. 32. Power channel differences to the mean for steady state coupled simulations (MW) for Cernavoda and KANUPP. A negative value means the participant has lower channel power than the average.

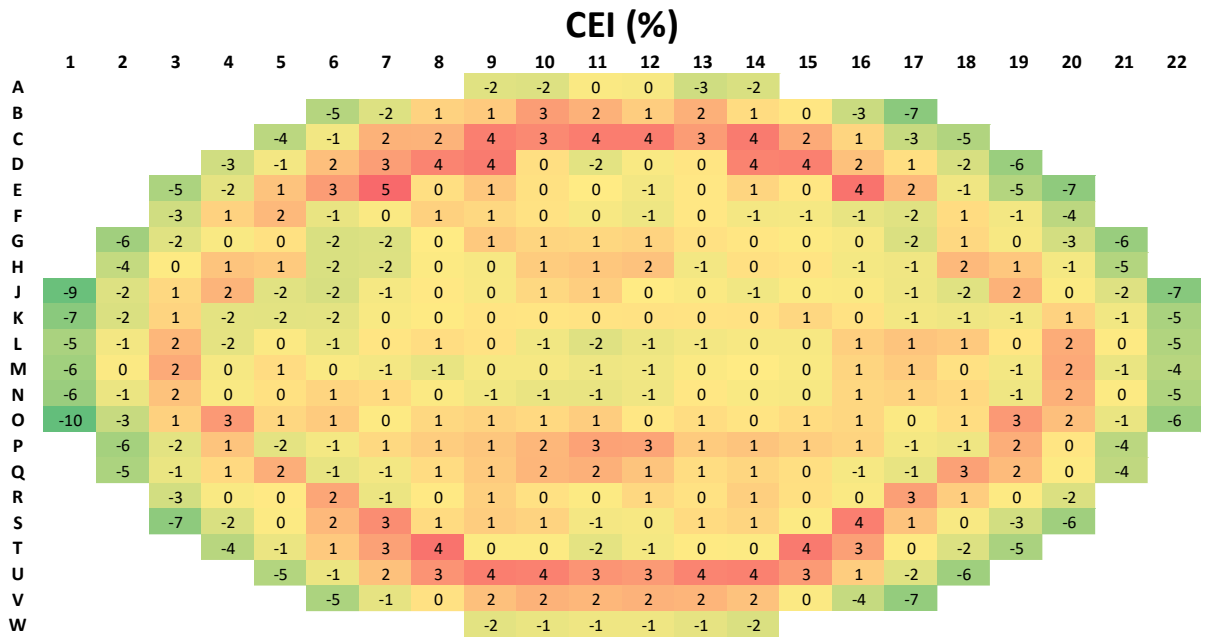
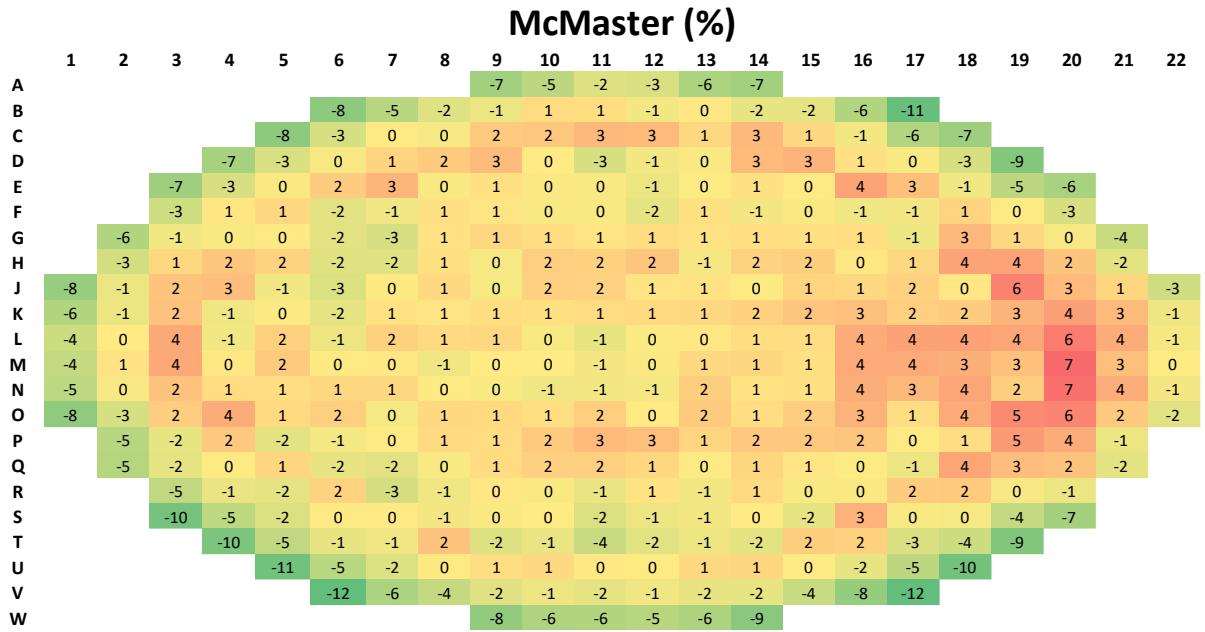


FIG. 33. Power channel differences to the mean for steady state coupled simulations (MW) for McMaster and CEI. A negative value means the participant has lower channel power than the average.

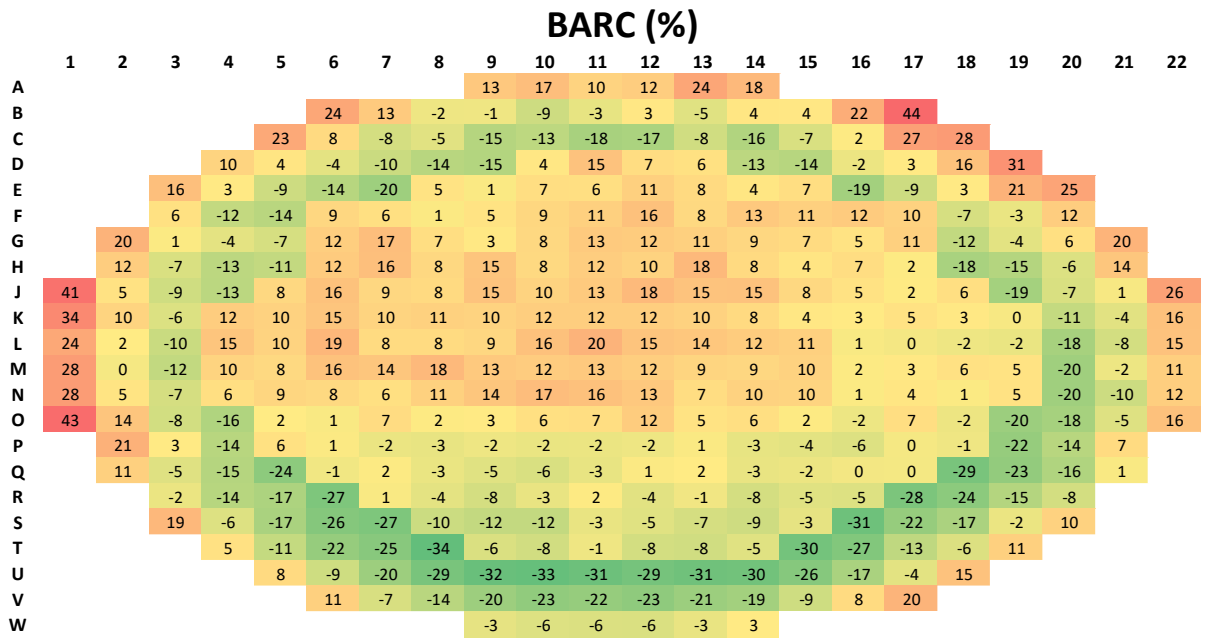
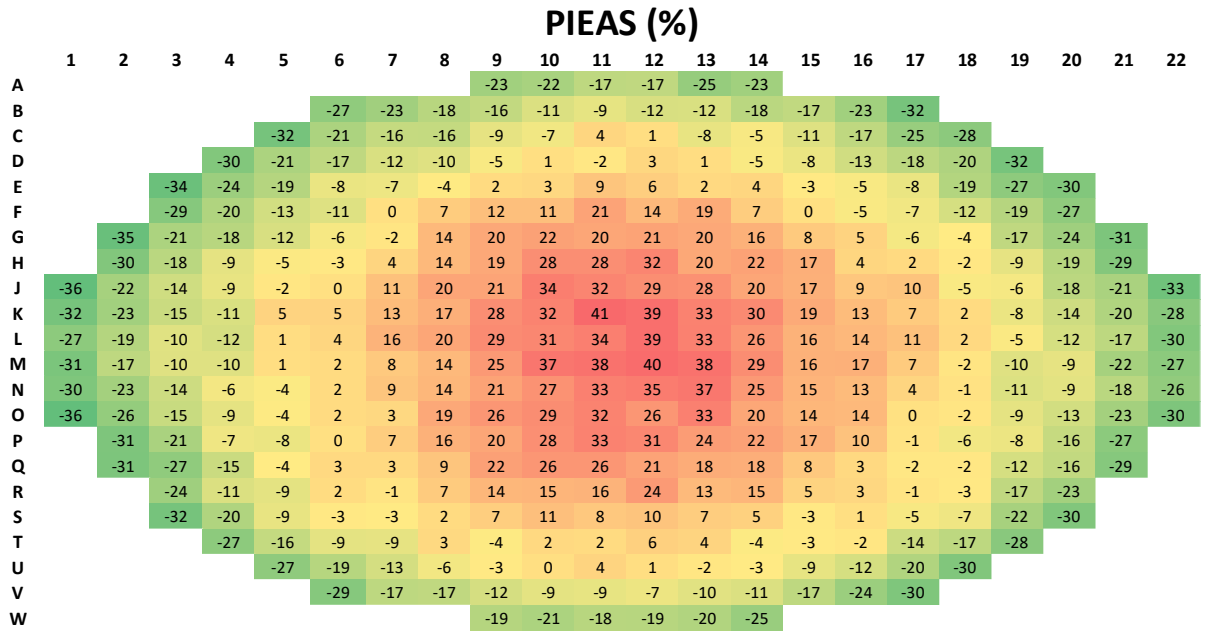


FIG. 34. Power channel differences to the mean for steady state coupled simulations (MW) for PIEAS and BARC. A negative value means the participant has lower channel power than the average.

Mean (°C)												
	1	2	3	4	5	6	7	8	9	10	11	12
1	329	464	581	653	699	744	753	724	687	614	501	372
2	331	468	582	644	673	711	719	694	673	610	500	372
3	334	477	598	666	697	737	745	720	694	624	508	374
4	337	491	631	721	773	827	838	803	762	673	537	385
5	309	406	495	566	636	676	685	661	599	532	448	356
6	310	407	495	566	627	663	671	650	596	528	445	354
7	313	418	515	593	675	723	734	705	635	561	466	363
8	328	459	575	650	699	742	749	720	682	614	503	373
9	330	464	579	645	681	721	728	701	675	617	507	374
10	331	469	588	659	687	723	730	706	689	626	512	375
11	337	490	631	726	792	847	856	816	762	676	540	387
12	307	400	485	554	620	658	666	644	588	528	447	356
13	308	403	491	564	626	660	668	647	597	531	448	355
14	311	412	508	588	667	712	721	691	624	553	461	360
15	326	455	568	642	695	743	753	723	684	613	500	371
16	333	474	594	662	702	747	755	725	688	619	506	374
17	336	486	614	687	717	758	766	738	713	635	513	376
18	336	489	626	711	775	830	840	804	748	660	528	383
19	304	389	465	526	586	622	632	614	566	511	436	351
20	313	418	518	599	670	712	720	694	632	552	458	360
21	313	418	515	592	671	717	727	699	632	558	465	363
22	326	455	568	640	689	732	739	709	670	605	498	370
23	331	470	592	667	708	754	761	729	699	632	514	376
24	333	477	605	683	718	761	768	740	716	646	522	379
25	335	487	626	719	774	826	834	798	756	672	537	385
26	306	396	477	542	606	641	648	627	574	516	440	352
27	311	414	514	599	675	718	727	700	636	559	463	362
28	312	416	512	588	668	713	722	694	627	559	467	363

Relative standard deviation [%]												
	1	2	3	4	5	6	7	8	9	10	11	12
1	2	5	6	5	5	5	5	5	5	6	4	1
2	2	5	6	5	4	4	4	4	5	5	4	2
3	2	5	7	6	5	4	4	4	6	6	4	1
4	2	6	8	8	8	8	8	8	8	8	6	2
5	2	4	7	8	10	10	10	10	9	7	5	3
6	1	3	5	6	7	7	7	7	6	5	4	2
7	2	5	8	10	11	12	12	11	10	9	6	3
8	2	5	7	6	5	5	5	5	5	6	5	2
9	2	5	5	5	4	4	4	4	4	4	4	2
10	2	6	8	8	6	5	5	5	7	7	6	2
11	2	4	5	4	4	3	3	4	4	5	4	2
12	2	4	5	6	7	8	7	7	6	5	4	2
13	1	4	6	7	8	8	8	8	7	6	4	2
14	3	7	10	13	14	15	15	14	13	12	9	4
15	1	4	5	5	5	5	5	5	5	5	4	1
16	2	6	7	6	5	5	5	5	5	6	4	1
17	2	6	7	7	5	5	5	5	6	6	5	2
18	2	6	8	8	8	8	8	8	8	8	6	2
19	1	3	5	7	7	8	8	7	6	5	4	2
20	1	4	6	8	9	9	9	9	7	6	4	2
21	2	5	8	10	11	11	11	11	10	8	6	3
22	2	6	7	6	5	5	5	4	5	6	5	2
23	2	6	7	6	5	5	5	5	6	6	5	2
24	2	5	7	7	5	5	5	5	6	6	5	1
25	2	6	8	8	7	7	7	7	8	8	6	2
26	2	5	6	7	7	7	7	7	6	6	4	2
27	1	4	6	8	9	9	9	9	8	7	5	2
28	2	5	8	9	11	11	11	11	10	9	7	3

FIG. 35. Mean thermal hydraulics group fuel temperature distribution and its relative standard deviation for steady state coupled simulations (°C).

Mean (°C)												
	1	2	3	4	5	6	7	8	9	10	11	12
1	262	265	269	274	280	285	291	295	299	302	305	305
2	262	265	269	274	279	284	289	293	298	301	303	304
3	262	265	269	274	279	284	289	293	298	301	303	304
4	262	265	270	275	280	286	292	297	302	306	308	309
5	262	265	269	274	280	286	292	298	302	306	308	309
6	262	265	269	274	279	285	291	296	301	304	306	307
7	262	265	270	276	282	289	296	302	307	310	311	311
8	262	265	269	274	279	284	289	294	298	302	304	305
9	262	265	269	274	278	284	289	293	297	301	303	304
10	262	265	269	273	278	283	288	293	297	300	303	304
11	262	265	270	276	282	288	294	299	303	307	309	310
12	262	265	269	274	280	287	293	299	303	307	309	309
13	262	264	268	273	279	285	290	296	300	304	306	307
14	262	265	269	275	282	288	295	301	305	309	310	310
15	262	265	269	273	278	284	289	294	298	302	304	305
16	262	265	269	274	279	284	289	294	298	302	304	305
17	262	265	269	274	279	284	289	294	298	302	304	305
18	262	265	270	275	281	287	293	298	303	306	309	310
19	262	264	268	273	279	285	290	296	300	304	306	307
20	262	265	269	275	281	287	293	299	304	307	309	310
21	262	265	270	275	282	289	296	302	306	310	311	311
22	261	264	268	273	278	283	288	293	297	301	303	304
23	261	264	269	273	278	284	289	294	298	302	304	305
24	261	264	269	274	279	284	289	294	298	302	304	305
25	262	265	269	274	280	286	291	296	301	305	308	308
26	261	264	268	273	278	284	290	295	300	303	305	306
27	261	264	269	274	280	287	293	299	304	307	310	310
28	261	265	269	275	282	289	295	301	306	309	311	311

Relative standard deviation [%]												
	1	2	3	4	5	6	7	8	9	10	11	12
1	0.3	0.4	0.6	0.8	1.2	1.5	1.7	1.9	1.6	1.4	1.2	1.2
2	0.3	0.3	0.3	0.5	0.6	0.8	1.0	1.2	1.3	1.3	1.3	1.3
3	0.3	0.3	0.4	0.5	0.6	0.8	1.0	1.2	1.2	1.3	1.3	1.3
4	0.3	0.3	0.3	0.3	0.4	0.5	0.6	0.7	0.8	0.8	0.8	0.8
5	0.4	0.4	0.4	0.5	0.6	0.8	0.9	1.0	1.1	1.2	1.2	1.2
6	0.4	0.4	0.4	0.4	0.5	0.5	0.6	0.6	0.7	0.7	0.7	0.7
7	0.4	0.5	0.6	0.9	1.1	1.4	1.6	1.8	1.8	1.6	1.4	1.2
8	0.3	0.4	0.4	0.5	0.6	0.8	0.9	1.0	1.1	1.1	1.1	1.1
9	0.3	0.4	0.5	0.7	1.0	1.3	1.6	1.8	1.7	1.6	1.5	1.5
10	0.3	0.3	0.3	0.4	0.6	0.7	0.9	1.0	1.1	1.1	1.1	1.1
11	0.4	0.5	0.8	1.1	1.4	1.7	2.0	1.7	1.4	1.2	1.0	1.0
12	0.4	0.4	0.5	0.6	0.7	0.8	0.9	1.0	1.0	1.0	0.9	0.7
13	0.4	0.4	0.4	0.4	0.5	0.5	0.6	0.7	0.7	0.8	0.8	0.8
14	0.4	0.4	0.6	0.9	1.3	1.6	2.0	2.2	2.4	2.4	2.2	2.1
15	0.4	0.4	0.4	0.5	0.6	0.8	0.9	1.0	1.1	1.1	1.1	1.2
16	0.3	0.3	0.3	0.4	0.6	0.8	0.9	1.0	1.1	1.1	1.2	1.2
17	0.3	0.3	0.3	0.4	0.6	0.8	1.0	1.1	1.2	1.2	1.1	1.1
18	0.4	0.4	0.4	0.5	0.6	0.6	0.7	0.7	0.8	0.8	0.8	0.8
19	0.4	0.4	0.4	0.5	0.6	0.7	0.8	0.9	0.9	1.0	1.0	1.0
20	0.4	0.4	0.4	0.4	0.5	0.5	0.6	0.7	0.8	0.8	0.8	0.8
21	0.4	0.4	0.5	0.7	0.9	1.1	1.2	1.4	1.5	1.4	1.3	1.1
22	0.4	0.4	0.4	0.6	0.7	0.9	1.0	1.1	1.2	1.2	1.3	1.3
23	0.4	0.4	0.4	0.5	0.6	0.8	1.0	1.1	1.2	1.2	1.2	1.2
24	0.4	0.4	0.4	0.5	0.7	0.9	1.0	1.1	1.2	1.2	1.1	1.1
25	0.4	0.4	0.4	0.4	0.5	0.6	0.7	0.8	0.8	0.8	0.9	0.9
26	0.4	0.4	0.4	0.5	0.5	0.5	0.5	0.6	0.6	0.6	0.6	0.6
27	0.4	0.4	0.4	0.5	0.6	0.6	0.7	0.8	0.9	0.9	0.9	0.8
28	0.4	0.5	0.6	0.8	1.1	1.3	1.5	1.7	1.7	1.5	1.3	1.1

FIG. 36. Mean thermal hydraulics group coolant temperature distribution for steady state coupled simulations (°C).

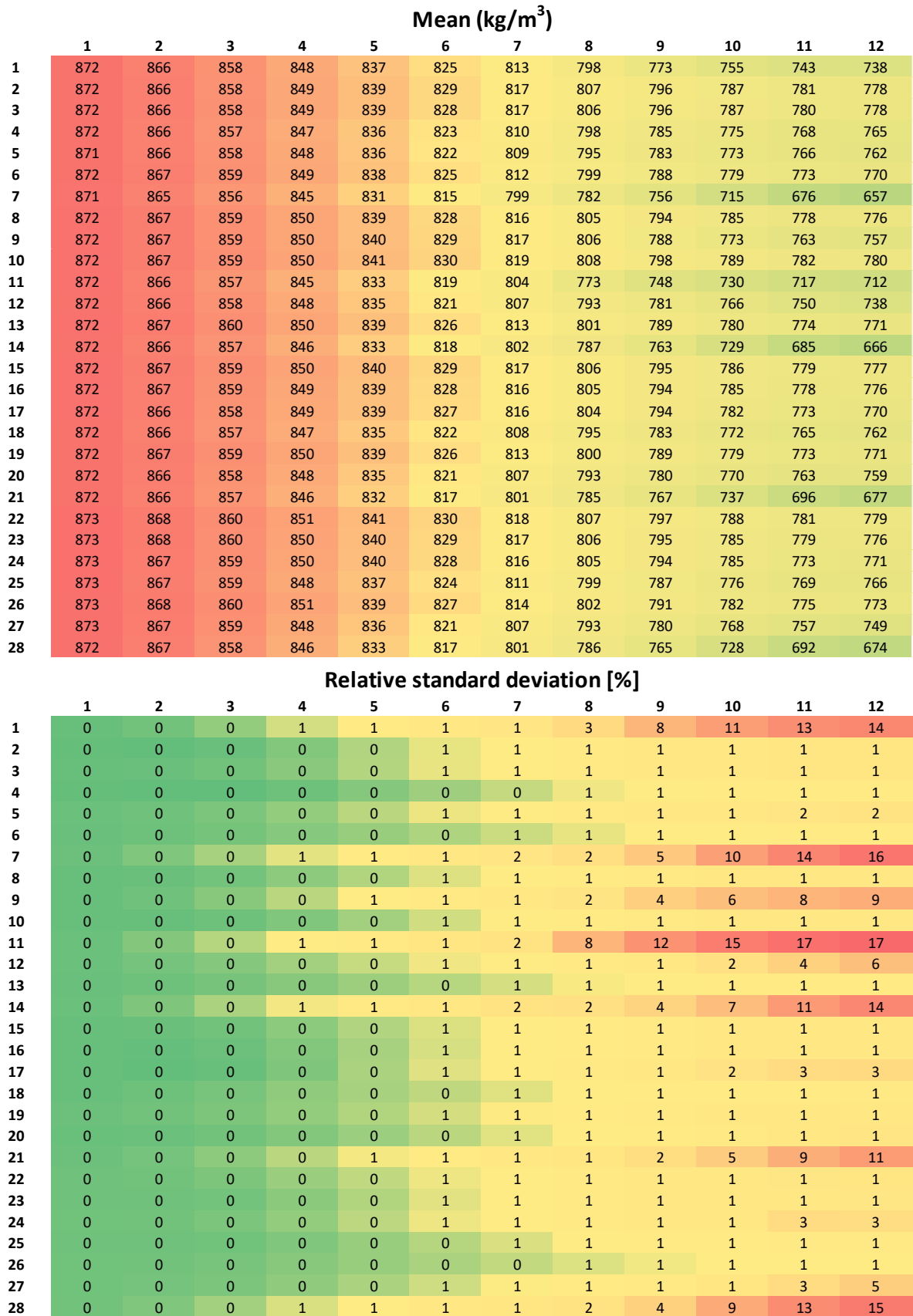


FIG. 37. Mean thermal hydraulics group coolant density distribution for steady state coupled simulations (kg/m³).

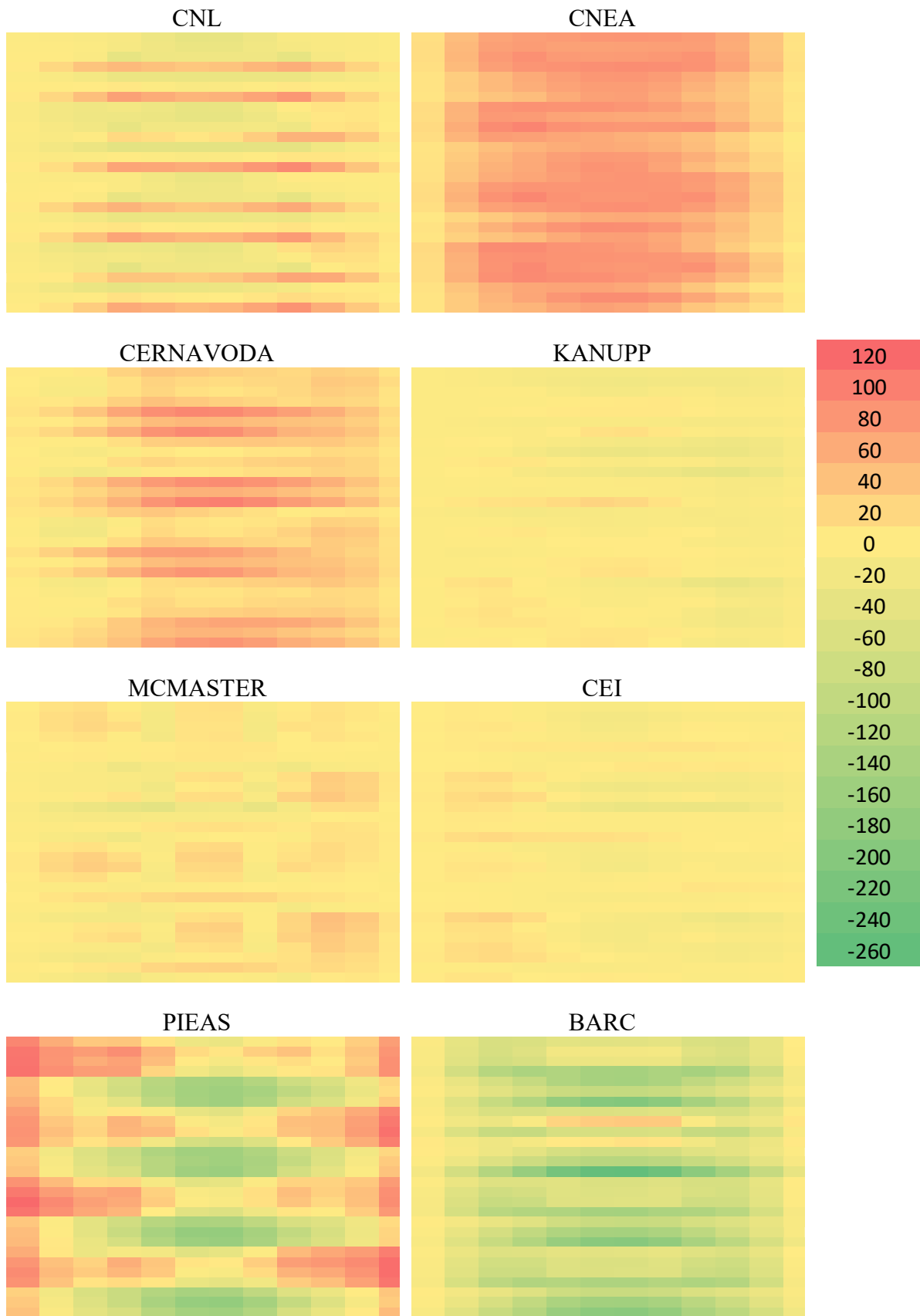


FIG. 38. Differences to mean thermal hydraulics group fuel temperature distribution for steady state coupled simulations ($^{\circ}\text{C}$). A negative value means the participant has lower temperature than the average.

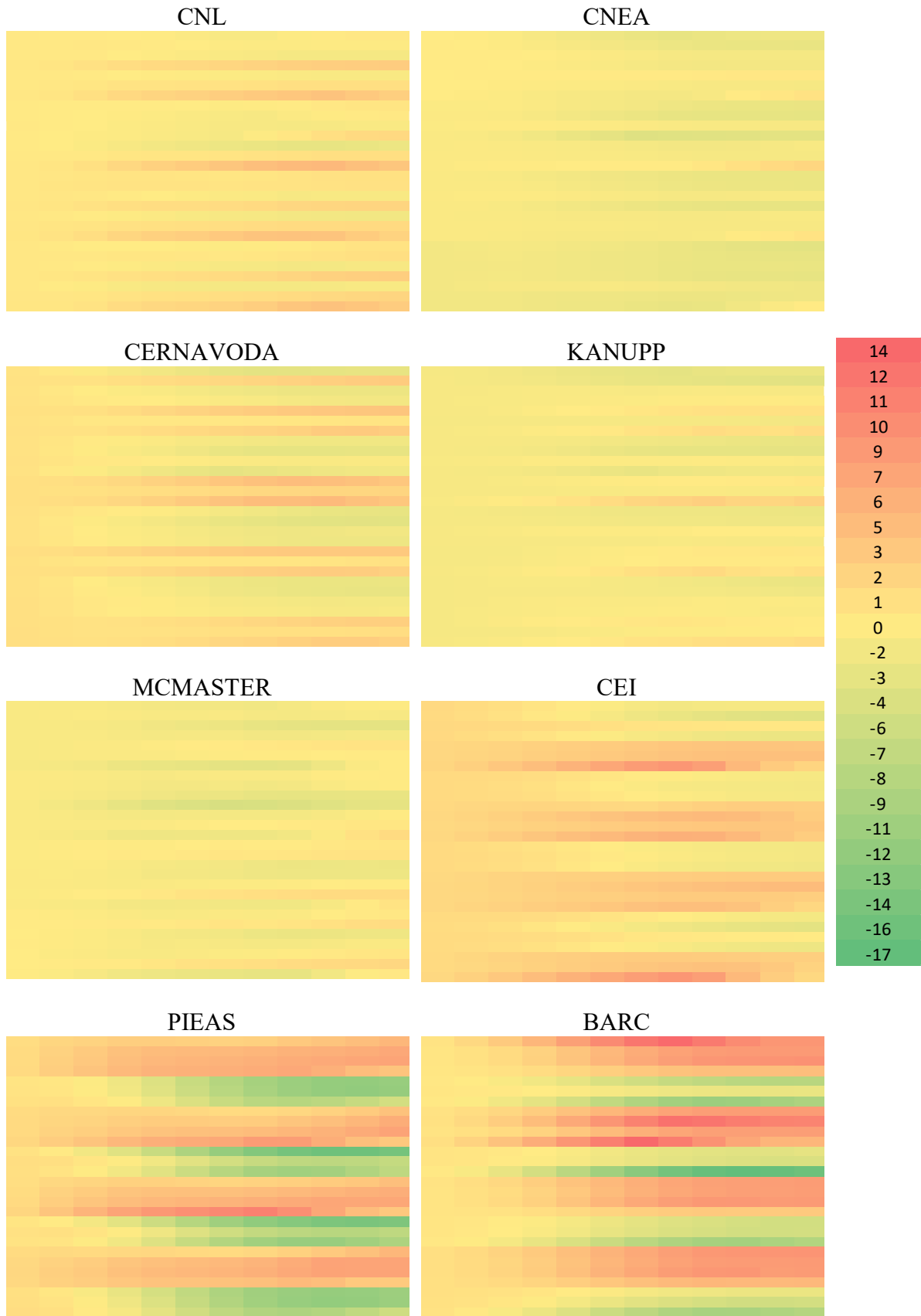


FIG. 39. Differences to mean thermal hydraulics group coolant temperature distribution for steady state coupled simulations($^{\circ}\text{C}$). A negative value means the participant has lower temperature than the average.

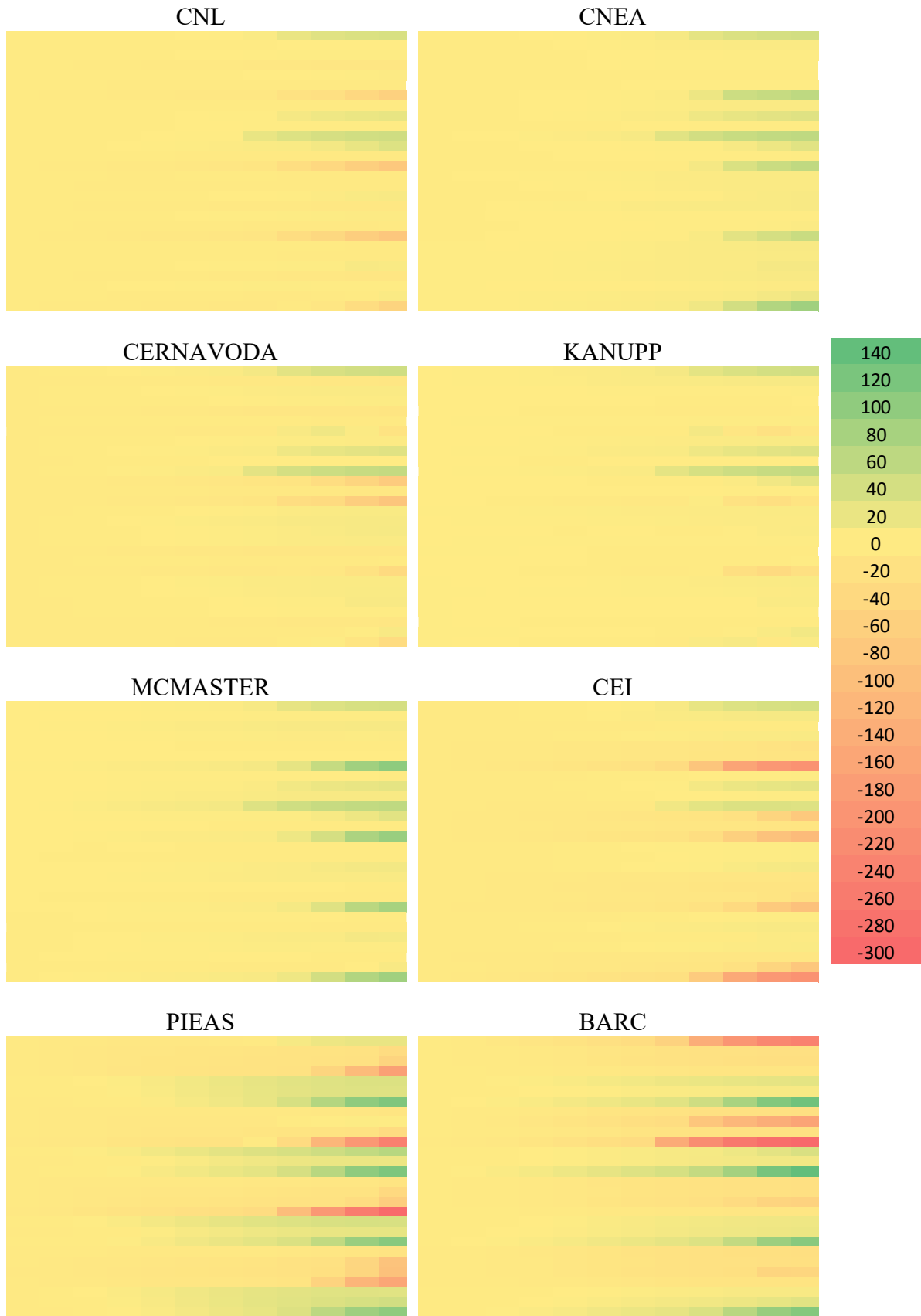


FIG. 40. Differences to mean thermal hydraulics group coolant density distribution for steady state coupled simulations (kg/m^3). A negative value means the participant has lower temperature than the average.

5.2.2. Standalone neutronics: diffusion versus transport

A simplified specification was provided to support transport-based solutions. This serves two purposes: to enable future work based on transport solutions, and to provide a cross check that diffusion-based solutions will provide adequate accuracy for the neutronics solutions.

Two participants, GATECH and PIEAS, have used neutronics transport based methods for full core simulations: COMET and OpenMC, respectively. However, the specifications for transport based neutronics solutions, described in Section 3.3.1, were used by GATECH only, whereas PIEAS used a model based on the neutronics model specifications described in Section 3.2, albeit with some notable simplifications, such as the use of a 21 points burnup values distribution. Therefore, the PIEAS results are included and discussed in Section 5.2.1.

GATECH used COMET to obtain the multigroup reference solutions for the following cases: full core voided, full core checkerboard voided and half-core checkerboard voided cases, with each case being performed both with and without the presence of adjuster rods. Since the Monte Carlo method was used to generate the response function library for COMET, the geometry details and material heterogeneities were fully modelled in the fuel bundle, adjuster rods and reflector. For consistency with the deterministic transport and diffusion models, the external circular core boundary was approximated as corrugated rectangular meshes, although COMET can model the exact (circular) boundary, and no-re-entry boundary condition was assumed in COMET core calculations.

For this problem, CNSC contributed with results produced by NESTLE-C Version 3.0 to enable a limited comparison between transport and diffusion based solutions for a standalone steady state physics case. All elements of the core model, including burnup distribution, adjusters' types, etc., were adjusted to match the model proposed for the transport based solution. The notable difference is the use of the two groups macroscopic diffusion cross sections to model the fuel bundle, adjuster rods and reflector. Results for two solution methods, the FDM and NEM with transport correction using the average discontinuity factors included in the library of diffusion cross sections, were reported. For consistency with the generation of the response function library for COMET, results using the more refined options available in the NESTLE-C code for treatment of saturable fission products were not reported.

The following tables and figures summarize few selected key results. Table 21 shows relevant scalar output values including: k_{eff} , the steady state neutron multiplication factor for the reference, unperturbed, nominal state, CVW1, reactivity worth associated with full core checkerboard voiding, CVW2, reactivity worth associated with ½ core checkerboard voiding, and ADJW, adjuster rods reactivity worth.

TABLE 21. MAIN OUTPUT PARAMETERS

Output	Unit	Value		
		NESTLE-C (FDM)	NESTLE-C (NEM)	COMET
k_{eff}	N/A	1.0003974	0.9999711	0.99626
CVW1	mk	16.44	16.49	16.41
CVW2	mk	4.54	4.48	4.67
ADJW	mk	15.23	15.39	14.99

Table 22 shows the maximum channel and bundle power values (kW) and positions for each code and problem variant.

TABLE 22. MAXIMUM CHANNEL AND BUNDLE POWERS AND POSITION FROM DIFFUSION AND TRANSPORT COMPARISON

		NESTLE-C				COMET	
		FDM		NEM		-	
		Position	Power (kW)	Position	Power (kW)	Position	Power (kW)
Channel maximum	Ref.	F12	6773.9	F13	6823.4	F13	6892.9
	ADJW	L13	7986.0	L13	8030.1	L13	8216.5
	CVW1	F13	6766.6	F13	6809.0	G13	6898.0
	CVW2	L5	7112.1	N7	7144.8	N7	7511.8
Bundle maximum	Ref.	E12-6	850.6	E12-6	842.1	F13-6	856.8
	ADJW	L13-7	1145.0	L13-7	1141.0	L13-7	1180.6
	CVW1	E12-6	848.7	E12-6	839.3	F13-6	858.5
	CVW2	E9-7	875.1	F10-7	873.0	M4-6	901.7

Figure 41 present the ratios of channel powers for the reference, un-perturbed, nominal state. Panel a) displays the ratio of the NESTLE-C (FMD) calculated channel powers to the COMET calculated channel powers. The orange and green regions represent over predictions and under predictions of NESTLE-C (FDMD) relative to COMET, respectively. The colour scale is shown on the right and is shared for all sub-plots. Panel b) presents the ratio of the NESTLE-C (FMD) calculated channel powers to the NESTLE-C (NEM) calculated channel powers. Finally, panel c) displays the ratio of the NESTLE-C (NEM) calculated channel powers to the COMET calculated channel powers.

The results show a good agreement between the NESTLE-C diffusion and COMET transport solutions for this stylized problem. The small differences are as expected and explained mainly by the more refined modelling of the geometry details and material heterogeneities in COMET.

More significantly, the results indicate that, in general, solutions based on finite difference implementations of the neutron diffusion solution can be expected to compare well to transport-based solutions.

5.3. ADJUSTER WITHDRAWAL TEST PROBLEM

5.3.1. Standalone neutronics

Four participants contributed results for this problem: CNL, CNEA, KANUPP and McMaster. Table 23 shows the maximum channel and bundle power at the end of the transient and its location for each participant. The standard deviation of those values and the maximum of the mean channel power distribution are also reported.

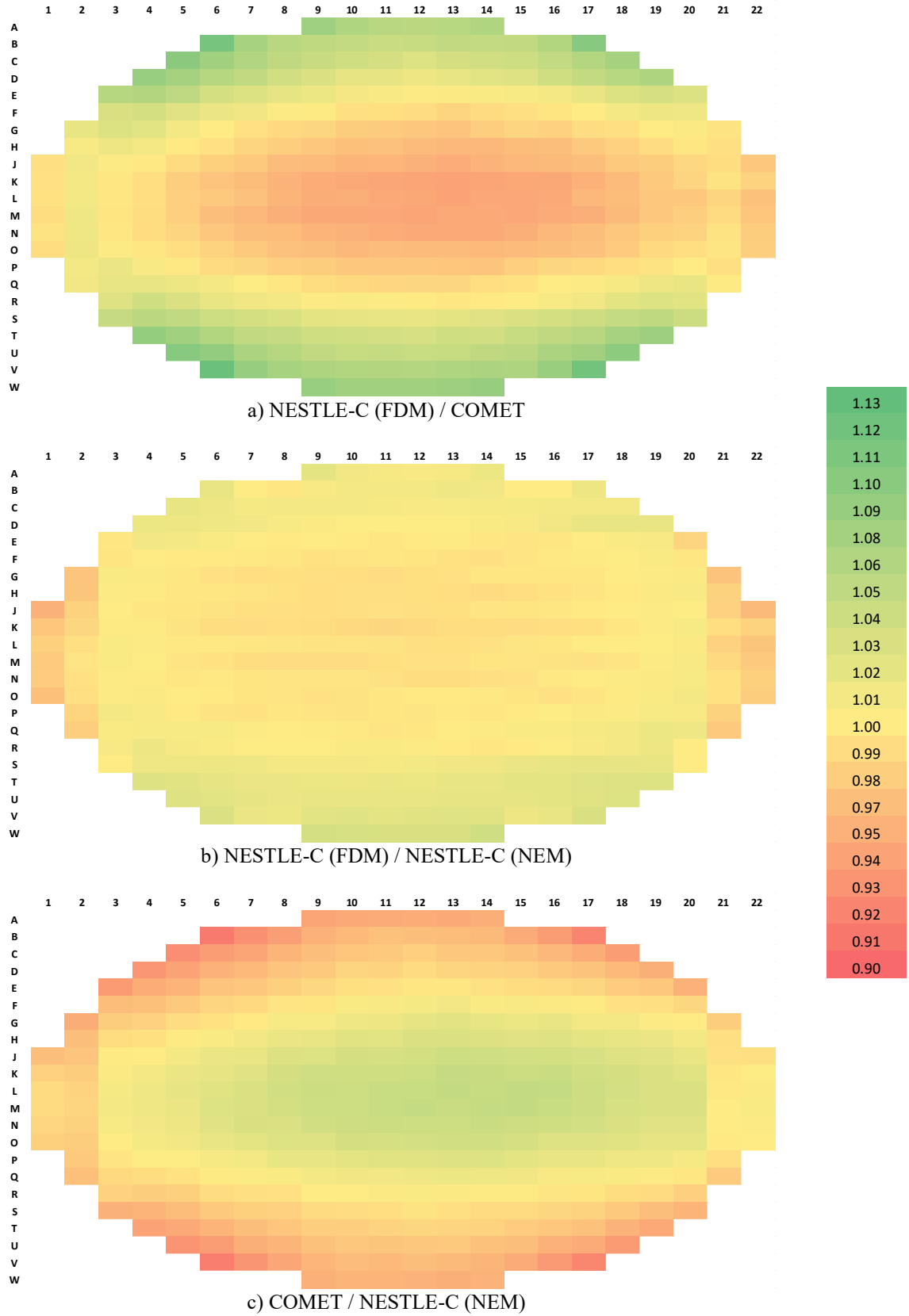


FIG. 41. Heat maps of channel power distribution ratios. Panel a) NESTLE-C with FDM solution divided by COMET solution results. Panel b) Ratio of NESTLE-C FDM to NEM solutions. Panel c) COMET solutions divided by NESTLE-C NEM solution. Heat maps use identical colouring scheme.

TABLE 23. MAXIMUM POWER VALUE AND LOCATION AT THE END OF STNDALONE NEUTRONIC ADJUSTER WITHDRAWAL TRANSIENT

FOM	Maximum channel power at 25 s	Maximum channel power location	Maximum bundle power at 25 s	Maximum bundle power location
Unit	MW	-	kW	-
Mean	10.682	L18	1464	P6_L18
Std. Dev.	0.66	-	104	-
CNL	10.94	T13	1378	P6_L18
CNEA	11.07	L18	1492	P6_L18
KANUPP	10.01	L18	1364	P6_L18
McMaster	11.86	L18	1622	P6_L18

Figure 42 shows the evolution of reactivity and reactor thermal power, relative to the steady state condition. All participants present similar behaviour regarding reactivity, with a maximum value of 0.78 mk and a minimum value of 0.65 mk at 25 s. These differences on reactivity result in a maximum power difference of 456 MW at 25 s, which represent a 22% of the initial power. Power evolutions tend to differentiate after 20 s.

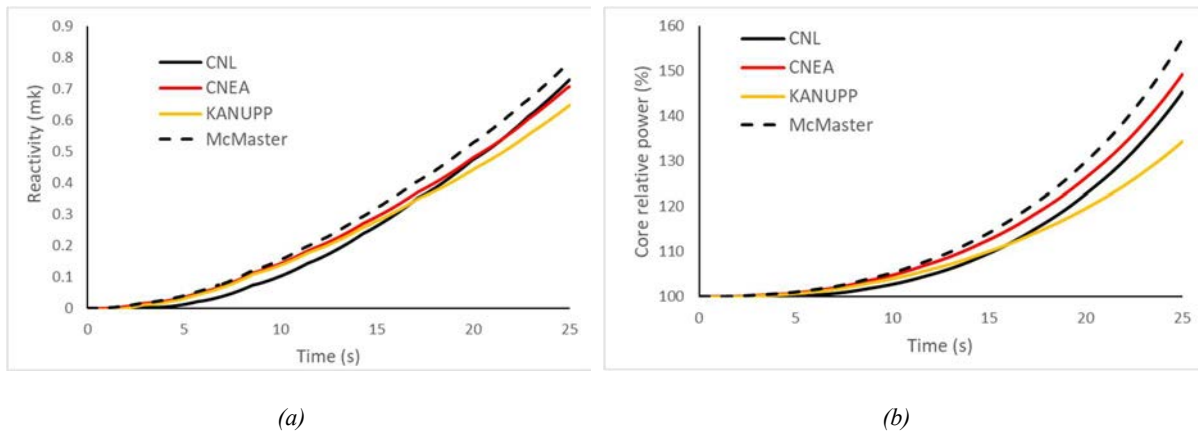


FIG. 42. Evolution of (a) reactivity and (b) thermal power for standalone neutronic adjuster withdrawal transient.

Figure 43 shows the mean channel power distribution, the relative standard deviation and the channel power maps for each participant, calculated at the end of the transient. Average and standard deviation distributions use their own heat map colouring scale. However, all the participant contributions use the same scale, in order to emphasise absolute variations between them. Green is used for lower power and red for higher power. The results present differences of 6% in most of the channels, with a slightly increase in the regions perturbed by liquid zones, where the standard deviation reach up to 9%. The results from the individual contributions reflect the difference in power shown in Fig. 42.

Figure 44 shows the mean channel power distribution normalized by total power. This was done with the intention of further analysing differences in power distributions without it being overridden by differences in total power. Average and standard deviation distributions use their own heat map colouring scale. Participant contributions use the same scale. Green is used for lower power and red for higher power. Overall differences are lower compared to non-normalized values, and the zones with higher dispersion of results are shifted towards the lower and upper most side of the core. CNL's higher predicted power towards the lower part of the

core relates to a similar behaviour observed in coupled steady state calculations. It is also noticeable that the zones with liquid zones have a higher dispersion of results than adjacent ones.

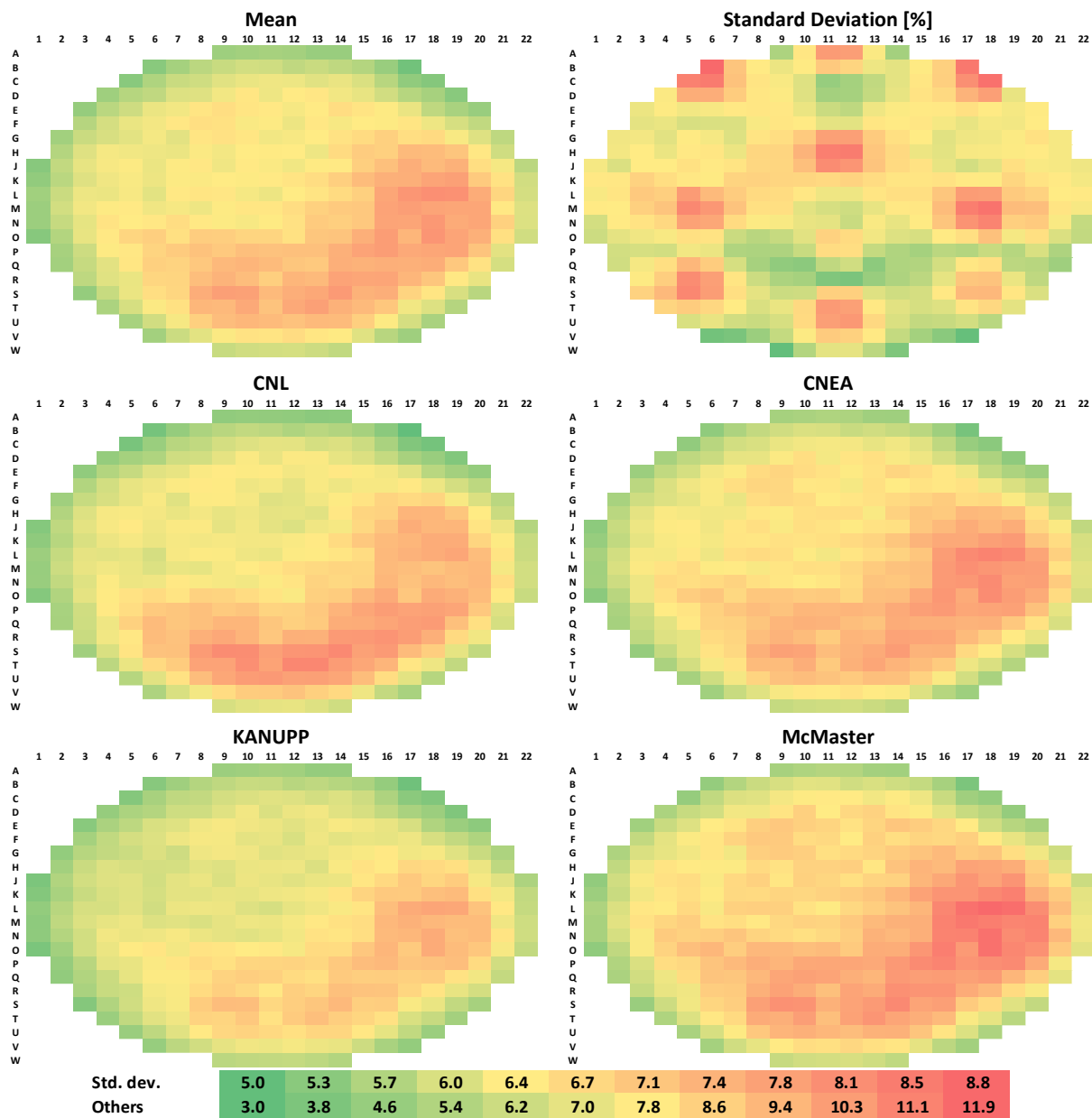


FIG. 43. Channel power (MW) distribution at the end of standalone neutronic adjuster withdrawal transient.

The discrepancies in results do not point to significant differences in neutronic models. The biggest differences in power are found in the regions that contain liquid zone controllers. Power distributions, normalized by total power, show higher discrepancies in the lower and upper part of the core.

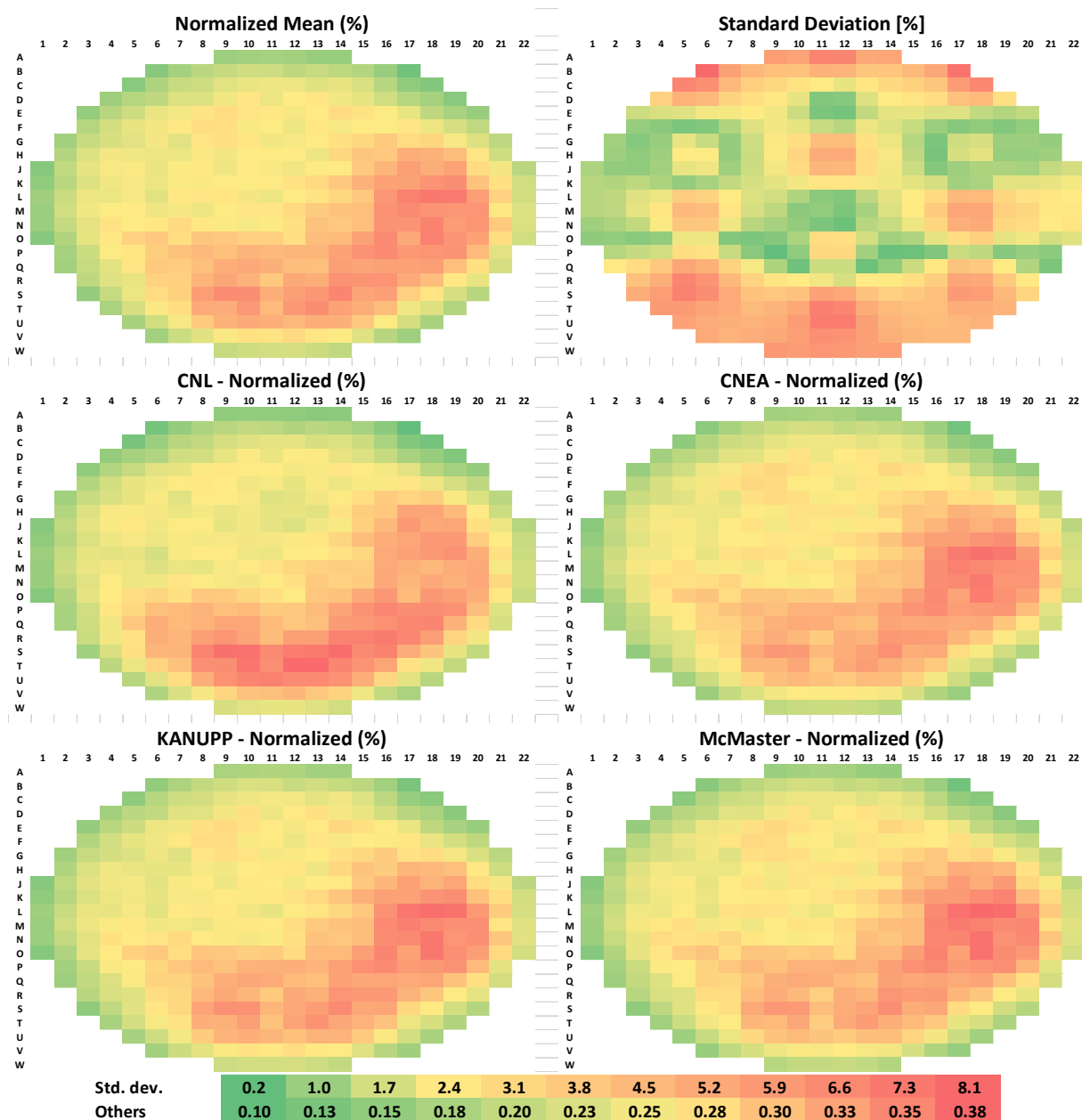


FIG. 44. Channel power distribution normalized by total power at the end of standalone neutronic adjuster withdrawal transient.

5.3.2. Standalone thermal hydraulics

Figures 45, 46 and 47 present the time evolution of the coolant pressure, coolant temperature, and void fraction for inlet header 2 obtained by all participants. Participant results are in general agreement with the exception of a single outlier (Cernavoda). Excluding the outlier, all inlet header pressures are bounded between 12.5 MPa and 13.0 MPa, at 25 s. The coolant temperature and void at 25 s are bounded by 262°C and 0.13, respectively. Inlet header coolant temperature increases in response to the withdrawal of adjuster rods approximately after 15 s BARC and Cernavoda. Cernavoda and BARC inlet header coolant temperature response to rod withdrawal is not as significant as the rest of the participants. For Cernavoda, this is consistent with the pressure response at the inlet header but for BARC the same explanation cannot be given.

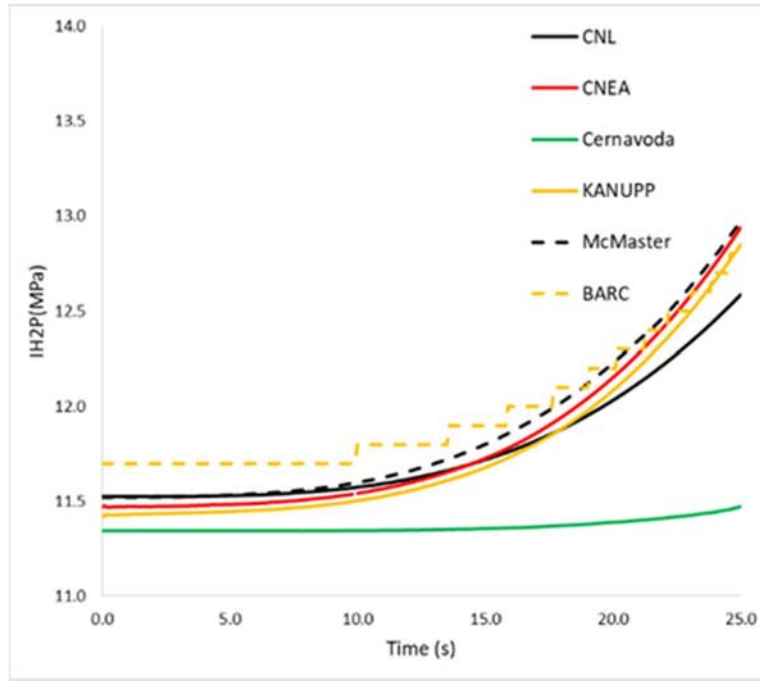


FIG. 45. Inlet header coolant pressure evolution in the standalone adjuster withdrawal problem.

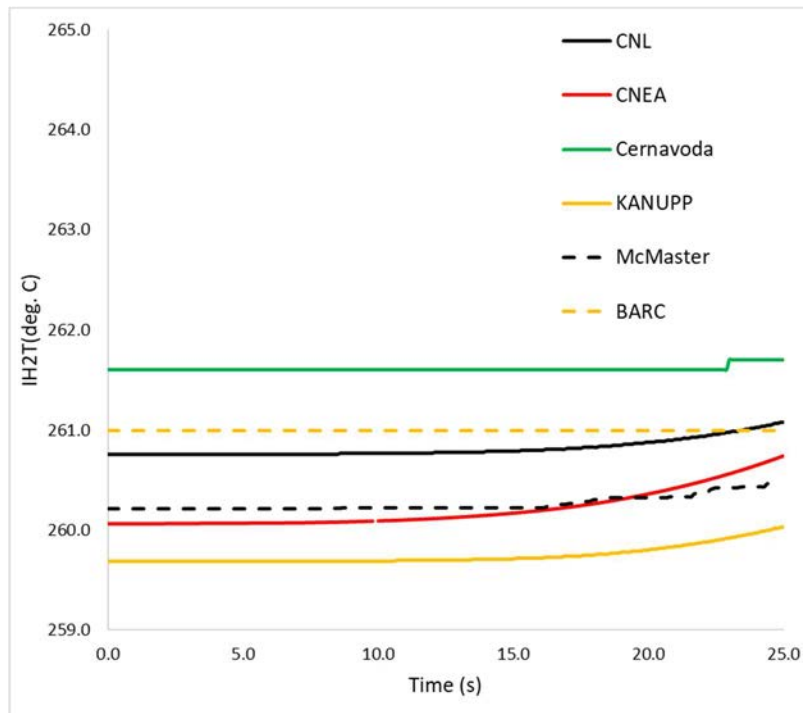


FIG. 46. Inlet header coolant temperature evolution in the standalone adjuster withdrawal problem.

Figures 48 to 50 presents the distributions of the coolant temperature, pressure, and void fraction within the thermal hydraulics network at 25s. Pressure and temperature distributions follow a common profile for all participants, however some significant variations in coolant pressure are noted in one participant (Cernavoda). This is consistent with the lower inlet header pressure observed earlier for Cernavoda. Voiding is noted in the outlet headers for all participants with varying degrees. BARC and Cernavoda void in loop-1(OHD1 and OHD3) in particular, are higher than the rest at, both over 0.1, or 10%, void. Although Cernavoda is an outlier in this particular scenario, the pressure and temperature response are consistent. Given

that void fraction at the outlet headers are also higher, one possible explanation in the case of Cernavoda is that the steam generators are removing more heat than expected. This can point to an inconsistency in the heat removal boundary conditions applied at the boilers. Alternatively, it may be that the pressurizer is keeping the pressure more stable and more void is generated

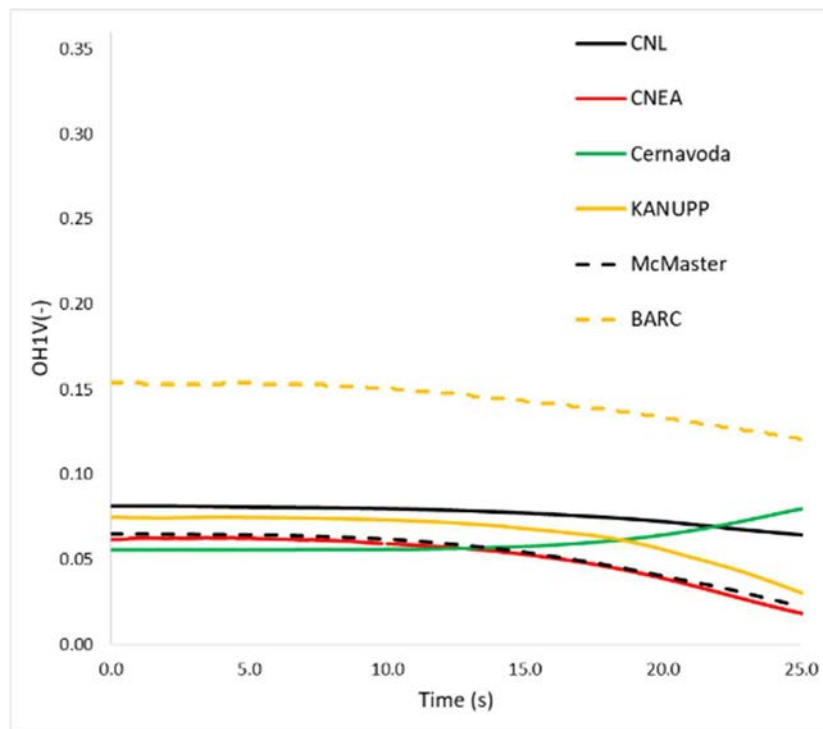


FIG. 47. Inlet header void evolution in the standalone adjuster withdrawal problem.

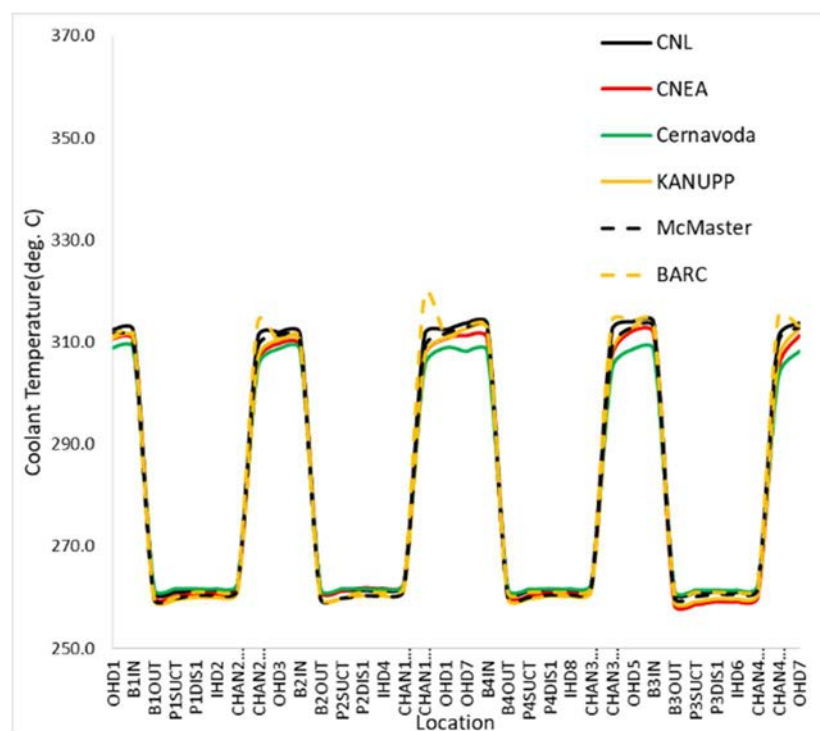


FIG. 48. Coolant temperature in the network after 25s.

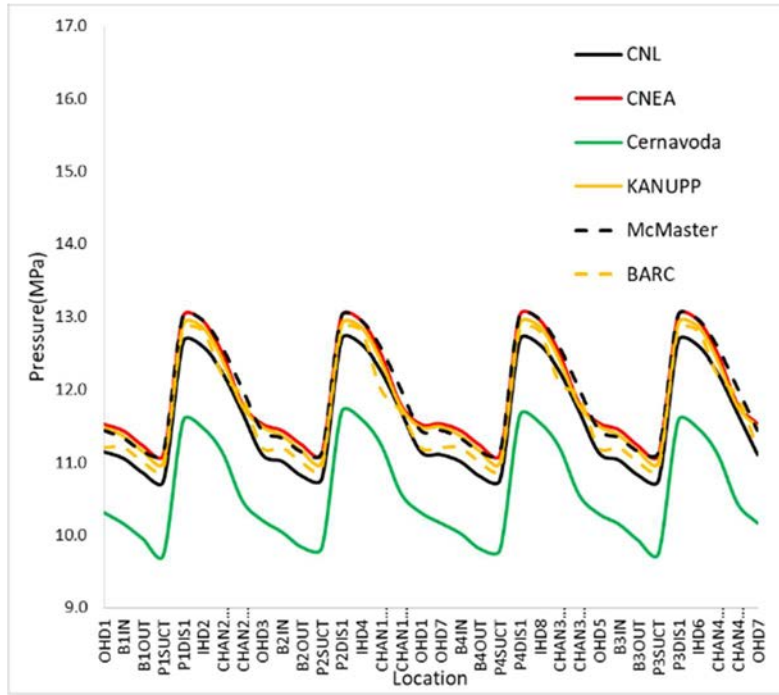


FIG. 49. Coolant pressure in the network after 25s.

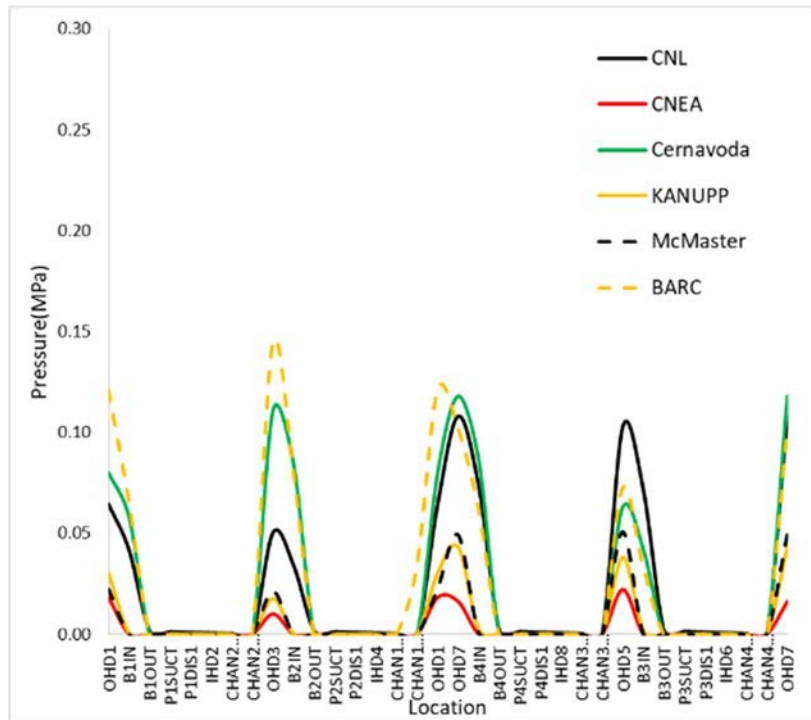
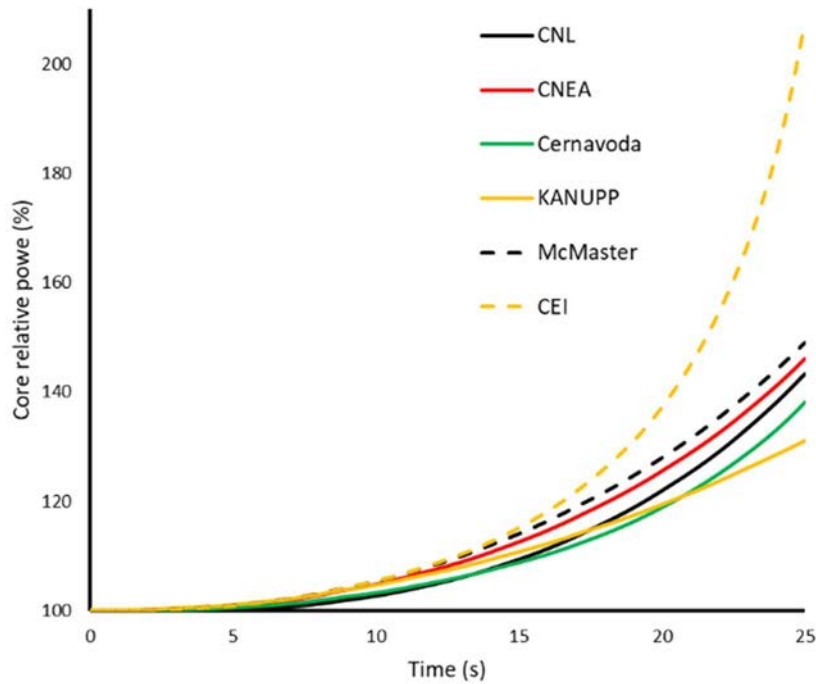


FIG. 50. Coolant void fraction in the network after 25s.

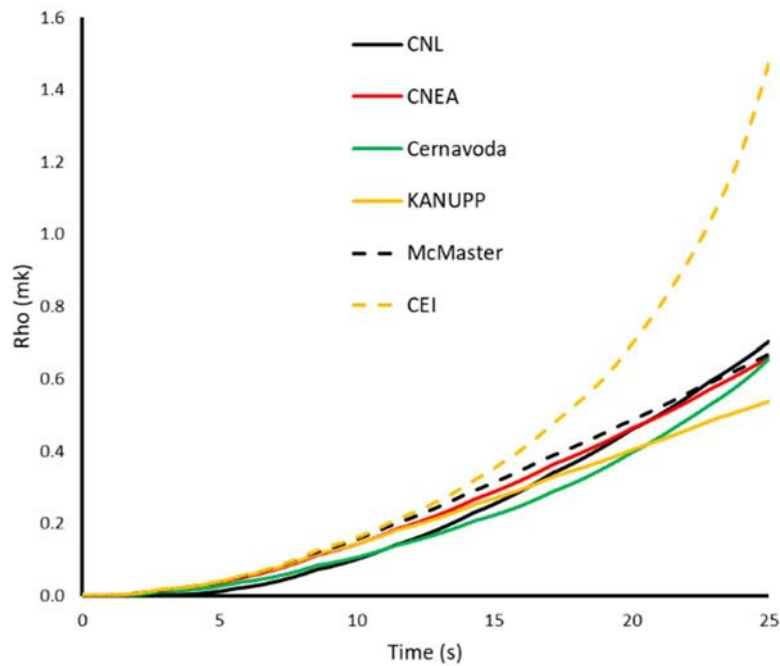
5.3.3. Coupled converged case

Figure 51 presents the time evolution of the core power and reactivity obtained by all participants. Power evolution tracks reactivity, and participant results are in general agreement with the exception of a single outlier. Excluding the outlier, reactivity at 25 s is bounded by 0.7 mk and core relative power between 130%–150%. The relative ranking of the core relative power magnitudes at 25 s do not correlate to any of the following factors: thermal hydraulics

code family (TRACE/RELAP vs ARIANT/CATHENA), steady state coolant voiding worth (CVW1 and CVW2), or steady state ADJW. A review of participant's detailed time evolution data for inlet header pressures, temperatures, and void fractions presents no insight. CEI and Cernavoda results differ despite using the same codes (RFSP/CATHENA). As noted previously, differences can be attributed to the use of different methods to comply with the test problem specifications. In addition, the coupling frameworks used by both teams were developed independently.



(a)



(b)

FIG.51. (a) Core power and (b) reactivity evolution in the coupled adjuster withdrawal problem.

Figures 52, 53 and 54 present the distributions of pressure, temperature, and void fraction within the thermal hydraulics network at 25 s. Pressure and temperature distributions follow a common profile for all participants, however some significant variations in absolute pressures are noted. Voiding is noted in the outlet headers for three participants: Cernavoda, CEI, and CNL. These participants made use of thermal hydraulics models based on either CATHENA3 or ARIANT. What is noteworthy is that there is no obvious link between void fractions (or coolant pressures) and the relative ranking of core powers presented in Fig. 51.

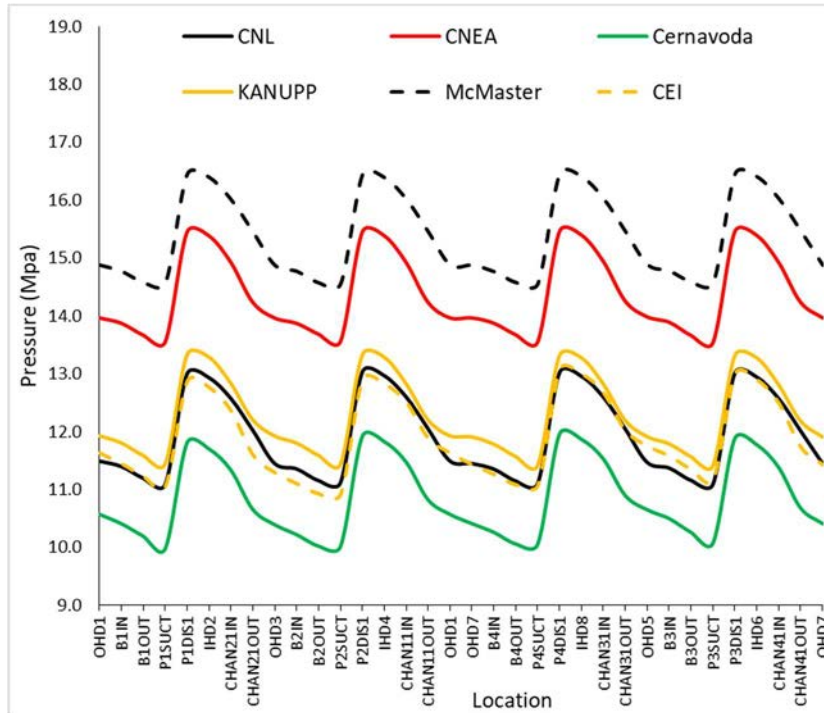


FIG.52. Coolant pressure in the network after 25 s.

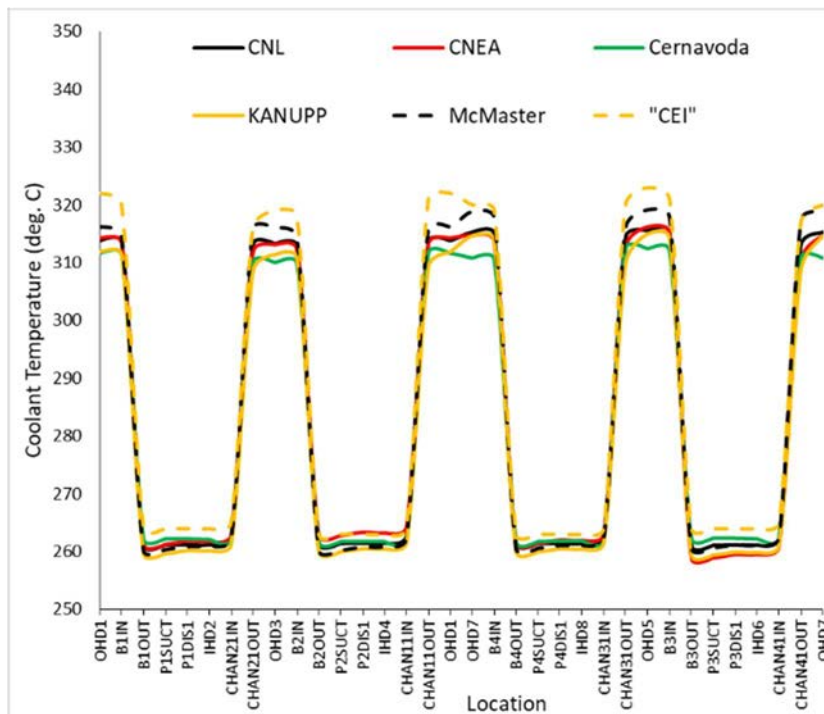


FIG. 53. Coolant temperature in the network after 25 s.

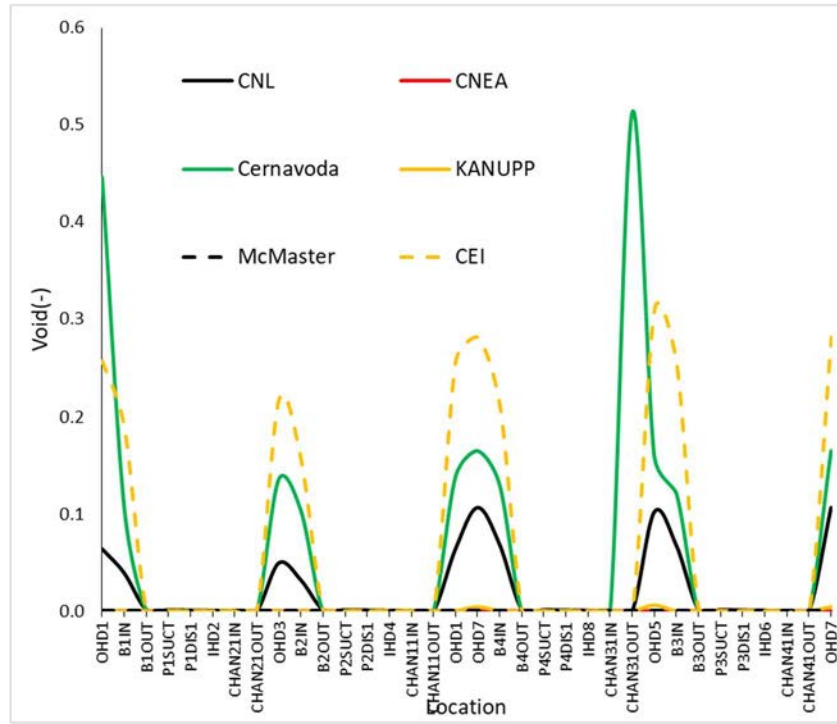


FIG. 54. Coolant void fractions in the network after 25 s.

Figure 55 presents a heat map of the mean and standard deviation of the in-core coolant density distribution. These densities are volumetrically averaged over the volume occupied by the coolant within a core fuel lattice cell. Data are reported in kg/m^3 . Each row represents one of the 28 thermal hydraulics channels, and there is one column for each of the 12 axial nodal positions corresponding to the location of a fuel bundle. Columns are sorted from reactor inlet to outlet. Green is used for high density, red for low density. Separate colour bars are used because of differences in scale.

Figure 56 presents the detailed results obtained by the participants. The colour bar used is the same as for the mean values. The CEI, CNL, and Cernavoda teams all present significant voiding in the downstream axial positions in channels 7, 14, 21, and 28. These teams made use of the CATHENA3 or ARIANT codes. Results from the KANUPP, McMaster and CNEA teams present a much less significant contrast in voiding between different thermal hydraulic channels. These teams all made use of TRACE or RELAP base solvers. A global drop in the in-core coolant mass does not appear to be sufficient to explain the differences in power evolution noted in Fig. 51.

The relative change in the in-core coolant mass, relative to the steady state was estimated as follows. Equilibrium in-core coolant densities from the coupled steady state, were summed; as were the densities presented in Fig. 56. The percent drop in the sums were then computed. The three most significant drops were observed for the CEI team (7.6%), the Cernavoda team (3.2%), and the CNL team (1.8%). While the power at 25 s was highest for the CEI team, the maximum power obtained by the CNL team was inferior to that of the McMaster team, despite a larger relative change in in-core coolant mass.

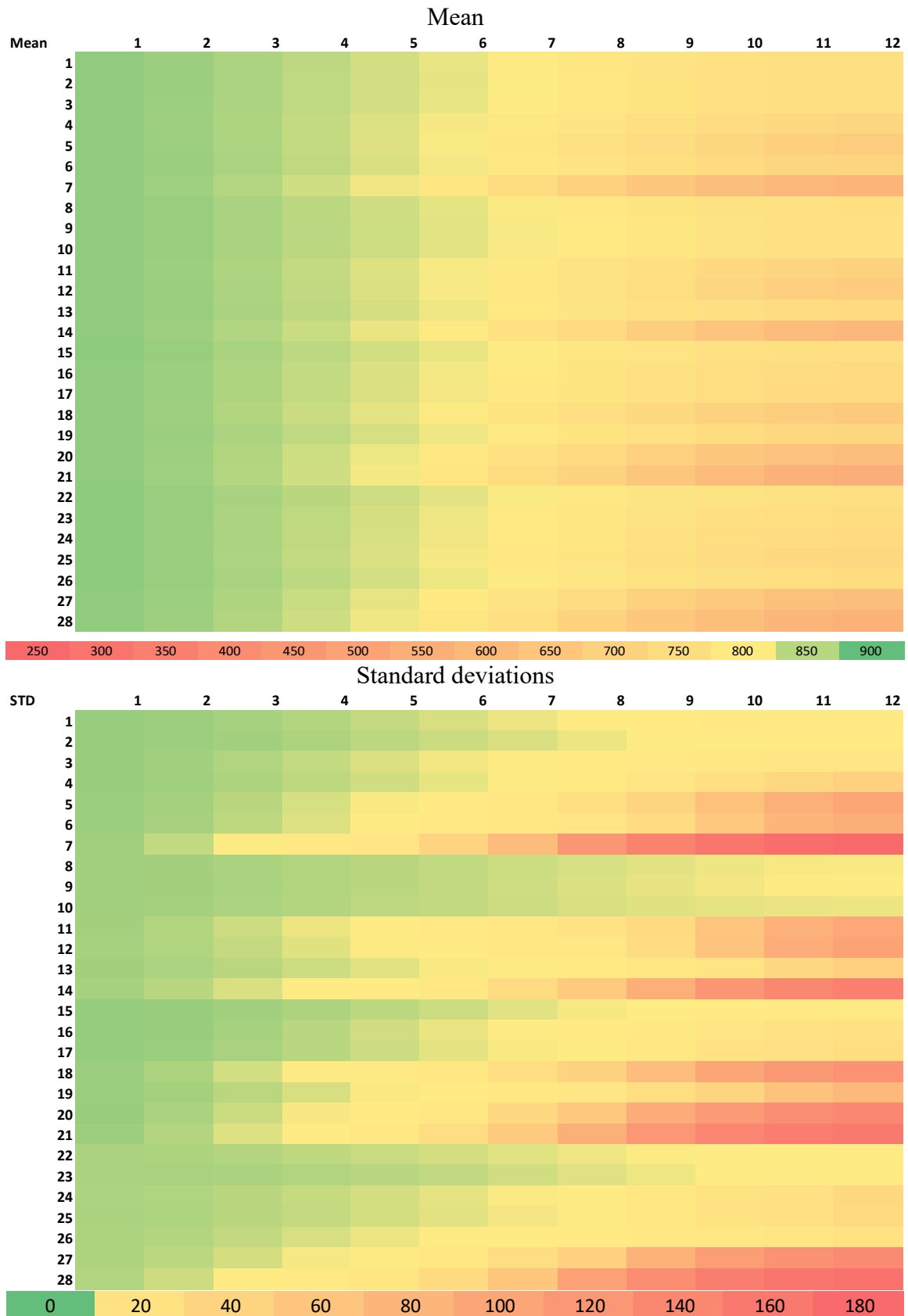


FIG.55. Distribution of mean and standard deviations for in-core coolant densities, in kg/m^3 , at 25 s. Each row represents one of the 28 thermal hydraulics channels, and each column one of the twelve axial fuel bundle positions. The right-hand side of each figure lies at the downstream end of the flow.

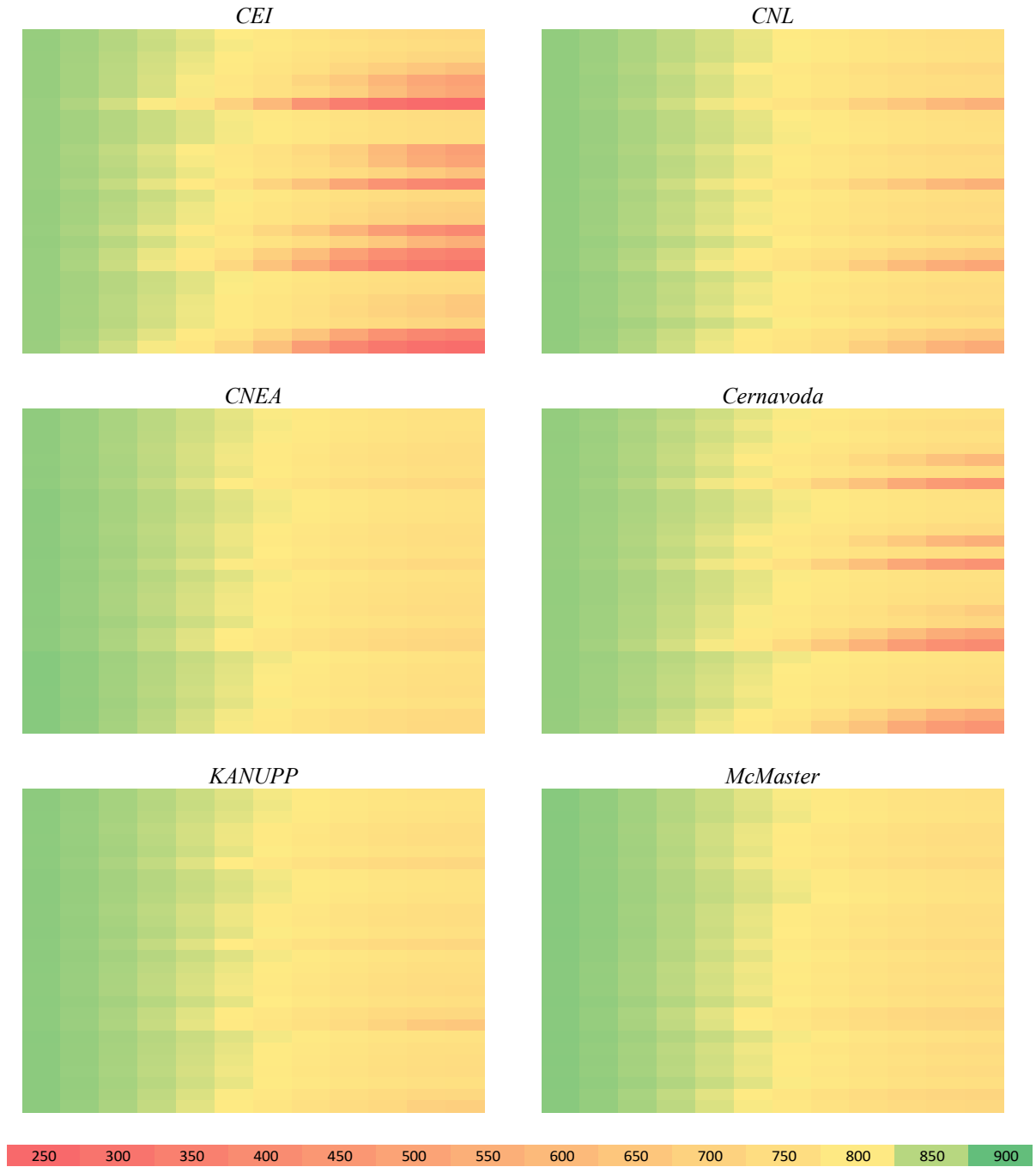


FIG. 56. Distribution of in-core coolant densities, in kg/m^3 , at 25 s. The colour map corresponds to the mean values from Fig. 55.

Figure 57 presents heat maps of the mean and standard deviations of the in-core fuel temperatures. These temperatures, reported in $^{\circ}\text{C}$, are averaged over all fuel elements within each fuel bundle position. Separate colour bars are used for the mean and standard deviation, owing to the differences in scale. Figure 58 presents the individual participant contributions and makes use of the same colour scheme as for the mean data. The CEI and CNEA team results feature the highest overall fuel temperatures, In-core temperature distributions follow a common pattern for all participants. Thermal hydraulics channels 4, 11, 18, and 25 generally present the highest temperatures, while channels 1, 7, 14, and 21 generally present the lowest. This is generally consistent with the mapping of thermal hydraulics channels presented in Fig 5 and the channel power distribution. The removal of the adjuster leads to a change in the steady

state power distribution (below); however, this change has two components: a core wide increase which competes with a localized increase in the vicinity of fuel channel M-18.

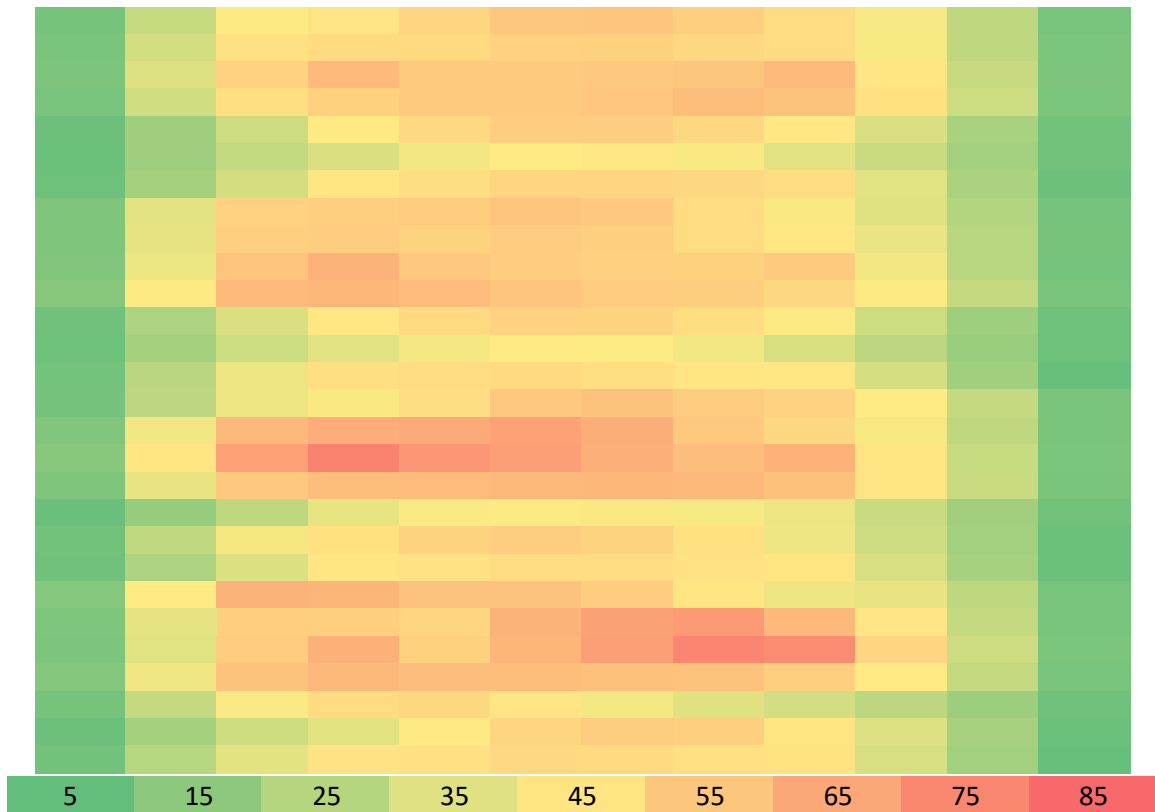
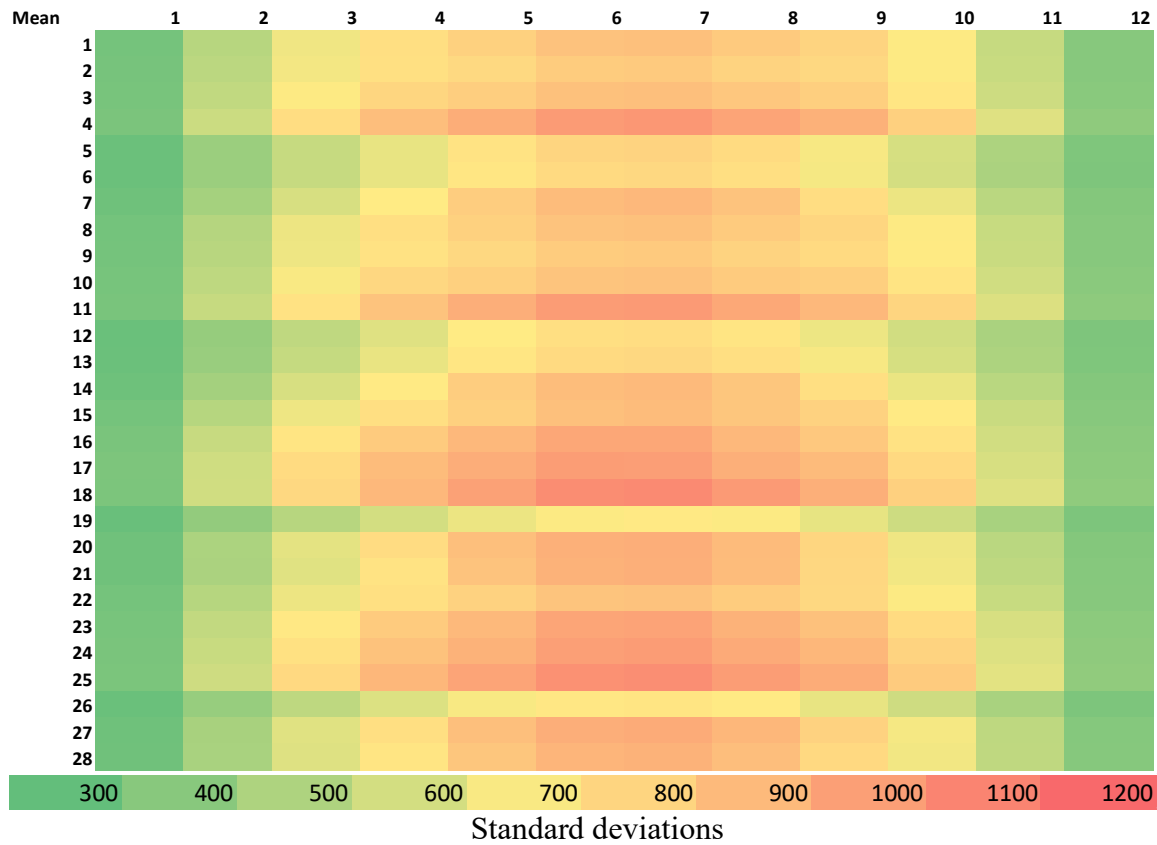


FIG. 57. Distribution of mean and standard deviations for in-core fuel temperatures, °C, at 25 s. Each row represents one of the 28 thermal hydraulics channels, and each column one of the twelve axial fuel bundle positions. The right-hand side of each figure lies at the downstream end of the flow.

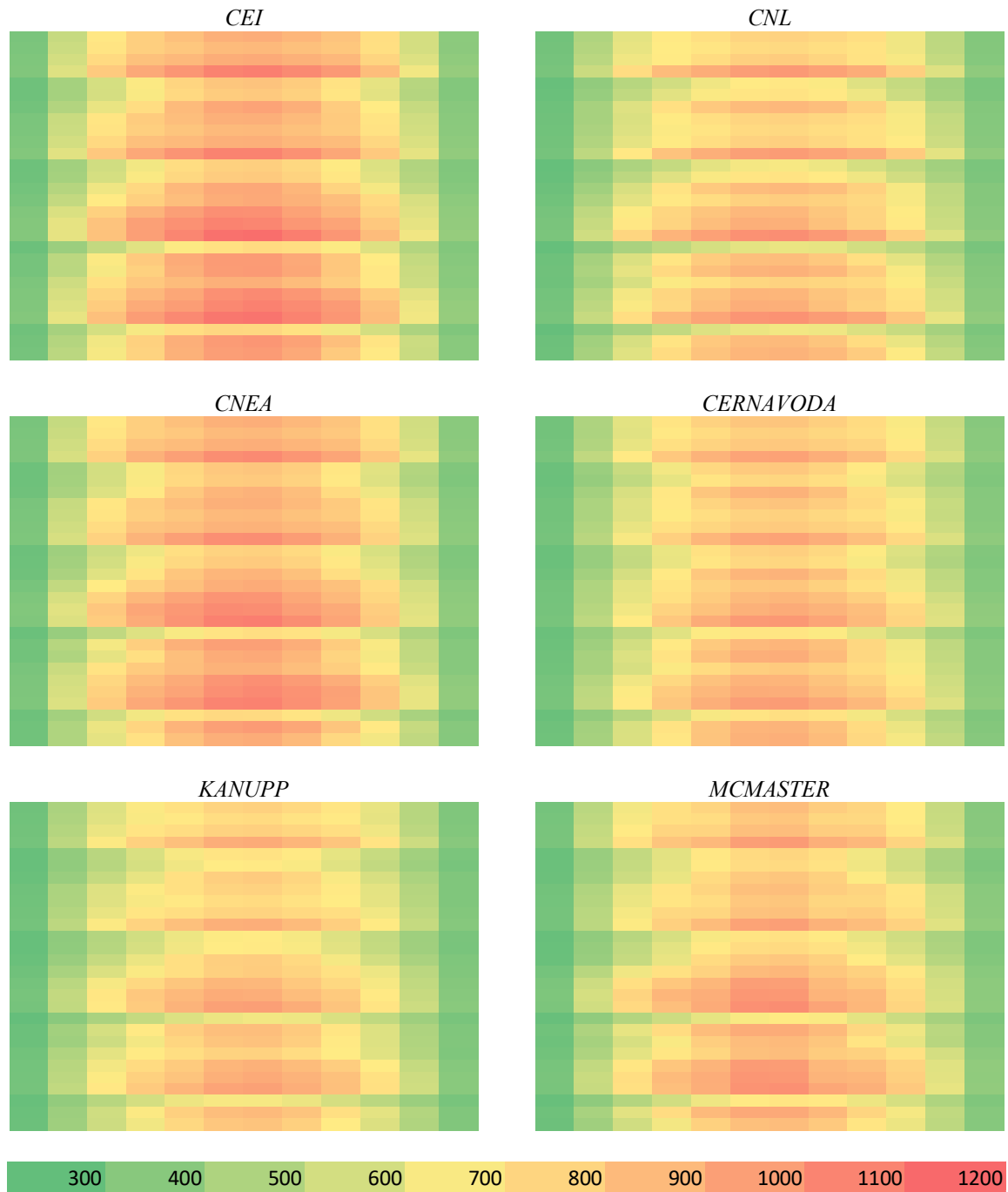
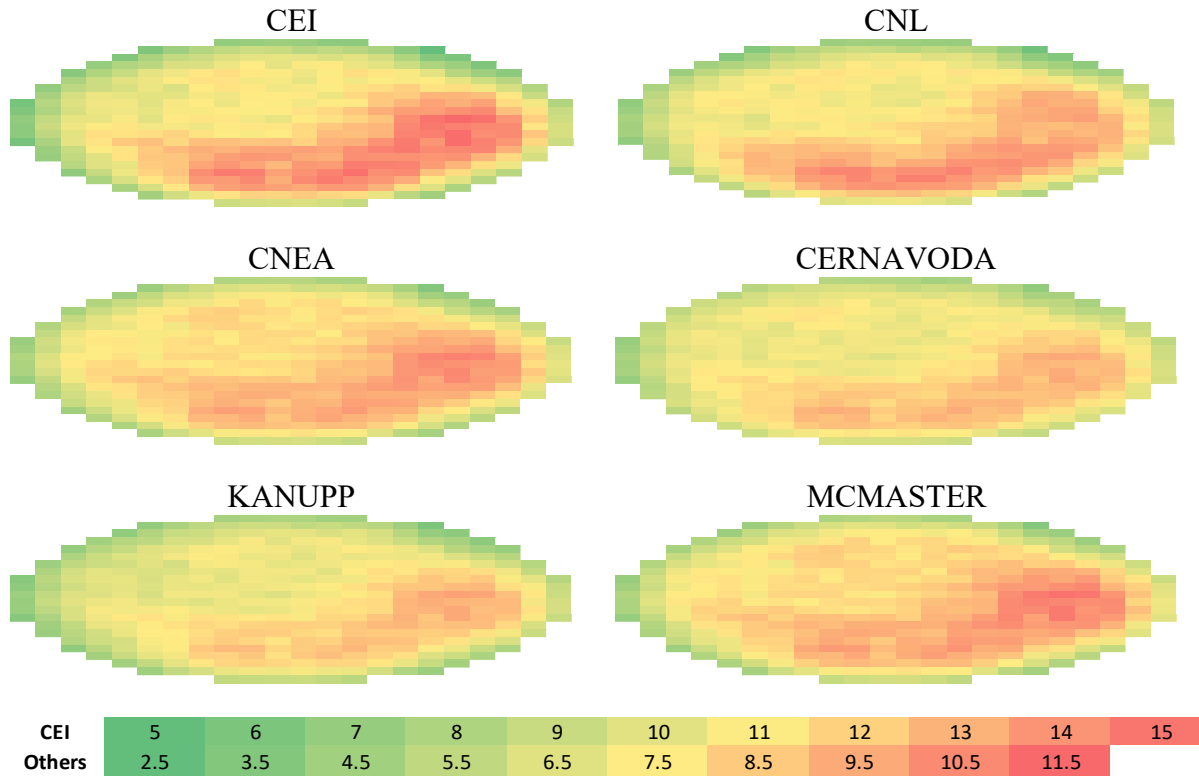


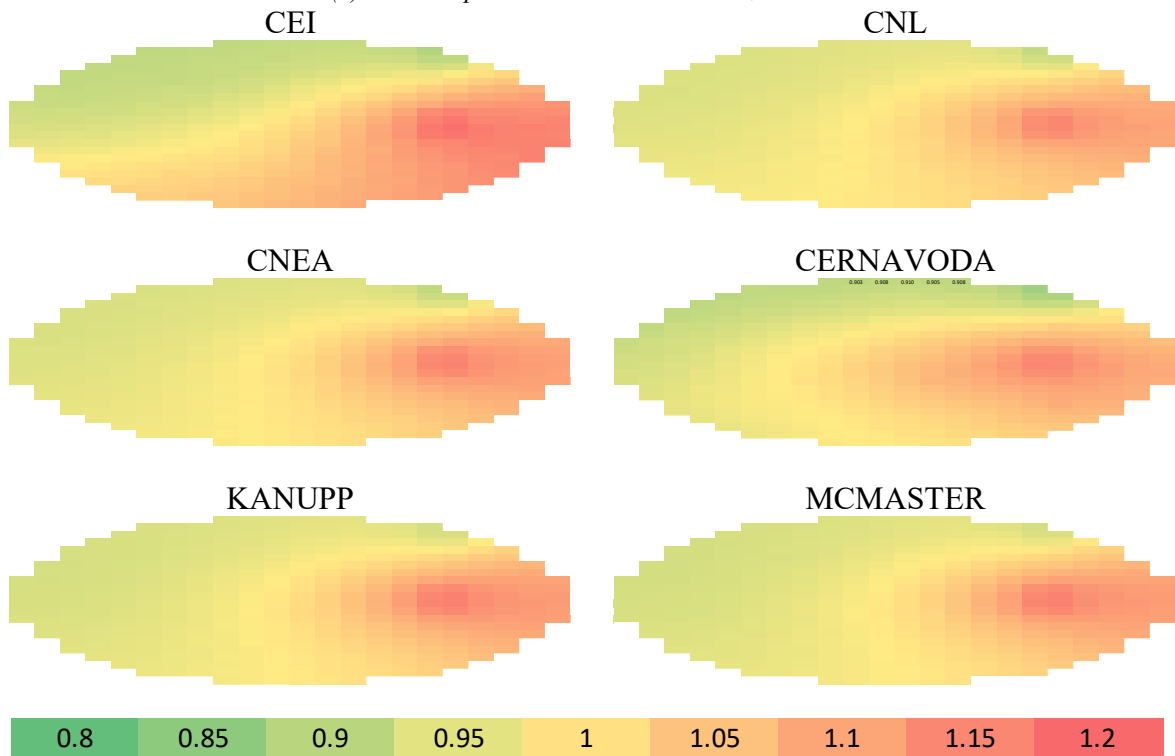
FIG. 58. Distribution of in-core fuel temperatures, in $^{\circ}\text{C}$, at 25 s. The colour bar is the same as for the mean values in Fig. 57.

Panel (a) in Fig. 59 presents the channel power distribution at 25 s. The heat maps use the colour red to indicate high power, however each sub plot uses a separate heat map scale. This decision was made to highlight changes in power distribution relative to the steady state and was necessitated by the large difference between the mean and maximum core relative power results. Relative to the steady state power distributions, all participants report a net power increase across all channels, with additional peaking in the general vicinity of fuel channel M18. This is consistent with the location of the two adjuster rods which are perturbed in this exercise. Panel (b) in Fig. 59 illustrates the effect. Channel powers at 25 s were normalized by participant's respective stead-state channel power distributions and core relative power at 25 s. Using this normalization scheme highlights that most participants predict similar relative

increases in regional core power. It is noteworthy that the CEI result presents the greatest relative change in core tilt, which may partially explain why this team also recorded the highest total core power increase.



(a) Channel power distributions at 25 s, in MW.



(b) Normalization by steady state power and final core relative power (dimensionless)

FIG. 59. Channel power distributions at 25 s. Panel (a) presents the channel power distributions. Panel (b) corrects the data by dividing out the respective steady state channel powers and final core relative powers reported by participants. Note use of different colour bars. All participants predict similar relative regional shifts relative to the steady state.

Figure 60 presents the critical channel power ratio. For each channel, the critical channel power ratio (CCPR) is computed as

$$CCPR = \frac{\text{Reference}}{\text{Cha power}} \quad (18)$$

Where the reference power distribution is presented in Fig. 61. This reference distribution was adapted from data commonly used by industry. A CCPR ratio below unity is indicative of a potential dry-out condition and a prelude to fuel failure. A simple three point colour scheme is used to highlight safe channels in green (CCPR > 1.1), channels in potential dry out in red (CCPR < 1), and channels at risk (yellow). Owing to the large core relative power, CCPR < 1 for all channels in the CEI contribution. For the other participants, the number of channels at risk of dry out varies based on the core relative power and individual channel power distributions.

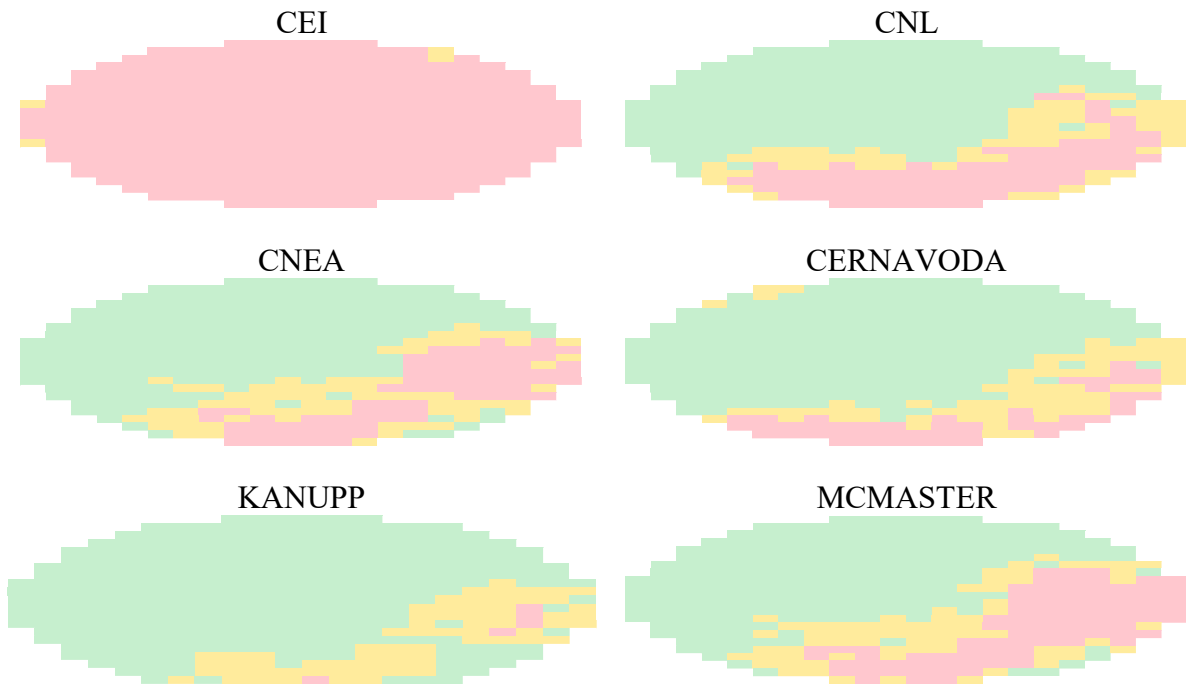


FIG. 60. CCPR distribution with three point colour scheme. Red CCPR < 1, Yellow: $1.0 \leq CCPR \leq 1.1$, and Green: CCPR > 1.1. A CCPR ratio below unity is indicative of a potential dry-out condition.

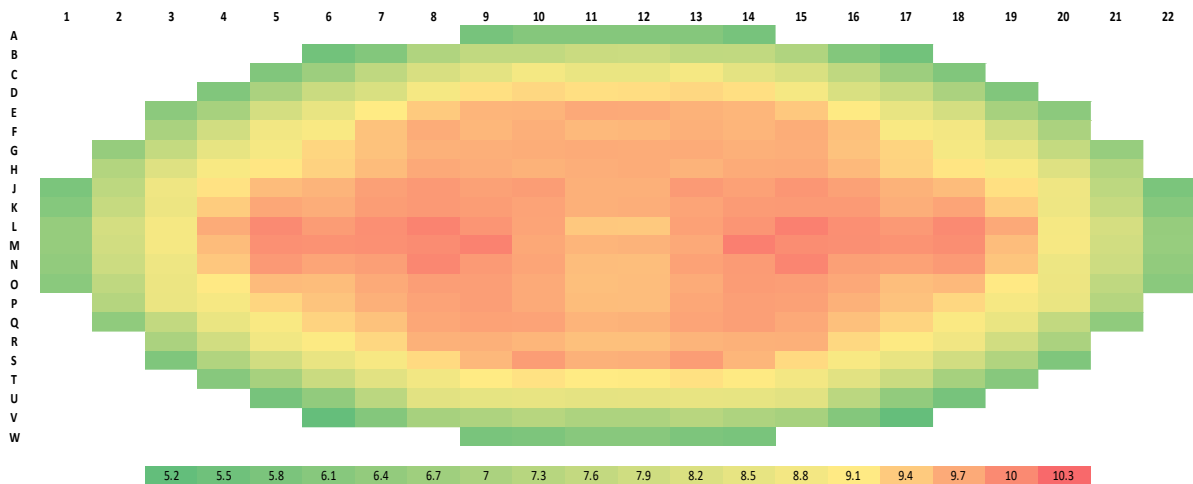


FIG. 61. Reference critical channel power distribution, all values in MW.

5.4. PUMP TRIP TEST PROBLEM

5.4.1. Standalone neutronics

This problem is attempted by CNL, CNEA, KANUPP, and McMaster. Figure 62 shows variation of the core relative power (%) with time for the prescribed simulation time of 25 s following the transient. The graph is plotted on a semi log scale as the power rises exponentially in later stage of the transient. The trend of power variation predicted by all the participants is similar in general; a linear increase up to first 17.5 s followed by an exponential increase in the power. The results obtained by all the participants are in close agreement during the first stage of linear increase. However, a huge deviation in results is observed during the second stage. After the specified simulation time, CNL has highest power rise (114,733.40 %) followed by CNEA (44,890.64 %), McMaster (4,073.9 %) and KANUPP (2,152.56 %) after. The power rise predicted by KANUPP is comparatively lowest.

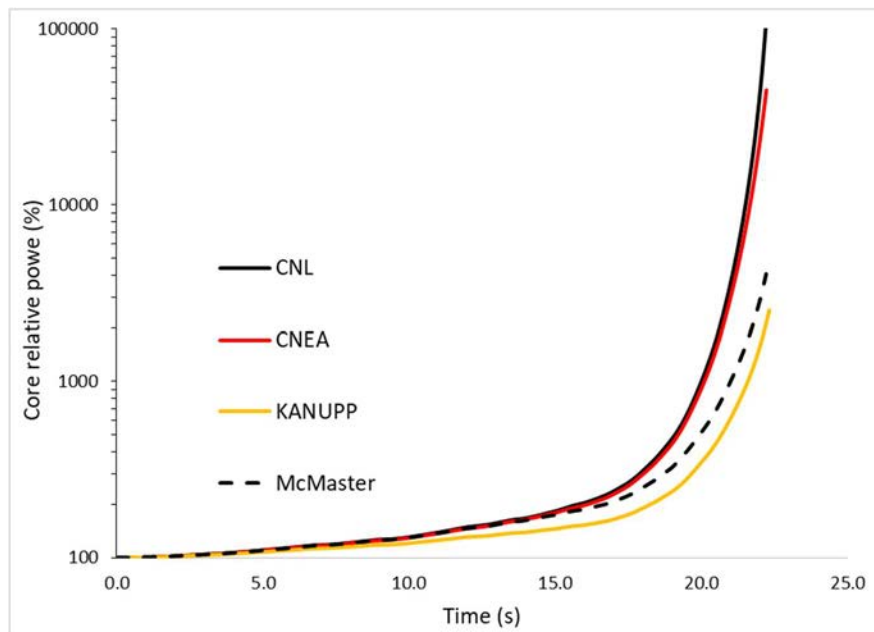


FIG.62. Time evolution of relative core power (%) for the pump run down standalone neutronics variant problem.

TABLE 24. MAXIMUM CHANNEL AND BUNDLE POWER

FOM	Maximum channel power at 15 s	Maximum channel power location	Maximum bundle power at 15 s	Maximum bundle power location
Unit	MW	-	kW	-
Mean	12.55	-	1534	-
Max-Min.	3.85	-	425	-
CNL	14.36	S9	1724	S9P7
CNEA	12.91	S9	1578	S9P7
KANUPP	10.51	S9	1299	S9P7
McMaster	12.42	S9	1534	S9P7

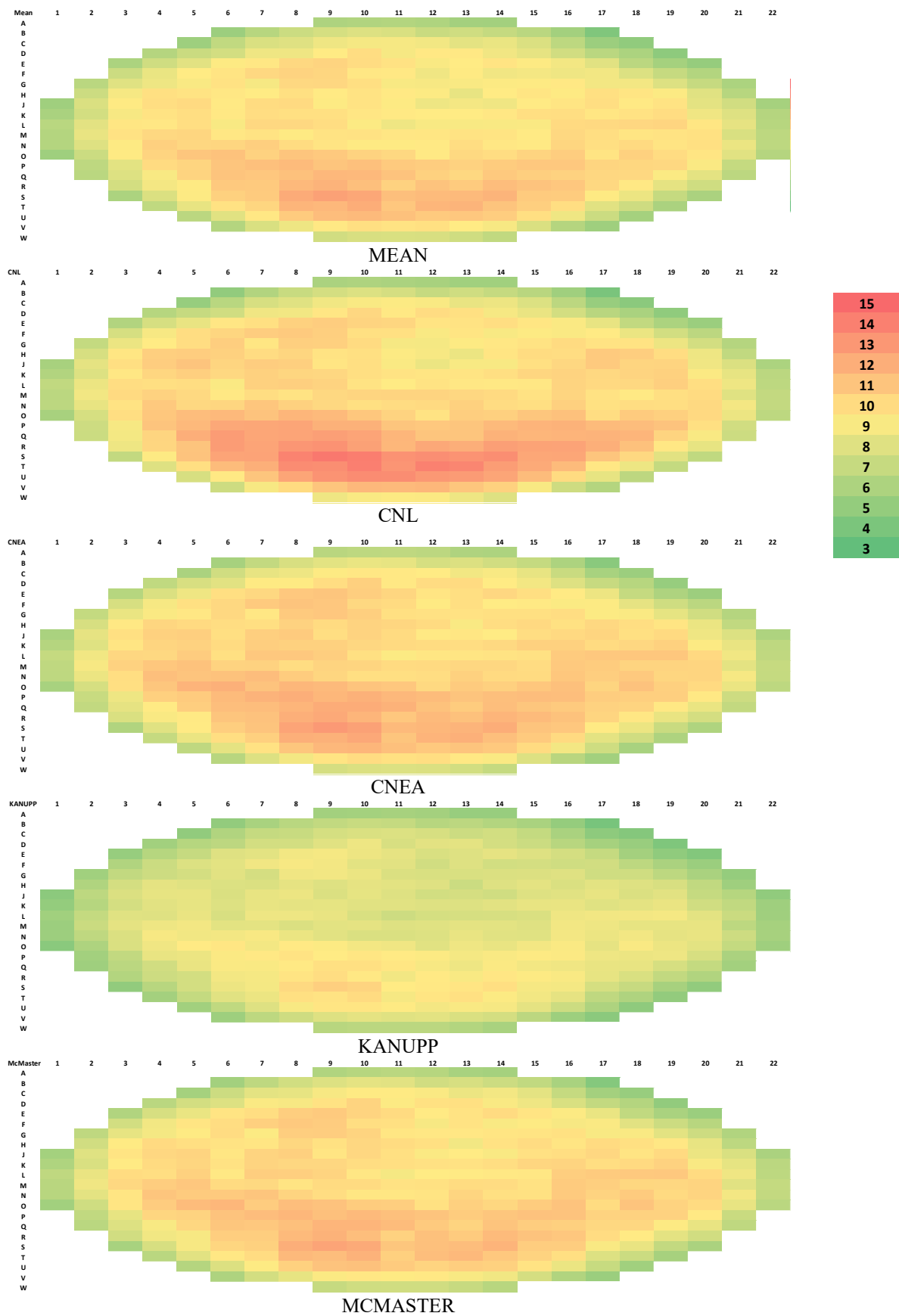


FIG. 63. Cross sectional view of the distributions of in-core channel power in MW at 15 s. The same colour scheme is used for all heat maps.

The mean of channel powers of all participants' data and individual contributors channel power data at 15 s following transient is presented in Fig. 63. It can be seen from this figure that the channel power is not symmetrical over the core cross section rather it is concentrated toward lower half for the case of CNL, CNEA, KANUPP and toward left half in case of McMaster. The channel powers reported by McMaster are much higher than the rest of the participants. The results of McMaster have affected the mean of channel powers.

The maximum channel and bundle powers are given in Table 24. All the participants predicted have the same location (S9) of the maximum channel power whereas the location of maximum bundle power predicted by McMaster (S9P6) is just one plane away then the rest of the participants (S9P7). The maximum bundle power and channel power values of the McMaster team are higher than the other participants.

5.4.2. Standalone thermal hydraulics

Figure 64 shows variation of pressure with time obtained by all participants except Cernavoda and CEI teams. Figure 65 presents the corresponding void evolution. With pump rundown, a linear increase is observed followed by an exponential increase in the reactor pressure. This observed behaviour is interrelated to the difference in heat generation and removal. The imbalance is small at the start of transient as the flow does not stop immediately due to inertia and keeps on increasing with pump coast down. The added heat results in increased temperature of the system thereby increasing void as observed in the figure on right. The positive void feedback reactivity causes further increase in power. The mismatch in heat generation and removal grows exponentially giving rise to a rapid increase in pressure.

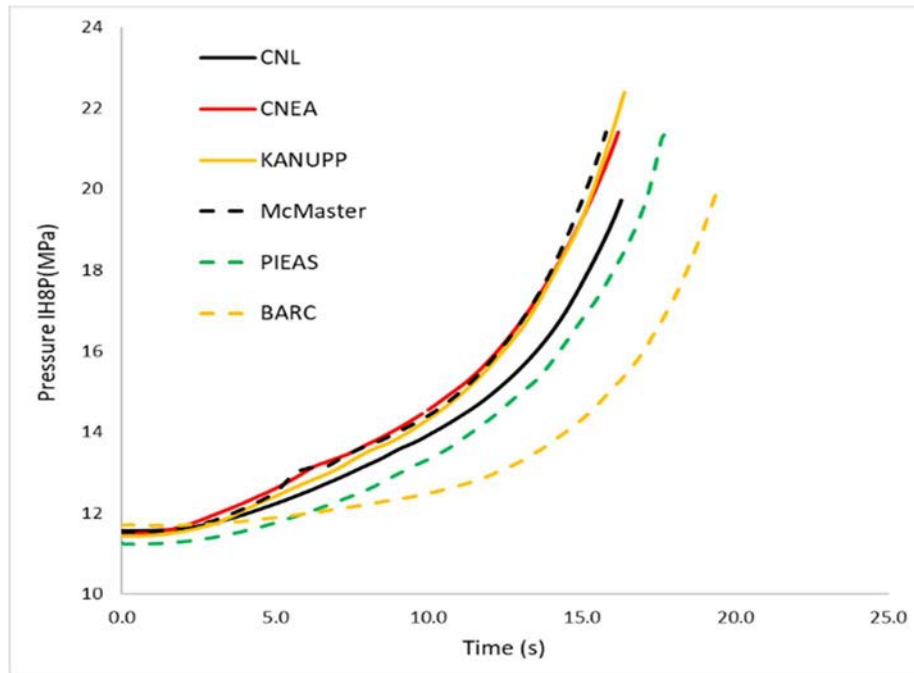


FIG. 64. Pressure at IH8 in the standalone thermal hydraulic variant problem.

Enormous increase in pressure results in inversion of void fraction as predicted all of the participants except BARC for which case it keeps on increasing monotonously. The trend of pressure and void fraction evolution by different participants is similar. The pressure and void fraction predicted by CNEA, KANUPP and McMaster, all RELAP/TRACE users, are very close to each other whereas there is a notable difference in pressures and void fraction predicted

by rest of the participants. The transient is terminated due to error of properties out of range or code limitations when pressure reaches critical point (22 MPa).

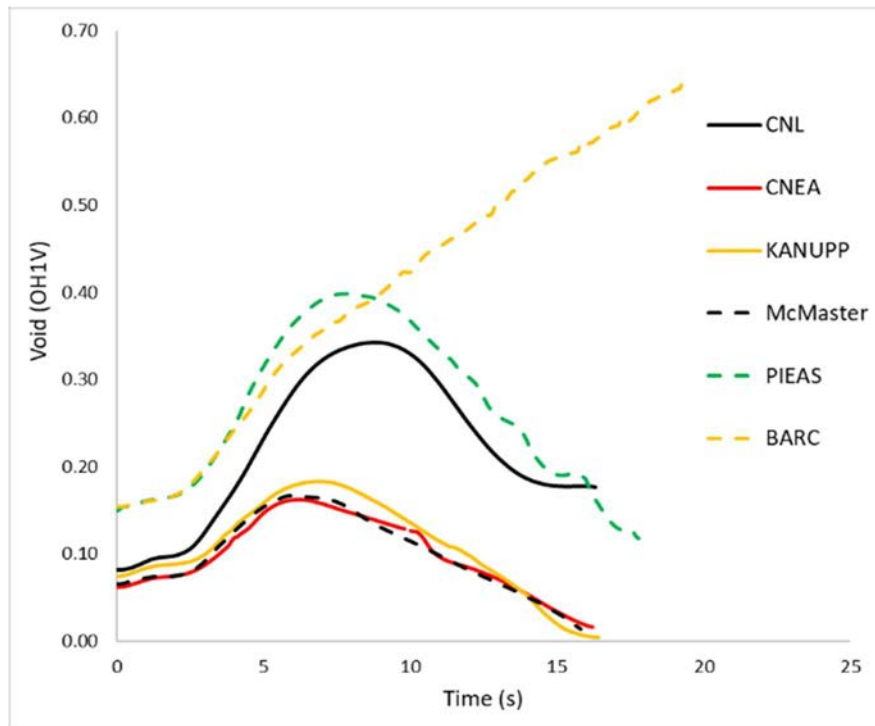


FIG. 65. Void at OH1 in the standalone thermal hydraulic variant problem.

Figures 66, 67 and 68 present the distributions of pressure, temperature, and void fraction within the thermal hydraulics network at 15 s. Pressure, temperature and void distributions are similar only magnitude of these parameters differ for different participants.

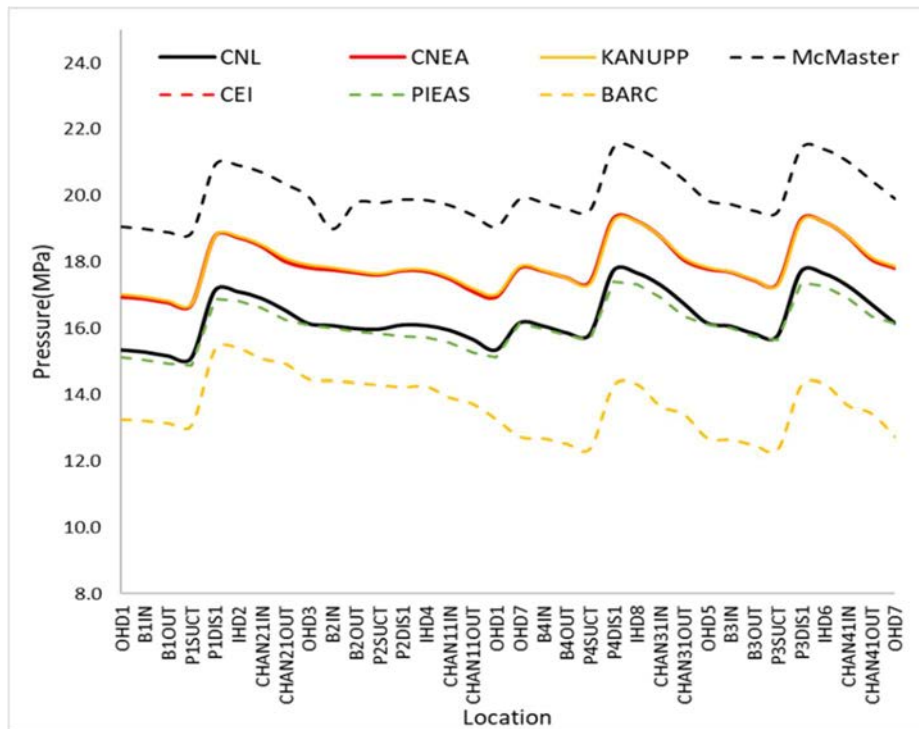


FIG. 66. Coolant pressure in the network after 15 s.

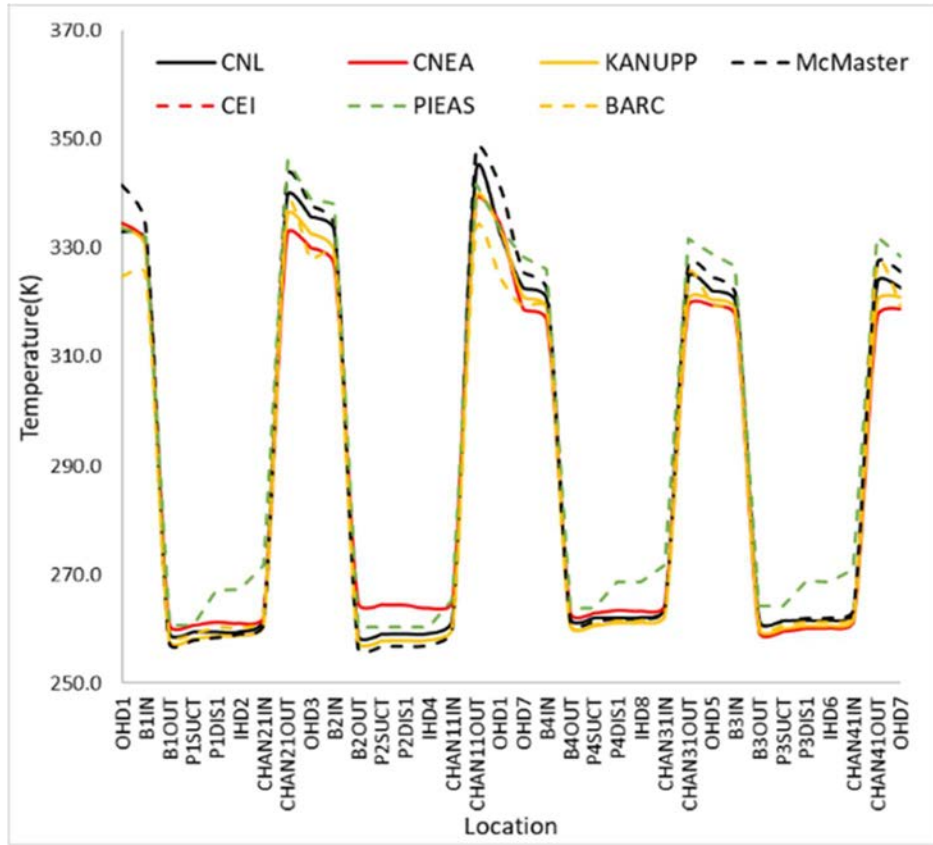


FIG. 67. Coolant temperature in the network after 15 s.

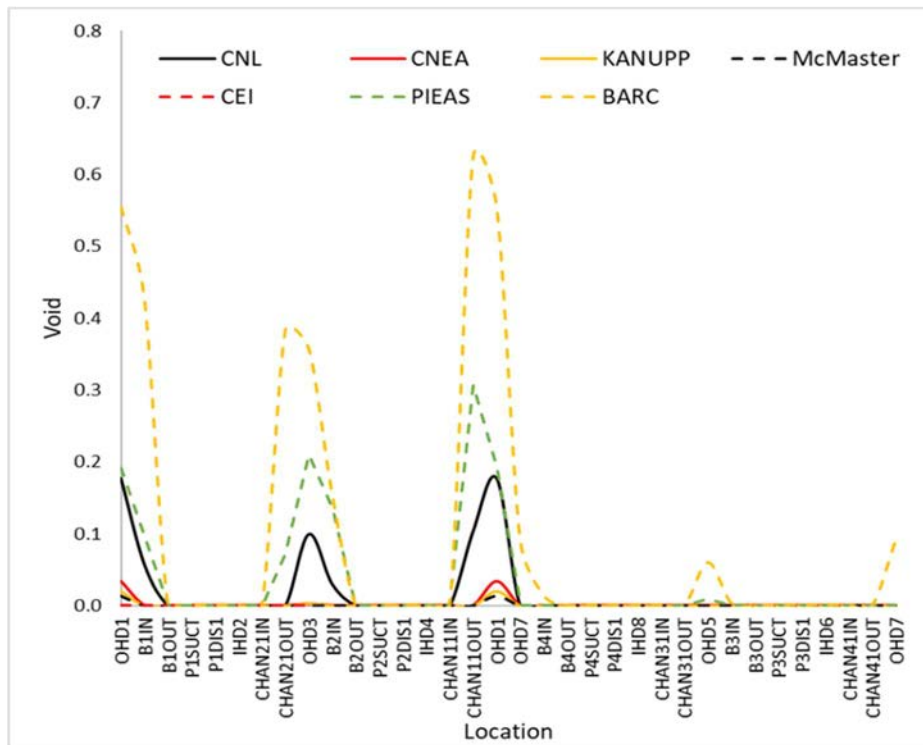


FIG. 68. Void fraction in the network after 15 s.

5.4.3. Coupled converged case

Seven participants presented results for this problem: CNL, CNEA, Cernavoda, KANUPP, McMaster, CEI and BARC.

Table 25 presents several scalar FOM from the coupled pump rundown problem. Mean and standard deviations, where applicable, are also reported. The integrated enthalpy in the core (IENTHL), is computed from the time integral of the total core power from 0–5 s. The maximum energy deposited in a fuel bundle (MAXHB), is computed using the following procedure. The bundle power time series at each location of the core are integrated separately, converted to kJ units, and divided by a reference fuel mass of 27.014 kg. The maximum value is then reported, as is the fuel bundle position where the maximum was found. Neither of these figures of merit account for heat removal due to cooling, and readers are reminded that decay heat was excluded from the problem specifications. In most cases, MAXHB lies in the range 450–505 kJ/kg. The result from the CEI team is an outlier, however this is consistent with the larger power pulse which was reported.

TABLE 25. SELECTED SCALAR FIGURES OF MERIT FROM COUPLED PUMP RUNDOWN TRANSIENT AT 15 s

FOM	IENTHL	MAXHB	MAXHB location
Unit	MJ	kJ/kg	-
Mean	34,034	595	n/a
Std. dev	3,530	324	n/a
CNL	33,619	289	T-12-7
CNEA	31,827	502	S-9-7
CERNAVODA	37,086	-	--
KANUPP	31,633	-	--
CEI	41,312	1,224	--
BARC	31,260	460	M-4-6*
McMaster	31,500	505	S-9-7

*Indistinguishable from M-4-6,M-6-6,M-8-6,M-10-6,N-5-6,N-7-6,N-9-6,N-11-6,O-6-6,O-8-6,O-10-6 M-4-7,M-6-7,M-8-7,M-10-7,N-5-7,N-7-7,N-9-7,N-11-7,O-6-7,O-8-7,O-10-7.

Table 26 shows a comparison of the maximum channel and bundle power at 15 s and their location of each participant. The standard deviation of those values and the maximum of the mean channel power distribution are also reported. A good agreement is found regarding position of maximum channel power and bundle, with the exception of BARC. However, that participant is not simulating differences in power within a TH group, so differences are to be expected.

There is a significant discrepancy in the results, but it is expected, given the important differences in total power presented in Fig. 69, which shows the time dependent reactor thermal power, related to the steady state condition. Important differences are observed, and they could be grouped by the thermal hydraulic code family: RELAP/ TRACE users simulate an increase in power lower than 20% while CATHENA/ARIANT users reach higher values, even leading to interruption of simulation before the specified time.

TABLE 26. MAXIMUM BUNDLE AND CHANNEL POWER AT 15 s

FOM	Maximum channel power at 15 s	Maximum channel power location	Maximum bundle power at 15 s	Maximum bundle power location
Unit	MW	-	kW	-
Mean	110	-	1351.4	-
Std.Dev.	4.8	-	589.5	-
CNL	9.7	S9	1167	S9P7
CNEA	7.7	S9	953	S9P7
Cernavoda	11.5	S9	1413	S9P7
CEI	21.3	S9	2620	S9P7
BARC	7.1*	N11 M10 O10 N9 M8 N7 M6 O6 N5 M4	871.2*	(N11 M10 O10 N9 M8 N7 M6 O6 N5 M4)-(06 07)
KANUPP	7.8	S9	969	S9P7
McMaster	12.42	S9	1534	S9P7

* BARC maximum channel and bundle powers at N11, M10, O10, N9, M8, O8, N7, M6, O6, N5, and M4 are identical.

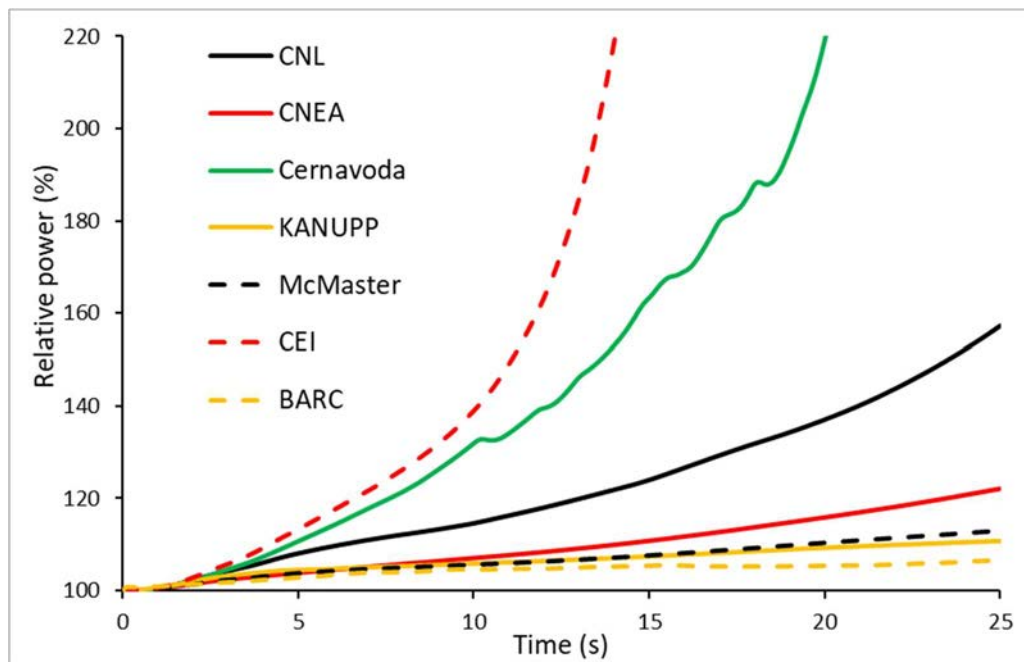


FIG. 69. Relative power evolution during coupled pump rundown transient.

Figure 70 shows mass flow evolution through pump 2. There are important differences in reported results. In this case again different behaviours can be observed between RELAP/TRACE and CATHENA/ARIANT users, the latter simulate a more oscillating response while the former's decreases in a monotonous manner.

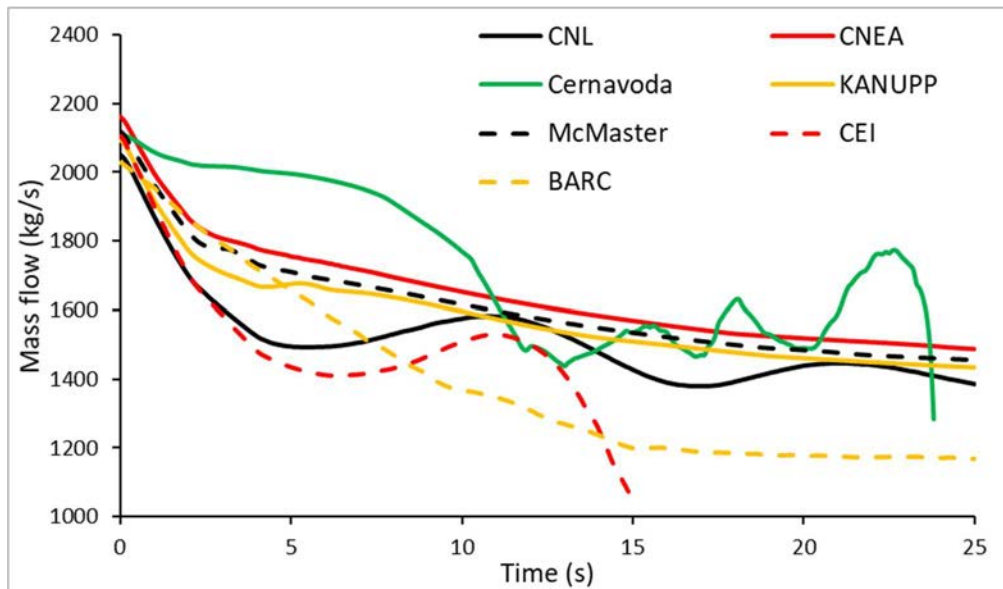


FIG. 70. Pump 2 mass flow evolution during coupled pump rundown transient.

Figure 71 shows pressure evolution in IHD8 component and Fig. 72 shows void fraction evolution for the OHD1 component. These variables are closely related, and it can be observed that some participants simulate a steeper pressurization during the first seconds of the transient. This prevents high void fractions from appearing. Due to the positive void fraction, this in turn moderates power increase and the effect of the positive feedback loop between power and void generation.

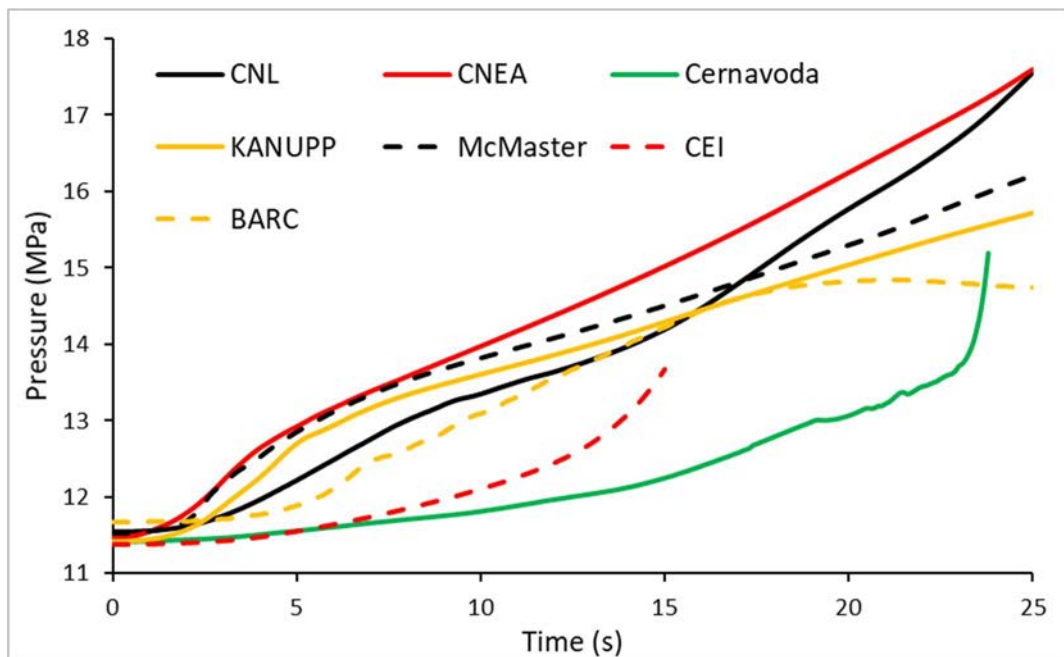


FIG. 71 Pressure evolution in IH8 component evolution during coupled pump rundown transient.

It would be expected that a totally liquid pressurizer would produce a steeper increase in pressure in the event of a decrease in coolant density produced by an increase in power, moderating void production; this effect would be milder if the pressurizer had a steam mattress, allowing a higher void production. This approximately correlates with reported results, with

higher pressurizations obtained by participants with initially filled pressurizers. The exception is Cernavoda.

Figures 73 and 74 show profiles of respectively coolant temperature and pressure within the circuit at 15 s. Higher dispersions on temperature are found in components in the core region, where differences reach up to 20 °C. Differences are bigger for the affected loop; in the other one, the bulk of the participants present differences lower than 10 °C, with the exception of CEI, who has the highest temperatures with differences up to more than 10 °C with the other contributions. Differences on pressure are much more significant, up to near 4 MPa, without any apparent relation between family codes or pressurizer level.

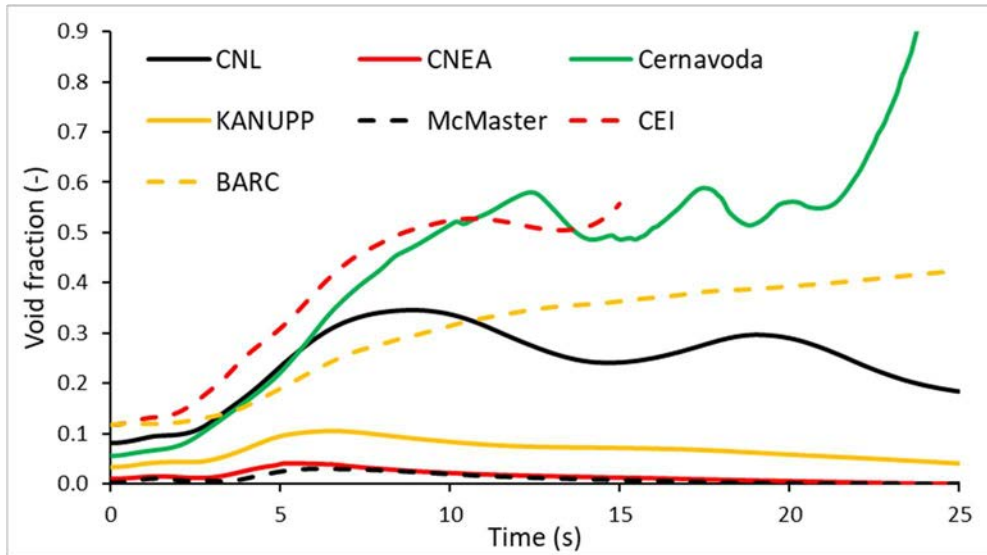


FIG. 72. Void fraction evolution in OHI component evolution during coupled pump rundown transient.

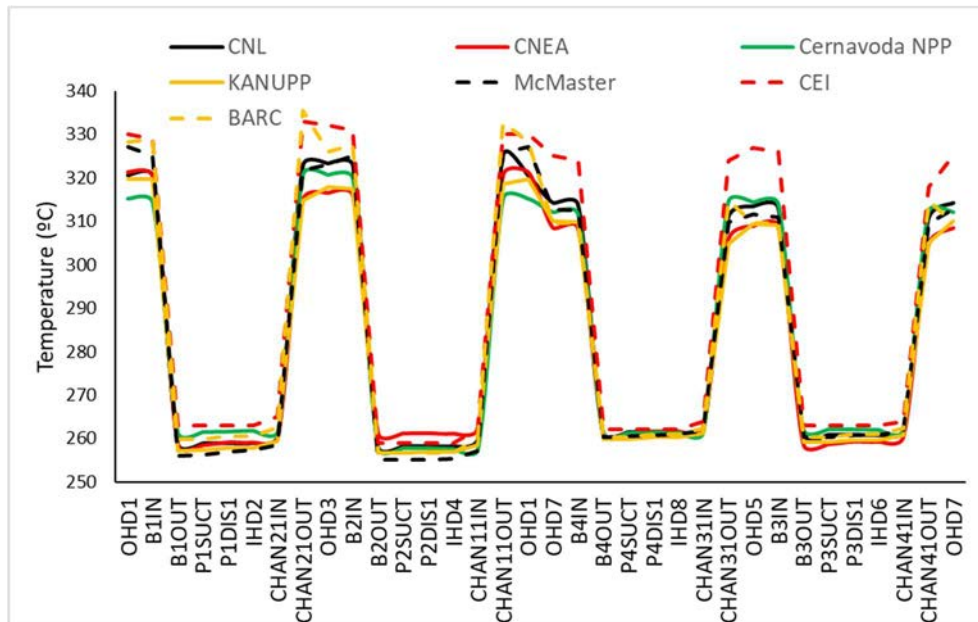


FIG. 73. Coolant temperature profile at 15 s of coupled pump rundown transient.

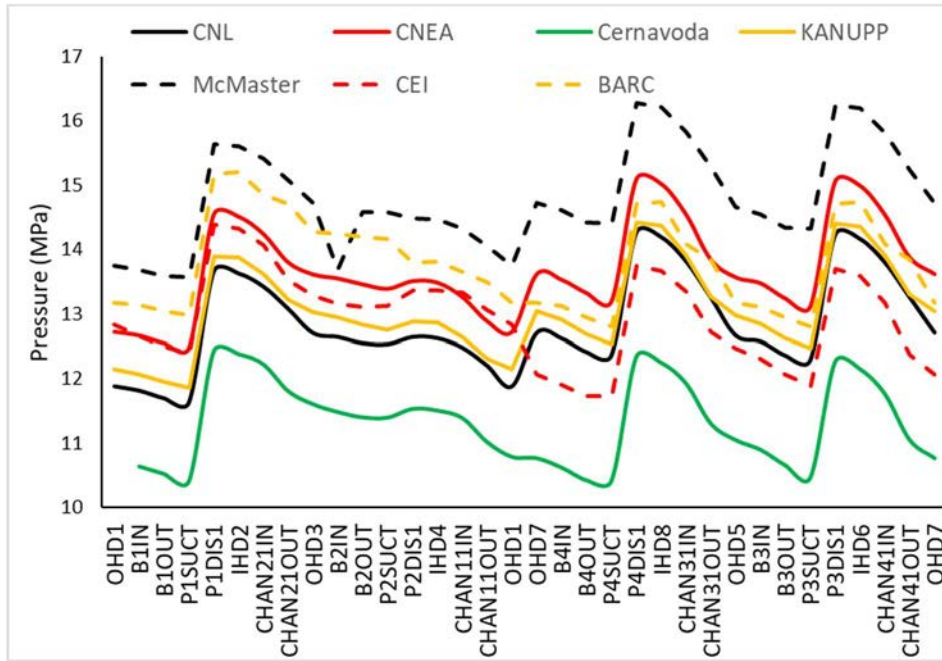


FIG. 74. Pressure profile at 15 s of coupled pump rundown transient.

Figure 75 shows void fraction at 15 s of the transients. Differences of up to over 0.6 can be observed in the loop that corresponds to pump 2. The components that are part to the other loop have differences of up to 0.2. Higher void fractions correspond to the participants with higher predicted power, with the exception of BARC that has one of the highest void fractions but the lowest increase in power. However, the initial void values for BARC are higher, as it can be seen in the steady state results.

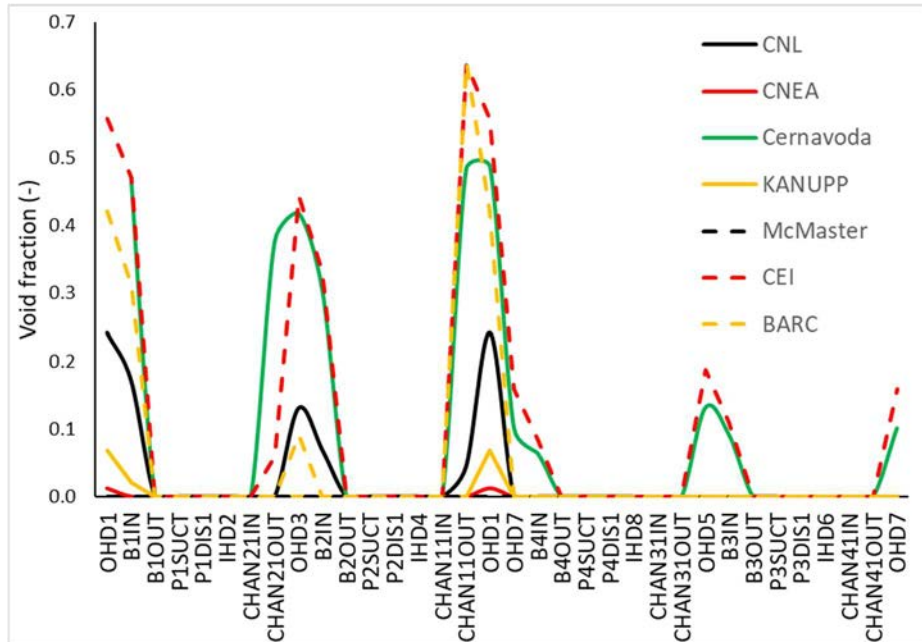


FIG. 75. Void fraction profile at 15 s of the transient.

Figure 76 shows the normalized mean channel power and the channel power maps of each participant, calculated at 15 s. A single colouring scheme is used. Participant's results were normalized using the total core power reported at 15 s and multiplying by 380. It is noticeable

the difference of distribution obtained by BARC, having three distinct zones of high, medium and low power, in addition to not modelling differences of power in channels within a thermal hydraulics group.

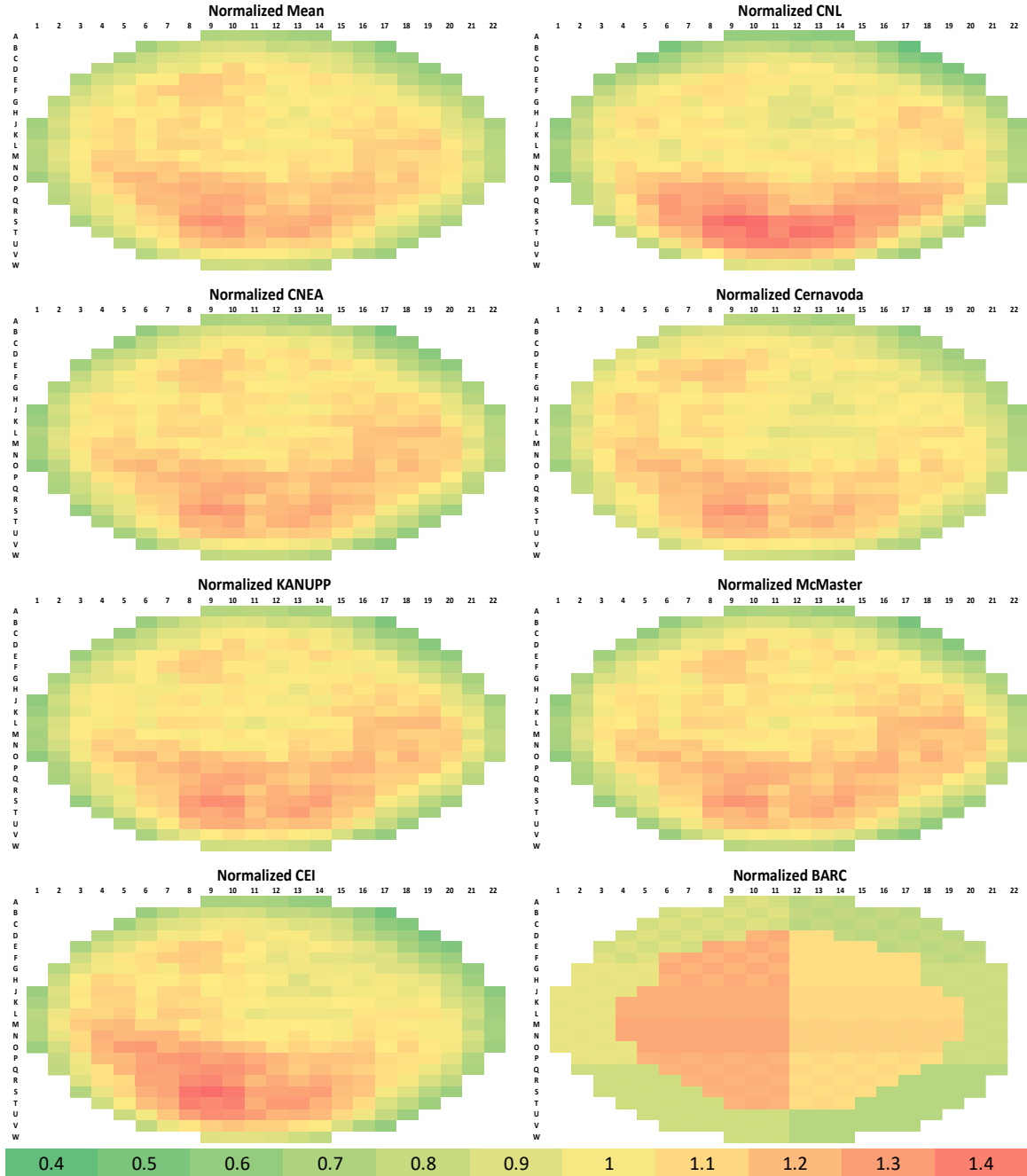


FIG. 76. Normalized channel power distributions at the end of coupled pump rundown transient (dimensionless).

Figure 77 shows standard deviation of power distribution per channel and standard deviation of power distribution per channel normalized by average power per channel. High dispersion can be observed in raw power distributions, mainly due to the BARC discretization if thermal hydraulics groups. In the normalized cases a much lower dispersion is observed when BARC is excluded from comparison and it tend to grow towards the periphery of the core.

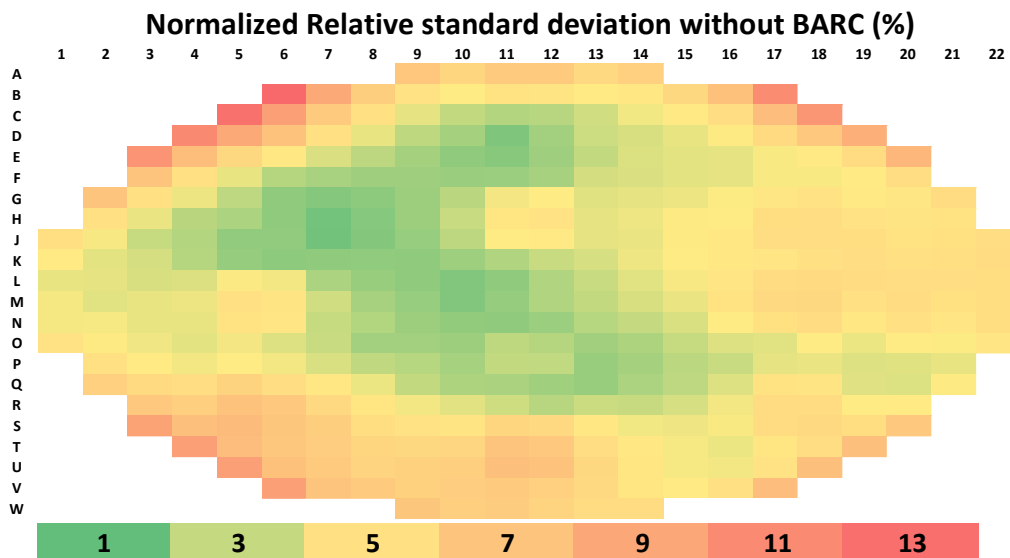
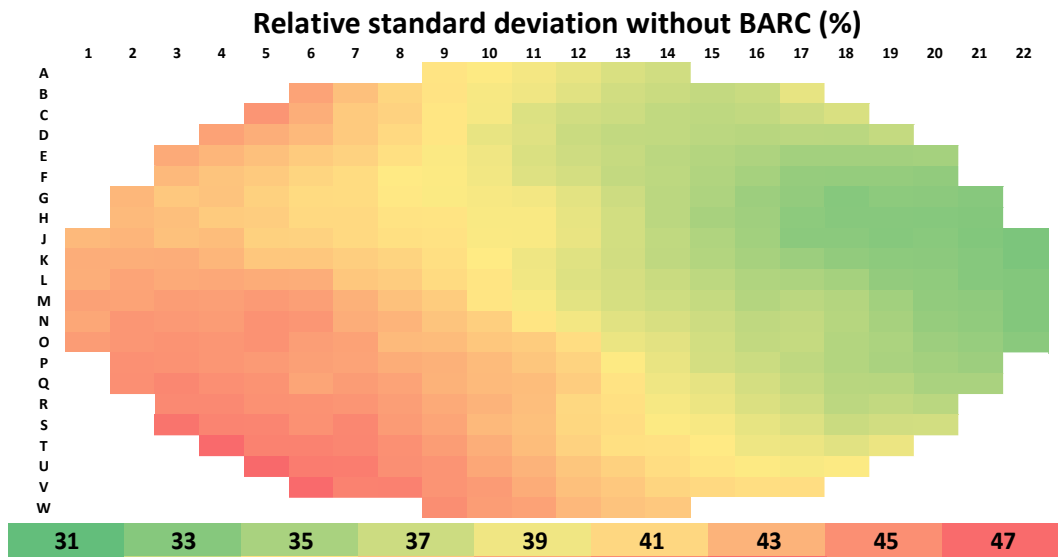
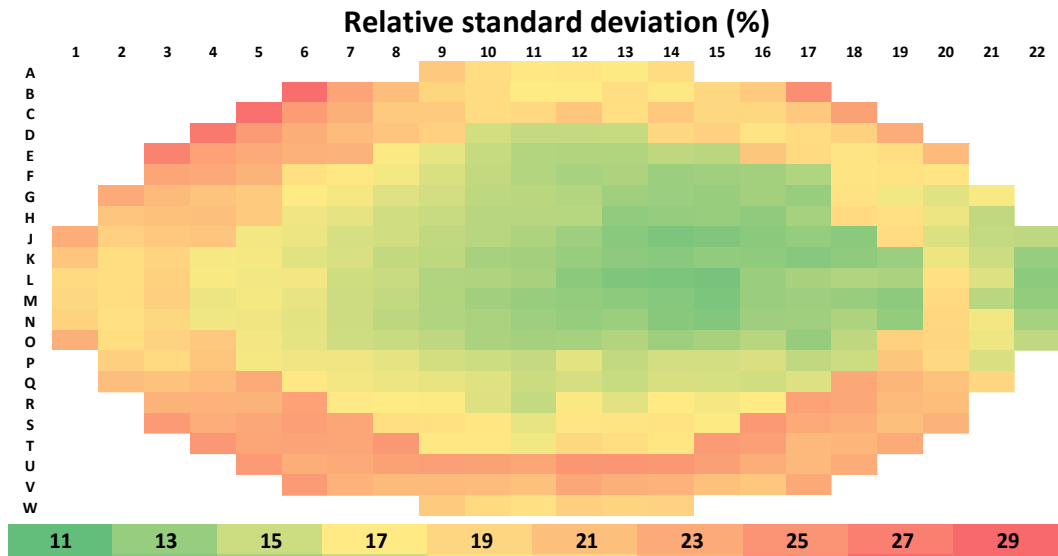


FIG. 77. Relative standard deviation for power distribution raw and normalized by total power.

Figure 78 shows fuel temperature profiles in the core at the end of the transient. Higher differences are observed in the middle of the outer most channel groups.

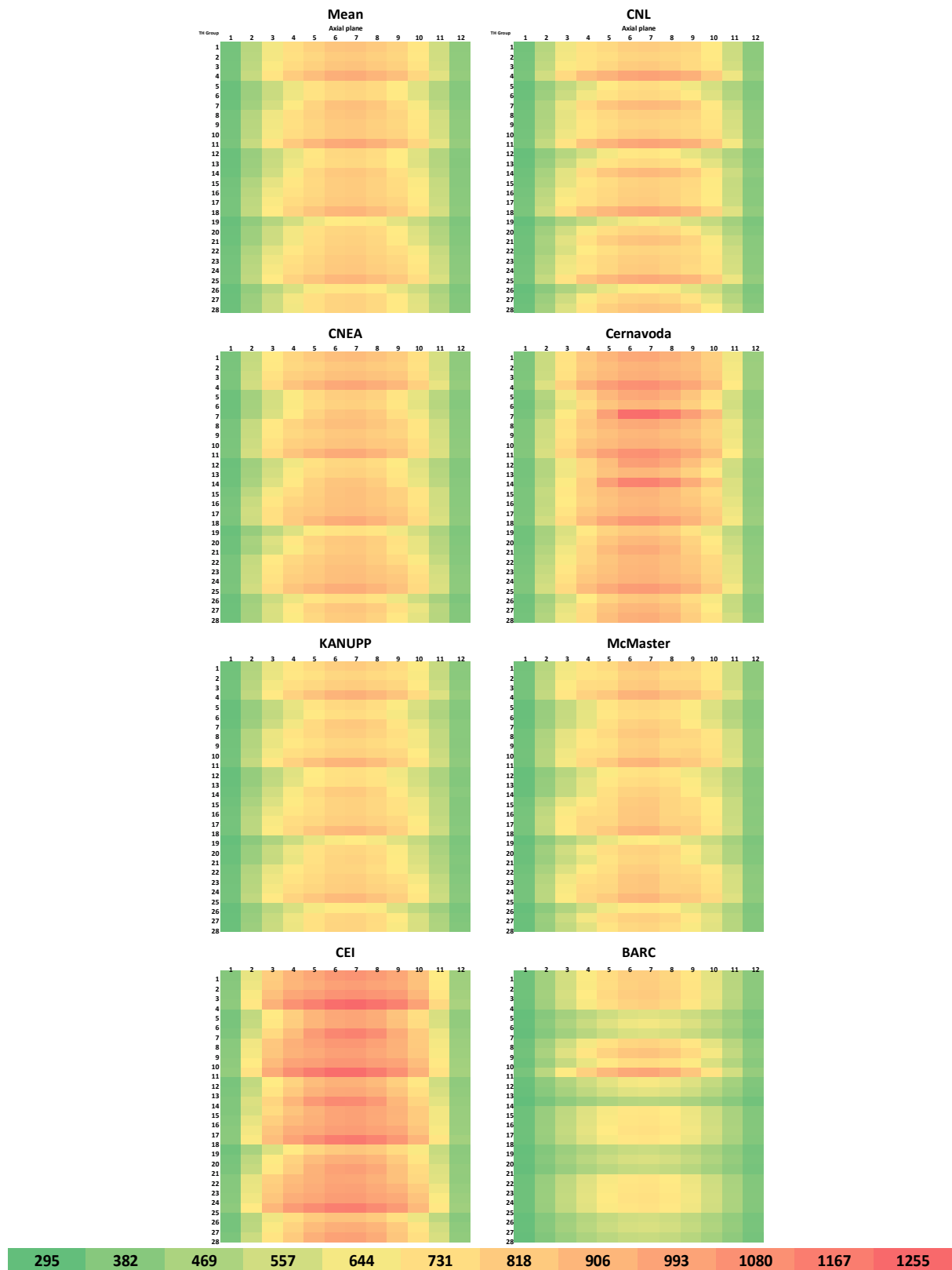


FIG. 78. Mean and participant fuel temperature distributions at the end of coupled pump rundown transient, °C.

Figure 79 presents the mean and participant results for the in-core coolant density distributions. Two different colour scales are required because of the overall magnitudes of the CEI team

results. Noticeable differences in relative voiding are observed between the participants, however there is no obvious link to the code families (TRACE/RELAP vs CATHENA/ARIANT).

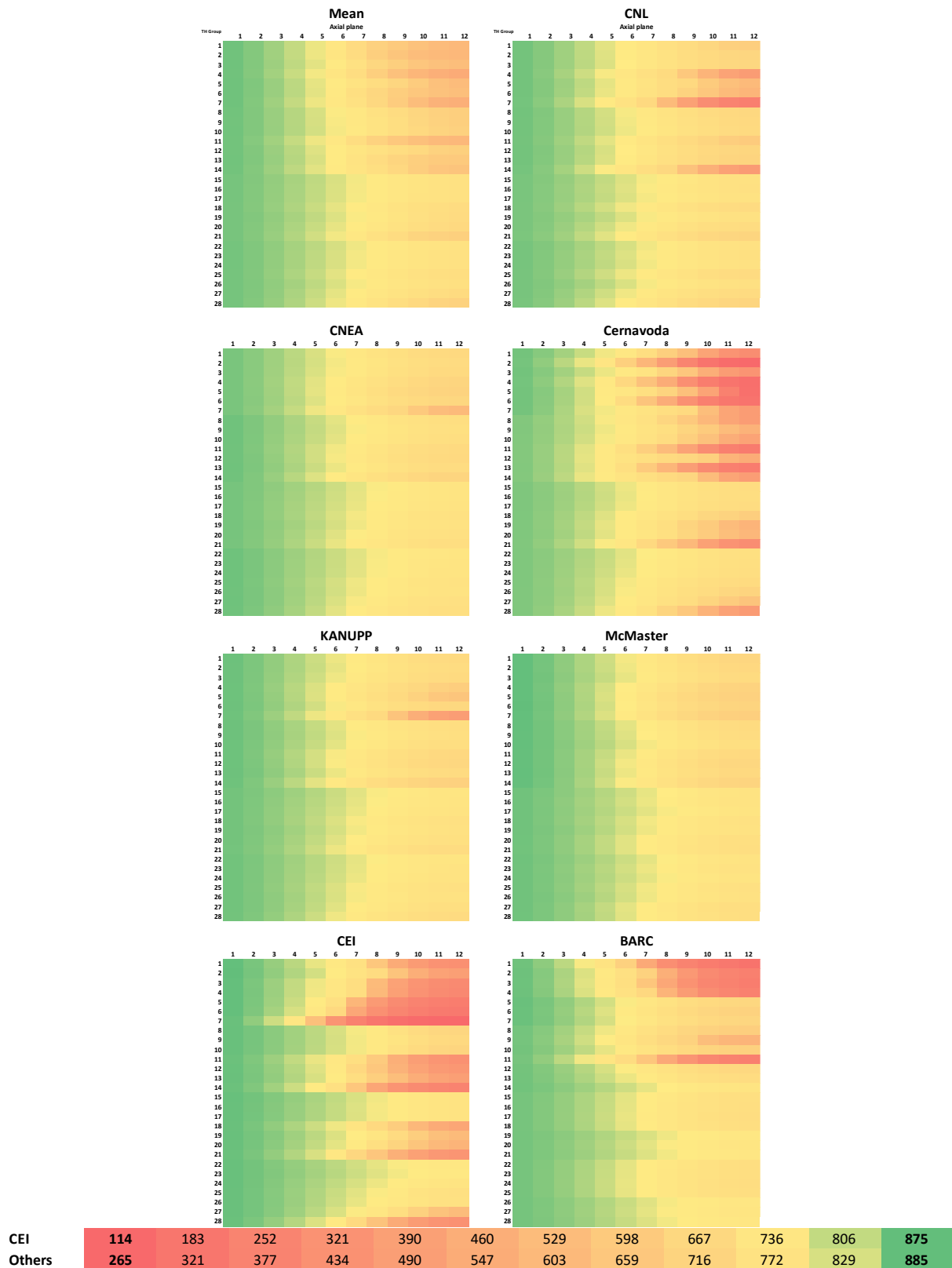


FIG. 79. Mean and participant coolant density distribution at the end of coupled pump rundown transient, kg/m^3 . Note the use of different colour scaling.

Figure 80 shows coolant temperature distributions mean values and relative standard deviations for the core. Participant distributions are not showed because the maximum standard deviation resulted lower than 3.5%.

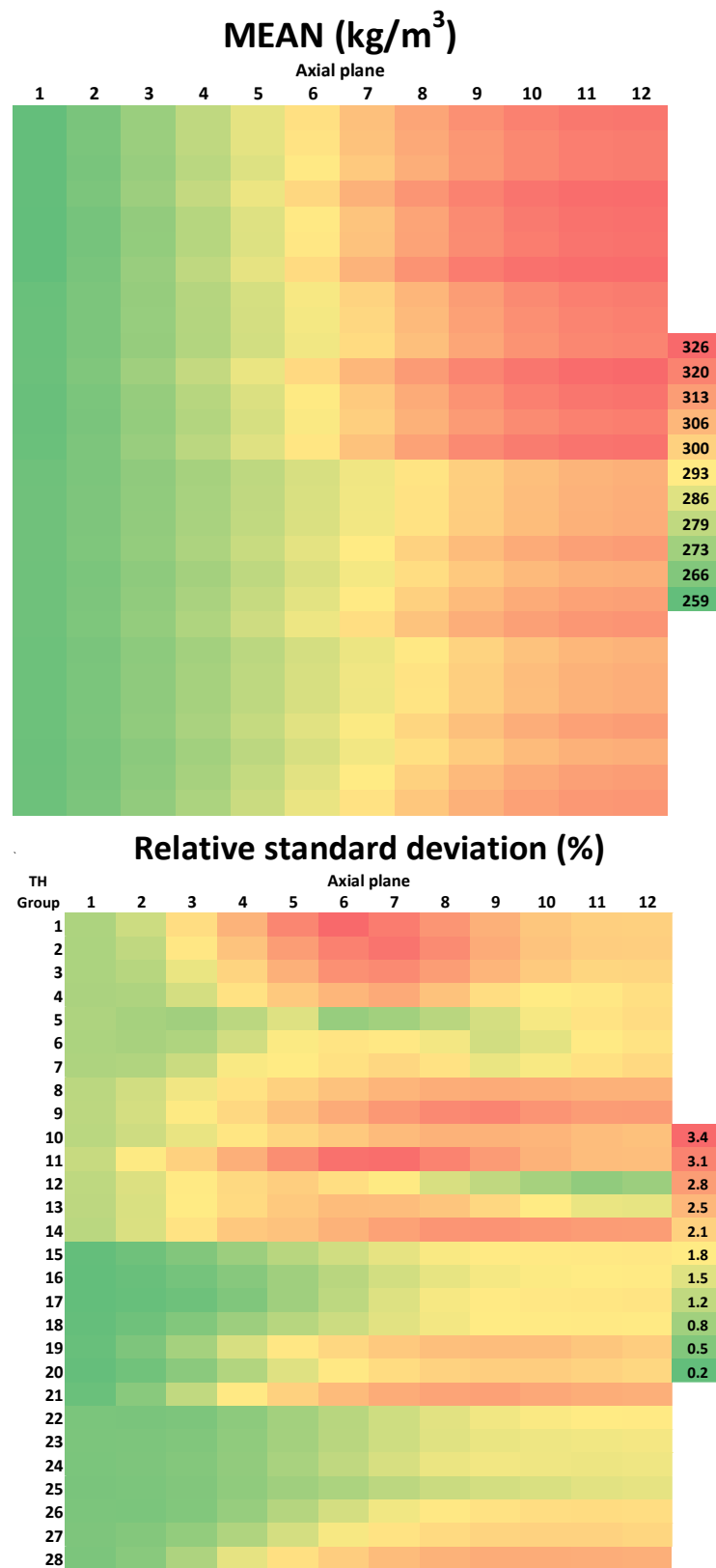


FIG. 80. Mean and relative standard deviation for coolant temperature distributions at the end of coupled pump rundown transient.

5.4.4. Discussion

There are widely dispersed results for the main part of the parameters reported, mainly due to high dispersion in total power achieved during transient. This is primarily thought to happen due to a lesser or higher void generation during the first seconds of the transients that in turn feeds to a lower or higher level of positive feedback loop between power and void.

In general, a better agreement can be found within users of RELAP/TRACE codes when compared to the total batch of participants, and the same can be said regarding CATHENA/ARIANT users.

Differences in pressure evolution could be one of the main reasons behind the differences in power increase and mass flow, as a more rapid increase in pressure limits the generation of void. Because of this, differences in pressurizer models or initial conditions seem to have a more significant impact on this transient evolution than in the other two transient problems analysed.

Parametric analysis was carried out with RELAP models and similar results to CATHENA/ARIANT calculations could be obtained by employing a lower initial pressurizer level as a starting value before reaching steady state. The sources of these differences could be further analysed for better understanding.

5.5. INLET HEADER BREAK TEST PROBLEM

5.5.1. Standalone neutronics

Four participants present the results for this problem: CNL, CNEA, KANUPP and McMaster.

Table 27 shows a comparison of SCRAM initiation times. The standard deviation of those values and the maximum of the mean channel power distribution are also reported. There is good agreement in the trip time, with differences lower than 0.04 s between participants.

TABLE 27. SCRAM BEGINNING TIME IN STANDALONE NEUTRONIC HEADER BREAK TRANSIENT.

FOM	Unit	Mean	Std Dev	CNL	CNEA	KANUPP	McMaster
Time_120	s	0.72	0.014	0.72	0.70	0.72	0.74

Figures 81 and 82 present the evolution of reactivity and reactor thermal power, relative to the steady state condition. In spite of the good agreement in the time when the SCRAM starts, there are significant differences in the evolution of these parameters. There is a significant difference in the time and magnitude of the power peak, with a difference of approximately 25% between maximum (CNL) and minimum (KANUPP) values.

These differences are consistent with initial reactivity evolution of the for each case, with KANUPP's reactivity peak occurring 0.3 s earlier than CNL's. There is also a significant difference in final reactivity achieved between KANUPP and the rest of the participants, that has an impact in power evolution after SCRAM.

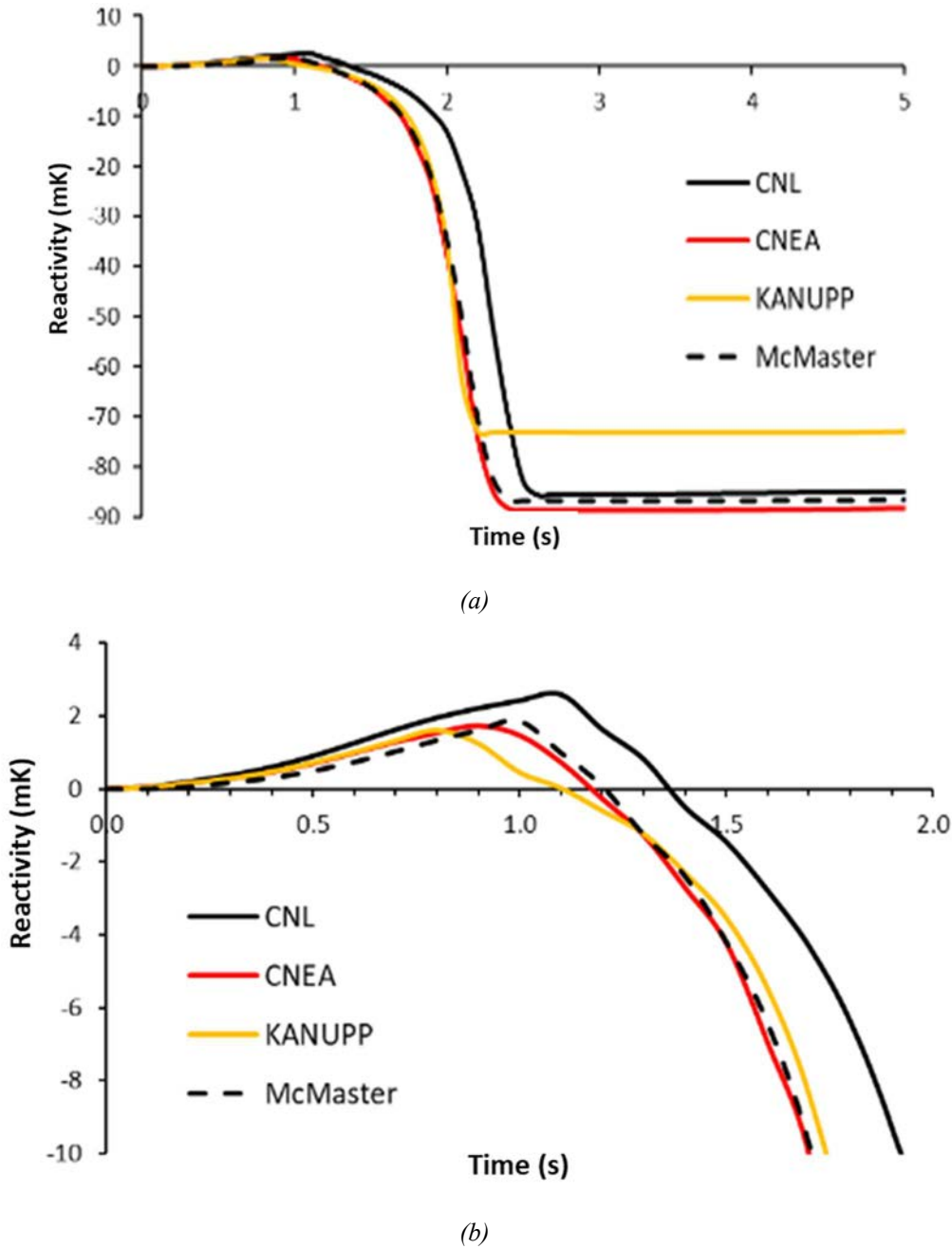
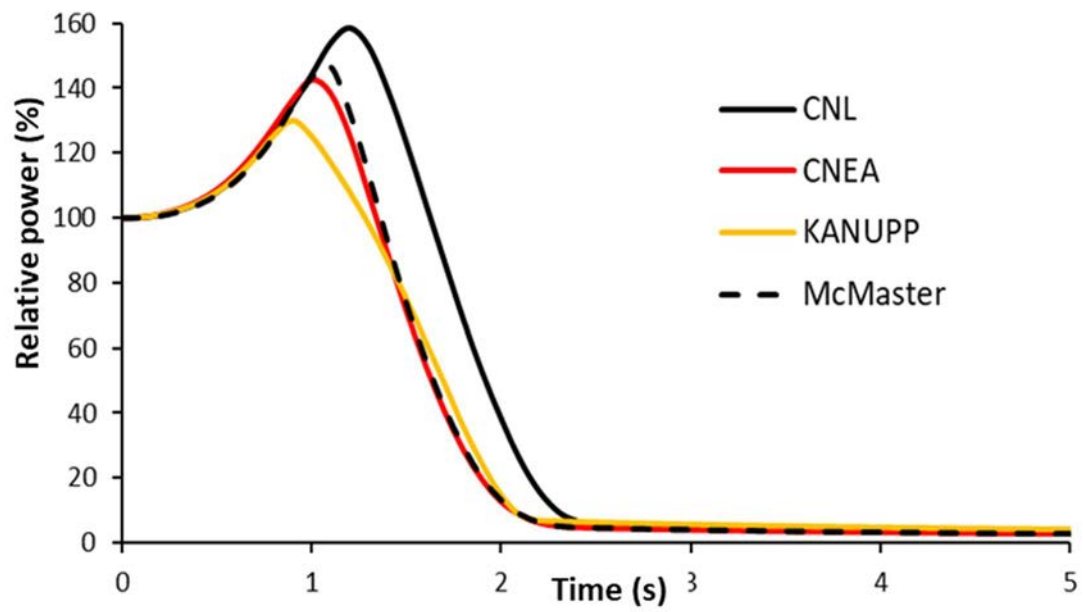
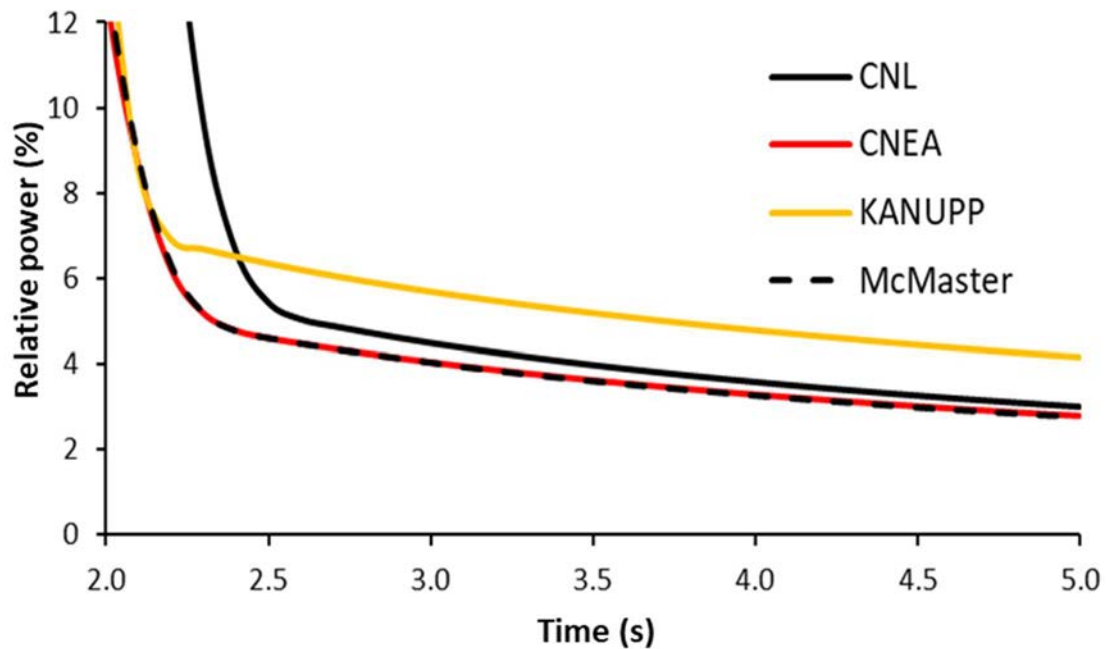


FIG. 81. Evolution of reactivity standalone neutronic header break transient (a) complete transient, (b) SCRAM.

Figure 83 shows mean channel power distribution, relative standard deviation and channel power maps for each participant, calculated at 25 s. Mean values and individual participant results use a common colour bar. A separate colour bar is provided for the standard deviations. Results from individual contributions reflect the difference in decay power between KANUPP and the rest of the participants. This difference affects only to the circuit that suffers the header break and produce a high dispersion of results on half of the reactor core, where the relative standard deviation of results reaches up to 65%. The undamaged half remains with differences of up to 20% in the lower region, and lower than 10% in the rest. These differences may point to difference in how the control devices and SCRAM sequence are simulated.



(a)



(b)

FIG. 82 Evolution of thermal power for standalone neutronic header break transient: (a) complete transient, (b) SCRAM.

Differences in power peak time and magnitude may have an impact in coupled simulations as the integrated energy varies in a relevant manner. There seem to be some differences in control devices and SCRAM modelling impacts power peak and power produced after SCRAM.

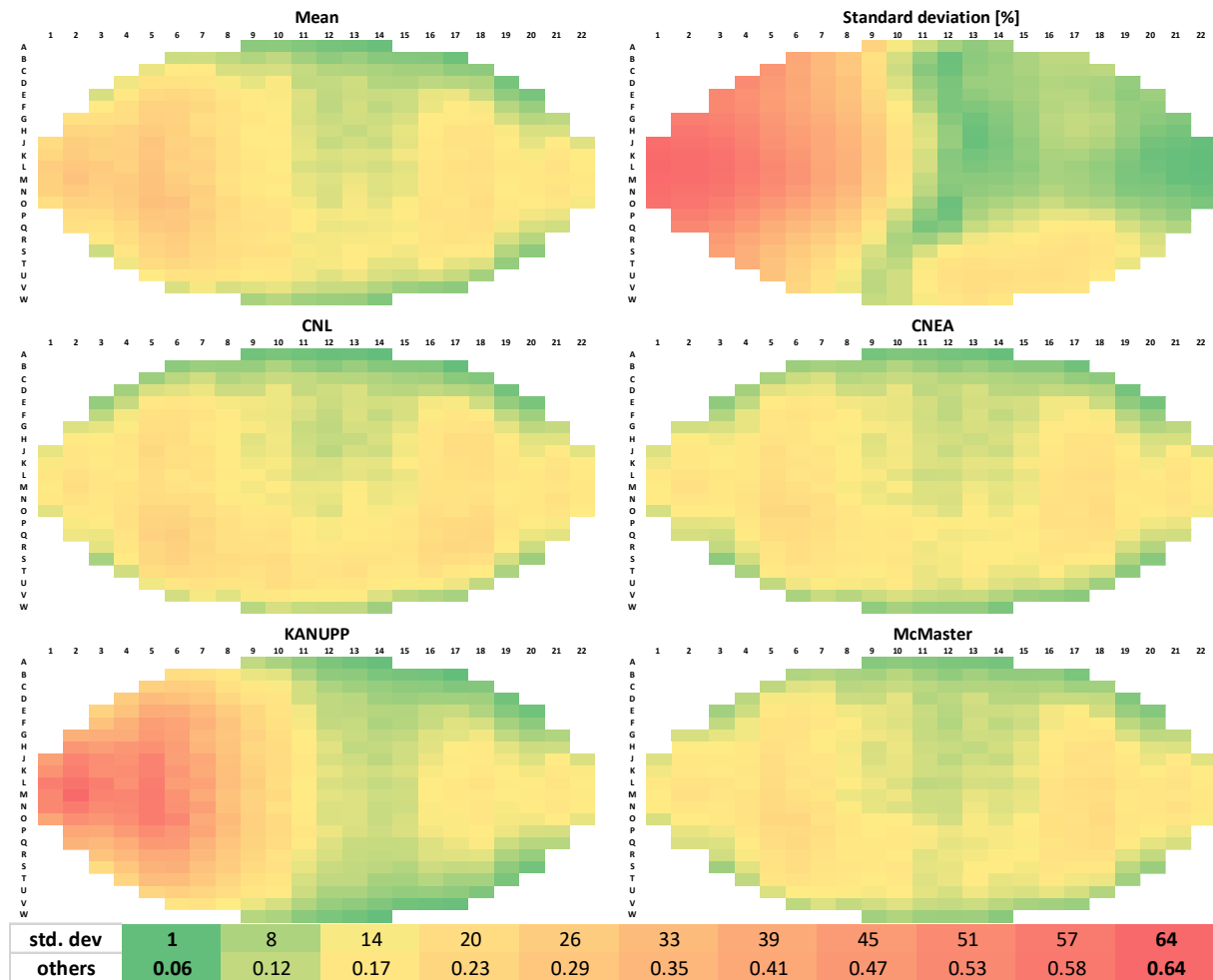
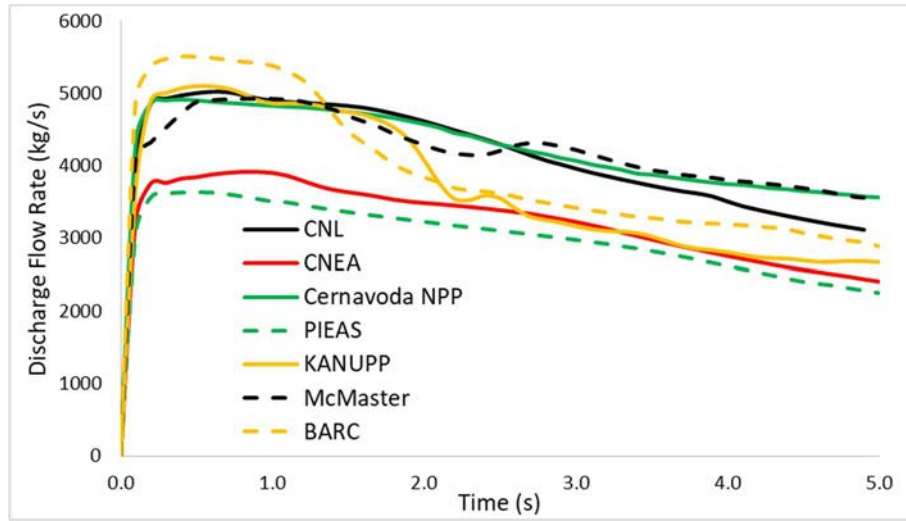


FIG. 83. Channel power [MW] distribution at the end of standalone neutronic header break transient. Average and standard deviation distributions use their own heat map colouring scale. Participant contributions use a shared colour scale. Red indicates higher values.

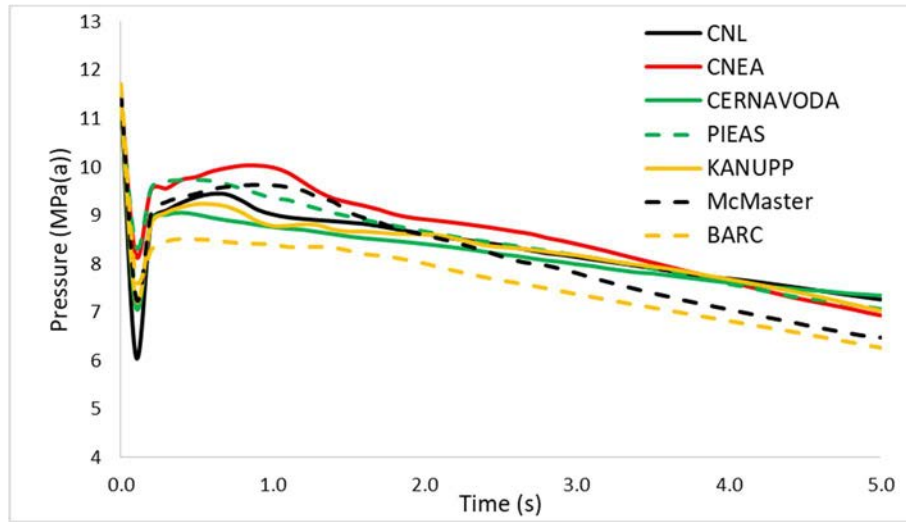
5.5.2. Standalone thermal hydraulics

The top panel of Fig. 84 presents the time evolution of the discharge mass flow rate out of the broken IHD2 and the broken header pressure obtained by all participants. Break discharge profiles are similar for all participants: a strong initial excursion which slowly decays. The magnitude of the excursions range from 3,750 to 5,500 kg/s. Asymptotic decay rates are similar for all participants. The BARC, KANUPP, and McMaster teams report discharge mass flow rates which present large variations compared to the asymptote. There is no obvious segregation of results based on the thermal hydraulics code family (CATHENA3/ARIANT and TRACE/RELAP5). However, the majority of RELAP users, with the exception of BARC, predict a flow peak around 3,800 kg/s if KANUPP's modifications of Section 4.7.5 are considered.

The pressure evolution of IHD2, which is in the broken pass, is presented in the bottom panel of Fig. 84. All participants report similar immediate de-pressurization, followed by a partial recovery and subsequent decay. The CNL team reported the largest depressurization pulse, the CNEA team the smallest. The asymptotic pressure loss rates are similar for all participants, but there is a spread of nearly 1.5 MPa (a) in the pressure values following the depressurization pulse. CNL and Cernavoda results are in close agreement. The spread in results is found in the remaining contributions, all based on either TRACE or RELAP codes.



(a)



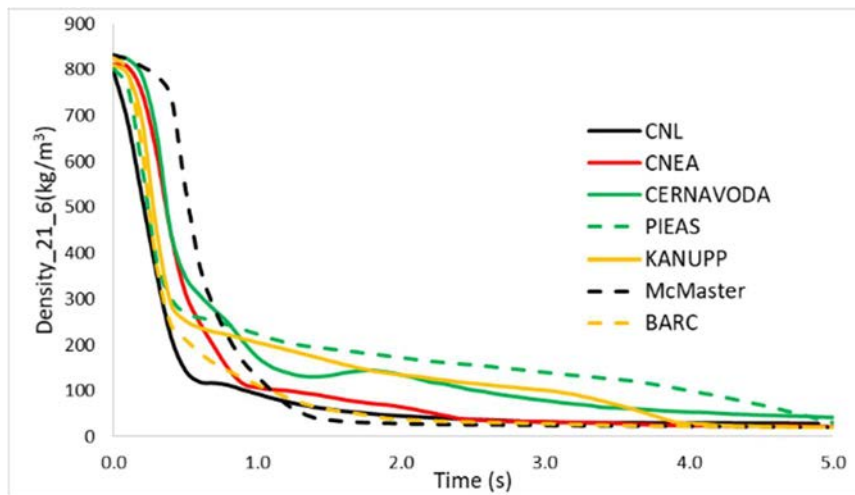
(b)

FIG. 84. (a) Discharge mass flow rate and (b) IHD2 (broken header) pressure evolution for the standalone thermal hydraulics header break problem.

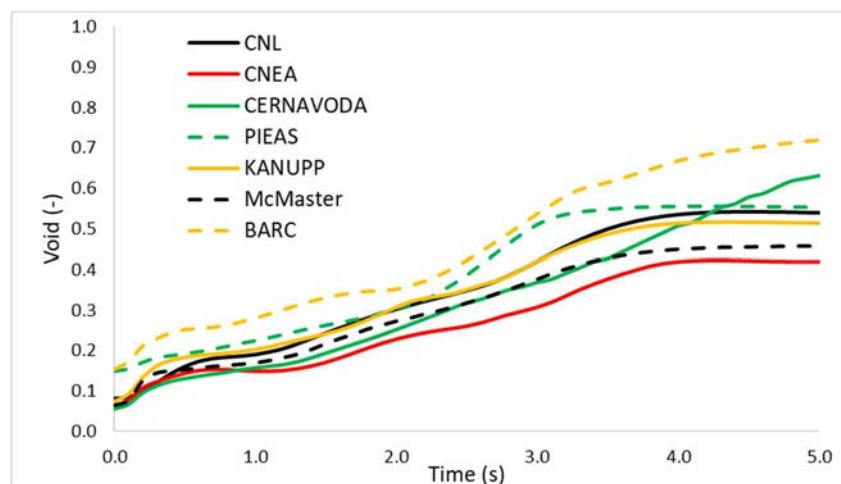
The (a) panel of Fig. 85 presents the coolant density in thermal hydraulic group CHAN21 at axial location 6. This channel is connected directly to the broken header, and the axial location is representative of a mid-core region. Comparing density evolutions is important because of the strong coolant void reactivity coefficient, which would govern reactivity feedback in coupled problems. In the coupled problem, participants reported trip times before 1.0s. As seen in Fig. 85, all participants report a rapid drop in the density before 1.0s, however some differences in the response are noted. Note that a direct comparison of this density evolution with the coupled result cannot be made, owing to differences between coupled and standalone problem specifications which could not be resolved owing to lack of time. The CNL team reported the most rapid change in density. The McMaster team reported a short duration slow decrease, followed by a very rapid decrease. All other participants reported changes in density which are bounded by these two team's results in the first 1.0s of the transient. CERNAVODA, PIAS, and KANUPP team results present densities after 1.0s which are markedly higher than those of the other participants.

The (b) panel of Fig. 85 presents the time–evolution of the OHD1 void fraction. Outlet Header 1 is the connected to the broken IHD2 via the fuel channels. All participants report a general increase in void with some differences in the overall rate of increase. CNL and Cernavoda results are in close agreement, which is interesting when one considers that they differ when CHAN21 densities are considered.

Figure 86 presents the distributions of pressure, temperature, and void fraction within the thermal hydraulics network at 5 s. Mean, maximum, and minimum values are listed for clarity. Maximum, minimum, and mean pressure profiles are similar. The maximum to minimum gap is approximately 1.5 MPa (a). With the exception of locations in the vicinity of CHAN21OUT, there coolant temperature profiles present very narrow gaps. CNEA reported a large coolant temperature which distorts the profile. The team indicated that the affected channels were virtually fully voided, and large differences in fluid and vapour temperatures were observed. Differences in the maximum and minimum void profile are indicative greater variability reported by participants. However, a review of individual participant outputs failed to reveal any patterns.



(a)



(b)

FIG. 85. (a) Thermal hydraulic group CHAN21 coolant density and (b) OHD1 void fraction evolution for the standalone thermal hydraulics header break problem.

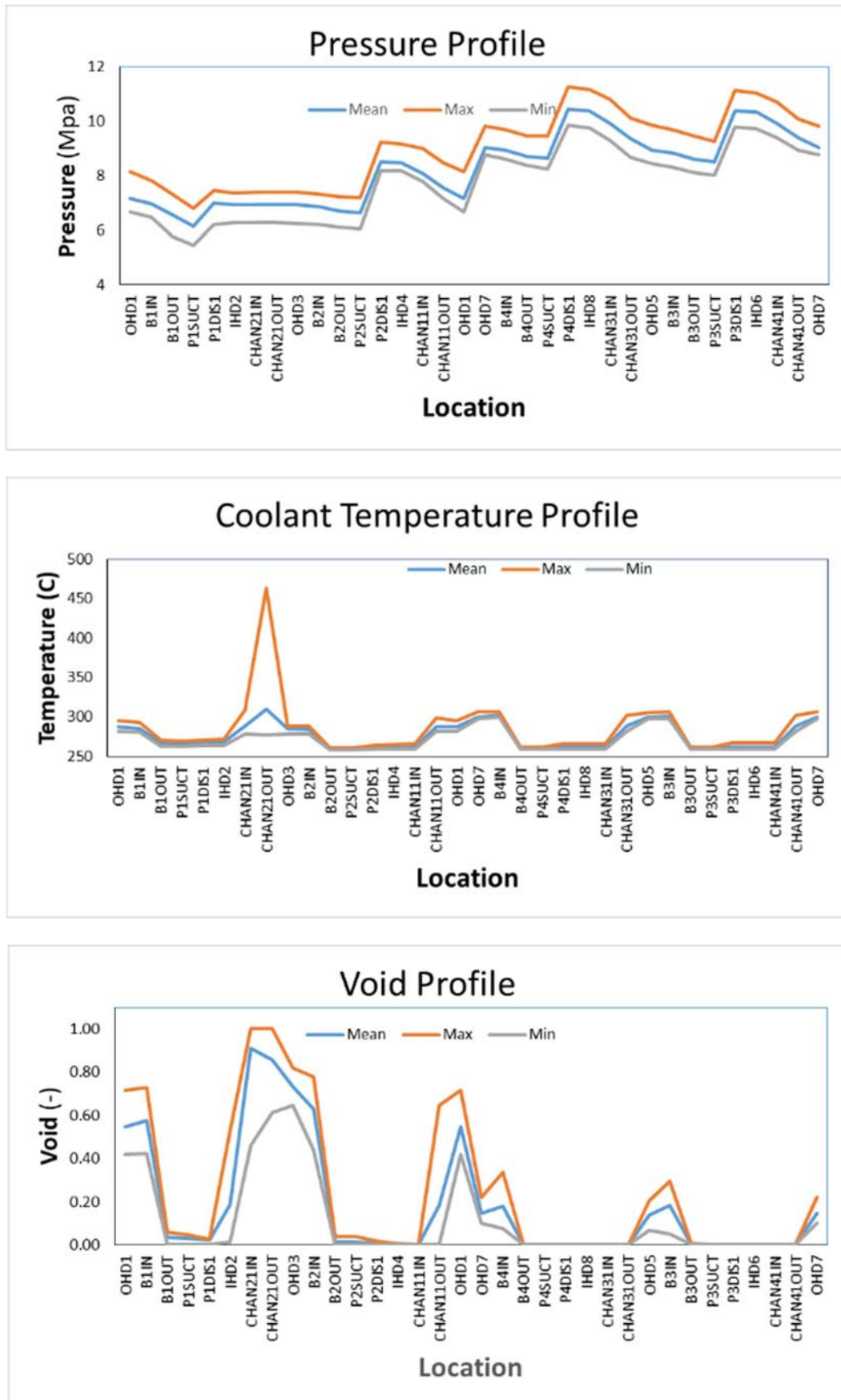


FIG. 86. Key thermal hydraulics network properties after 5 s.

5.5.3. Coupled converged case

5.5.3.1. With reactor shutdown

Table 28 presents several scalar FOM from the coupled header break transient problem. Mean and standard deviations, where applicable, are also reported. The integrated enthalpy in the core (IENTHL), is computed from the time integral of the total core power from 0–5 s. The maximum energy deposited in a fuel bundle (MAXHB), is computed using the following procedure. The bundle powers at each of the 4,560 bundle locations of the core were integrated separately, converted to kJ units, and divided by a reference fuel mass of 27.014 kg. The maximum value was then reported, as is the fuel bundle position where the maximum was found. The maximum energy deposited in a fuel channel (MAXHC) is computed in a similar manner. The channel powers at each of the 380 fuel channels in the core were integrated separately. The maximum value was reported along with the location of the maximum. None of these figures of merit account for heat removal due to cooling, and readers are reminded that decay heat was excluded from the problem specifications. The nominal trip time is reported as the time where the total core relative power would reach 120%.

There is no apparent link between the ordering of IENTHL, MAXHB, and MAXHC results. CNL presents the lowest estimates for MAXHB and MAXHC, yet the estimate for IENTHL is near the mean. With the exception of BARC, all reporting teams agree that the location of MAXHB is S-8-7. The differential result from the BARC team may be due to the differences in model realization, particularly the thermal hydraulics channel groupings. Similar statements may be made for the MAXHC parameter.

TABLE 28. SELECTED SCALAR FIGURES OF MERIT FROM COUPLED HEADER BREAK TRANSIENT

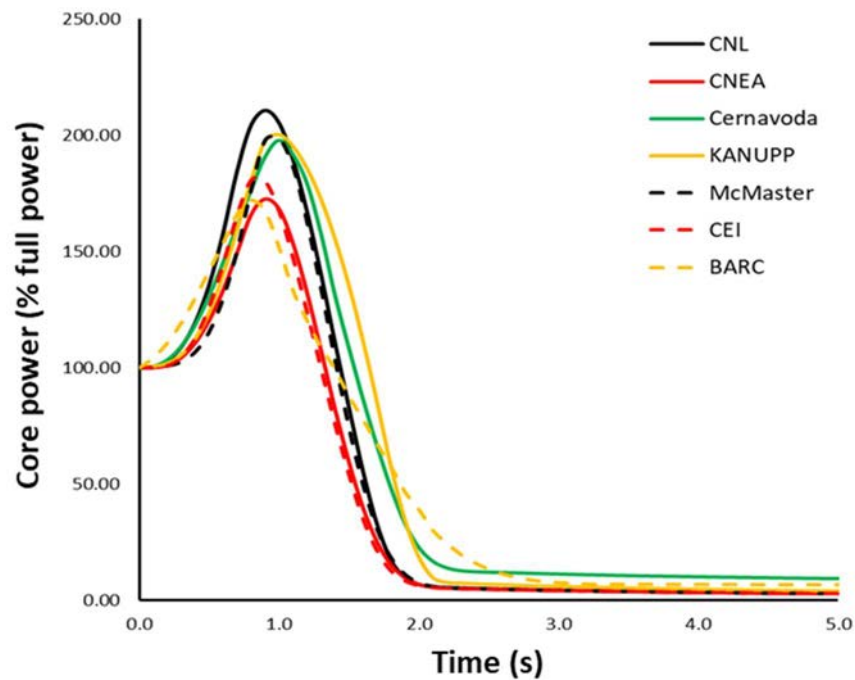
FOM	IENTHL	MAXHB	MAXHB location	MAXHC	MAXHC location	Trip
Unit	MJ	kJ/kg		MJ		s
Mean	5088	91	-	19.1	-	0.44
Std. dev	498	17	-	3	-	0.07
CNL	5134	59	S-8-7	13.2	S-8	0.41
CNEA	4365	89	S-8-7	19.5	S-9	0.50
CERNAVODA	5778	-	-	-	-	0.41
KANUPP	5677	-	-	-	-	0.47
CEI	4555	111	--	20.3	-	0.45
BARC	5282	96	M-4-6*	21.1	M-4**	0.31
McMaster	4827	100	S-8-7	21.6	S-9	0.53

* Indistinguishable from M-6-6,M-8-6,M-10-6,N-5-6,N-7-6,N-9-6,N-11-6,O-6-6,O-8-6,O-10-6 M-4-7,M-6-7,M-8-7,M-10-7,N-5-7,N-7-7,N-9-7,N-11-7,O-6-7,O-8-7,O-10-7.

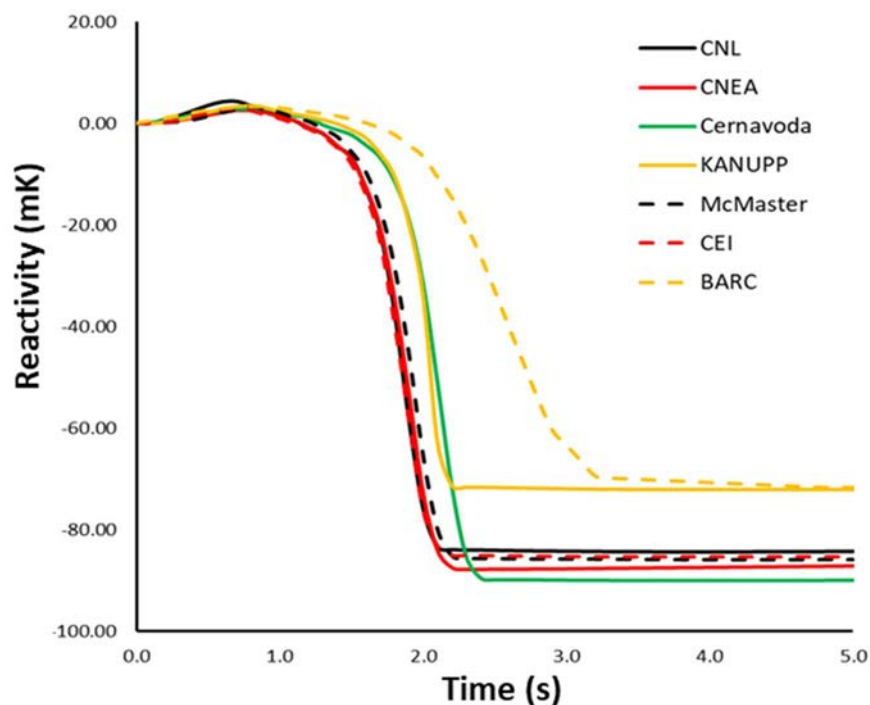
** Indistinguishable from M-4,M-6,M-8,M-10,N-5,N-7,N-9,N-11,O-6,O-8,O-10.

Figure 87 presents the time evolution of the core power and reactivity obtained by all participants. In general, good agreement is seen by participants, particularly in the core power results. One can observe to groupings of core power results: 1. A higher peak power group that includes CNL, McMaster, Cernavoda, and KANUPP, and 2. A lower peak power group that includes CNEA, CEI, and BARC. The peak power for group 1 is around 200 %FP, while the

peak power for group 2 is around 175–180 %FP. These differences will be discussed in more detail below. The relative ranking of the peak core relative power magnitudes does not correlate to the thermal hydraulics code family (TRACE/RELAP vs ARIANT/CATHENA), or steady state coolant voiding worth (CVW1 and CVW2).



(a)



(b)

FIG. 87. (a) Core power and (b) reactivity evolution in the coupled header break problem.

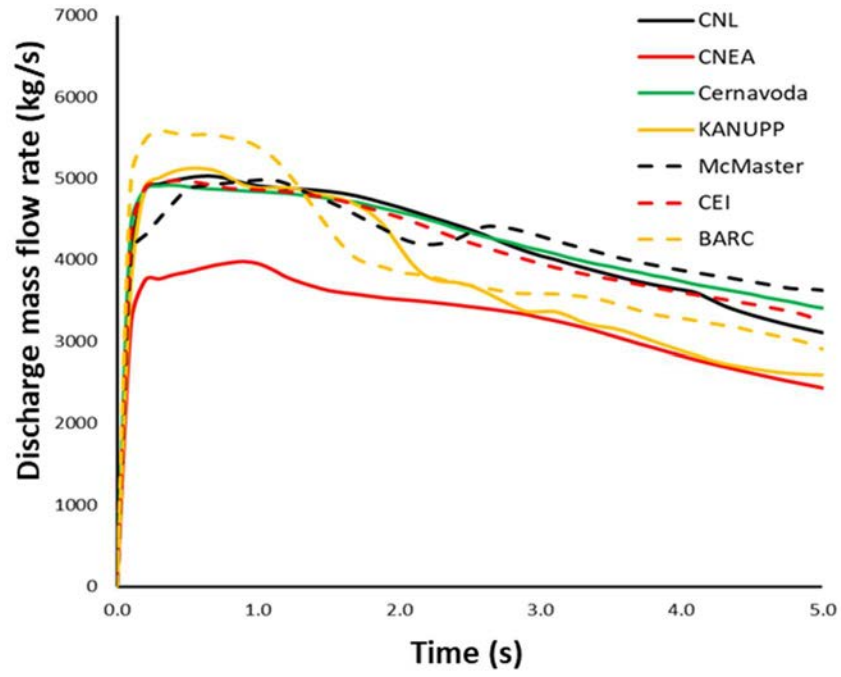
Figure 88 presents the time evolution of the discharge mass flow rate out of the broken IHD2 and the broken header pressure obtained by all participants. It is well known that the major driver of the power excursion during a loss of coolant accident in a CANDU styled reactor is the positive void reactivity that results from coolant depressurization. The rate of depressurization is in turn driven by the mass flow rate of the coolant discharging from the broken header.

In general, good agreement is seen by participants on both parameters. Relating back to the peak core power, one can clearly see that the CNEA discharge mass flow rate is markedly less than other participants, which helps explain the correspondingly smaller peak core power. This result correlates to the lower flow through the break observed by the majority of RELAP users in their standalone thermal hydraulic case. From discussion between some participants, it is known that the header break was modelled on the ends of the headers, while it is assumed that all other participants modelled the break on the side of the header. Sensitivity cases run in TRACE by McMaster showed that differences in location of the break in the header could produce the observed differences in discharge mass flow rate and peak core power. However, similar behaviour wasn't observed in RELAP simulations done by CNEA. This observation does not hold for the other group 2 participants: CEI, and BARC. In fact, BARC shows the highest initial discharge rate, which would suggest that their peak core power should be higher than most other participants, which is not the case. Furthermore, the CEI discharge mass flow rate compares well with the other group 1 participants, despite them showing a significantly lower peak core power. For group 1 participants, the discharge mass flow rates compare well, which helps explain the tight grouping of peak core powers shown in Figure 87.

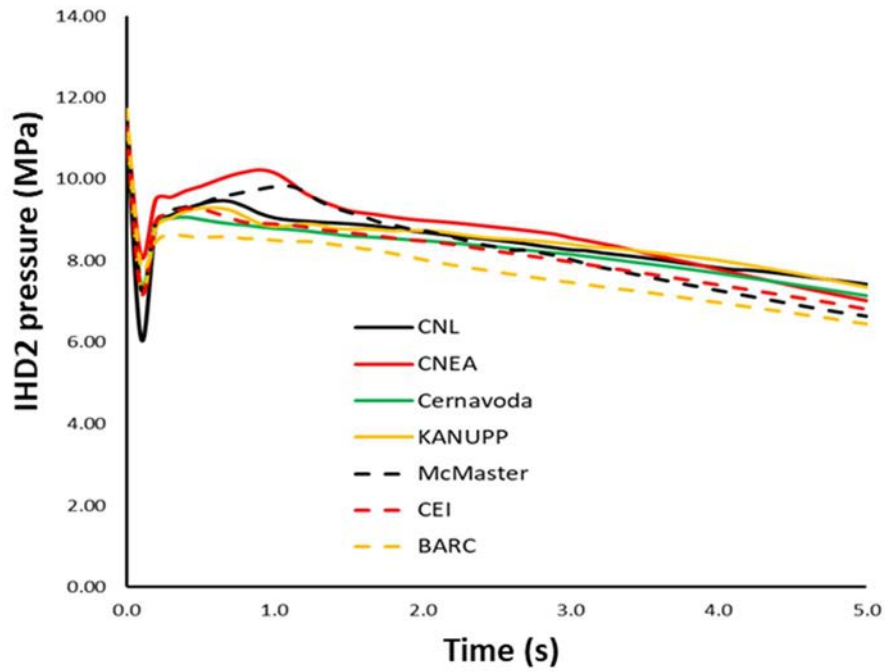
The behaviour of the header pressure does not offer any insight; however, it is encouraging to see that all participants have a similar prediction.

Figure 89 presents the coolant density in thermal hydraulic group CHAN21, which is connected directly to the broken header, and the OHD1 void fraction. Outlet Header 1 is the connected to the broken IHD2 via the fuel channels. The plot (a) shows the rapid decrease in coolant density during the first second of the transient, which is the major driver of the positive void reactivity. Again, in general, agreement here is good, however, the results do not correlate with the peak power results discussed above. It is worth noting that this is only 1 of 7 fuel channel groups, so one would not necessarily expect perfect correspondence between the rate of change of the coolant density and the magnitude of the peak core power. For future benchmarks or follow up activities, it may be worth analysing the core average coolant density as a function of time, or the average coolant density in the broken pass of the broken loop to gain more insight.

Examining the void fraction plot, it is worth noting that many participants had non-zero void in the outlet header at the start of the transient. During previous discussions with the working group of participants, it was noted that the initial void fraction in the outlet header can have a major impact on the transient progression. Interestingly, both CEI and BARC show higher initial void fractions than the other participants, despite having lower peak core powers.

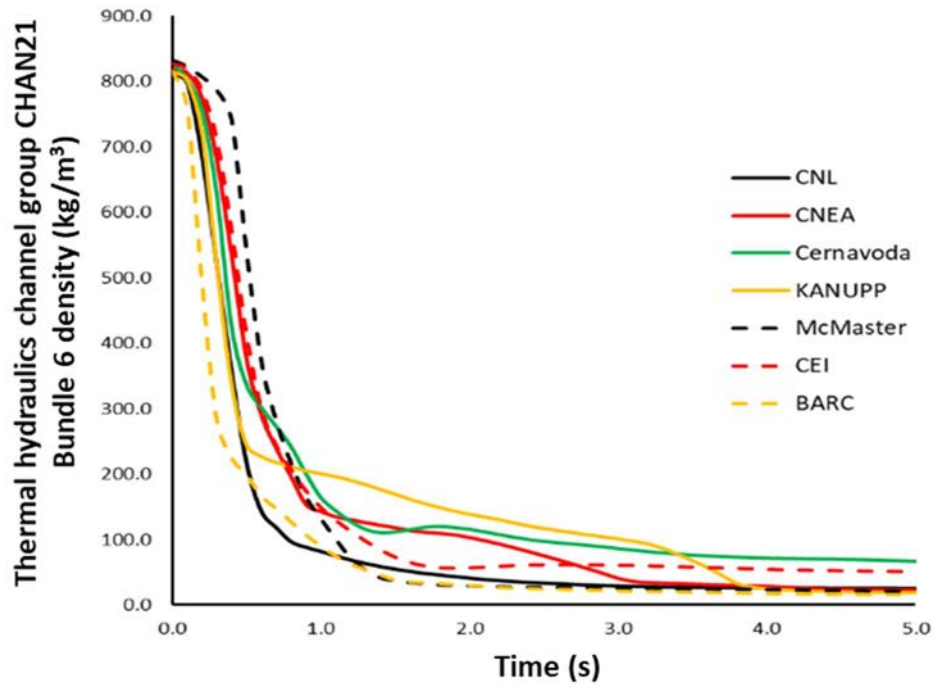


(a)

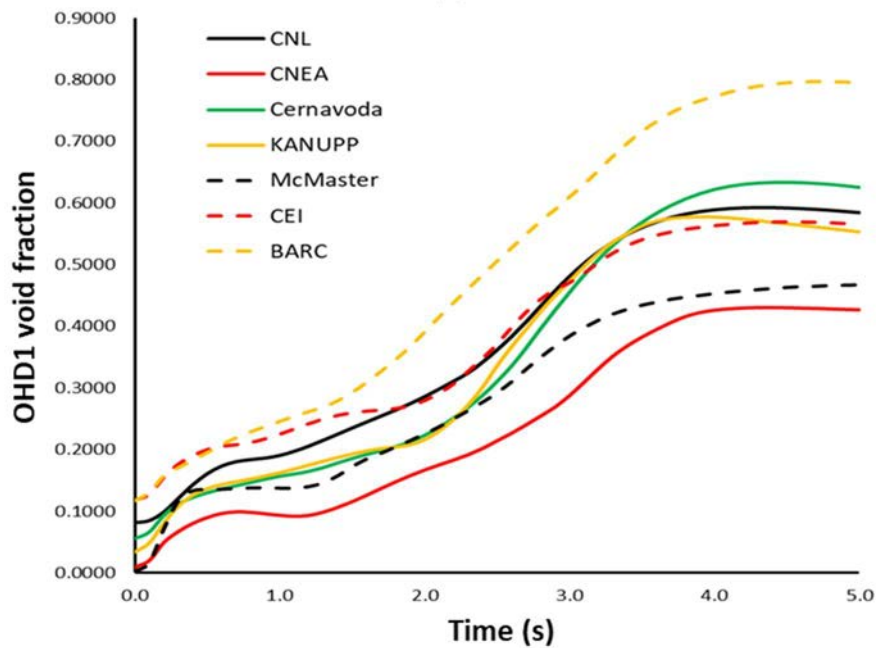


(b)

FIG.88. Discharge mass flow rate and IHD2 pressure evolution during the coupled header break problem: (a) discharge mass flow rate, (b) pressure (broken header).



(a)



(b)

FIG. 89. (a) Thermal hydraulics group CHAN21 coolant density and (b) OHD1 void fraction evolution during the coupled header break problem.

Figures 90, 91 and 92 present the distributions of pressure, temperature, and void fraction within the thermal hydraulics network at 5 s. Pressure and temperature distributions follow a common profile for all participants, except for the high CHAN21IN temperature for CEI and the high CHAN21OUT temperature for CNEA. At first glance these two results seem unlikely, both due to the more reasonable temperature predicted by all other participants, and due to the extremely high temperatures predicted by these two participants. However, it is worth noting that these temperatures correspond to the coolant temperature in bundle 1 (CHAN21IN) and bundle 12 (CHAN21OUT) only. As such, it is likely that for these two participants, the flow in this fuel channel group has stagnated or nearly stagnated, and the coolant has reached a superheated

state. For CEI, it is also likely that some flow reversal has occurred, which explains why the inlet of the channel is hotter than the outlet. This is supported by the void fraction plot, which shows that almost all participants have 100% void in CHAN21IN and OUT. The lower temperatures observed by other participants suggests that they reached a superheated state later in the transient. High coolant temperatures may have also been predicted by other participants, but just in different fuel channel groups. The McMaster team confirmed that this occurred in their contributed solution to this problem.

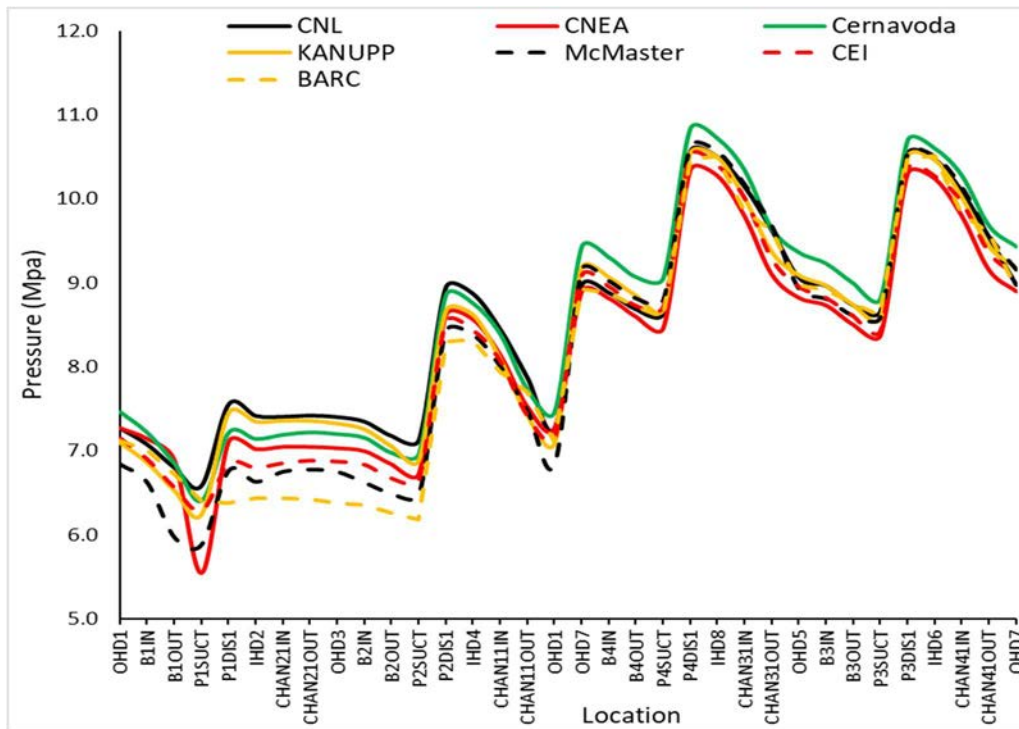


FIG. 90. Coolant pressure in the network after 5 s.

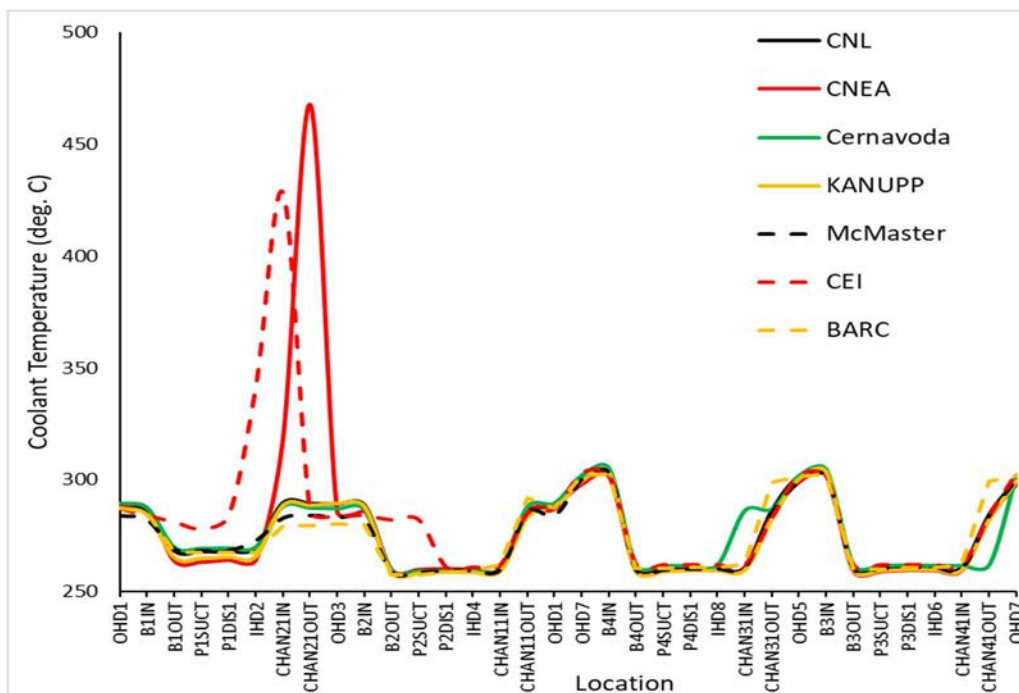


FIG.91. Coolant temperature in the network after 5 s.

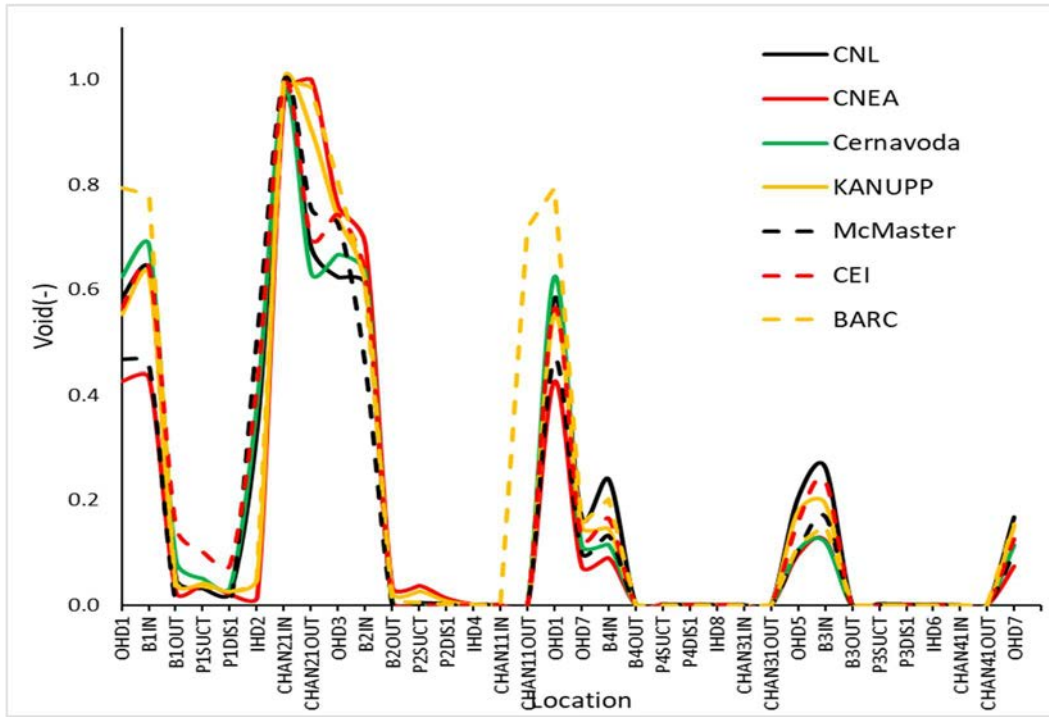


FIG.92. Void fraction in the network after 5 s.

Figures 93 and 94 present a heat map of the in-core coolant density obtained by all participants. Data are reported in kg/m^3 . Each row represents one of the 28 thermal hydraulics channels, and there is one column for each of the 12 axial nodal positions corresponding to the location of a fuel bundle. Columns are sorted from reactor inlet to outlet. Green is used for high density, red for low density. In general, all participants show good agreement in these plots, with only small variations compared to the mean density. It is worth noting that these plots may be slightly misleading, due to the large difference in coolant density between the intact channels and the broken channels. For example, a coolant density of 10 kg/m^3 and 50 kg/m^3 would both show up as almost the same colour.

Figures 95 and 96 present heat maps of the in-core fuel temperatures. Red is used for high temperatures and green is used for low temperatures. Again, in general, all participants show good agreement in these plots, with only small variations compared to the mean temperature. Furthermore, there is a correspondence between low density fuel bundles/channels, and high temperature fuel bundles/channels, as one would expect.

Figure 97 presents the channel power distribution at 5 s. The heat maps use the colour red to indicate high power, however each sub plot uses a separate heat map scale. This decision was made to highlight changes in power distribution relative to the steady state and was necessitated by the large difference between the mean and maximum core relative power results. There is a large variation in the channel power distributions predicted by participants, however, it is worth noting these plots correspond to a shutdown state, and do not give any insight into the overall accident progression. For future benchmarks or follow up activities, it may be worth plotting the channel power distribution at the time of the peak core power, to gain more insight.

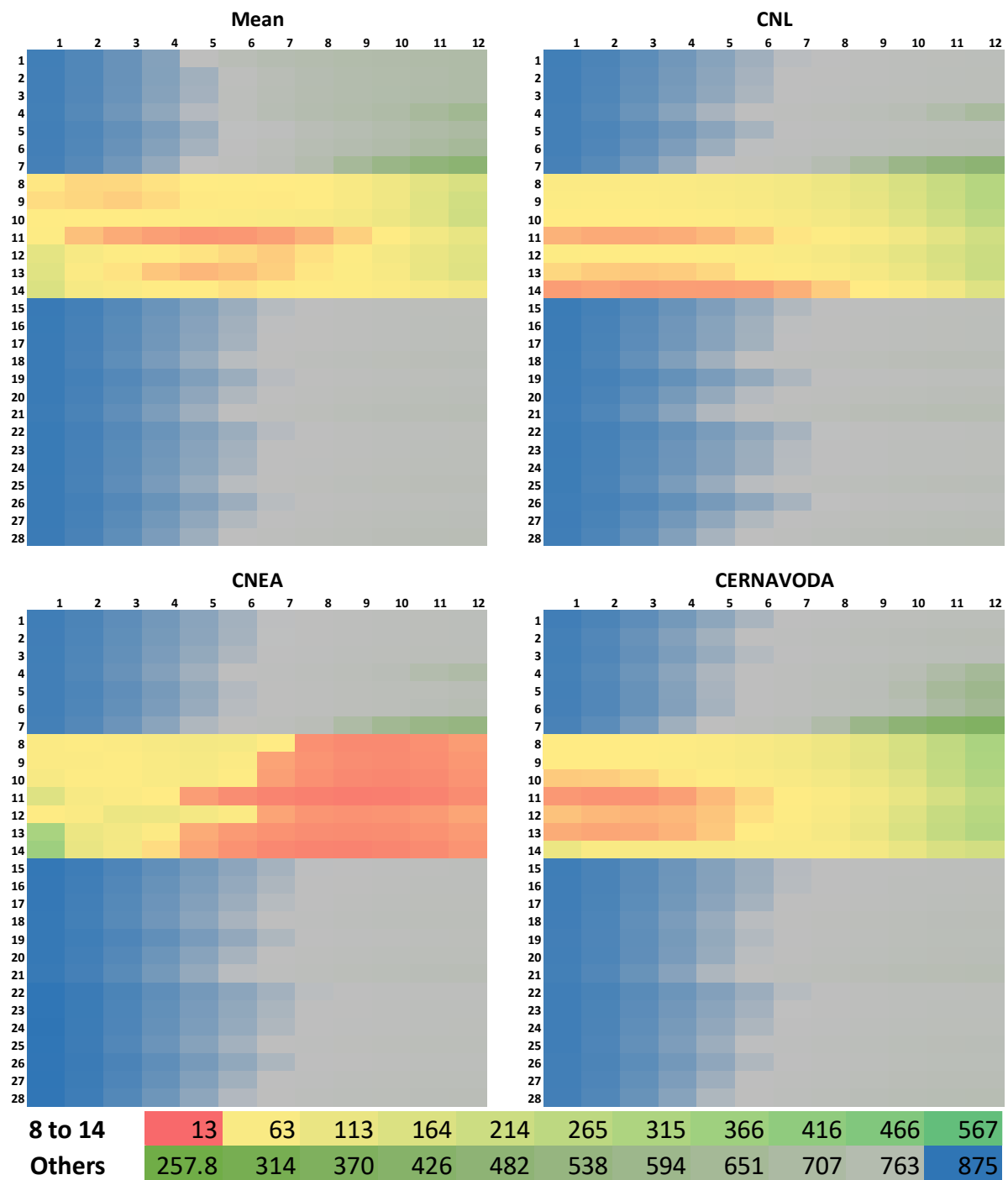


FIG.93. Distribution of in-core coolant densities, in kg/m^3 , at 5 s. Mean and three participants. Note the use of different colour bars for thermal hydraulics groups 8–14 in the broken pass.

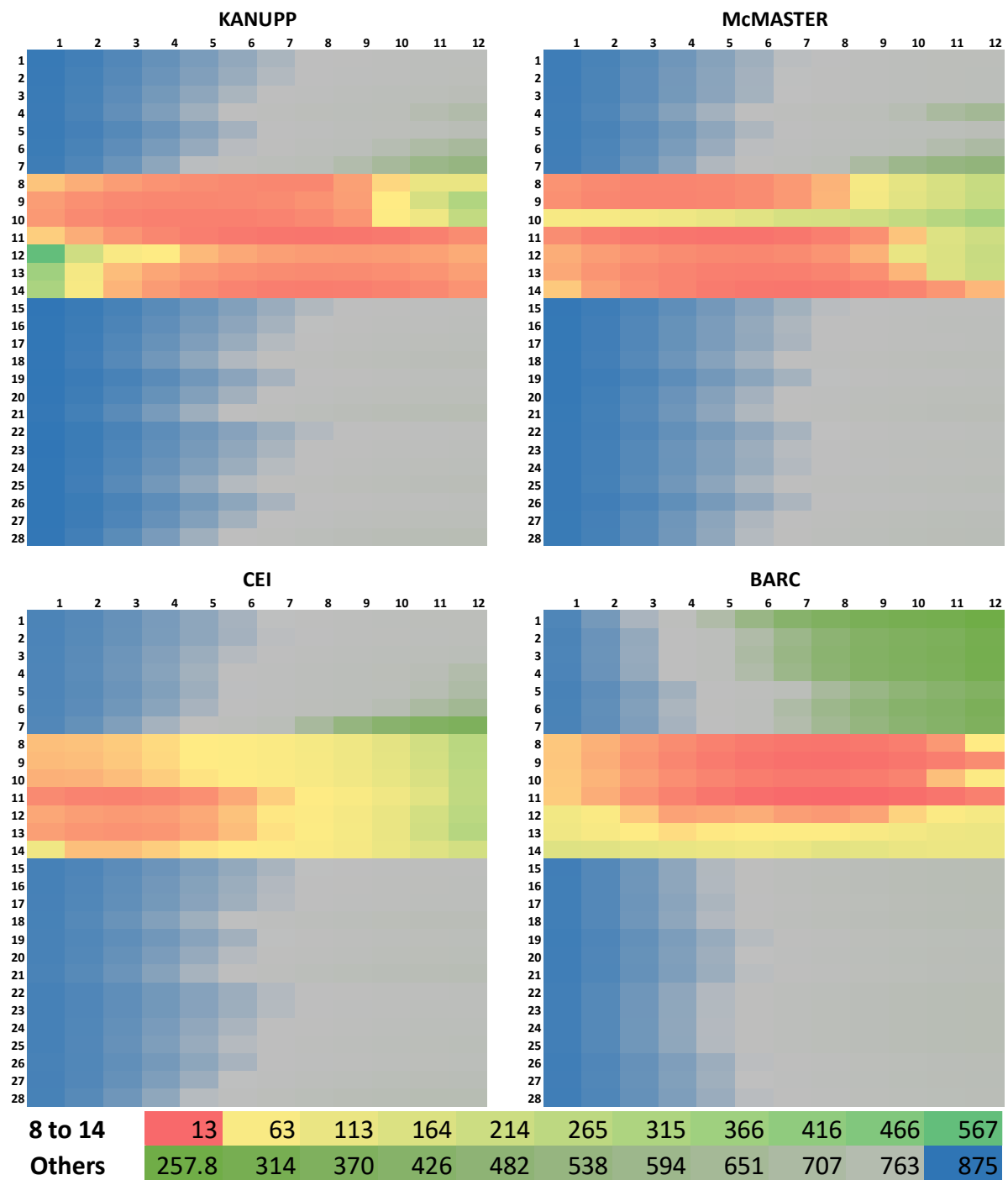


FIG.94. Distribution of in-core coolant densities, in kg/m^3 , at 5 s. Remaining participants. The colour scaling from the previous figure is retained.

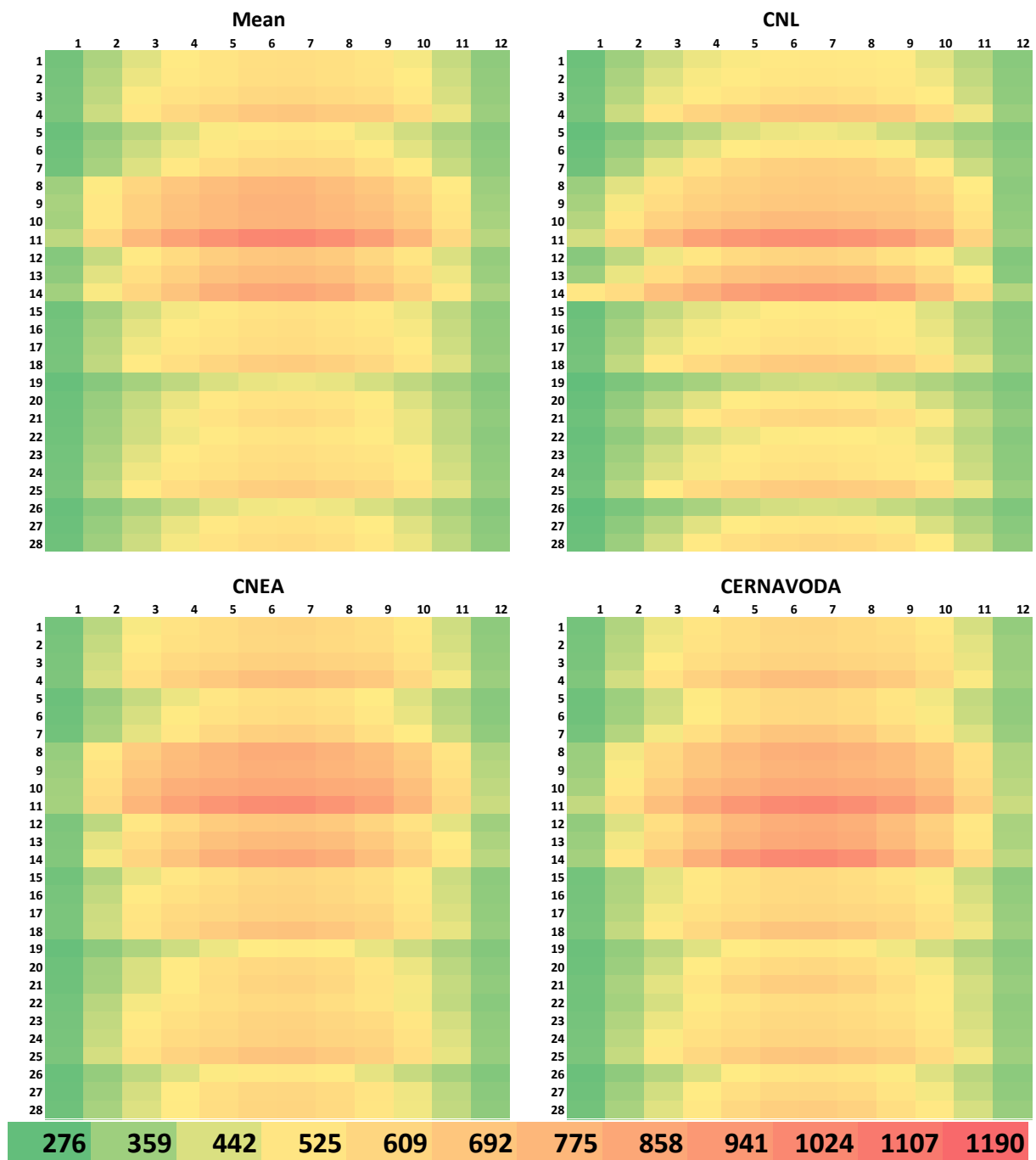


FIG. 95. Distribution of in-core fuel temperatures, in °C, at 5 s. Mean and three participants.

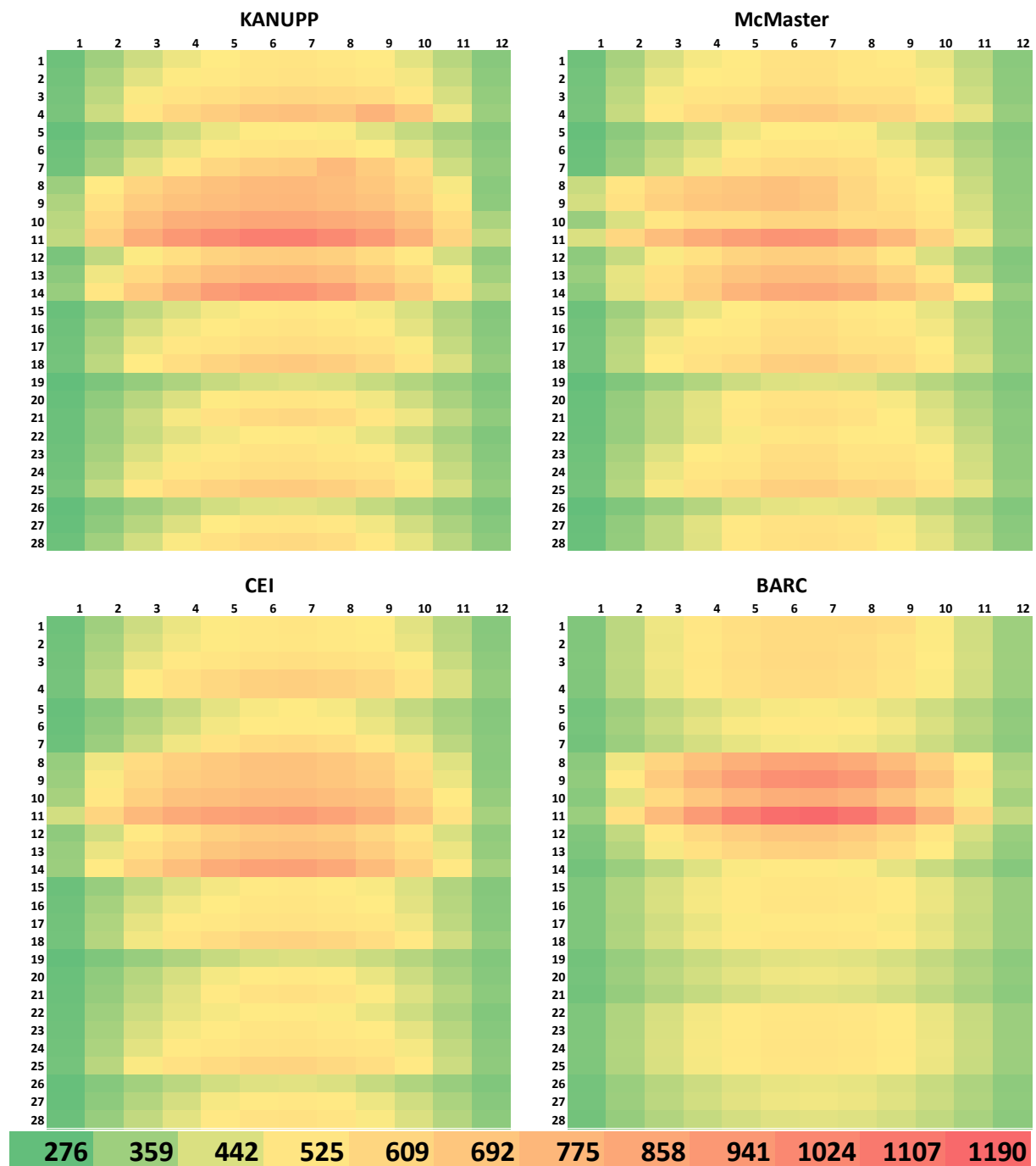


FIG.96. Distribution of in-core fuel temperatures, in °C, at 5 s. Remaining participants. The colour scaling from the previous figure is retained.

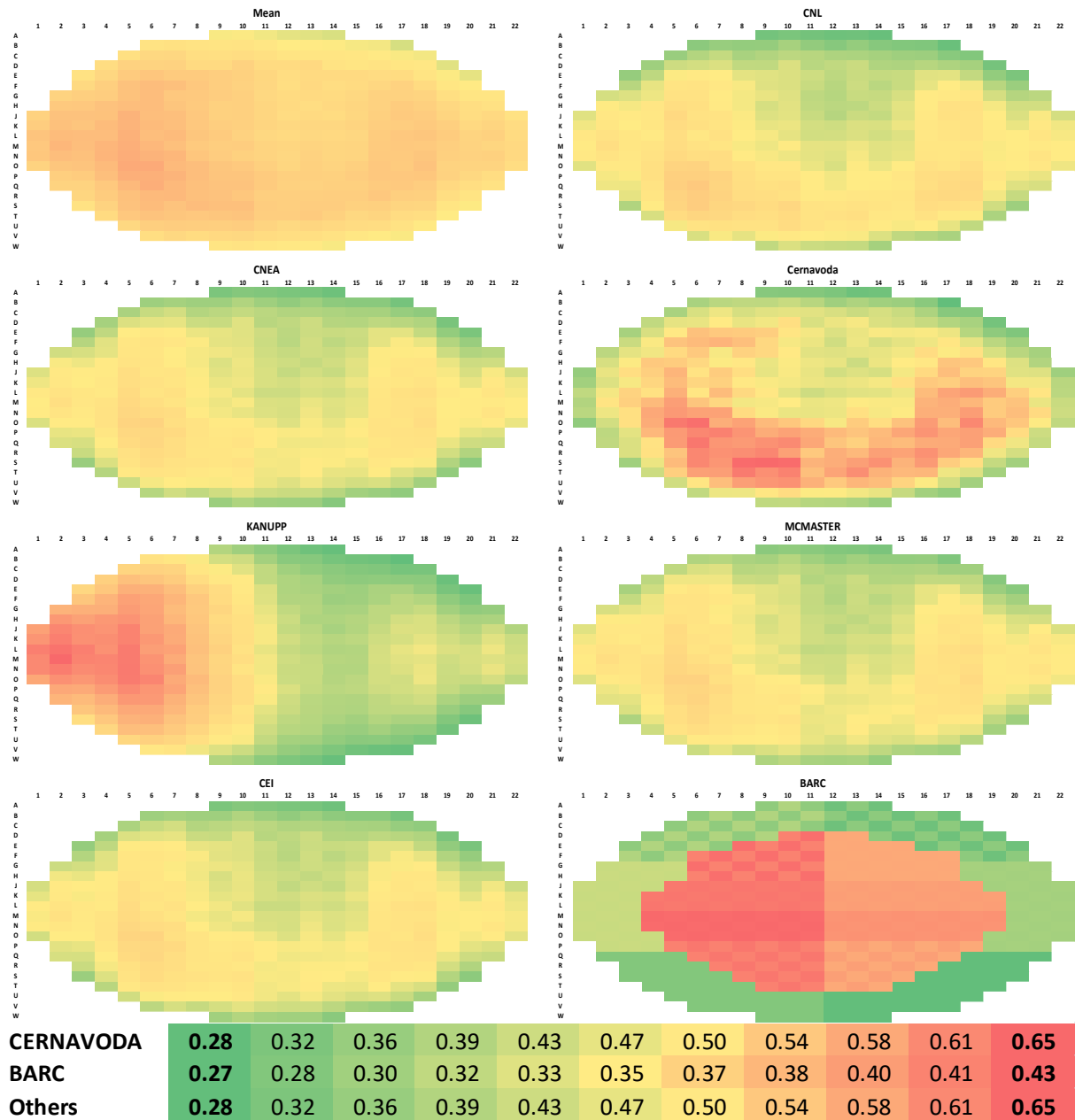
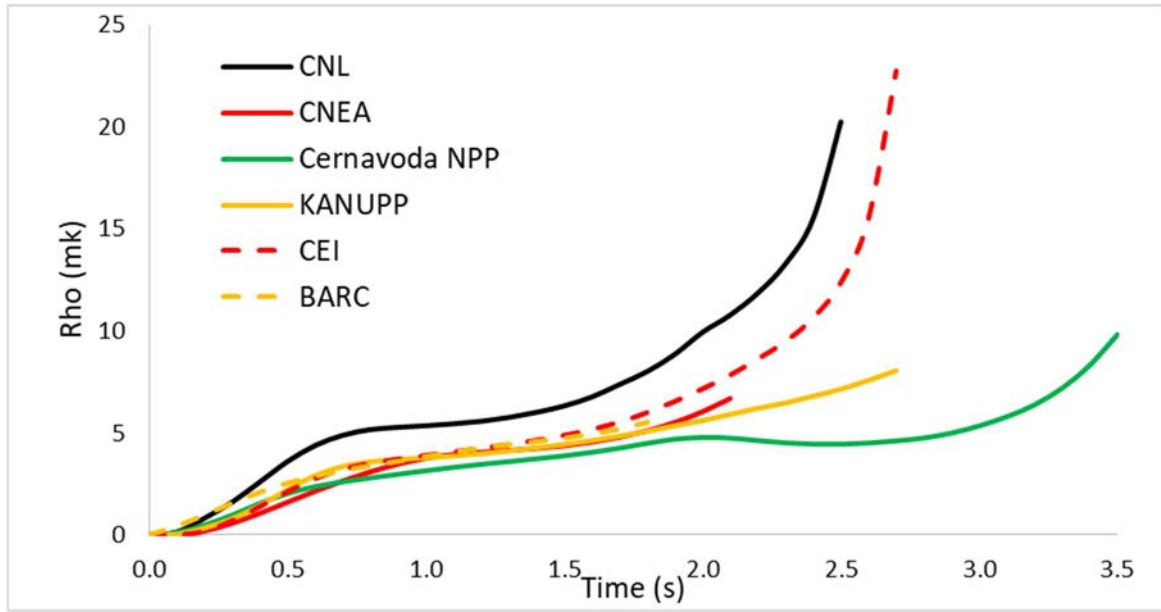


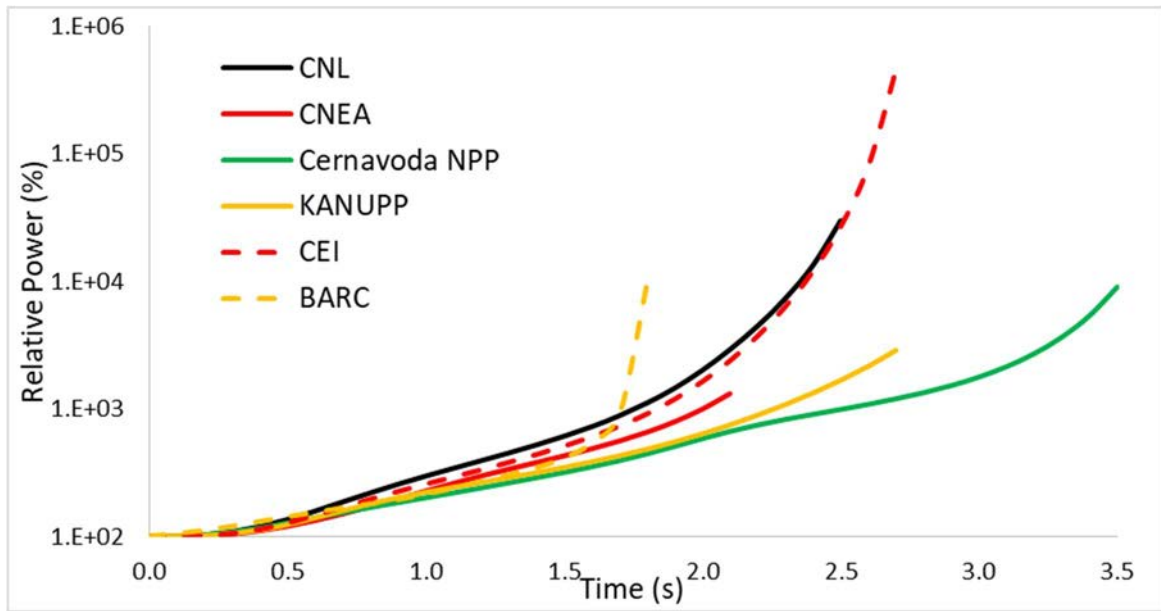
FIG. 97. Channel power distributions at 5 s. Note use of different heat map scales.

5.5.3.2. Without reactor shutdown

Figure 98 presents the time evolution of the core power and reactivity obtained by all participants. Power evolution tracks reactivity. All participants achieve good agreement for relative power as well as reactivity up to 1.7 s. A sharp rise in power is predicted by BARC at 1.7 s. For other participants the power rise is sluggish. The maximum relative percentage power predictions show large deviation, ranging from 700% to 450,000% of original power. The transient time simulated by participants also varies from 1.8–3.5 s.



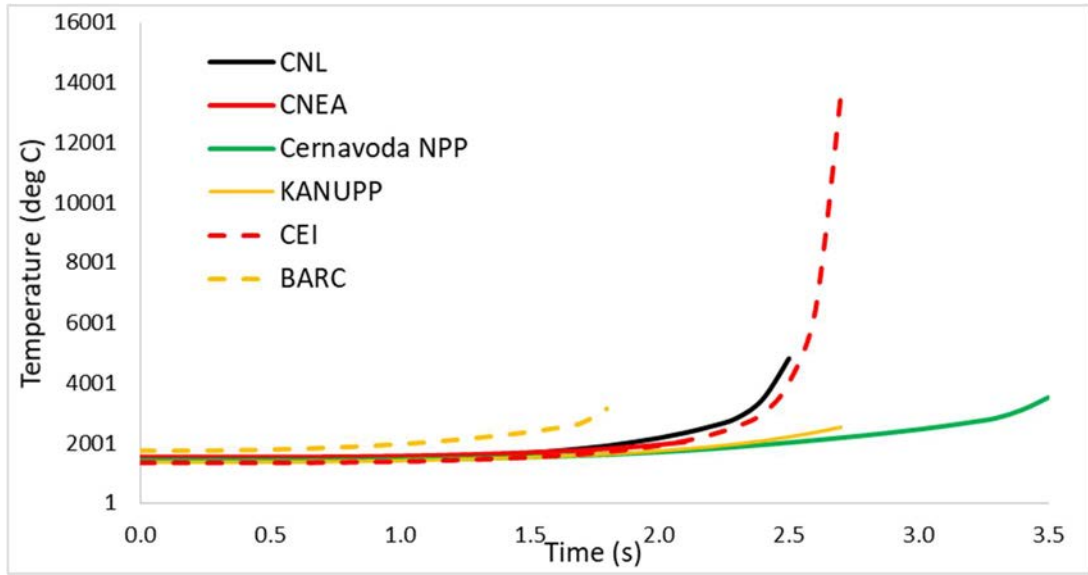
(a)



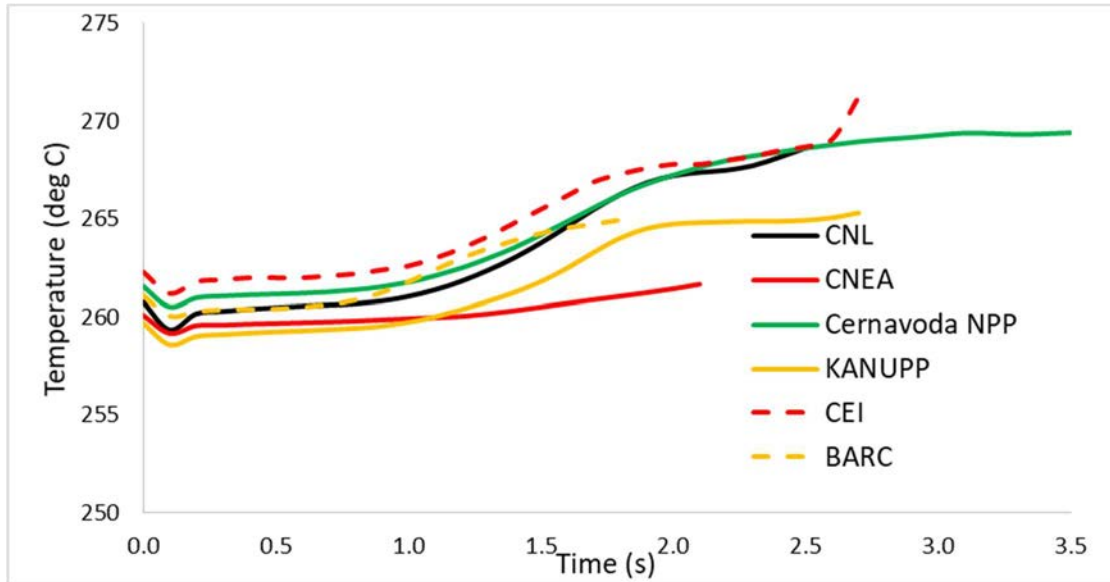
(b)

FIG.98. Core power and reactivity evolution in the coupled inlet header break without shutdown problem: (a) power, (b) reactivity.

Figures 99 and 100 present the time evolution of maximum centreline temperature of fuel, inlet header pressure, inlet header coolant temperature and outlet header void fraction. Pressure and temperature distributions follow similar trends for all participants up to 1.8 s. Maximum fuel centreline temperature prediction shows a rise towards the end of the transient for each participants with the maximum value ranging between 2,000 °C and 4,000 °C, except for CEI, where the maximum centreline temperature is an order of magnitude higher (14,000 °C). A drop in the inlet header pressure at the time of break initiation, followed by recovery of pressure, is captured well by all participants. The absolute pressure and coolant temperature for the inlet header and void fraction for the outlet header show significant deviations beyond 1.8 s. Evolution of void fraction at the outlet header by all participants show deviations within the range of 0.0–0.3.



(a)

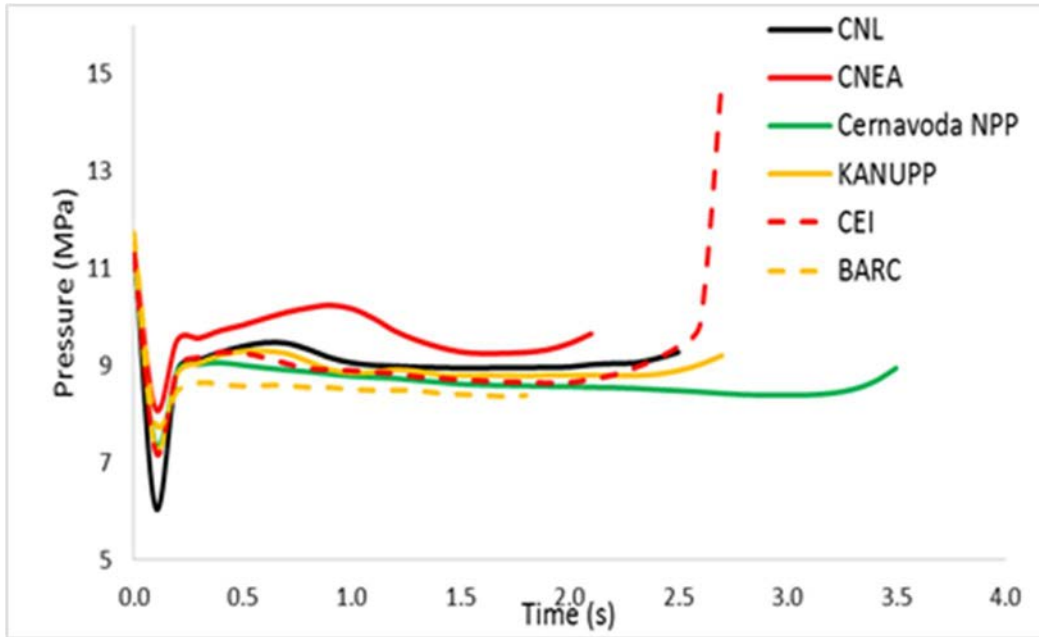


(b)

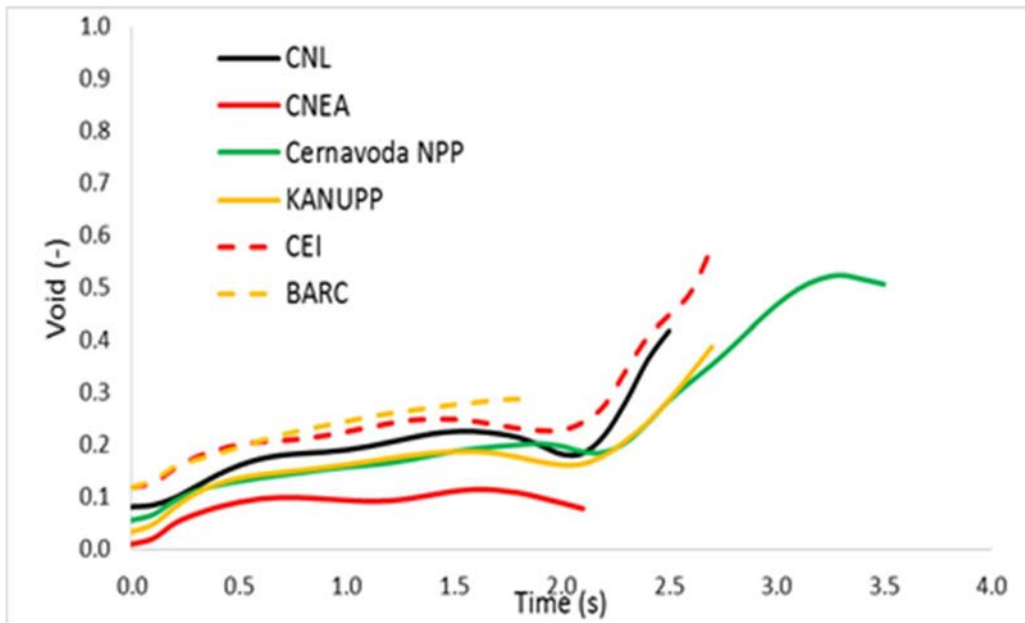
FIG. 99. Time evolution of thermal hydraulics parameters by different participants: (a) maximum fuel temperature ($^{\circ}\text{C}$) and (b) coolant temperature at inlet header 2 ($^{\circ}\text{C}$).

Figure 101 presents the normalized core channel power distributions obtained by all participants at the end of the transient. Each heat map uses the same colour scheme. Data are dimensionless, based on the normalization scheme: for each participant heat map, the channel powers were divided using the total core power and multiplying by 380. The mean values of all normalized values were then computed to generate the mean heat map. The left side of each heat map represents the power distribution in coolant loop 1 (broken loop) whereas right side represents coolant loop 2 (unbroken loop) of the reactor. Green colour represents lowest channel power whereas red colour represents highest channel power. Maximum power is observed to be in the loop 1 for all participants. This is consistent with significant void generation in loop 1 due to break at inlet header. Among the participants, CNL has indicated maximum power of 7,067 MW and CNEA has observed maximum power of 134 MW. The overall pattern of core channel power map appears consistent for all the participants except for BARC. In case of BARC, the

coupling across the loops is weak, and hence, increase in power in loop 1 (due to voiding) does not affect power of loop 2. Since the control rods were not active, the large power leads to a quasi-null ratio in BARC's loop 2 results.



(a)



(b)

FIG. 100. Time evolution of thermal hydraulics parameters by different participants: (a) coolant pressure at inlet header 2, and (b) void fraction at outlet header 1.

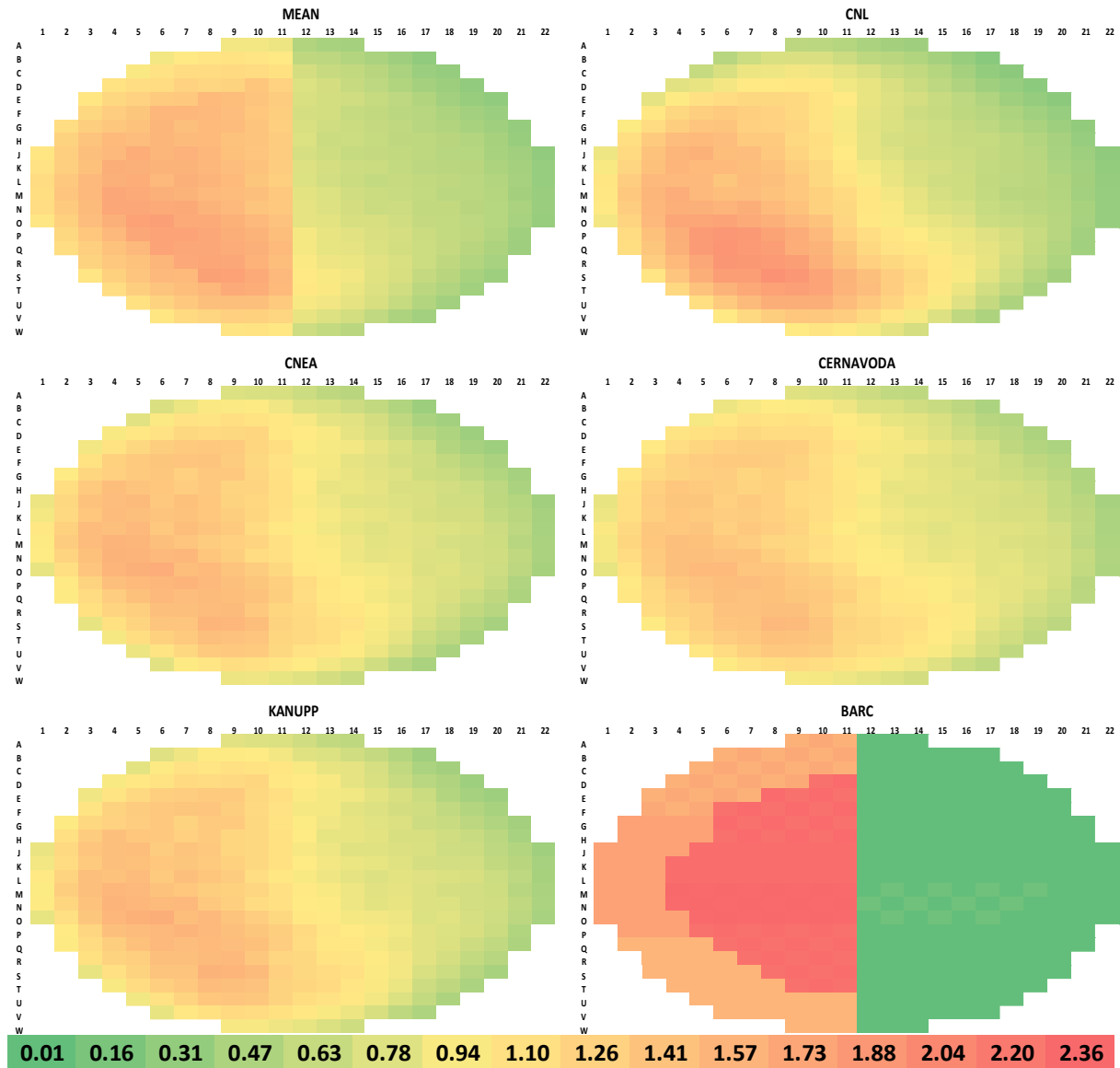


FIG. 101. Normalized core channel power presented by all participants at end of transient in the coupled Inlet header break without shutdown problem.

Figure 102 presents a heat map of the in-core coolant density obtained by all participants. The colour scaling is common for all heat maps, with values reported in kg/m^3 . Each row represents one of the 28 thermal hydraulics channels, and there is one column for each of the 12 axial nodal positions corresponding to the location of a fuel bundle. Columns are sorted from reactor inlet to outlet. Green is used for high density, red for low density. First figure represents the mean values of density of all the participants. Low coolant density (high void fraction) is observed in all the axial positions in channels 8 to channel 14 for all the participants. These channels belong to loop 1 of the core.

Figure 103 presents a heat map of the in-core volumetric average core fuel temperature obtained by all participants. Data are reported in $^{\circ}\text{C}$. Each row represents one of the 28 thermal hydraulics channels, and there is one column for each of the 12 axial nodal positions corresponding to the location of a fuel bundle. Columns are sorted from reactor inlet to outlet. Green is used for low temperature, red for high temperature. First figure represents the mean values of temperature of all the participants. Maximum volumetric average temperature $4,651^{\circ}\text{C}$ is obtained by CNL in channel number 11 and 7th axial position. Temperature predicted in

almost all nodes by CNL is much higher than other teams. For all the participants Loop 1 shows higher average fuel bundle temperature as compared to Loop 2.

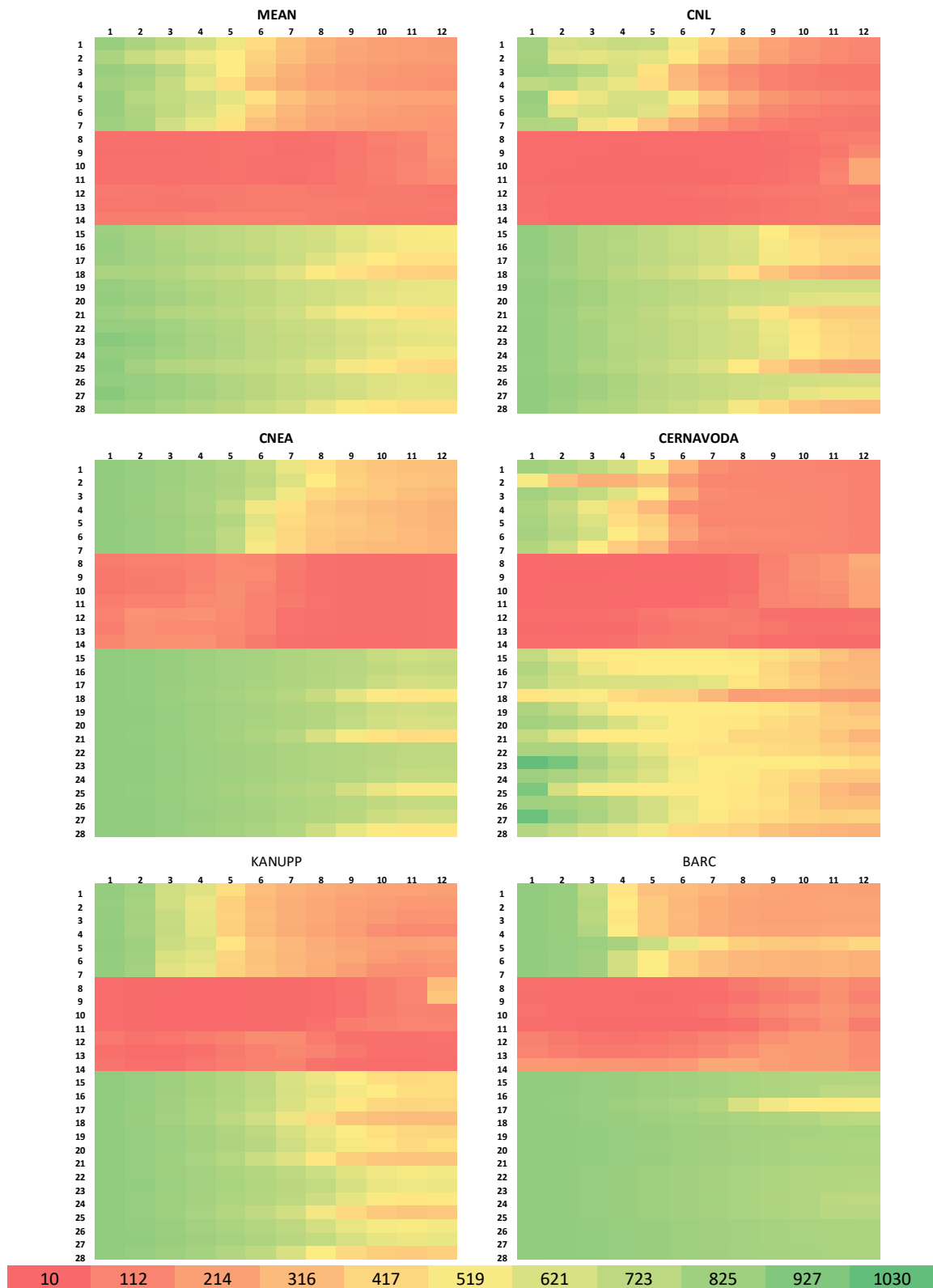


FIG. 102. Distribution of in-core coolant densities (kg/m^3) at end of transient in the coupled Inlet header break without shutdown problem.

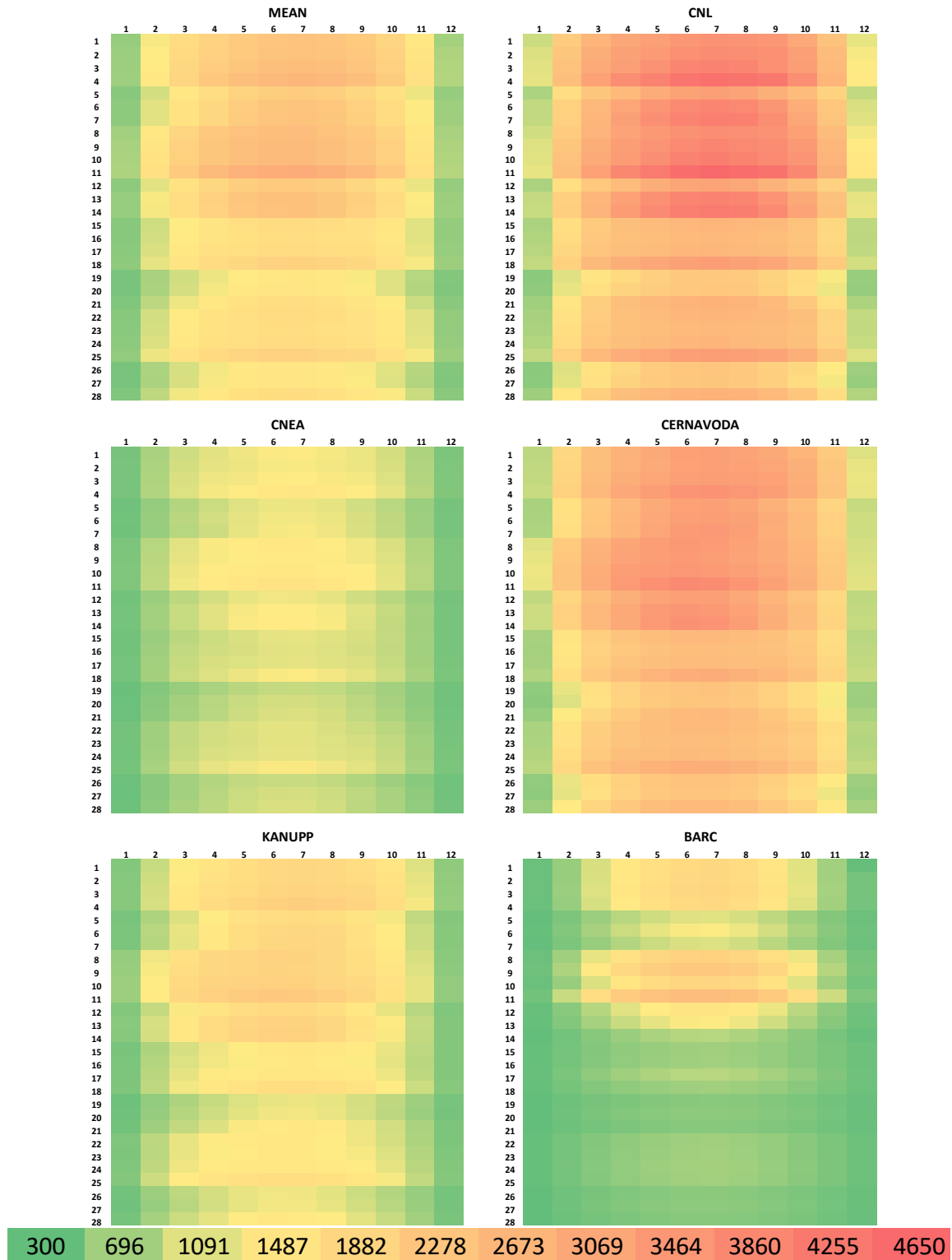


FIG. 103 Distribution of volumetric average core fuel temperature (°C) at end of transient by different participates in the coupled Inlet header break without shutdown problem.

Summary of results (comparison among participants)

Different countries have been participated in a multiphysics numerical benchmarking exercise for PHWRs. Key thermal hydraulic parameters are compared among the all the participants. Figures 98 and 99 show different parameters of all the participants. The time evolutions of relative power and reactivity are found to be in good agreement for initial period of the transient.

Large deviations are observed beyond 1.7 s. After 2.5 s, significant variations in absolute pressures, coolant temperature and void are observed. The core channel power maps as well as bundle power maps show similar trends for all participants except for BARC. The coolant density distribution and mean fuel average temperature maps shows similar patterns. Some discrepancy is observed for the coolant density data of Cernavoda NPP. The maximum core channel power among all participants is observed by CNL and it is 7,067 MW.

6. LESSONS LEARNED

6.1. PROCESS OVERVIEW

This IAEA ICSP is a first-of-a-kind approach to develop a set of standardized numerical multiphysics test problems for selected postulated transients in PHWR. Experts from ten organizations representing six Member States, five of which have operating PHWRs, contributed to an elicitation process, carried out during a four-day Technical Meeting, to define the framework and philosophy. The process comprises the following main steps:

1. Selection of a representative, albeit stylized, section of a PHWR plant design as the basis for identifying the key components and data for the multiphysics simulator. Using the generic layout illustrated in Fig. 104, it was first proposed to retain the system's components in the red circuit. Additional simplifications, such as replacement of the steam generators with suitable boundary conditions, were made. Further simplifications were adopted during the conversion of the selected system to the primary heat transport system network model and the reactor core model.
2. Selection of the key components and data for the multiphysics simulator. Based on the generic and stylized system developed in step 1, the main components, i.e., simulation methods, and data illustrated in Fig. 105 were selected. Notable simplifications are the elimination of cross-sections generation component, replaced using an existing 2-groups cross-section library for diffusion simulations, and elimination of the fuel behaviour simulation component, replaced by a simplified component for derivation of fuel related FOM. These simplifications are justified by the main objective of the multiphysics test problems; see also step 3.
3. Setting guidelines for development and execution of the numerical multiphysics test problems. The following key elements define the adopted philosophy:
 - i. Simplified and stylized:
 - a. Exaggerated to test feedback effects, coupling, and to limit computing time.
 - b. Specified conditions but flexible modelling.
 - c. Self-consistent and tested IC and BCs.
 - d. Users can group channels and/or axial segments and zones, chose their own data, modelling parameters, and methods.
 - ii. No specified reference solution:
 - a. Analytical solution unfeasible.
 - b. Integral-effect test data sparse.
 - c. No preference for specific method and codes.

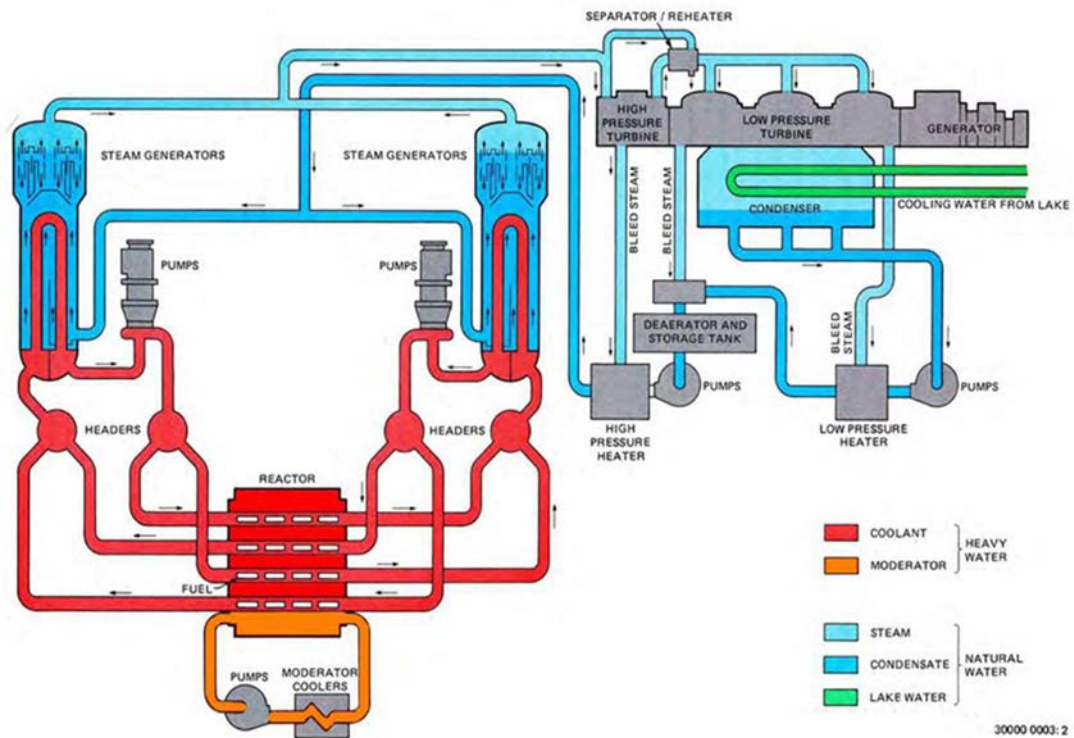


FIG. 104 Key systems in a generic PHWR system based on horizontal fuel channels.

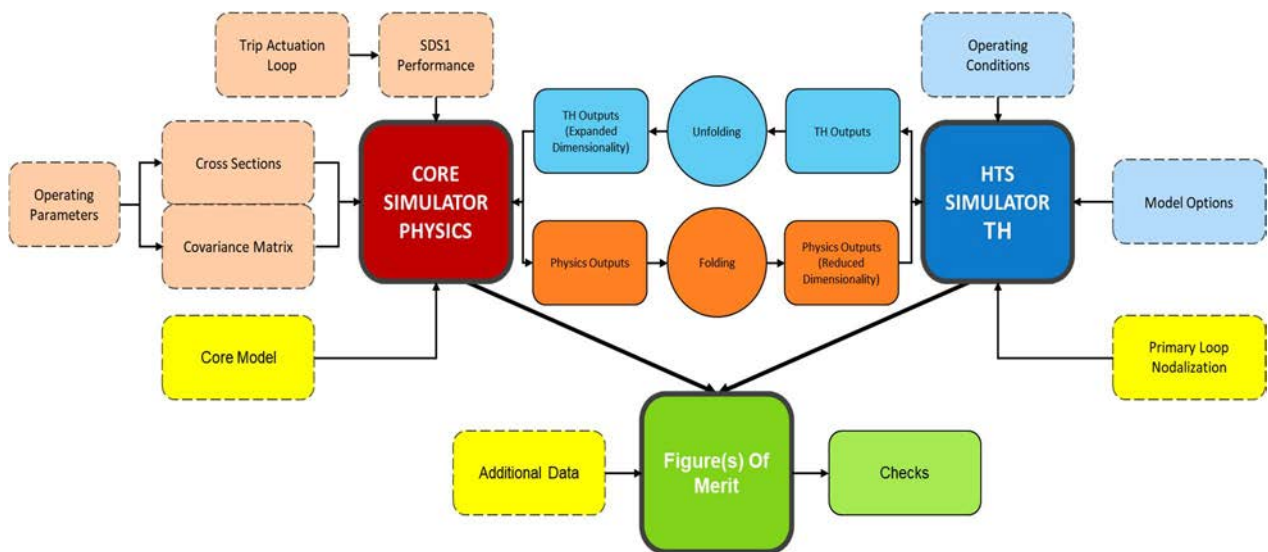


FIG. 105 Generic components of coupled reactor transient simulation systems.

4. Selection of postulated transients for a first set of standardized numerical multiphysics test problems and a structure of check-point sub-problems to facilitate the processing of the results. Each test problem is limited to representing reactor physics and system thermal hydraulics phenomena. A steady state problem is first considered for (a) testing of coupling methods and sensitivities, plus ‘tuning of models’ in order to (b) achieve similar starting conditions for better comparison of challenging problems results. Two additional sub-problems are defined under each test problem:

- a. Neutronics simulations with postulated thermal hydraulics conditions.
- b. TH simulations with postulated power transient.

The purpose of these additional sub-problems is (a) separate testing of neutronics and

thermal hydraulics methods and codes, in order to (b) gather complete information for better comparison of the challenging test problem results. The sub-problems play a significant role in the discussion of the results and identification of main contributors to the differences.

5. Selection of a lead group of experts to prepare and document the specifications. The CNL group of experts was selected to lead the implementation of this step.

The technical specifications initially released by the CNL team were used by participants to prepare initial solutions to the proposed problems. A technical meeting was held to review these initial results. Significant differences in all problems, including the steady state, were noted. These were traced to various inconsistencies and ambiguities in the numerical test problem specifications, which necessitated revisions.

6.2. PREPARATION OF PROBLEM SPECIFICATIONS

The problem specification was prepared and documented by one of the participating organizations (CNL, Canada). Although assigning the task of problem specification to one participant may not necessarily be unusual, it was inevitable that some of the models used in solving similar problems by CNL staff have affected specifications of reactor components and boundary conditions. For example, it turned out during the execution of the ICSP exercises that, not all participants had similar capability to model fuel gap heat transfer. This necessitated the development of an equivalent modelling strategy to account for fuel-sheath gap heat transfer. Similar but minor issues arose in the interpretation of control systems (even though CNL tried to keep these to a minimum) that required minor revisions of the specifications or further simplifications to accommodate all participants.

The lesson learned under this category, therefore, is to ensure that each participant is engaged during the 'problem specification' stage before commencing the exercises. This would also save considerable time and make working group meetings more effective.

6.3. PROPAGATION OF CHANGES

During the execution of the ICSP, there was considerable email traffic on specifications between the participants and CNL. Since there has not been a protocol established for reporting issues on specs or underlying models, these emails were considered one at a time and questions/issues were dispositioned by CNL one at a time. Every effort by CNL was made to inform other participants from revisions to specs or resolution of issues resulting from participant questions.

The lesson learned is that, right from the beginning, a protocol has to be established to keep track of issues identified in the specifications. This could be achieved and tracked through a 'living' database throughout the exercise. Such a database would include:

- a) The reporting participant and date;
- b) Description of the issue;
- c) Participant responsible to address the issue (in most cases this would be the same organization who prepared the initial specs);
- d) Priority (set levels of priority), required to ensure high priority items are addressed first;
- e) Resolution (or workaround) and date;
- f) Reference to revised specification documents, if applicable.

6.4. ORGANIZATIONAL COMMITMENT

There are two main factors that play an important role in the level of commitment to the ICSP, organizational commitment and individual commitment. The lesson learned is that participants right from the outset to confirm their organization's as well as their own (if applicable, their replacement) commitment over a multiyear exercise with supporting evidence.

6.5. GENERATION OF RESULTS

During the initial stages of the ICSP, majority of questions arose from the interpretation of specifications provided by CNL. One of the main reasons for this was that CNL plant representation and input formalism was influenced by the CNL code, ARIANT and its predecessor, CATHENA. Issues that surfaced during the generation of results often underlined these difficulties in the interpretation of specifications.

6.5.1. Issues arising from interpreting specifications

- There were several specifications that were not used and were in some cases cause of confusion. Examples are certain control systems which would never have been activated due to changes in the problem specification after the first year of the exercise. For example, after the LBLOCA simulation window was limited to 5 s, trip condition due to low header pressures became unnecessary;
- Volume components have very few specified parameters (specifications provided only the volume of such components). This could lead to discrepancies as not all codes have such components and other physical parameters may be needed to fully specify them;
- Pump specifications were not initially provided in full. CNL later provided this data and the cases had to be re-run, resulting in inefficiencies;
- Use of 'L-' and 'R-' prefixes for connections was not clear. This is a CATHENA/ARIANT method of specification and is not necessarily the way network connections are specified in other codes;
- Application of reversible losses, whether to some or all components was not clear. If they are not specified, default condition was not provided. RELAP users had to make modifications to specs since localized K factors cannot be specified at a component other than a junction.

Lessons learned:

- The specifications should avoid code-specific syntax and be as neutral as possible in the description of the network geometry, boundary and initial conditions;
- Given the boundary conditions and plant geometry data, the specification could mention that the initial conditions are established on a specific code estimation and that they may not be considered as imposed conditions.

6.5.2. Issues in interpretation of required output

- Interpretation of certain calculated output variables (e.g. IENTHL and MAXHB) were open to interpretation;
- The interpretation of physics data and code capability to use the technical specification was a source of differences observed (CNEA), both for the steady state or transient simulations.

Lesson learned:

The output variables and, if applicable, formulas for the calculation of more complex output variables are to be fully provided and clearly specified.

6.5.3. Examples of issues arising from different code capabilities

- RELAP users had to make certain modifications as components with a higher value of $\text{Area} \times \text{Length}$ than Volume (as given in the specs) could not be specified;
- The specification as given has certain expectations on geometry inputs, model constants, etc. which are not universally applicable across all thermal hydraulics codes (e.g., codes like TRACE require inputs and geometry within a different context).

Lesson learned:

Same as under Section 6.5.1 ‘Issues arising from interpreting specifications.’

Appendix I

THERMALHYDRAULICS MATERIAL PROPERTIES

I.1. CARBON STEEL, STAINLESS STEEL, AND INCONEL

The volumetric heat capacity, ρC_p , may be calculated from the thermal conductivity and diffusivity by:

$$\rho C_p = K / \alpha_g \quad (19)$$

where the thermal diffusivity, α_g , and conductivity, K , are determined by interpolation from the following tables:

- TABLE 29 THERMAL PROPERTIES OF CARBON STEEL;
- TABLE 30. THERMAL PROPERTIES OF STAINLESS STEEL (SS347);
- TABLE 31. THERMAL PROPERTIES OF INCONEL.

For temperatures outside the range of the table the limits of the tabulated values are used. Data for these materials is based on [51].

TABLE 29 THERMAL PROPERTIES OF CARBON STEEL

Temperature	Thermal Conductivity	Thermal Diffusivity
K	$\text{W m}^{-1} \text{K}^{-1}$	$10^{-5} \text{m}^2 \text{s}^{-1}$
273.15	46.0	1.28
323.15	45.8	1.25
373.15	45.3	1.19
423.15	44.7	1.14
473.15	43.3	1.08
523.15	40.9	1.03
573.15	37.5	0.97
623.15	34.5	0.89
673.15	32.0	0.83
723.15	30.0	0.83
773.15	28.2	0.75
823.15	27.1	0.67
873.15	26.0	0.58
923.15	25.0	0.56
973.15	24.4	0.47

TABLE 30. THERMAL PROPERTIES OF STAINLESS STEEL (SS347)

Temperature	Thermal Conductivity	Thermal Diffusivity
K	$\text{W m}^{-1} \text{K}^{-1}$	$10^{-6} \text{m}^2 \text{s}^{-1}$
273.15	14.60	3.50
342.95	14.90	3.55
432.95	15.70	3.70
520.95	17.10	3.95
622.95	18.50	4.16
725.95	20.20	4.43
815.95	21.60	4.53
885.95	22.40	4.75
1012.95	23.80	4.95
1072.95	24.80	5.05
1112.95	25.40	5.10
1173.95	25.90	5.16
1273.15	25.90	5.20

TABLE 31. THERMAL PROPERTIES OF INCONEL

Temperature	Thermal Conductivity	Thermal Diffusivity
K	$\text{W m}^{-1} \text{K}^{-1}$	$10^{-6} \text{m}^2 \text{s}^{-1}$
273.15	11.70	4.08
298.15	11.70	4.08
324.15	12.10	4.10
349.15	13.00	4.12
413.15	13.60	4.19
473.15	14.2	4.26
573.15	16.00	4.45
673.15	17.50	4.67
773.15	19.40	4.92
873.15	21.50	5.14
980.15	23.80	5.30
1078.15	26.00	5.32
1177.15	28.20	5.32
1273.15	30.10	5.32
1375.15	32.40	5.32
1473.15	34.00	5.32
1573.15	34.00	5.32

I.2. ZIRCALOY

The thermal conductivity, K , is given by [52]:

$$K = 7.67 \times 10^{-9}T^3 - 1.45 \times 10^{-5}T^2 + 2.09 \times 10^{-2}T + 7.51 \quad (20)$$

The volumetric heat capacity is determined from the product of density and the specific heat, where C_p is determined by interpolation from data provided in Table 32. In addition, the user has the option of specifying the hydrogen concentration, Hppm (H in parts per million) in the Zircaloy through the input file. The hydrogen concentration adds an additional term to the specific heat interpolated from data provided in Table 32. The specific heat for this option is determined through:

$$C_p = C_{p(table)} + C_{pH} \quad (21)$$

where $C_{p(table)}$ refers to the heat capacity provided in Table 33, and

$$C_{pH} = A \times \frac{2.679 \times 10^{10}}{T^2} e^{\frac{-4401}{T}} \quad (22)$$

where

$$A = \begin{cases} \frac{1}{e^{T_{ur}+1}} & \text{for } T_{ur} > -10 \text{ and } T_u < 10 \cdot T_0 \\ 1 & \text{for } T_{ur} \leq -10 \text{ and } T_u < 10 \cdot T_0 \\ 0 & \text{for } T_u \geq 10 \cdot T_0 \end{cases}$$

$$T_{ur} = \frac{T_u}{T_0} \quad T_u = \frac{T-T_0}{0.02} \quad T_0 = \frac{4401}{\log(1.332 \times 10^5)/H_{ppm}}$$

The density is assumed constant at 6,440 kg/m³.

For temperatures outside the range of the table the limits of the tabulated values are used.

TABLE 32. ZIRCALOY PROPERTIES

Temperature K	Density kg m ⁻³	Heat capacity J kg ⁻¹ K ⁻¹	Conductivity W m ⁻¹ K ⁻¹)
300	6440.00	281	12.68
350	6440.00	291.5	13.38
400	6440.00	302	14.04
450	6440.00	308.04	14.68
500	6440.00	314.08	15.29
550	6440.00	320.12	15.89
600	6440.00	326.17	16.49
650	6440.00	331.98	17.08
700	6440.00	336.87	17.67
750	6440.00	341.76	18.26
800	6440.00	346.64	18.88
850	6440.00	351.53	19.51
900	6440.00	356.42	20.17
950	6440.00	361.31	20.85
1000	6440.00	366.2	21.58
1050	6440.00	371.09	22.35
1100	6440.00	532.8	23.16
1150	6440.00	703.4	24.03
1200	6440.00	717.15	24.96
1250	6440.00	356	25.96
1300	6440.00	356	27.03
1350	6440.00	356	28.17
1400	6440.00	356	29.4
1450	6440.00	356	30.71
1500	6440.00	356	32.12
1550	6440.00	356	33.63
1600	6440.00	356	35.25
1650	6440.00	356	36.97
1700	6440.00	356	38.82
1750	6440.00	356	40.79
1800	6440.00	356	42.88
1850	6440.00	356	45.11
1900	6440.00	356	47.48
1950	6440.00	356	50
2000	6440.00	356	52.67
2050	6440.00	356	55.5
2100	6440.00	356	58.49
2150	6440.00	356	61.65
2200	6440.00	356	64.98
2250	6440.00	356	68.49
2300	6440.00	356	72.2
2350	6440.00	356	76.09
2400	6440.00	356	80.18
2450	6440.00	356	84.47
2500	6440.00	356	88.98
2550	6440.00	356	93.7
2600	6440.00	356	98.64
2650	6440.00	356	103.8
2700	6440.00	356	109.2
2750	6440.00	356	114.84
2800	6440.00	356	120.72
2850	6440.00	356	126.85
2900	6440.00	356	133.24

TABLE 33. THERMAL PROPERTIES OF ZIRCALOY

Temperature (K)	300	400	640	1090	1093	1113	1133	1053	1173	1193	1213	1233	1248	5000
Heat capacity (J kg ⁻¹ K ⁻¹)	281	302	331	375	502	590	615	719	816	770	619	469	356	356

I.3. IRRADIATED FUEL

I.3.1. Volumetric heat capacity

The heat capacity at constant pressure, C_p , is calculated from:

$$C_p = \left(\frac{C_1 \theta^2 e^{\theta/T}}{T^2 (e^{\theta/T} - 1)^2} \right) + C_2 T + \frac{0.5 F_0 C_3 \eta}{RT^2} e^{\left(\frac{-\eta}{RT} \right)} \quad (23)$$

where T is the temperature in K, and the remaining constants are listed in Table 5. The volumetric heat capacity, ρC_p , is computed using $\rho = 10.6 \times 10^3 \text{ kg} \cdot \text{m}^{-3}$.

TABLE 34. FUEL HEAT CAPACITY CONSTANTS

Constant	Value	Unit
C_1	296.7	J kg ⁻¹ K ⁻¹
C_2	2.43×10^{-2}	J kg ⁻¹ K ⁻²
C_3	8.745×10^7	J kg ⁻¹ K
θ	535.285	K
η	1.577×10^5	J mol ⁻¹
R	8.314	J mol ⁻¹ K ⁻¹
F_0	2.0	—

I.3.2. Thermal conductivity

At temperatures greater than, or equal to 3,110 K, the thermal conductivity (in W m⁻¹ K⁻¹) is computed using the electronic contribution only:

$$K^{elec} = 5.2997 \times 10^{-3} T \left(1 + 0.169 \times \left[\frac{13358}{T} + 2 \right]^2 \right) \times e^{-13358/T} \quad (24)$$

where T is the temperature in K.

Below 3,110 K, the additional terms are used:

$$K = \frac{C_v \rho F}{\left[\frac{\partial C_v}{\partial T} \times (A + B \beta_T) \times (1.0 + \beta(1.0 - \rho_F)) \right]} + K^{elec} \quad (25)$$

In this expression, the specific heat at constant volume, C_v , and its' derivative is given with:

$$C_v = \frac{296.79 \times (535.285/T)^2 \times e^{535.285/T}}{(e^{535.285/T} - 1)^2} \quad (26)$$

$$\frac{\partial C_v}{\partial T} = 1 + 3 \left(10^{-5}T - 3 \times 10^{-3} + 4 \times 10^{-2} \times e^{-5000/T} \right) \quad (27)$$

ρ_F is the effective fuel density, $A = 0.339$, and $B = 6.867 \times 10^{-2}$.

The porosity correction factors β and β_T are temperature dependent and are computed as per Table 35.

TABLE 35. FORMULAS FOR POROSITY CORRECTION FACTORS

Temperature limits for β	Formula for β
$T < 1364.647\text{K}$	$\beta = 6.5 - 4.69 \times 10^{-3}T$
$1364.647\text{K} \leq T < 1833.647\text{K}$	$\beta = 15.811308 - T(0.01833647 - 5 \times 10^{-6}T)$
$T \geq 1833.647\text{K}$	$\beta = -1.0$
Temperature limits for β_T	Formula for β_T
$T < 1800.0\text{K}$	$\beta_T = T$
$1800.0\text{K} \leq T < 2300.0\text{K}$	$\beta_T = -3240.0 + T(4.6 - 10^{-3}T)$
$T \geq 2300.0\text{K}$	$\beta_T = 2050.0$

I.3.3. Fuel properties in tabular form

Fuel properties are shown in Table 36.

TABLE 36. FUEL PROPERTIES

Temperature	Density	Heat capacity	Conductivity
K	kg m ⁻³	J kg ⁻¹ K ⁻¹	W m ⁻¹ K ⁻¹)
300	10600	236.38	10.94
350	10600	253.56	10.04
400	10600	265.84	9.18
450	10600	274.99	8.41
500	10600	282.07	7.74
550	10600	287.71	7.15
600	10600	292.36	6.63
650	10600	296.28	6.17
700	10600	299.67	5.77
750	10600	302.64	5.41
800	10600	305.31	5.09
850	10600	307.74	4.81
900	10600	309.98	4.55
950	10600	312.06	4.32
1000	10600	314.03	4.11
1050	10600	315.89	3.92
1100	10600	317.69	3.74
1150	10600	319.43	3.58
1200	10600	321.15	3.43
1250	10600	322.85	3.29
1300	10600	324.59	3.17
1350	10600	326.37	3.05
1400	10600	328.24	2.94
1450	10600	330.23	2.84
1500	10600	332.4	2.75
1550	10600	334.78	2.67
1600	10600	337.43	2.59
1650	10600	340.4	2.52
1700	10600	343.76	2.46
1750	10600	347.55	2.4
1800	10600	351.84	2.35
1850	10600	356.68	2.31
1900	10600	362.13	2.28
1950	10600	368.25	2.25
2000	10600	375.08	2.24
2050	10600	382.67	2.24
2100	10600	391.07	2.25
2150	10600	400.31	2.26
2200	10600	410.43	2.29
2250	10600	421.46	2.32
2300	10600	433.43	2.36
2350	10600	446.33	2.41
2400	10600	460.2	2.46
2450	10600	475.04	2.52
2500	10600	490.85	2.58
2550	10600	507.63	2.64
2600	10600	525.36	2.71
2650	10600	544.05	2.78
2700	10600	563.67	2.85
2750	10600	584.2	2.93
2800	10600	605.62	3.01
2850	10600	627.91	3.1
2900	10600	651.04	3.19

I.3.4. Gap properties in alternate form

For those participants where gap properties cannot be specified in terms of a gap conductance or surface emissivity, a workaround is presented here where an equivalent gap conductivity may be used.

The specifications provide a gap conductance, h , and surface emissivity for the fuel and the clad. The total heat flux from fuel to sheath through the gas is given by,

$$q = h(T_1 - T_2) + \sigma(T_1^4 - T_2^4) / \left[\frac{1}{\epsilon_1} + \frac{A_1}{A_2} \left(\frac{1}{\epsilon_2} - 1 \right) \right] \quad (28)$$

where h is the gap conductance given in the specifications. T_1 and T_2 are the outside surface temperature of fuel and inside surface temperature of the clad, respectively.

The above equation can be simplified further. In the fuel gap specifications $\epsilon_1 = \epsilon_2 = \epsilon$. Furthermore, since the fuel gap is small, it can be assumed that $A_1 \approx A_2$. Thus, equating the simplified form of total gap heat flux to heat flux by conduction, one can show that,

$$h(T_1 - T_2) + \frac{\sigma}{E}(T_1^4 - T_2^4) = \frac{k_{eff}(T_1 - T_2)}{\delta} \quad (29)$$

where δ is the gap size. The Eq. (29) can further be solved for the effective conductivity as follows:

$$k_{eff} = \delta \left\{ h + \frac{\sigma}{E}(T_1 + T_2)(T_1^2 + T_2^2) \right\} \quad (30)$$

The above form gives k_{eff} as a function of temperature and requires specification of equivalent gap conductivity in a lookup table in terms of surface temperatures. This is too complex and not required given the fact that gap surface emissivity in the specifications are small ($\epsilon = 0.01$). It will now be shown that the radiation component can be ignored in an order of magnitude analysis.

$$\sigma \sim O(-8)$$

$$E \sim O(2)$$

$$T \sim O(3)$$

$$h \sim O(4)$$

Thus, the above equation in an order-of-magnitude form becomes:

$$k_{eff} \sim \delta \left\{ O(4) + \frac{O(-8)}{O(2)} O(3) O(6) \right\} = \delta \{ O(4) + O(-1) \} \quad (31)$$

Therefore, the approximation $k_{eff} = \delta \cdot h$ can be used if a gap radiation model is not available.

Appendix II

PUMP CHARACTERISTICS

Table 37 shows the ANS pump model data, Table 38 provides data for the ANC pump function $m(\alpha_g)$, Table 39 shows data for pump torque curve, and the data for the ANC pump function $n(\alpha_g)$ are given in Table 40.

TABLE 37. ANC PUMP MODEL DATA (REVERSE PUMP ROTATION)

	Single-phase pump curve	Two-phase pump curve
Q^*/ω^*	$\frac{H_1^*}{(\omega^*)^2}$	$\frac{(H_1^* - H_2^*)}{(\omega^*)^2}$
0.00	0.95	0.00
0.20	1.10	-0.34
0.40	1.29	-0.65
0.60	1.45	-0.93
0.80	1.70	-1.19
1.00	1.95	-1.47
1.11	2.09	-1.12
1.25	2.18	-0.80
1.43	2.49	-0.47
1.67	2.79	-0.11
2.00	3.60	0.28
2.50	5.00	0.81
4.00	12.16	2.40
10.00	75.00	13.00
1,000.00	7.50×10^5	1.10×10^5

TABLE 38. ANC PUMP FUNCTION, $m(\alpha_g)$

α_g	$m(\alpha_g)$
0.0	0.0
0.08	0.0
0.20	1.0
0.90	1.0
1.00	0.0

TABLE 39. ANC PUMP TORQUE CURVE (FORWARD PUMP ROTATION)

Q^*/ω^*	$\frac{T_1 P}{(\omega^*)^2}$
-1,000.0	8.00×10^5
-10.00	80.00
-5.00	22.50
-2.00	4.00
-1.50	2.25
-1.00	1.05
-0.75	0.62
-0.50	0.40
-0.30	0.35
0.00	0.45
0.40	0.72
1.00	1.00
1.60	1.20
2.00	1.00
3.00	0.00
5.00	-3.75
10.00	-25.00
1,000.00	-3.00×10^5

TABLE 40. ANC PUMP FUNCTION, $n(\alpha_g)$

α_g	$n(\alpha_g)$
0.0	0.00
0.17	0.08
0.30	0.56
0.65	0.62
0.80	0.62
1.00	0.50

REFERENCES

- [1] POUNDERS, J. et al., “A 3D stylized half-core CANDU benchmark problem,” *Ann. Nucl. Energy* **38** (2011) 876–896.
- [2] MOSHER, S., F. RAHNEMA, AND R. STAMM’LER, “Lattice Database Development for Static and Transient Analyses,” CNSC Report, NAZ CNSC 0102R (2002).
- [3] AYDOGDU, K., Radiation Heating Report, 98–03320–AR–004, 2001 February.
- [4] ALEXANDER, J., Assessment of Energy Deposition Distribution in Lattices in Pressure Tube Heavy Water Reactors with Uranium and Thorium–Based Fuels, CNL technical report 153–123740–REPT–036, Revision 0, 2018 April.
- [5] VILLARINO, E.A., et al., “HELIOS: Angularly Dependent Collision Probabilities”. *Nucl. Sc. Eng.* **112** 16 (1992).
- [6] STAMM’LER, R.J.J., ABBATE, M.J., *Methods of Steady–State Reactor Physics in Nuclear Design*, Academic Press, London (1983).
- [7] GRANT, C., CNEA, Manual Del Sistema “PUMA” Versión 6. MCO–06REC–2 Rev. 0.
- [8] INFORMATION SYSTEMS LABORATORIES INC, “RELAP5/MOD3.3 Code Manual,” Idaho Falls, ID, December 2001.
- [9] RIBES, A., CAREMOLI, C., “SALOME platform component model for numerical simulation,” in: COMPSAC 07: Proceeding of the 31st Ann. Int. Computer Software and App. Conf., IEEE Computer Society (2007).
- [10] AYDEMIR, N.U., A. TROTTIER, T. XU, M. ECHLIN, T. CHIN, “Coupling of reactor transient simulations using the SALOME platform,” *Ann. Nucl. Energy*, **126** (2019) 434–442.
- [11] AYDEMIR, N. U., “Recent developments in CATHENA4: A fully–implicit network thermalhydraulics code,” in: NURETH–15, Pisa, Italy, May 12–17, 2013.
- [12] AYDEMIR, N.U., “A discussion of hyperbolicity in CATHENA4: virtual mass and phase–to–interface pressure differences,” in *Kerntechnik* **77** (2012) 128–133.
- [13] TURINSKY, P. AND H. SARSOOR, NESTLE–C: Few–group Neutron Diffusion Equation Solver Utilizing the Nodal Expansion Method for Eigenvalue, Adjoint, Fixedsource Steady–state and Transient Problems, CANDU Version. North Carolina State University. Tech.rep. (2003).
- [14] TURINSKY, P., R. AL–CHALABI, P. ENGRAND, H. SARSOOR, F. FAURE, M. GUO, NESTLE: Few–group neutron diffusion equation solver utilizing the nodal expansion method for eigenvalue, adjoint, fixed–source steady–state and transient problems. Tech. Rep. NC 27695–7909. North Carolina State University (2003).
- [15] LEPPÄNEN, J., M. PUSA, T. VIITANEN, V. VALTAVIRTA, T. KALTIAISENAHO, “The SERPENT Monte Carlo code: Status, development and applications,” *Ann. Nucl. Energy* **82** (2015) 142–150.
- [16] TROTTIER A., S. PFEIFFER, D. SERGHIUTA, “SERPENT–based Few–Group Cross Section Data for NESTLE–C,” M&C 2019 Int. Conf. on Mathematics and Computational Methods applied to Nucl. Sc. Eng., Portland, Oregon, USA 2019 August 25–29.
- [17] TROTTIER, A. H. ABDEL–KHALIK, Multigroup reference and covariance cross section data libraries for NESTLE–C, CNSC Project 598.2 final technical report (2019).

- [18] SARSOOR, H. P., TURINSKY, Reactor Physics Aspects of LOCA Analysis: Phase 2, CNSC Project 87055–0273, April 2003.
- [19] “NESTLE: Code System to Solve the Few Group Neutron Diffusion Equation Utilizing the Nodal Expansion Method for Eigenvalue Adjoint, and Fixed–Source Steady State and Transient Problems, Version 5.2.1,” RSICC CCC–641, June 2003.
- [20] MALDONADO, G. I., J. GALLOWAY, H. HERNANDEZ, K. T. CLARNO, E. L. POPOV, M. A. JESSEE, “Integration of the NESTLE Core Simulator with SCALE,” Trans. Am. Nucl. Soc. **100** (2009) 619–620.
- [21] HART, S., G. I. MALDONADO, “Modernization of the NESTLE–CANDU Reactor Simulator and Coupling to SCALE–Processed Cross Sections,” Proc. 24th Nucl. Sim. Symp., Ottawa, 2012 October 14–16.
- [22] RAHNEMA, F., D. ZHANG, “Continuous energy coarse mesh transport (COMET) method”, Ann. Nucl. Energy **115** (2018) 601–610.
- [23] ROUBEN, B., “RFSP–IST, the Industry Standard Tool Computer Program for CANDU Reactor Core Design and Analysis,” Proc. 13th Pacific Basin Nucl. Conf., Shenzhen, China (2002).
- [24] HANNA, B.N., “CATHENA: a thermalhydraulic code for CANDU analysis,” Nucl. Eng. Des. **180** (1998) 113–131.
- [25] DOWNAR, T., D. LEE, Y. XU, T. KOZLOWSKI, PARCS v2.7 U.S. NRC Core Neutronics Simulator User Manual, Purdue University Report, School of Engineering.
- [26] T DOWNAR, T., D. LEE, Y. XU, T. KOZLOWSKI, PARCS v2.7 U.S. NRC Core Neutronics Simulator Theory Manual. Purdue University Report, School of Engineering.
- [27] BAJOREK, S., TRACE V5.0 Patch 5 User’s Manual Volume 1: Input Specification, United States Nuclear Regulatory Commission Report (2017).
- [28] BAJOREK, S., TRACE V5.0 Patch 5 User’s Manual Volume 2: Modeling Guidelines.” United States Nuclear Regulatory Commission Report (2017).
- [29] S BAJOREK, S., TRACE V5.0 Patch 5 Theory Manual: Field Equations, Solution Methods and Physical Models.” United States Nuclear Regulatory Commission Report (2017).
- [30] REARDEN, B. T., M. A. JESSEE, SCALE 6.2.2 Code System User’s Manual, Oak Ridge National Laboratory Report (2017).
- [31] JESSEE, M. A., M. D. DEHART, NEWT: A NEW Transport Algorithm for Two–Dimensional Discrete–Ordinates Analysis in Non–Orthogonal Geometries, Oak Ridge National Laboratory Report (2016).
- [32] JESSEE, M. A., D. WIARDA, K. T. CLARNO, U. MERTYUREK, K. BEKAR, TRITON: A Multipurpose Transport, Depletion, and Sensitivity and Uncertainty Analysis Module, Oak Ridge National Laboratory Report (2017).
- [33] LEPPANEN, J., “The Serpent Monte Carlo code: Status, development and applications in 2013,” Ann. Nucl. Energy **82** (2015) 142–150.
- [34] WARD, A., Y. XU, T. DOWNAR, GenPMAX–v6.2 User’s Manual–Code for Generating the PARCS Cross Section Interface File PMAXS, University of Michigan Report (2016).
- [35] FLETCHER, C.D., R.R. SCHULTZ, RELAP5/MOD3 Code Manual, Idaho National Engineering Laboratory Report, Idaho Falls, ID (1995).

- [36] INTERNATIONAL ATOMIC ENERGY AGENCY, Comparison of Heavy Water Reactor Thermalhydraulic Code Predictions with Small Break LOCA Experimental Data, IAEA-TECDOC-1688 (2012).
- [37] SANTOSH K. PRADHAN, K OBAIDURRANHMAN, KANNAN N. IYER, AVINASH J. GAIKWAD, Development, validation and application of multi-point kinetics model in RELAP5 for analysis of asymmetric nuclear transients, Nucl. Eng. Des. **300** (2016) 506–516.
- [38] P.D. Krishnani, CLUB, A Multigroup Integral Transport theory code for analysis of cluster lattices, Annals of Nuclear Energy, Vol. 9, pp 255 to 260, 1982.
- [39] FOWLER, T. B., VONDY, D. R., CUNINGHAM, G. W., Nuclear Reactor Core Analyses Code CITATION, ORNL-TM-2496 Rev. 2 (1971).
- [40] ROMANO, P.K., et al., OpenMC: A state-of-the-Art Monte Carlo code for research and development, France: EDP Sciences (2013).
- [41] ASKEW, J.R., F.J. FAYERS, AND P.B. KEMSHELL, “General description of the lattice code WIMS”, J. Brit. Nucl. Energy Soc. **5** (1966) 564–85.
- [42] ALLISON, C.M., et al. “The Development of RELAP5/SCDAPSIM/MOD40 for Reactor System Analysis and Simulation,” in Book of Abstracts of 7th Int. Conf. on Nucl. Option in Countries with Small and Medium Electricity Grids, Croatia (2008).
- [43] SCHWANKE P., RFSP-IST User’s Manual, SQAD-12-5022, Rev. 0 (2013).
- [44] McARTHUR R. RFSPCB Development Log, CW-117370-SSDL-001, Rev.0, (2010).
- [45] BEUTHE, T.G. AND B. N. HANNA, CATHENA MOD-3.5d Rev.2 Input Reference, 153-112020-UM-001 (2005).
- [46] ZHANG, D., F. RAHNEMA, “Continuous-energy COMET solution to the stylized AHTR benchmark problem”, Ann. Nucl. Energy **121** (2018) 284–294.
- [47] ZHANG, D., AND F. RAHNEMA, “COMET Neutronics Solutions to the Prismatic VHTR Benchmark Problem”, Nucl. Eng. Des. **358** (2020) 110395.
- [48] ULMER R., F. RAHNEMA, K. CONNOLLY, “A neutronic benchmark specification and COMET solution for the Advanced Burner Test Reactor,” Ann. Nucl. Energy **87** (2016) 76–106.
- [49] MOSHER, S., F. RAHNEMA, “The Incident Flux Response Expansion Method for Heterogeneous Coarse Mesh Transport Problems,” Transport Theory and Statistical Physics **34** (2006) 1–26.
- [50] ZHANG, D., F. RAHNEMA, “An Efficient Hybrid Stochastic/Deterministic Coarse Mesh Neutron Transport Method,” Ann. Nucl. Energy **41** (1012) 1–11.
- [51] TOULOUKIAN Y.S., Ed., Thermalphysical properties of high temperature solid materials, MacMillan Co., New York (1967).
- [52] MATPRO-Version 11 (Revision 1) A handbook of material properties for use in the analysis of light water reactor fuel rod behaviour Rev 1, NUREG/CR-0497, TREE-1280, (1980).

ANNEX I: SUPPLEMENTARY FILES – DATA

The supplementary files for this publication can be found on the publication's individual web page at: www.iaea.org/publications.

I-1. Core_specs.xlsx

Neutronics core geometry data, burnup distribution and data library;

I-2. Device_specs.xlsx

Neutronics data/geometry for reactivity control devices;

I-3. Transport_neutronics.xlsx

Burnup distribution and data library for use with transport neutronics codes;

I-4. TH_network_specs.xlsx

Network thermal hydraulics geometry and data;

I-5. SA_neutronics.xlsx

This file provides the neutronics response for use with standalone thermal hydraulics simulations;

I-6. SA_thermalhydraulics.xlsx

Provides the corresponding thermal hydraulics response data for use with standalone neutronics simulations.

ANNEX II: SUPPLEMENTARY FILES – PARTICIPANT INFORMATION

Participant information and a summary of the contributions are below. The contribution can be found in full in the supplementary files for this publication, which can be found on the publication's individual web page at: www.iaea.org/publications.

COMISIÓN NACIONAL DE ENERGÍA ATÓMICA (CNEA)

Country	Argentina
Organization	Comisión Nacional de Energía Atómica
Technical contact name	Juan Beliera, Santiago Bazzana and Roberto Hilal
Technical contact email	jbeliera@cnea.gob.ar sbazzana@cnea.gob.ar hilal@cnea.gov.ar
Neutronics code name and version	PUMAv6.0.5
Thermal hydraulics code name and version	RELAP5 3.3
Summary of participant contributed solutions	All problems with exception of the standalone steady state neutronics transport problem (Section 3.3).

CANADIAN NUCLEAR LABORATORIES (CNL)

Country	Canada
Organization	Canadian Nuclear Laboratories
Technical contact name	Alexandre Trottier and Nusret Aydemir
Technical contact email	Alexandre.trottier@cnl.ca Nusret.aydemir@cnl.ca
Neutronics code name and version	NESTLE-C 3.1.2
Thermal hydraulics code name and version	ARIANT 1.0.0.24
Summary of participant contributed solutions	All problems with exception of the standalone steady state neutronics transport problem (Section 3.3).

CANADIAN NUCLEAR SAFETY COMMISSION (CNSC)

Country	Canada
Organization	Canadian Nuclear Safety Commission
Technical contact name	Marcus Secor Dumitru Serghiuta
Technical contact email	Marcus.secor@canada.ca Dumitru.serghiuta@canada.ca
Neutronics code name and version	NESTLE-C Version 3.0
Thermal hydraulics code name and version	N/A
Summary of participant contributed solutions	CNSC contributed neutron diffusion solutions for comparison with transport-based solutions to steady state problem (Section 5.2.2).

CANDU ENERGY INC. AND THE CANDU OWNER'S GROUP (CEI)

Country	Canada
Organization	CANDU Energy Inc., on behalf of the CANDU Owner's Group
Technical contact name(s)	R. Farkas, M. Dahmani
Technical contact email	Robert.Farkas@snclavalin.com , Mohamed.Dahmani@snclavalin.com
Neutronics code name and version	RFSP version 3.5.2
Thermal hydraulics code name and version	CATHENA version 3.5.5.1
Summary of participant contributed solutions	Contributed solutions to the steady state, adjuster withdrawal, pump rundown, and header break coupled problems. The CANDU Owner's Group provided financial support for the completion of the steady state and header break contributions listed in this publication. All contributions from this team are included as 'CEI' in the main text.

MCMASTER UNIVERSITY (MCMMASTER)

Country	Canada
Organization	McMaster University
Technical contact name	Kai Groves and Dr. Novog
Technical contact email	groveskj@mcmaster.ca novog@mcmaster.ca
Neutronics code name and version	PARCS v32m21co

Thermal hydraulics code name and version	TRACE v5p5
Summary of participant contributed solutions	Contributed to all problems with two exceptions: standalone steady state neutronics transport problem (Section 3.3) and the header break without shutdown rod action (Section 3.5.4.1).

BHABHA ATOMIC RESEARCH CENTRE (BARC)

Country	INDIA
Organization	BARC
Technical contact name	Dr. Onkar Gokhale Dr. Mithilesh Kumar Dr. Mukhopadaya, Deb
Technical contact email	onkarsg@barc.gov.in mithiles@barc.gov.in

Neutronics code name and version	RELAP5/ mod 3.2
Thermal hydraulics code name and version	RELAP5/ mod 3.2
Summary of participant contributed solutions	BARC contributed solutions to all coupled problems with the exception of the adjuster withdrawal problem (Section 3.5.2). Furthermore, BARC also provided solutions for the standalone thermal hydraulics variants of the transient problems.

KARACHI NUCLEAR POWER PLANT (KANUPP)

Country	PAKISTAN
Organization	KANUPP
Technical contact name	Adam Noora
Technical contact email	adam@knpc.gov.pk
Neutronics code name and version	CITATION-II
Thermal hydraulics code name and version	RELAP5/SCDAP Version 3.4
Summary of participant contributed solutions	All problems with exception of the standalone steady state neutronics transport problem (Section 3.3).

PAKISTAN INSTITUTE OF ENGINEERING AND APPLIED SCIENCES (PIEAS)

Country	Pakistan
Organization	Pakistan Institute of Engineering & Applied Sciences (PIEAS)
Technical contact name	Muhammad Ilyas Nasir Hayat Hengra Muhammad Sajjad
Technical contact email	ilyas@pieas.edu.pk mailto:Alexandre.trottier@cnl.ca milyas323@gmail.com mailto:Nusret.aydemir@cnl.ca
Neutronics code name and version	OpenMC 0.11.0, WIMSD/4
Thermal hydraulics code name and version	RELAP/SCDAPSIM Mod 4.0
Summary of participant contributed solutions	PIEAS contributed a coupled solution to the steady state problem and standalone thermal hydraulics solutions to all transient problems.

CERNAVODA NUCLEAR POWER STATION (CERNAVODA)

Country	ROMANIA
Organization	CERNAVODA NPP
Technical contact name	ISTRATE EMANOIL-RELU TOMA VICTOR
Technical contact email	relu.istrate@cne.ro victor.toma@cne.ro
Neutronic code name and version	RFSP, version 3.5.4.1
Thermal hydraulics code name and version	CATHENA MOD-3.5d Rev.2
Summary of participant contributed solutions	CERNAVODA contributed solutions to all coupled problems as well as standalone thermal hydraulics variants of the transient problems.

GEORGIA INSTITUTE OF TECHNOLOGY (GATECH)

Country	USA
Organization	Georgia Institute of Technology
Technical contact name	Farzad Rahnema Dingkang Zhang
Technical contact email	farzad@gatech.edu dingkang.zhang@gatech.edu

Neutronics code name and version	COMET
Thermal hydraulics code name and version	N/A
Summary of participant contributed solutions	GATECH provided transport solutions for the standalone steady state neutronics transport problem (Section 3.3).

ABBREVIATIONS

ADF	Assembly Discontinuity Factor
CNL	Canadian Nuclear Laboratories
ECC	Emergency Core Cooling
FDM	Finite Difference Method
FOM	Figure of Merit
ICSP	International Computational Standard Problem
IHD	Inlet Header
LBLOCA	Large-Break Loss-Of-Coolant Accident
NEM	Nodal Expansion Method
OHD	Outlet Header
PHWR	Pressurized Heavy Water Reactor

CONTRIBUTORS TO DRAFTING AND REVIEW

Aydemir, N..	Canadian Nuclear Laboratories (CNL), Canada
Bazzana, S.	Comisión Nacional de Energía Atómica (CNEA), Argentina
Beliera, J.	Comisión Nacional de Energía Atómica (CNEA), Argentina
Dahmani, M.	CANDU Energy Inc. (CEI), Canada
Farkas, R.	CANDU Energy Inc. (CEI), Canada
Gokhale, O.	Bhabha Atomic Research Centre (BARC), India
Groves, K.	McMaster University, Canada
Hengra, N.H.	Pakistan Institute of Eng. & App. Sciences (PIEAS), Pakistan
Hilal, R.	Comisión Nacional de Energía Atómica (CNEA), Argentina
Ilyas, M.	Pakistan Institute of Eng. & App. Science (PIEAS), Pakistan
Istrate, R.	Society National Nuclearelectrica (SNN), Romania
Jevremovic, T.	International Atomic Energy Agency
Krause, M.	International Atomic Energy Agency
Kumar, M.	Bhabha Atomic Research Centre (BARC), India
Mukhopadaya, D.	Bhabha Atomic Research Centre (BARC), India
Noora, A.	Karachi NPP (KANUPP), Pakistan
Novog, D.	McMaster University, Canada
Sajjat, M.	Pakistan Institute of Eng. & App. Sciences (PIEAS), Pakistan
Secor, M.	Canadian Nuclear Safety Commission (CNSC), Canada
Serghiuta, D.	Canadian Nuclear Safety Commission (CNSC), Canada
Rahnema, F.	Georgia Institute of Technology, GA, USA
Rehman, H.	International Atomic Energy Agency
Toma, V.	Society National Nuclearelectrica (SNN), Romania
Trottier, A.	Canadian Nuclear Laboratories (CNL), Canada
Zhang, D.	Georgia Institute of Technology, GA, USA

Technical Meetings

Ottawa, Canada: 9–12 August 2016

Vienna, Austria: 21–24 August 2017, 4–7 September 2018, 26–29 November 2019



IAEA

International Atomic Energy Agency

No. 26

ORDERING LOCALLY

IAEA priced publications may be purchased from the sources listed below or from major local booksellers.

Orders for unpriced publications should be made directly to the IAEA. The contact details are given at the end of this list.

NORTH AMERICA

Bernan / Rowman & Littlefield

15250 NBN Way, Blue Ridge Summit, PA 17214, USA

Telephone: +1 800 462 6420 • Fax: +1 800 338 4550

Email: orders@rowman.com • Web site: www.rowman.com/bernan

REST OF WORLD

Please contact your preferred local supplier, or our lead distributor:

Eurospan Group

Gray's Inn House

127 Clerkenwell Road

London EC1R 5DB

United Kingdom

Trade orders and enquiries:

Telephone: +44 (0)176 760 4972 • Fax: +44 (0)176 760 1640

Email: eurospan@turpin-distribution.com

Individual orders:

www.eurospanbookstore.com/iaea

For further information:

Telephone: +44 (0)207 240 0856 • Fax: +44 (0)207 379 0609

Email: info@eurospangroup.com • Web site: www.eurospangroup.com

Orders for both priced and unpriced publications may be addressed directly to:

Marketing and Sales Unit

International Atomic Energy Agency

Vienna International Centre, PO Box 100, 1400 Vienna, Austria

Telephone: +43 1 2600 22529 or 22530 • Fax: +43 1 26007 22529

Email: sales.publications@iaea.org • Web site: www.iaea.org/publications

**International Atomic Energy Agency
Vienna**